The multifunctional role of Semaphorin6A during brain development and disease

Moving forward with reverse signaling

Marieke G. Verhagen

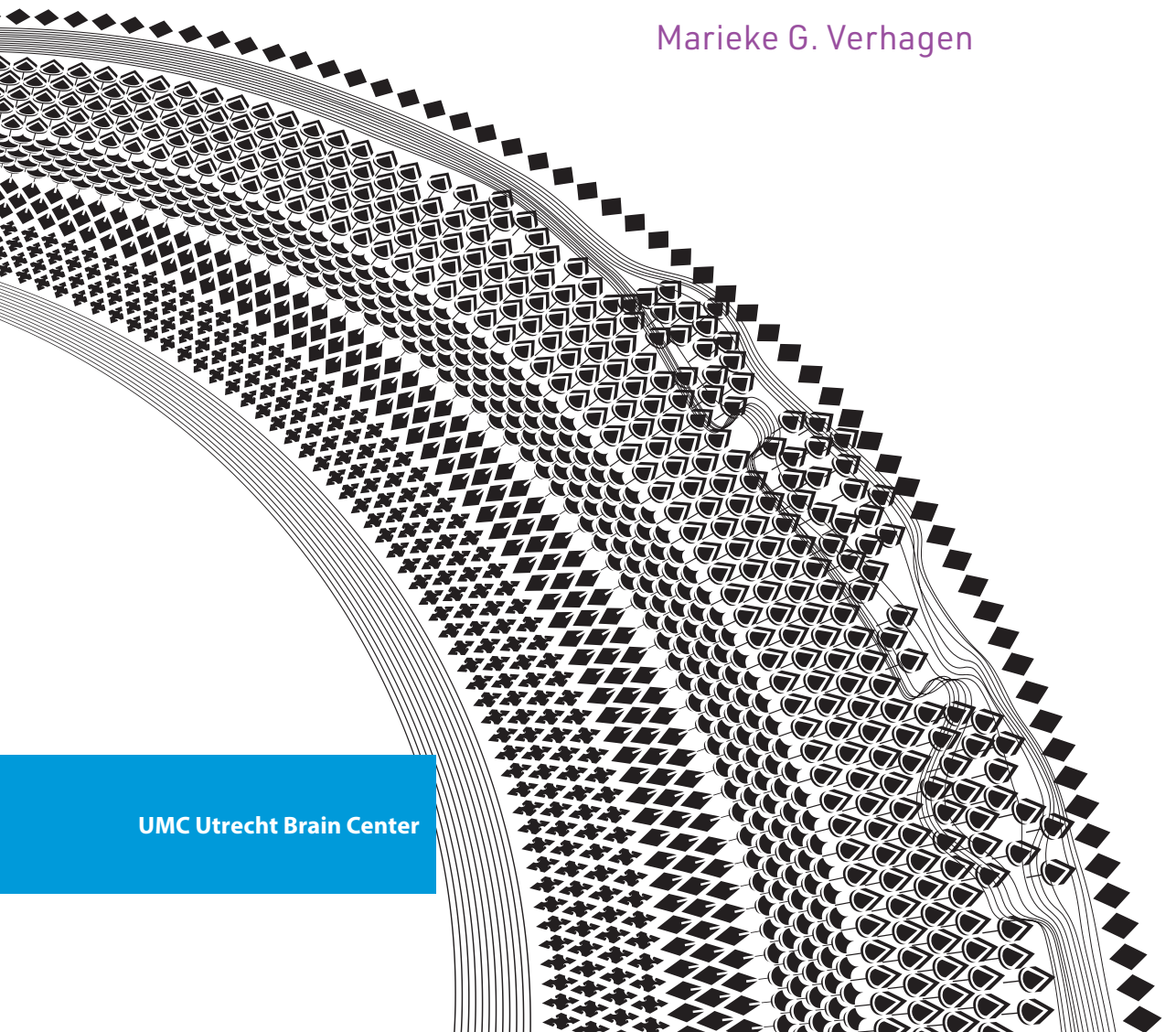

UMC Utrecht Brain Center

The multifunctional role of Semaphorin6A during brain development and disease

Moving forward with reverse signaling

Marieke Geerte Verhagen

Cover design Marieke G. Verhagen
Layout Proefschrift-All in One | www.proefschrift-aio.nl
ISBN 978-94-93184-99-2

The multifunctional role of Semaphorin6A during brain development and disease

Moving forward with reverse signaling

De multifunctionele rol van Semaforine6A tijdens de ontwikkeling van de hersenen en hersenziekten

Voorwaarts met tegengestelde signalering

(met een samenvatting in het Nederlands)

Proefschrift

ter verkrijging van de graad van doctor aan de
Universiteit Utrecht
op gezag van de
rector magnificus, prof.dr. H.R.B.M. Kummeling,
ingevolge het besluit van het college voor promoties
in het openbaar te verdedigen op

donderdag 14 oktober 2021 des ochtends te 10.15 uur

door

Marieke Geerte Verhagen

geboren op 10 juli 1989
te Gouda

Promotor:
Prof. dr. R.J. Pasterkamp

Copromotor:
Dr. G.M.J. Ramakers

CONTENTS

CHAPTER 1

General Introduction

GENERAL INTRODUCTION

Preface

The development of the brain is a highly complex process that encompasses cellular and molecular events starting from early embryonic development onwards. The determination of these events is essential for understanding brain development and disorders. Semaphorins are axon guidance molecules that play a key role during the development of the brain. By providing direction and context-specific signals, semaphorins trigger signaling events controlling a wide variety of developmental processes such as axon guidance, cell migration, dendrite morphology, laminar segregation and synaptogenesis. These processes are essential for the correct organization and formation of the brain. Studying brain development in mice in which semaphorin function has been genetically manipulated, helps to understand their role during neurodevelopmental disorders. This thesis focuses on previously unexplored signaling mechanisms and essential cellular functions of a member of the semaphorin protein family, Semaphorin6A, during the development of the nervous system.

Introduction

The brain is a complex and versatile organ that undergoes various phases of development (**BOX I**). This thesis focuses on the moment when neurons migrate from their birthplace to different brain areas and start to make connections with other cells to form neural circuits. During this phase, axon guidance molecules play an important role in establishing proper neural organization and connectivity. The principle of axon guidance is that growing axons and migrating cells rely on intermediate targets and guidance cues presented over short or long distances along their paths in order to establish neuronal connections (Fig. 1). Growing axons extend their growth cones to scan the environment and respond to axon guidance cues that provide direction towards or away from specific regions (Fig. 1) [1-4]. Semaphorins are axon guidance molecules that are well-known for their function as attractants or repellents. Although only a limited set of semaphorins has been identified, accumulating evidence indicates that distinct molecular mechanisms act to diversify the effects of semaphorins, making semaphorins multifunctional molecules that control a wide variety of cellular events. **Chapter 2** comprises an extended introduction and description of general features and novel aspects of semaphorin function and signaling, including the role of their receptors; plexins and neuropilins. The focus is on the contribution of these molecules to the regulation of

cell migration and the formation of neuronal connections. Semaphorin6A (Sema6A) is an example of a member of the semaphorin protein family that plays a key role in the nervous system, yet we know very little about its multifunctional role and diverse signaling mechanisms. In this thesis, the aim is to determine and specify these Sema6A signaling events during the development of the brain. Throughout the subsequent chapters of the thesis, three topics will be addressed: 1. Sema6A reverse signaling *in vivo* (**Chapters 3 and 4**) 2. Sema6A *cis* interaction and the specific structural domains involved in this interaction (**Chapter 5**) and 3. Novel functions of Sema6A in the diseased brain (**Chapter 6**).

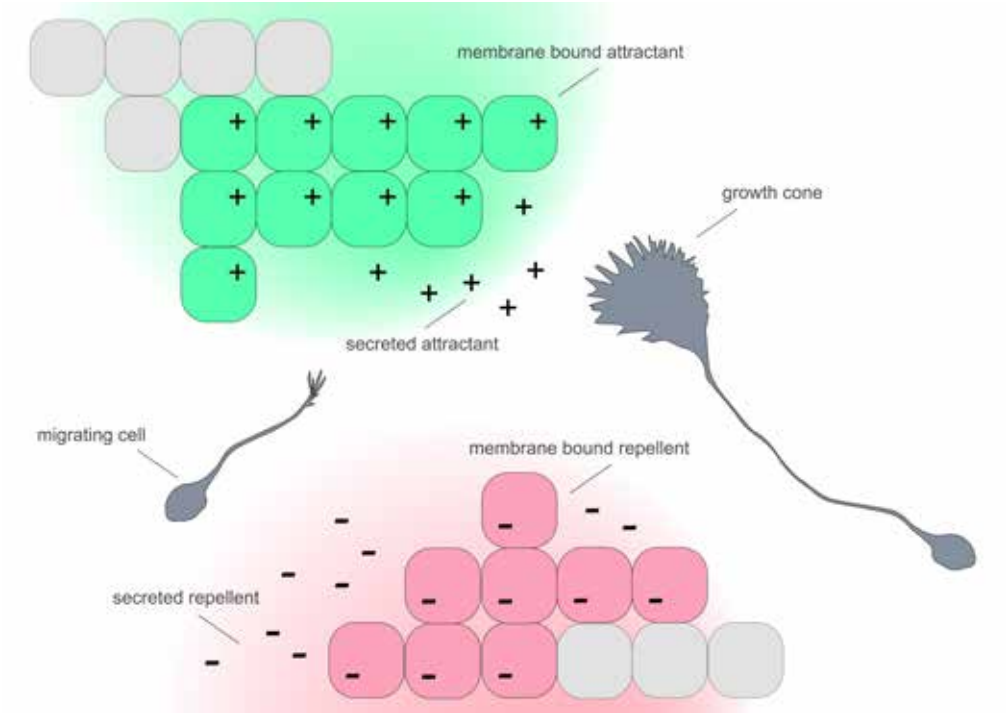

Figure 1. Principle of axon guidance. Schematic overview showing axon guidance effects. Axon guidance cues can be membrane-bound or secreted attractants or repellents. Repulsive signals repel migrating cells or growth cones away or along an inappropriate region (red). Attractive signals provide permissive regions to continue growth towards a target region (green). The process of axon guidance ensures over short or long distances is essential in order to establish neuronal connections during brain development.

BOX I Brain development

The development of the brain is a remarkable process that includes multiple processes: neurulation, neurogenesis, migration, apoptosis, synaptogenesis, gliogenesis and myelination (Fig. 2). These processes are highly conserved in mammalian species and shared between humans and mice [5,6]. During neurulation cells differentiate into neural stem cells that increase dramatically in number by undergoing symmetric cell division creating new stem cells that also continue to proliferate [7]. Around embryonic day (E) 10, neural stem cells shift to asymmetric division to create one new stem cell and one post-mitotic cell. This hallmarks the start of neurogenesis. Post-mitotic cells become a neuron or glial cell [7,8]. At this stage, many different types of neurons are formed that vary in shape, size and function. To settle in the correct region of the brain, these newborn cells follow specific paths over short or long distances during the process of migration, when axon guidance molecules start to play an important role. At this time, different brain structures are formed for example, the cerebral cortex that further divides into different subregions and layers [9]. Axons travelling over long distances enter the cerebral cortex to establish connections to form for example the corpus callosum and other major white matter tracts [10]. The organization of the brain continues after migration is complete with axonal and dendritic development and maturation, synapse formation (synaptogenesis), programmed cell death (apoptosis), glial proliferation (gliogenesis) and myelination [5,6,11]. All these processes contribute to the formation of different functional regions in the brain that form connections and complex neural networks. The determination of the molecular and cellular events involved during development in mice contributes to a dramatic increase in knowledge and is essential to understand brain development and disorders.

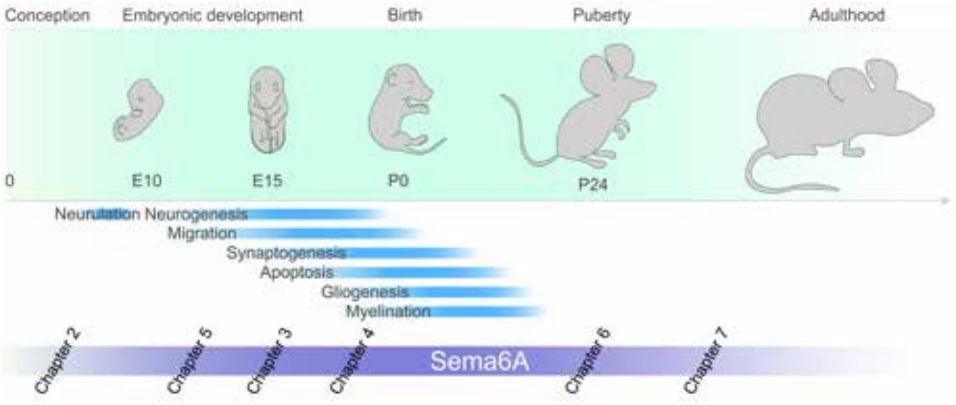

Figure 2. Mouse brain development. Schematic overview of developmental processes during mouse brain development focusing on embryonic and early postnatal stages. The development of the brain starts with the process of neurulation at early embryonic stages and continues with neurogenesis and migration that finishes around birth. Synaptogenesis, apoptosis, gliogenesis and myelination continue during postnatal stages. Blue lines show timing of specific process. Some of these processes occur simultaneously, as indicated. The different chapters in this thesis are indicated, by approximation, at the developmental stage and timepoint studied. The chapters included the following topics: 3. The role of Sema6A during brain development, 4. Sema6A reverse signaling during cortical development, 5. Structural domains involved in *cis* interaction and 6. Sema6A and puberty onset and disease. The general introduction and discussion of this thesis are found in Chapter 1 and Chapter 7, respectively. Chapter 2 provides an extensive introduction on semaphorin, plexin and neuropilin signaling during the development of the brain.

Sema6A is a transmembrane semaphorin originally identified as a repulsive cue when interacting as a ligand with PlexinA receptors in the forward signaling fashion [12]. In the absence of Sema6A, axonal dysconnectivity and cellular disorganization phenotypes are found in the neocortex, anterior commissure, lateral olfactory tract, piriform cortex, hippocampus, corticospinal tract, fornix, cerebellum and retina [13–27]. These neuroanatomical phenotypes described for Sema6A knockout mice (*Sema6A*$^{-/-}$) have been linked to the etiology of psychiatric disorders in humans and are therefore highly informative to start understanding the mechanisms behind neurodevelopmental disorders such as schizophrenia and autism [20,28]. In **Chapter 2**, a few recent studies are presented that highlight how semaphorins, plexins and/or neuropilins contribute to brain disorders.

Over the recent years it has become clear that there are a few possible modes of interaction between Sema6A and PlexinA interactors, contributing to the multifunctionality of Sema6A in different biological effects. Sema6A can mediate forward signaling (ligand function) and also reverse signaling (receptor function) depending on the molecular and cellular context [29–34]. While there are examples for the role of Sema6A as a ligand in forward signaling, there is limited information about its role as a receptor in reverse signaling. However, several studies suggest that reverse signaling could also play an important role during vertebrate neuronal circuit development [30,32,34–36]. When and where Sema6A functions as a ligand and/or as a receptor during development is largely unknown.

To study the bidirectional role of Sema6A and to distinguish between ligand and receptor functions *in vivo* we developed a new mouse model: a conditional transgenic mouse model, Sema6AΔcyto, that lacks the intracellular domain of Sema6A (**Chapter 3**). In this mouse model, we aim to analyze specifically the intracellular domain of Sema6A *in vivo*. Immunohistochemical analysis revealed developmental defects in axon pathfinding and organization of the anterior commissure, piriform cortex, lateral olfactory tract, thalamocortical axons, corticospinal tract and mossy fiber projections in the hippocampus, and cellular positioning in the cerebral cortex and cerebellum. These findings indicate that the intracellular domain of Sema6A is essential for proper development of these brain regions and axonal tracts and provide insight into the importance of the signaling pathways downstream of this transmembrane semaphorin.

In **Chapter 4**, we continue to study a specific developmental defect found in the cerebral cortex of Sema6AΔcyto mice. We identify a novel role for Sema6A receptor function during cortical neuron positioning and laminar formation in the cortex. A well-characterized effect of semaphorins is their ability to restrict and organize neurites into specific well-defined lamina in the retina and hippocampus [17,23–25,34,37–39]. In **Chapter 4**, we find a novel role for Sema6A in the anatomical segregation and patterning of neurons and projections to establish functional neural circuits. In the absence of the Sema6A receptor, layer 2/3 pyramidal neurons formed ectopic neuronal clusters in cortical layer 1, displayed altered morphology and were intermingled with neighboring neurons and other cell types. Overall, our findings in **Chapter 4** indicate that Sema6A receptor function is essential for proper development of the cerebral cortex.

Sema6A interactions with PlexinAs occur *in trans*, when receptor and ligand are expressed on different cells, but also *in cis* when they are expressed on the same cell (Renaud et al., 2008; Haklai-Topper et al., 2010). The interplay between *trans* and *cis* interactions is crucial for the regulated development of complex neural circuitry [40], but the underlying molecular mechanisms remain uncharacterized. In **Chapter 5**, we discovered a mode of interaction through which the *Drosophila* semaphorin Sema1b and mouse Sema6A mediate binding *in cis* to their cognate plexin receptors. High-resolution structural, biophysical and *in vitro* analyses demonstrate that monomeric semaphorins can mediate a distinctive plexin binding mode. The *cis* interaction involves specific binding domains that are identified and discussed in **Chapter 5**. These findings suggest that the interplay between monomeric versus dimeric states also contributes to the multifunctionality of Sema6A.

Sema6A is known to be involved in multiple developmental defects discovered over the past years and interestingly, additional novel roles are still found to date. In **Chapter 6** we describe a role for Sema6A in the GnRH neuronal system and puberty onset. Puberty is the maturational process of the reproductive endocrine system that results in the achievement of adult height and body proportion, in addition to development of the genital organs and the capacity to reproduce [41]. Puberty onset is driven by the pulsatile release of GnRH hormone by the hypothalamic GnRH-secreting neurons. Defects in the GnRH neuronal system and altered secretion of GnRH result in low levels of gonadotropins with consequently disruption of puberty development [42–47]. The specific Sema6A genetic mutation studied here is predicted to be damaging and disease causing. In **Chapter 6**, we study the impact of the identified Sema6A mutation on protein structure, localization, stability and function and the physiological role of Sema6A in GnRH neuron development.

Thesis aim

This thesis provides an overview of recent developments in the field of axon guidance research focusing on semaphorins, including the role of their interactors; plexins and neuropilins (**Chapter 2**). Furthermore, it focuses on Sema6A, which is known to play important roles during the development of the nervous system. The overall aim of this thesis is to study the multifunctional character of Sema6A by selectively exploring functions of the intracellular domain (**Chapter 3**) and reverse signaling events (**Chapter 4**),interactors and regulators involved in Sema6A signaling pathways (**Chapter 4**), *cis* interaction domains (**Chapter 5**) and to specify novel roles during puberty onset and neuronal disease (**Chapter 6**). These previously unexplored functions help to understand the complexity of semaphorin signaling pathways and provide an extensive and in-depth overview of Sema6A signaling during brain development. The findings described in this thesis contribute to the knowledge of complex and dynamic cellular and molecular events that help to understand brain development and disorders.

REFERENCES

1. Pasterkamp, R. J. & Giger, R. J. Semaphorin function in neural plasticity and disease. *Current Opinion in Neurobiology* (2009). doi:10.1016/j.conb.2009.06.001
2. Tran, T. S., Kolodkin, A. L. & Bharadwaj, R. Semaphorin Regulation of Cellular Morphology. *Annu. Dev.Biol.* (2007).
3. Yoshida, Y. Semaphorin Signaling in Vertebrate Neural Circuit Assembly. *Front. Mol. Neurosci.* (2012). doi:10.3389/fnmol.2012.00071
4. Koropouli, E. & Kolodkin, A. L. Semaphorins and the dynamic regulation of synapse assembly, refinement, and function. *Curr. Opin. Neurobiol.* 27, 1–7 (2014).
5. Finlay, B. L. & Darlington, R. B. Linked regularities in the development and evolution of mammalian brains. *Science (80-.).* (1995). doi:10.1126/science.7777856
6. Molnár, Z. & Clowry, G. Cerebral cortical development in rodents and primates. in *Progress in Brain Research* (2012). doi:10.1016/B978-0-444-53860-4.00003-9
7. Rakic, P. A small step for the cell, a giant leap for mankind: a hypothesis of neocortical expansion during evolution. *Trends Neurosci.* (1995). doi:10.1016/0166-2236(95)93934-P
8. Rakic, P. Mode of cell migration to the superficial layers of fetal monkey neocortex. *J. Comp. Neurol.* (1972). doi:10.1002/cne.901450105
9. Marin-Padilla, M. Dual origin of the mammalian neocortex and evolution of the cortical plate. *Anat. Embryol. (Berl).* (1978). doi:10.1007/BF00315920
10. Kostović, I. & Jovanov-Milošević, N. The development of cerebral connections during the first 20-45 weeks' gestation. *Semin. Fetal Neonatal Med.* (2006). doi:10.1016/j.siny.2006.07.001
11. Ferrer, I., Bernet, E., Soriano, E., Del Rio, T. & Fonseca, M. Naturally occurring cell death in the cerebral cortex of the rat and removal of dead cells by transitory phagocytes. *Neuroscience* (1990). doi:10.1016/0306-4522(90)90281-8
12. Xu, X. et al. The Transmembrane Protein Semaphorin 6A Repels Embryonic Sympathetic Axons. 20, 2638–2648 (2000).
13. Leighton, P. A. et al. Defining brain wiring patterns and mechanisms through gene trapping in mice. Nature 410, 174–179 (2001).
14. Rünker, A. E., Little, G. E., Suto, F., Fujisawa, H. & Mitchell, K. J. Semaphorin-6A controls guidance of corticospinal tract axons at multiple choice points. Neural Dev. 3, 34 (2008).
15. Renaud, J. & Chédotal, A. Molecular and Cellular Neuroscience Time-lapse analysis of tangential migration in Sema6A and PlexinA2 knockouts. Mol. Cell. Neurosci. 63, 49–59 (2014).
16. Lilley, B. N. *et al.* Genetic access to neurons in the accessory optic system reveals a role for Sema6A in midbrain circuitry mediating motion perception. *J. Comp. Neurol.* (2019). doi:10.1002/cne.24507

17. Matsuoka, R. L. et al. Transmembrane semaphorin signalling controls laminar stratification in the mammalian retina. Nature 470, 259–263 (2011).
18. Mitsogiannis, M. D., Little, G. E. & Mitchell, K. J. Semaphorin-Plexin signaling influences early ventral telencephalic development and thalamocortical axon guidance. Neural Dev. 12, 6 (2017).
19. Sun, L. O. et al. Functional Assembly of Accessory Optic System Circuitry Critical for Compensatory Eye Movements. Neuron 86, 971–984 (2015).
20. Rünker, A. E. et al. Mutation of Semaphorin-6A Disrupts Limbic and Cortical Connectivity and Models Neurodevelopmental Psychopathology. PLoS One 6, e26488 (2011).
21. Little, G. E. et al. Specificity and Plasticity of Thalamocortical Connections in Sema6A Mutant Mice. PLoS Biol. 7, e1000098 (2009).
22. Kerjan, G. et al. The transmembrane semaphorin Sema6A controls cerebellar granule cell migration. Nat. Neurosci. 8, 1516–1524 (2005).
23. Sun, L. O. et al. On and Off Retinal Circuit Assembly by Divergent Molecular Mechanisms. Science (80-.). 342, 1241974–1241974 (2013).
24. Belle, M., Parray, A., Belle, M., Chédotal, A. & Nguyen-Ba-Charvet, K. T. PlexinA2 and Sema6A are required for retinal progenitor cell migration. Dev. Growth Differ. 58, 492–502 (2016).
25. Suto, F. *et al.* Interactions between Plexin-A2, Plexin-A4, and Semaphorin 6A Control Lamina-Restricted Projection of Hippocampal Mossy Fibers. *Neuron* (2007). doi:10.1016/j.neuron.2007.01.028
26. Okada, T., Keino-Masu, K., Suto, F., Mitchell, K. J. & Masu, M. Remarkable complexity and variability of corticospinal tract defects in adult Semaphorin 6A knockout mice. *Brain Res.* (2019). doi:10.1016/j.brainres.2018.12.041
27. Renaud, J. *et al.* Plexin-A2 and its ligand, Sema6A, control nucleus-centrosome coupling in migrating granule cells. *Nat. Neurosci.* (2008). doi:10.1038/nn2064
28. Håkansson, K. *et al.* Semaphorin 6A knockout mice display abnormalities across ethologically-based topographies of exploration and in motor learning. *Neurosci. Lett.* (2017). doi:10.1016/j.neulet.2017.01.043
29. Toyofuku, T. *et al.* Guidance of myocardial patterning in cardiac development by Sema6D reverse signalling. *Nat. Cell Biol.* (2004). doi:10.1038/ncb1193
30. Mauti, O., Domanitskaya, E., Andermatt, I., Sadhu, R. & Stoeckli, E. T. Semaphorin6A acts as a gate keeper between the central and the peripheral nervous system. Neural Dev. 2, 28 (2007).
31. Perez-Branguli, F. et al. Reverse Signaling by Semaphorin-6A Regulates Cellular Aggregation and Neuronal Morphology. PLoS One 11, e0158686 (2016).
32. Bernard, F. et al. Role of transmembrane semaphorin Sema6A in oligodendrocyte differentiation and myelination. Glia 60, 1590–1604 (2012).

33. Battistini, C. & Tamagnone, L. Transmembrane semaphorins, forward and reverse signaling: Have a look both ways. *Cellular and Molecular Life Sciences* (2016). doi:10.1007/s00018-016-2137-x
34. Sun, L. O. *et al.* Functional Assembly of Accessory Optic System Circuitry Critical for Compensatory Eye Movements. *Neuron* (2015). doi:10.1016/j.neuron.2015.03.064
35. Andermatt, I. et al. Semaphorin 6B acts as a receptor in post-crossing commissural axon guidance. Development 141, 3709–3720 (2014).
36. Burkhardt, C. et al. Semaphorin 4B interacts with the post-synaptic density protein PSD-95/SAP90 and is recruited to synapses through a C-terminal PDZ-binding motif. FEBS Lett. 579, 3821–3828 (2005).
37. Huberman, A. D., Clandinin, T. R. & Baier, H. Molecular and cellular mechanisms of lamina-specific axon targeting. *Cold Spring Harbor perspectives in biology* (2010). doi:10.1101/cshperspect.a001743
38. Tawarayama, H., Yoshida, Y., Suto, F., Mitchell, K. J. & Fujisawa, H. Roles of Semaphorin-6B and Plexin-A2 in Lamina-Restricted Projection of Hippocampal Mossy Fibers. *J. Neurosci.* (2010). doi:10.1523/JNEUROSCI.0073-10.2010
39. Matsuoka, R. L., Sun, L. O., Katayama, K. ichi, Yoshida, Y. & Kolodkin, A. L. Sema6B, Sema6C, and Sema6D Expression and Function during Mammalian Retinal Development. *PLoS One* (2013). doi:10.1371/journal.pone.0063207
40. Seiradake, E., Jones, E. Y. & Klein, R. Structural Perspectives on Axon Guidance. Annu. Rev. Cell Dev. Biol. 32, 577–608 (2016).
41. Herbison, A. E. Control of puberty onset and fertility by gonadotropin-releasing hormone neurons. *Nature Reviews Endocrinology* (2016). doi:10.1038/nrendo.2016.70
42. Boehm, U. *et al.* Expert consensus document: European Consensus Statement on congenital hypogonadotropic hypogonadism-pathogenesis, diagnosis and treatment. *Nature Reviews Endocrinology* (2015). doi:10.1038/nrendo.2015.112
43. Stamou, M. I. & Georgopoulos, N. A. Kallmann syndrome: phenotype and genotype of hypogonadotropic hypogonadism. Metabolism 86, 124–134 (2018).
44. Cariboni, A. *et al.* Dysfunctional SEMA3E signaling underlies gonadotropin-releasing hormone neuron deficiency in Kallmann syndrome. *J. Clin. Invest.* (2015). doi:10.1172/JCI78448
45. Känsäkoski, J. *et al.* Mutation screening of SEMA3A and SEMA7A in patients with congenital hypogonadotropic hypogonadism. *Pediatr. Res.* (2014). doi:10.1038/pr.2014.23
46. Marcos, S. *et al.* Defective signaling through plexin-A1 compromises the development of the peripheral olfactory system and neuroendocrine reproductive axis in mice. *Hum. Mol. Genet.* (2017). doi:10.1093/hmg/ddx080
47. Hanchate, N. K. *et al.* SEMA3A, a Gene Involved in Axonal Pathfinding, Is Mutated in Patients with Kallmann Syndrome. *PLoS Genet.* (2012). doi:10.1371/journal.pgen.1002896

CHAPTER 2

Axon Guidance: Semaphorin/Neuropilin/ Plexin Signaling

Marieke G. Verhagen[1] and R. Jeroen Pasterkamp[1]

[1] Department of Translational Neuroscience, UMC Utrecht Brain Center, University Medical Center Utrecht, Utrecht University, The Netherlands

Cellular Migration and Formation of Neuronal Connections - 2nd edition, Chapter 5
Axon Guidance: Semaphorin/Neuropilin/Plexin Signaling

ABSTRACT

The semaphorin protein family controls a wide variety of developmental processes in the nervous system such as axon guidance, cell migration, dendrite morphology and synaptogenesis. The best characterized function of semaphorins is their ability to attract or repel neurites, directing these structures towards or away from specific regions. Although only a limited set of semaphorins has been identified, accumulating evidence indicates that distinct molecular mechanisms act to diversify the effects of these guidance cues, allowing them to control a disproportionally large number of different cellular events. In this chapter, we discuss general features and novel aspects of semaphorin function and signaling, including the role of their receptors; plexins and neuropilins. The focus is on the contribution of these molecules to the regulation of cell migration and the formation of neuronal connections. In addition, we highlight a few recent studies that examine how semaphorins, plexins and/or neuropilins contribute to neurological diseases.

Keywords

Semaphorin; Axon guidance; Development; Signaling; Plexin; Neuropilin; Cell migration; Neuronal connectivity

INTRODUCTION

To establish functional neuronal connections during development, axons follow specific paths that are marked by instructive proteins known as axon guidance proteins. These proteins act to attract or repel axons and function over short or long distances. Although initially identified for their role in axon guidance, axon guidance proteins are now known to have much broader functions, both within and outside the nervous system. In the nervous system, axon guidance proteins are, for example, involved in the regulation of cell migration, dendrite morphology and synaptogenesis[1–4]. Our nervous system consists of millions of neurons and glial cells, axonal connections and synaptic contacts, but only a limited set of axon guidance cues (~ 100) has been identified that can regulate the formation of this complex organ[5,6]. Accumulating evidence indicates that distinct molecular mechanisms act to diversify the effects of axon guidance cues, allowing them to control a disproportionally large number of different cellular events. Several different families of axon guidance cues have been identified[5,6]. but the focus of this chapter is on the largest family of canonical axon guidance proteins, the semaphorins.

The first semaphorins were reported in the early 1990s, i.e. collapsin-1 (now called Sema3A[7]) and Fasciclin IV (now called Sema-1a[8]). Since then 25 additional semaphorins have been identified and categorized into 8 subclasses on basis of sequence similarity and structural features [9,10]. Classes 1 and 2 contain invertebrate semaphorins; classes 3-7 contain vertebrate semaphorins; and class V contains viral semaphorins. Sema5c is an exception, as it is also found in invertebrates (Fig. 1). Semaphorins play important roles in various biological processes ranging from the regulation of immune responses to angiogenesis and tumorigenesis[11–14]. In addition to their role in axon guidance, semaphorins control the migration of various neuronal cell types such as neural crest cells in the peripheral nervous system[15], and GABA-ergic interneurons[16], Cajal-Retzius cells[17], cortical neurons[18] and cerebellar granule neurons[19–21] in the central nervous system. Other neural processes regulated by semaphorins include neuronal proliferation and polarity, neurite growth and pruning, synapse formation and function, and dendrite morphology[1–3].

Semaphorins exert their effects by binding to multi-subunit cell surface receptors. In neurons, plexins constitute the major semaphorin receptors. The first plexin receptor identified, Virus-Encoded Semaphorin Protein

Receptor (VESPR) (now known as PlexinC1), binds viral semaphorins and mediates cell adhesion[22–24]. Plexins are large transmembrane signaling molecules that are subdivided into 4 classes (PlexinA-D). In addition to their interaction with plexins, semaphorins can bind other (co-)receptors such as CD72[25], Tim2[26], integrins[27], proteoglycans[28] and neuropilins (Fig. 1). Intriguingly, semaphorins not only function as ligands, but some transmembrane semaphorins can also act as receptors, a process called reverse signaling, depending on the molecular and cellular context[29].

In this chapter, we further discuss the semaphorin, plexin and neuropilin protein families and provide an overview of their signature functions in the nervous system. First, we discuss general features and novel aspects of semaphorin, plexin and neuropilin molecules and of the signaling pathways activated downstream of these molecules, stressing general principles and recent insights. The focus here is on cell migration and the formation of neuronal connections. Second, we discuss examples of recent work showcasing how dysregulation of axon guidance proteins might cause pathological changes and neurological diseases, and we explore the potential these insights have for developing therapeutic strategies and improving functional recovery.

Structural features

Semaphorins are defined by a conserved characteristic feature called the semaphorin (sema) domain[9]. This extracellular N-terminal ~400 amino acid region facilitates homodimerization and interactions with semaphorin receptors. In addition, semaphorins, except class V (viral) semaphorins, contain a cysteine-rich plexin-semaphorin-integrin (PSI) domain located at the C-terminus[30,31]. Other class-specific domains are immunoglobulin (Ig)-like domains found in most semaphorins, a C-terminal basic domain specific for class 3 semaphorins[7] and thrombospondin domains that are specific for class 5 semaphorins[32]. Semaphorin classes 1, 4, 5 and 6 are composed of transmembrane proteins. Members of classes 2, 3 and V are secreted, and the only semaphorin in class 7 (Sema7A) is a glycosylphosphatidylinositol (GPI)-linked semaphorin[6,10,33,34].

Structural analysis of the sema domain revealed a propeller-like appearance composed of secondary structure ß-sheet twists[30,31]. The protein topology of the sema domain broadly conforms to the typical architecture of a seven-blade ß-propeller fold, which is a commonly found structural scaffold in various proteins[35]. Structural analysis revealed distinct insertions in

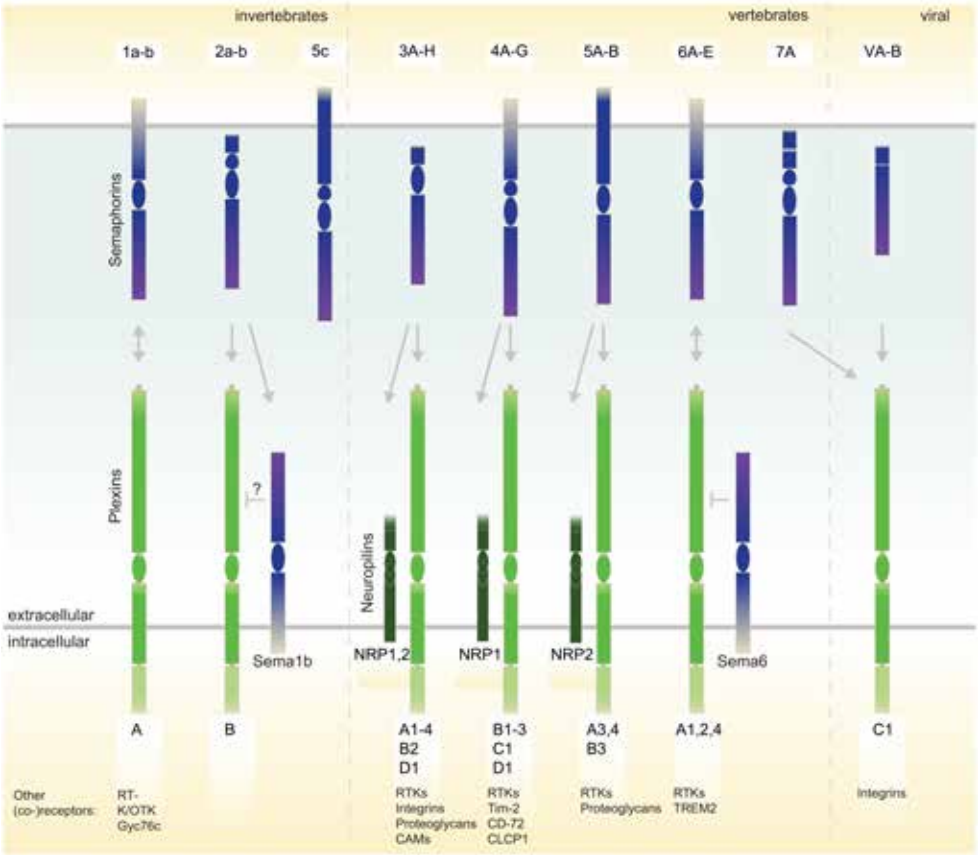

Figure 1. Semaphorins and semaphorin receptor complexes. Thirty semaphorins have been identified and can be categorized into eight classes based on structural similarities. In neural cells, semaphorins signal mainly through plexins. Eleven plexins have been identified (in both invertebrates and vertebrates) and these are subdivided into 4 classes (A-D). Sema3s signal through PlexinAs but require neuropilins (only detected in vertebrates) for activating plexins, with the exception of Sema3E. Sema3E binds PlexinD1 directly in the absence of neuropilins. Sema2a, Sema2b and Sema3s are secreted proteins. Transmembrane semaphorins are: Sema1a, Sema1b, and Sema5c in invertebrates and Sema4s, Sema5s, Sema6s in vertebrates. Sema7A is the only glycosylphosphatidylinositol (GPI)-linked semaphorin. SemaVA and SemaVB are found in viral genomes. Sema6s, and most likely other membrane-anchored semaphorins, can influence signaling through inhibitory *cis* interactions with PlexinAs. In addition, several transmembrane semaphorins function as receptors (reverse signaling). Neuronal semaphorin receptor complexes often contain co-receptors that can affect signaling outcome, for example: RTKs; receptor tyrosine kinases, OTK; off track, Gyc76c; guanylyl cyclase, proteoglycans, integrins, CAMs; immunoglobulin super family cell adhesion molecules, Tim-2; T-cell Ig and mucin domain containing protein 2, CD-72; B cell differentiation antigen CD72 , CLCP1; CUB, LCCL-homology, Coagulation factor V/VIII homology domains protein 1, TREM2; Triggering Receptor Expressed on Myeloid Cells 2.

different sema domains that determine binding specificity[36]. The sema and PSI domains of different semaphorins can differ slightly, and the various class-specific domains that follow the sema and PSI domains are likely to influence the stability of protein-protein complexes. These differences among semaphorins influence specific protein-protein interactions such as dimerization, semaphorin-plexin binding, and semaphorin-neuropilin interactions[37].

Like semaphorins, plexins contain a sema domain followed by PSI domains that together facilitate protein-protein interactions. These shared domains and the generic architecture of semaphorins and plexins suggest common modes of interaction and signaling. Additional domains found in plexins are Immunoglobulin-plexin-transcription (IPT) domains and a highly conserved intracellular region with a GTPase activating protein (GAP) homology domain (containing a Rho GTPase binding domain (RBD) insertion). The GAP homology domain mediates the repulsive effects of semaphorins through regulation of cytoskeletal components. Class A plexins (PlexinAs) are the best-characterized semaphorin receptors and cluster, along with PlexinBs, in the two largest subfamilies of plexins. PlexinC1 and D1 are phylogenetically the most distant classes of plexins[38].

Over the past decades crystal structures of distinct semaphorins and plexins, individually and in complexes, have been reported and highlight key residues and structural features required for protein-protein interactions and signaling[30,31,36,39–51] (see Box I). At the structural level, it has been observed that semaphorins and plexins interact in a 2:2 complex. The sema domain facilitates homodimerization of two semaphorin proteins[52]. Each protein binds a monomeric plexin protein through the sema domain[39,40,49,53]. PlexinA1, PlexinA2 and PlexinA4 exist in a ring-like conformation or in a less-frequent, twisted-open chair-like, conformation that may modulate PlexinA signaling[46]. In the absence of ligands, plexins are positioned on the membrane in a head to stalk conformation in *cis*, preventing cytoplasmic dimerization[46]. This mechanism of auto-inhibition provides spatiotemporal control over signaling and prevents premature activation of receptors. Upon ligand binding the PlexinA cytoplasmic domains dimerize, presumably because of intramolecular changes in protein conformation, and intracellular signaling is initiated (Fig. 2).

Box I. Structural studies of Semaphorin, Plexin and Neuropilin proteins and complexes

Molecule(s)								
Semaphorins	**Å**	**ref**	**Plexins**	**Å**	**ref**	**Neuropilins**	**Å**	**ref**
Sema3A$_{S}$	2.8	31	**PlexinA1$_{cyto}$-Rac1**	3.6	50	**NRP1$_{3}$**	1.9	44
Sema3A$_{S-P-I}$	3.3	49	**PlexinA2$_{1-4}$**	2.3	53	**Nrp1$_{1-4}$**	2.7	49
Sema3A$_{S-P}$-PlexinA2$_{1-4}$-Nrp1$_{1-4}$	7.0	49	**PlexinA2$_{S-P}$**	2.1	40	**NRP1$_{3-4}$**	1.8	43
SEMA4D$_{ecto}$	2.0	30	**PlexinA3$_{cyto}$**	2.0	42	**NRP1$_{2-4}$-FAB**	2.0	43
SEMA4D$_{ecto}$-PLXNB1$_{1-2}$	3.0	53	**PlexinA$_{ecto}$** **PlexinA1$_{1-10}$** **PlexinA1$_{7-10}$** **PlexinA2$_{4-5}$** **PlexinA4$_{1-10}$**	 4.0 2.2 1.36 7.5	46	**NRP1$_{3}$-FAB**	2.2	43
Sema6A$_{ecto}$	2.3	53	**PLXNB1$_{cyto}$-Rac1**	4.4	51	**NRP1$_{3-4}$**	2.4	159
Sema6A$_{S-P}$	2.5	40	**PLXNB1$_{cyto}$**	2.4	41	**NRP1$_{3-4}$-Tuftsin**	2.15	159
Sema6A$_{ecto}$-PlexinA2$_{1-4}$	2.2	53	**PlexinB2$_{cyto}$-PDZ-RhoGEF**	3.2-5.0	47	**NRP1$_{5}$**	2.24	160
Sema6A$_{S-P}$-PlexinA2$_{S-P}$	3.6	40	**PlexinC1$_{cyto}$**	3.3	48	**NRP2$_{3-4}$**	1.95	43
SEMA7A$_{S-P-I}$-PLXNC1$_{ecto}$	2.4	39	**PlexinC1$_{cyto}$-Rap1B**	3.3	48	**NRP2$_{3-4}$**	2.3	43
			PlexinD1$_{cyto}$	2.7	45	**NRP2$_{1-4}$-FAB***	2.75/3.1	43
			PlexinD1$_{cyto}$-GIPC1	3.2	45			

Semaphorin$_{S-P-I}$ = sema, PSI, Ig domains. Semaphorin$_{ecto}$ = ectodomain. Plexin$_{1-10/ecto}$ = 1-10 include sema, PSI, IPT domains/ectodomain. Neuropilin$_{1-5}$ = a1-a2 (CUB)$_{1-2}$, b1-b2 (coagulation factor V/VIII homology)$_{3-4}$, membrane proximal MAM (c)$_{5}$ domains. Plexin$_{cyto}$ = juxtamembrane (JM) segment, Rho GTPases binding RBD and GTPase activating protein (GAP) domains/cytoplasmic domain. GIPC1 = GAIP interacting protein, C-terminus 1. Tuftsin = VEGF HBD analog. Rac1 = Rho family small GTPases. Rap1B = Ras family small GTPases. PDZ-RhoGEF = PDZ domain guanine nucleotide exchange factor (GEF). *FAB = Fab fragment of anti-NRP antibody blocking either vascular endothelial growth factor (VEGF) 'anti-Nrp1^{B}' or Sema3 binding 'anti-panNrp1^{A}'. Å; resolution in Ångström, ref; reference

Multiple classes of semaphorins can directly interact with plexins, however, class 3 semaphorins, with the exception of Sema3E, require either neuropilin 1 (Nrp-1) or neuropilin 2 (Nrp-2) for assembling a holoreceptor Nrp/plexin signaling complex, [6,38,49,54,55] (Fig. 1). Neuropilins play an important role during neuronal development. Although a detailed discussion of Nrp

function is beyond the scope of this chapter, Nrps are multi-functional molecules well known for their role during cardiovascular development and other physiological and disease processes[56]. Neuropilins contain a CUB (a1/a2) domain, a two factor V/VIII homology domain (b1/b2), and a membrane proximal c (MAM) domain. These domains are required for sema domain binding of requisite interacting semaphorins and influence protein stability. Neuropilins contain a single transmembrane domain and a small cytoplasmic region[57]. In the nervous system, neuropilins bind class 3 semaphorins and interact with PlexinA1-4 to form a holoreceptor complex that can mediate growth cone collapse and axon guidance. The neuropilin co-receptor modulates and stabilizes the 2:2 semaphorin-plexin complex, creating a 2:2:2 complex shown for Sema3A, PlexinA1 and Nrp1[49]. The semaphorin-plexin and semaphorin-plexin-neuropilin complexes often contain additional proteins, such as receptor protein kinases and cell adhesion molecules, that modulate downstream intracellular signaling pathways critical for cellular function, often in a cell-type specific and tissue-specific manner[6].

Semaphorins and plexins can be expressed on separate cells and interact in *trans*, or on the same cell interacting in *cis* (Fig. 2). For example, axonal Sema6B interacts with PlexinA2 expressed at the chick floorplate in *trans* to induce commissural axon turning post-crossing. In the same system, *cis* interactions between Sema6B and PlexinA2 on pre-crossing commissural axons are thought to regulate Sema6B[58]. Interestingly, examination of Sema6A-PlexinA2 *trans* versus *cis* interactions *in vitro* reveals that *cis* interactions have a specific modulatory role and require different protein interfaces compared to those needed for *trans* binding[59]. Another example of an inhibitory semaphorin-plexin *cis* interaction is the binding of Sema6A and PlexinA4 on dorsal root ganglion neurons that prevents activation of PlexinA4 by Sema6A *in trans*[60]. Further, in a subset of starburst amacrine cells (SAC) in the mouse retina, Sema6A binds PlexinA2 in *cis* to control Sema6A repulsive responses *in vitro* and SAC stratification and morphology *in vivo*[61]. Interestingly, in *C. elegans* binding of the transmembrane semaphorin SMP-1 to Plex1 *in cis* triggers receptor signaling leading to the inhibition of synapse formation[62]. Thus, *cis* interactions constitute an excellent regulatory mechanism for providing tight spatiotemporal control of semaphorin-plexin signaling (for more details on semaphorin *trans* versus *cis* regulatory mechanisms, please see reference 60).

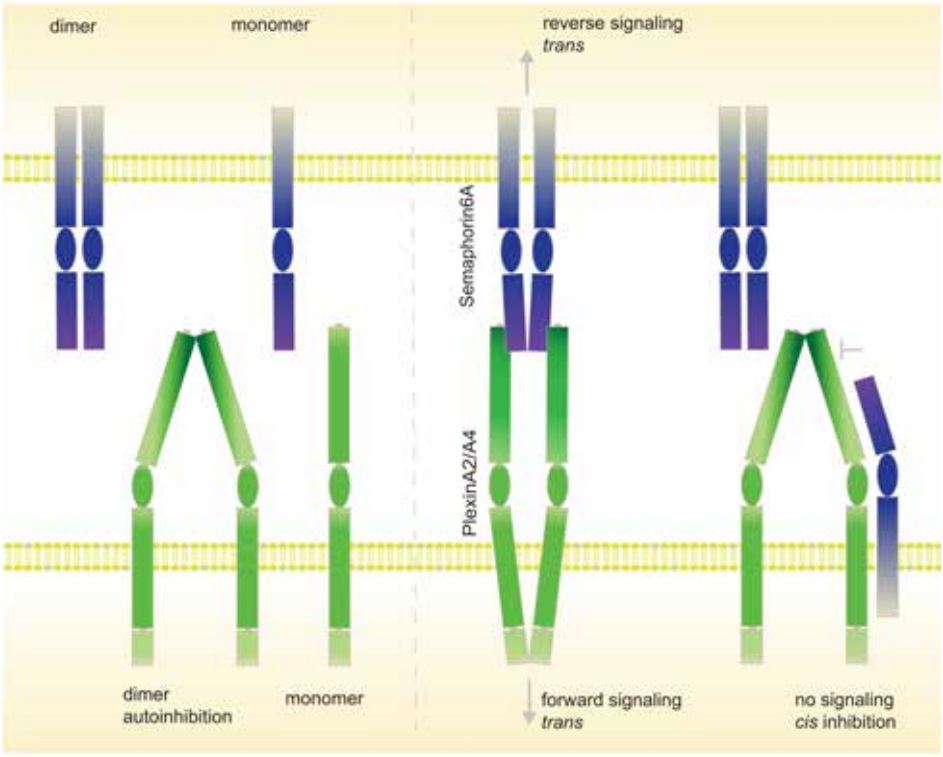

Figure 2. Structural basis of different modes of semaphorin-plexin signaling. Semaphorins and plexins exist as monomers and homodimers. During binding, semaphorin homodimers bind two plexin monomers to form a symmetrical 2:2 complex. Plexins engage in intramolecular head-to-stalk interactions in the absence of ligand. Semaphorin ligand binding *in trans* disrupts this state of plexin auto-inhibition. Consequently, the cytoplasmic domains of plexins dimerize to trigger downstream signaling. Plexins can also trigger signaling through transmembrane semaphorins, a process termed reverse signaling. Finally, transmembrane semaphorins can bind plexins *in cis* and inhibit plexin signaling.

Mechanisms of intracellular signaling

Interactions between semaphorins, plexins and neuropilins activate intracellular signaling pathways that trigger cell type- and tissue-specific responses. Intracellular events that initiate these functional outcomes of semaphorin-plexin-neuropilin complexes are only partially understood. The following section discusses mechanisms and modes of intracellular signaling involving semaphorins and their receptors during neural circuit development. Emphasis is on the role of small GTPases, which constitute the best-studied components of intracellular semaphorin signaling pathways.

Plexins trigger cytoplasmic signaling pathways through their intracellular GAP homology domain[63]. Different signaling routes have been described downstream of plexins that control different aspects of cellular morphology and function. Small GTPases play a crucial function downstream of semaphorins and plexins. GTPases occur in active or inactive states corresponding to their interaction with GTP or GDP, respectively[64,65,66]. Small GTPases are regulated by GTP/GDP exchange factors. GEFs (guanine nucleotide exchange factors) activate GTPases by increasing binding to GTP. GAPs (GTPase-activating proteins) terminate signal transduction by activating intrinsic GTPase activity to hydrolyze GTP to GDP[64,67]. In the developing nervous system, small GTPases regulate cell dynamics affecting actin dynamics, cell shape, movement, motility and position[68–70]. Small GTPases are one of the few intracellular signaling proteins that have been implicated in plexin signaling *in vivo*. For example, the distribution of dentate gyrus granule cells is controlled by Sema5A signaling through interactions of the PlexinA2 GAP homology domain and Rap1, a member of the Rap subfamily of Ras small GTPases. Loss of PlexinA2 GAP activity or the ablation of Rap1 in neurons results in malformation of the dentate gyrus[71]. In addition, the Rac-GAP β2-chimaerin has been shown to mediate Sema3F-dependent mossy fiber pruning in the hippocampus *in vivo*. During this process, NRP-2 selectively binds β2-chimaerin, and Sema3F binding activates this GAP to restrain Rac1-dependent effects on the cytoskeleton. Intriguingly, this pathway is required for Sema3F-mediated axon pruning but is dispensable for the effects of Sema3F on axon repulsion and spine remodeling[72].

Small GTPases are regulated by several other proteins such as receptor tyrosine kinases and serine/threonine kinases. For example, PlexinB1 associates with ErbB2 which is a transmembrane receptor tyrosine kinase. Sema4D ligand binding to PlexinB1 activates ErbB2 tyrosine kinase activity resulting in auto-phosphorylation and phosphorylation of PlexinB1. This triggers RhoGEF proteins to activate RhoA and RhoC GTPases enabling signal transduction[73]. Another example of GTPase regulation is seen in glioma cells. Sema5A binding to PlexinB3 promotes Rac1 recruitment to RhoGDI (RhoGDP dissociation inhibitor), which is a negative regulator of Rho GTPases that directly interacts with PlexinB3. RhoGDI inactivates Rac1 and reduces its membrane localization resulting in actin remodelling[74].

In addition to providing a link to the cytoskeleton, small GTPases also connect plexins to integrin signaling. For example, plexins negatively regulate integrin-mediated cell adhesion through FERM domain-containing

guanine nucleotide exchange factor (FARP2)[75]. Sema3A-Neuropilin interactions trigger FARP2 to dissociate from PlexinA1 and activation of FARP2 Rac GEF activity. Dissociation of FARP2 is essential for Sema3A-mediated axon repulsion as it causes inhibition of integrin function[76]. Other downstream processes required for Sema3A-mediated repulsion include recruitment of Rnd1 to PlexinA1 that causes downregulation R-Ras, a small GTPase that normally promotes cell adhesion[77]. Sema5A-PlexinA2 signaling also affects integrin receptors through small GTPases[71,78]. PlexinA2 inhibits Rap1 GTPase thereby negatively regulating integrin-mediated cell adhesion. Loss of plexin GAP activity or ablation of Rap1 results in aberrant granule cell distribution indicating that PlexinA2 forward signaling through Rap1 regulates granule cell migration and distribution during DG development[71]. For more information on other proteins associated with integrin signaling in cell-cell and cell-substrate adhesion events in the nervous system see references 76-79.

Different small GTPases interact directly with the plexin GAP homology domain to initiate downstream signaling events[79,80]. Centrally located in the GAP homology domain is the RBD (Rho GTPase binding domain) which is important for plexin dimerization and receptor activation[81]. Upon ligand binding, a weak plexin-plexin interaction of cytoplasmic RBD regions is triggered forming an intracellular dimer. These regions contain binding sites for distinct small GTPases. The Rho GTPases Rnd1 and Rac1 disrupt the plexin dimer leading to conformational changes and receptor activation[41]. Plexin family members have different binding affinities for Rho GTPases and consequently differ in the mechanism of GAP homology domain regulation. PlexinC1 and PlexinD1 seem to have different requirements of GTPases to regulate GAP activity[82] compared with members of the more extensively studied PlexinA and PlexinB classes[83].

Intracellular signaling through plexins can also occur through direct interaction with cytosolic proteins that function as binding partners of the intracellular part of the plexin receptor. In addition to small GTPases several other proteins can bind the plexin cytoplasmic domain or act further downstream. An intriguing example of a plexin-interacting protein is Molecule Interacting with CasL (MICAL)[84]. MICALs are large cytosolic proteins that negatively regulate and enzymatically modify actin through posttranslational residue oxidization resulting in remodeling and disassembly. SelR/MsrB antagonizes the effect of MICALs by restoring actin polymerization[85–87]. Another prominent group of plexin effectors are protein

kinases. For example, the tyrosine kinases Pyk2, Syk, FAK, Fer/Fes, Fyn and Scr play a role downstream of semaphorins and plexins[63]. A full description of these interactions is beyond the scope of this review and for more details see[6,33,88].

Semaphorins can mediate both forward (ligand function) and reverse (receptor function) signaling (Fig. 2). Class 4-6 semaphorins (Fig. 1) can trigger 'reverse signaling' pathways via their intracellular domains. Our knowledge of reverse signaling is mostly based on *in vitro* data and *in vivo* evidence is strongest for Sema1a in *Drosophila*[89-92]. However, several studies suggest that reverse signaling could also play an important role during vertebrate neuronal circuit development[58,93-97]. For example, at the chick spinal cord midline, Sema6B is expressed in commissural axons and is suggested to function cell-autonomously as a receptor. PlexinA2 expressed in floorplate cells acts as an instructive turning signal for commissural axons and it detected by axonal Sema6B[58]. Although it remains unclear how Sema6B signaling is mediated intracellularly in this particular example, some downstream effectors of semaphorin reverse signaling have been characterized. For example, during cardiac development, Sema6D reverse signaling through Abl mediates actin dynamics and regulates cell migration[98]. Sema6A can also act as a receptor through Abl in cultured neurons[59,99]. Chemically inducing multimerization of Sema6A receptors causes activation of Abl and other signaling proteins such as GSK3alpha/beta, p130CAS, Ezrin, Radixin, Moesin and MARCKS[59]. *In silico* predictions and biochemical studies reveal Ena/VASP like protein (EVL), involved in actin dynamics[100], as a potential interactor for Sema6A through its cytoplasmic zyxin domain[101] and Src as a potential interactor for Sema6B through its Src-homology 3 (SH3) domain[102]. Class 4 semaphorins have been suggested to function as receptors through their cytoplasmic PDZ-domain[103]. For more details on semaphorin reverse signaling please see[104].

Function in neural circuit development

In the nervous system, semaphorins control a wide variety of developmental processes such as axon guidance, cell migration, dendrite morphology and synaptogenesis[1-4]. The best characterized function of semaphorins is their ability to attract or repel axons, directing these structures towards or away from specific regions. A small selection of cellular functions of semaphorins and receptors in aspects of neural circuit development is discussed here.

The establishment of neural connections between distant brain regions is essential for normal nervous system function. A well-characterized effect of semaphorins is their ability to restrict neurites to specific lamina[105]. Functionally similar neuronal subtypes and projections are often anatomically segregated and patterned in order to establish functional neural circuits. The retina and hippocampus are two examples of systems that are organized into well-defined lamina. Many different semaphorins and receptors have been described to be involved in the development of retinal and hippocampal mossy fiber projections[61,97,106–110]. For example, Sema3E-mediated chemorepulsion through PlexinD1 was found to be important for the lamina-specific targeting of entorhinal cortex (EC) and mossy fiber axons in the hippocampus. The EC is the main source of excitatory input to the hippocampus and the establishment of connections between these brain regions is important for proper brain function[111]. In mice lacking Sema3E-PlexinD1 signaling, the EC-hippocampal pathway is disrupted and mossy fibers are misrouted. Sema3E-PlexinD1 signaling has also been implicated in Cajal-Retzius cell migration in the cortex[17], development of other neural connections in hippocampus[112] and synaptogenesis in the striatum[113].

In order to establish neuronal connections, axons grow over long distances and rely on intermediate targets and guidance cues along their route. For example, Sema6A was found to be involved in subpallial pathfinding of thalamocortical axons (TCAs)[114]. Thalamic axons are topographically sorted while extending through the subpallium en route to appropriate cortical areas. *Sema6A* knockout mice show subcortical misrouting of TCAs early during development. TCAs extend aberrantly in the ventral subpallium and initially fail to innervate the visual cortex. Interestingly, axons follow an alternative route and thalamocortical connectivity is re-established postnatally. PlexinA2 and PlexinA4 are not expressed by the misrouted axons but along the path of these axons, and therefore Sema6A is suggested to serve as a receptor on TCAs[115].

At later stages of development, after neuronal connections have been established, further refinement and modification of neuronal networks occurs. In order for immature neural circuits to transform into functionally mature networks the elimination of redundant synapses is crucial[116]. Sema3E and Sema7A function as retrograde signaling cues for climbing fiber (CF) to Purkinje cell (PC) synapses in the developing mouse cerebellum. Only strengthened CFs extend to dendrites of PCs. Weaker CFs are left on the PC soma and eliminated. Normally, PC-derived Sema3A

interacts with PlexinA4 and strengthens and maintains CFs. PC-derived Sema7A interacts with PlexinC1 and ß1-integrin. The downstream effectors of Sema7A cofilin and focal adhesion kinase (FAK) promote elimination of presynaptic CFs during postnatal cerebellar development[6,117]. Knockdown of Sema3A in postsynaptic cells accelerates elimination, while knockdown of Sema7A impairs synapse elimination during early postnatal development *in vivo*. Thus, the balance between different semaphorin proteins seems to be important for triggering synapse strengthening or elimination in the cerebellum. Also, the subcellular localization and specific distribution of these semaphorins in the cerebellum is important[118].

Semaphorins, Plexins and Neuropilins in neurological disorders

Defects in the expression or function of axon guidance cues have been linked to various neurological diseases. Many canonical axon guidance proteins have been implicated in neurological disease and for an overview of this work we direct the reader to other reviews[1,119–126]. Here, we highlight a few recent studies that examine how semaphorins, plexins and/or neuropilins contribute to neurological diseases that are characterized by pathological changes in neuronal connectivity.

Semaphorins, plexins and neuropilins have been linked to neurological disorders such as Autism Spectrum Disorder (ASD), Kallmann's syndrome, Spinal Muscular Atrophy (SMA), Epilepsy, congenital disorders, Schizophrenia and late onset brain neurodegenerative diseases such as Amyotrophic Lateral Sclerosis (ALS), Parkinson's disease and Alzheimer's disease. Our understanding of how semaphorin signaling is linked to these diseases derives from human studies but also from experiments using *in vitro* and animal models. A selection of neurological diseases in which semaphorins and their receptors may play a role is discussed here.

Autism spectrum disorder

Abnormal wiring of the brain is a hallmark of Autism Spectrum Disorder (ASD). ASD is believed to be caused by neural connectivity disturbances resulting in hypo- or hyperconnectivity between and within brain regions[123,127,128]. Axon guidance proteins may mediate these disturbances and human genetic studies implicate defective axon guidance protein function. For example, a *de novo* microdeletion of *SEMA5A* was found in a patient with ASD and intellectual disability[129]. Additional evidence for the involvement of *SEMA5A* gene deletions was found in a subset of patients with Cri du Chat syndrome showing autistic traits such as repetitive movements,

obsessive attachment to objects and social isolation[129]. In addition to Sema5A, multiple other axon guidance genes have been associated with ASD[119]. Genetic alterations in the integrin downstream signaling interactor SH3 and multiple ankyrin repeat domains 3 (SHANK3) were linked to ASD and other neuropsychiatric disorders such as schizophrenia, intellectual disability and manic-like-behavior[130–133]. In knockout mice, silencing of SHANK3 triggered increased Rap1 activity that activates integrin-mediated signaling leading to altered cell spreading and invasion, while restoration of SHANK3 improved autistic-like symptoms in mice[134]. Interestingly, similar to SHANK3, PlexinA2 GAP activity regulates Rap1 GTPases and *PlexinA2* knockout mice show schizophrenia-like behavior. It is therefore tempting to speculate that SHANK3, PlexinA3 and Rap1 are part of a common disease pathway[135].

Kallmann's syndrome

Kallmann's syndrome (KS) is a pathological condition characterized by aberrant GnRH neuron migration, reduced fertility and olfactory axon guidance defects. Mutations in *SEMA3A*, *SEMA3E*, *SEMA7A*, *PLXNA1*, *NRP1* and *NRP2* have been associated with this pathological condition[136–139]. Knockout mouse models showed that Sema3A is needed for guidance of GnRH neurons and that removal of Sema3A induces KS-like phenotypes[136,140]. *Sema3A* knockout mice, or Sema3A receptor knockout mice, display reduced fertility and failure of olfactory axons to grow to the hypothalamus. As a result, GnRH neurons stall or migrate aberrantly. Another essential cue for GnRH neurons to migrate towards the hypothalamus is Sema7A. Sema7A is expressed on olfactory axons which are used as a scaffold by GnRH neurons[141]. In the absence of Sema7A, olfactory axons grow normally, but GnRH neurons stall and fail to migrate into the brain. How specific semaphorin (receptor) mutations observed in patients cause KS remains incompletely understood. In addition to Sema3A and Sema7A, Sema4D may also be a potential candidate protein for KSs[142], however no mutations have been reported in *SEMA4D* in KS patients to date[143].

Amyothropic lateral sclerosis

Defects in semaphorins and receptors may also underlie the pathogenesis of amyotropic lateral sclerosis (ALS)[121]. ALS is characterized by loss of motor neurons and their axonal connections. In a mouse model for ALS, $SOD1^{G93A}$ mice, Sema3A expression is increased in terminal Schwann cells that surround neuromuscular junctions (NMJs)[144], while the Sema3A co-receptor Nrp-1 is located on axonal terminals at NMJs[145]. Human post

mortem tissue analysis also reveals that Sema3A expression is increased in ALS patients specifically in the motor cortex and to a lesser extent in the spinal cord[146]. These changes in Sema3A signaling may trigger loss of adhesion or repulsion of motor axons that cause muscle denervation and, consequently, motor neuron degeneration. Interestingly, *in vivo* antibody administration prolongs life span in SOD1^{G93A} mice[145]. However, disruption of Sema3A-Neuropilin1 signaling complex in knockout mouse models did not alter muscle re-innervation[147]. Therefore, the precise therapeutic potential of targeting Sema3A following neuromuscular injury or disease remains unclear. Interestingly, miR-126-5p was reported to be reduced at pre-symptomatic stages in ALS mouse models. miR-126-5p targets Sema3A and Nrp-1, and anti-Nrp-1 antibodies can rescue axonal degeneration and NMJ dysfunction *in vitro.* Similarly, overexpression of miR-126-5p was able to rescue axonal degeneration and NMJ disruption *in vitro* and *in vivo*. Together, these data identify miR-126-5p as a therapeutic target in ALS which may function by acting on aberrant Sema3A signaling[148]. Changes in the actin cytoskeleton are a hallmark of ALS and other progressive motor neuron diseases such as Spinal Muscular Atrophy (SMA)[149]. SMA is characterized by motor neuron degeneration due to deletions of survival of motoneuron 1 (SMN1). PlexinD1 is cleaved by metalloproteases (MPs), and in SMA mouse models cytoplasmic PlexinD1 fragments bind to actin aggregates that perturb cytoskeletal regulation in the growth cone[150]. If and how mislocalization of the PlexinD1 cytoplasmic domain leads to SMA remains to be investigated. Overall, further functional studies are needed to understand how the dysregulation of semaphorins and their receptors contributes to neurodegenerative diseases such as ALS and SMA.

Late onset neurodegenerative diseases

Expression profiling studies reveal changes in the expression of several axon guidance proteins in patients with Alzheimer's disease (AD) and Parkinson's disease (PD)[119]. Polymorphisms located in the coding regions of axon guidance genes have been established as risk factors using genome-wide association studies (GWAS) and meta-analyses. Recent studies provide evidence for new high-risk factors for PD[151] linked to semaphorins and also elucidate the roles of certain previously linked semaphorin signaling pathways in the pathogenesis of PD in mouse models[152]. Although axon guidance proteins play a crucial role in the development and maintenance of dopaminergic circuits[153], how their dysregulation contributes to the pathogenesis of PD remains to be established.

In AD, the expression of several semaphorins and receptors is changed as shown by profiling studies in patients[119]. The Sema3A signaling molecule collapsin response mediator protein-2 (CRMP2) also has been firmly linked to AD. Neurofibrillary tangles that characterize the disease contain hyperphosphorylated CRMP2 that might potentiate Sema3A-mediated repulsion. Amyloid-ß protein increases the phosphorylation of CRMPs through RhoA small GTPases *in vitro*, and levels of RhoA and CRMP2 surrounding amyloid plaques in the cortex are increased in a mouse model for AD (Tg2575)[154–157]. Interestingly, GWAS approaches identified a novel *PLXNA4* variant linked to AD pathogenesis. PlexinA4 affects tau phosphorylation, leading to neurofibrillary tangle formation in neurons [158]. These data suggest that *PLXNA4* variants may be linked to tau pathology in AD.

Overall, these data implicate semaphorins and their receptors in late onset neurodegenerative disease. It is unlikely that single gene mutations in semaphorins or their receptors cause neurodegenerative diseases, but they may contribute to disease risk, onset or progression. Functional studies are needed to assess the precise contribution of semaphorin and semaphorin receptor mutations to AD and PD.

Conclusions and perspectives

The semaphorin family of axon guidance molecules has been implicated in various aspects of neural circuit development. Novel insights into signaling pathways activated by semaphorins and their receptors, plexins and neuropilins, explain their ability to exert highly complex and tightly regulated functions. Transmembrane semaphorins function both as ligand and receptors, and can form, together with (co-)receptors, signaling complexes that are regulated through *cis* and *trans* interactions. In addition, pre-signaling autoinhibition of plexins contributes to the spatiotemporal control of semaphorin signaling. Important future challenges are to determine how different binding modes are initialized to trigger forward or reverse signaling pathways, and also *cis* or *trans* interactions. Further, we also need to know how appropriate downstream interactors are recruited in specific contexts *in vivo*. Structural work has significantly advanced our understanding of how semaphorins and receptors interact. The determination of intracellular binding interfaces also has aided the identification of novel downstream interactors involved in several semaphorin signaling pathways.

Altered expression and function of semaphorins plays a role in neurological disease. Understanding the fine-tuned regulation and mechanistic details of semaphorin signaling and function is a therefore an imperative step toward designing strategies to modulate neural injury and disease. Functional studies are needed to establish causality of patient-associated mutations and to understand underlying disease mechanisms.

REFERENCES

1. Pasterkamp, R. J. & Giger, R. J. Semaphorin function in neural plasticity and disease. *Current Opinion in Neurobiology* (2009). doi:10.1016/j.conb.2009.06.001
2. Tran, T. S., Kolodkin, A. L. & Bharadwaj, R. Semaphorin Regulation of Cellular Morphology. *Annu. Dev.Biol.* (2007).
3. Yoshida, Y. Semaphorin Signaling in Vertebrate Neural Circuit Assembly. *Front. Mol. Neurosci.* (2012). doi:10.3389/fnmol.2012.00071
4. Koropouli, E. & Kolodkin, A. L. Semaphorins and the dynamic regulation of synapse assembly, refinement, and function. *Curr. Opin. Neurobiol.* 27, 1–7 (2014).
5. Pasterkamp, R. J. & Kolodkin, A. L. Semaphorin junction: making tracks toward neural connectivity. *Curr. Opin. Neurobiol.* 13, 79–89 (2003).
6. Pasterkamp, R. J. Getting neural circuits into shape with semaphorins. 13, 605–618 (2012).
7. Luo, Y., Raible, D. & Raper, J. A. Collapsin: A protein in brain that induces the collapse and paralysis of neuronal growth cones. *Cell* 75, 217–227 (1993).
8. Kolodkin, A. L. *et al.* Fasciclin IV: Sequence, expression, and function during growth cone guidance in the grasshopper embryo. *Neuron* (1992). doi:10.1016/0896-6273(92)90237-8
9. Bamberg, J. A. *et al.* Unified nomenclature for the semaphorins/collapsins [1]. *Cell* (1999). doi:10.1016/S0092-8674(00)80766-7
10. Alto, L. T. & Terman, J. R. Semaphorins and their Signaling Mechanisms. in *Methods in Molecular Biology* 1–25 (2017). doi:10.1007/978-1-4939-6448-2_1
11. Casazza, A., Fazzari, P. & Tamagnone, L. Semaphorin signals in cell adhesion and cell migration: Functional role and molecular mechanisms. *Advances in Experimental Medicine and Biology* (2007). doi:10.1007/978-0-387-70956-7_8
12. Nishide, M. & Kumanogoh, A. The role of semaphorins in immune responses and autoimmune rheumatic diseases. *Nature Reviews Rheumatology* (2018). doi:10.1038/nrrheum.2017.201
13. Neufeld, G. *et al.* The role of the semaphorins in cancer. *Cell Adhesion and Migration* (2016). doi:10.1080/19336918.2016.1197478
14. Neufeld, G., Sabag, A. D., Rabinovicz, N. & Kessler, O. Semaphorins in angiogenesis and tumor progression. *Cold Spring Harb. Perspect. Med.* (2012). doi:10.1101/cshperspect.a006718
15. Osborne, N. J., Begbie, J., Chilton, J. K., Schmidt, H. & Eickholt, B. J. Semaphorin/neuropilin signaling influences the positioning of migratory neural crest cells within the hindbrain region of the chick. *Dev. Dyn.* (2005). doi:10.1002/dvdy.20258

16. Marín, O., Yaron, A., Bagri, A., Tessier-Lavigne, M. & Rubenstein, J. L. R. Sorting of striatal and cortical interneurons regulated by semaphorin-neuropilin interactions. *Science (80-.).* (2001). doi:10.1126/science.1061891
17. Bribián, A. *et al.* Sema3E/PlexinD1 regulates the migration of hem-derived Cajal-Retzius cells in developing cerebral cortex. *Nat. Commun.* (2014). doi:10.1038/ncomms5265
18. Chen, G. *et al.* Semaphorin-3A guides radial migration of cortical neurons during development. *Nat. Neurosci.* (2008). doi:10.1038/nn2018
19. Kerjan, G. *et al.* The transmembrane semaphorin Sema6A controls cerebellar granule cell migration. *Nat. Neurosci.* 8, 1516–1524 (2005).
20. Maier, V. *et al.* Semaphorin 4C and 4G are ligands of Plexin-B2 required in cerebellar development. *Mol. Cell. Neurosci.* (2011). doi:10.1016/j.mcn.2010.11.005
21. Renaud, J. *et al.* Plexin-A2 and its ligand, Sema6A, control nucleus-centrosome coupling in migrating granule cells. *Nat. Neurosci.* 11, 440–449 (2008).
22. Ohta, K. *et al.* Plexin: A novel neuronal cell surface molecule that mediates cell adhesion via a homophilic binding mechanism in the presence of calcium ions. *Neuron* (1995). doi:10.1016/0896-6273(95)90266-X
23. Comeau, M. R. *et al.* A poxvirus-encoded semaphorin induces cytokine production from monocytes and binds to a novel cellular semaphorin receptor, VESPR. *Immunity* (1998). doi:10.1016/S1074-7613(00)80552-X
24. Winberg, M. L. *et al.* Plexin A is a neuronal semaphorin receptor that controls axon guidance. *Cell* (1998). doi:10.1016/S0092-8674(00)81715-8
25. Ishida, I. *et al.* Involvement of CD100, a lymphocyte semaphorin, in the activation of the human immune system via CD72: Implications for the regulation of immune and inflammatory responses. *Int. Immunol.* (2003). doi:10.1093/intimm/dxg098
26. Kumanogoh, A. *et al.* Class iv semaphorin sema4a enhances t-cell activation and interacts with tim-2. *Nature* (2002). doi:10.1038/nature01037
27. Jongbloets, B. C. *et al.* Stage-specific functions of Semaphorin7A during adult hippocampal neurogenesis rely on distinct receptors. *Nat. Commun.* (2017). doi:10.1038/ncomms14666
28. Cho, J. Y., Chak, K., Andreone, B. J., Wooley, J. R. & Kolodkin, A. L. The extracellular matrix proteoglycan perlecan facilitates transmembrane semaphorin-mediated repulsive guidance. *Genes Dev.* (2012). doi:10.1101/gad.193136.112
29. Battistini, C. & Tamagnone, L. Transmembrane semaphorins, forward and reverse signaling: Have a look both ways. *Cellular and Molecular Life Sciences* (2016). doi:10.1007/s00018-016-2137-x
30. Love, C. A. *et al.* The ligand-binding face of the semaphorins revealed by the high-resolution crystal structure of SEMA4D. *Nat. Struct. Mol. Biol.* 10, 843–848 (2003).

31. Antipenko, A. *et al.* Structure of the Semaphorin-3A Receptor Binding Module. *Neuron* 39, 589–598 (2003).
32. Adams, R. H., Betz, H. & Püschel, A. W. A novel class of murine semaphorins with homology to thrombospondin is differentially expressed during early embryogenesis. *Mech. Dev.* (1996). doi:10.1016/0925-4773(96)00525-4
33. Jongbloets, B. C. & Pasterkamp, R. J. Semaphorin signalling during development. *Development* 141, 3292–3297 (2014).
34. Kolodkin, A. L. & Tessier-Lavigne, M. Mechanisms and molecules of neuronal wiring: A primer. *Cold Spring Harbor Perspectives in Biology* (2011). doi:10.1101/cshperspect.a001727
35. Fülöp, V. & Jones, D. T. β Propellers: Structural rigidity and functional diversity. *Current Opinion in Structural Biology* (1999). doi:10.1016/S0959-440X(99)00035-4
36. Janssen, B. J. C. *et al.* Structural basis of semaphorin–plexin signalling. *Nature* 467, 1118–1122 (2010).
37. Gherardi, E., Love, C. A., Esnouf, R. M. & Jones, E. Y. The sema domain. *Curr. Opin. Struct. Biol.* 14, 669–678 (2004).
38. Tamagnone, L. *et al.* Plexins Are a Large Family of Receptors for Transmembrane, Secreted, and GPI-Anchored Semaphorins in Vertebrates. *Cell* 99, 71–80 (1999).
39. Liu, H. *et al.* Structural Basis of Semaphorin-Plexin Recognition and Viral Mimicry from Sema7A and A39R Complexes with PlexinC1. *Cell* 142, 749–761 (2010).
40. Nogi, T. *et al.* Structural basis for semaphorin signalling through the plexin receptor. *Nature* 467, 1123–1127 (2010).
41. Tong, Y. *et al.* Structure and Function of the Intracellular Region of the Plexin-B1 Transmembrane Receptor. *J. Biol. Chem.* 284, 35962–35972 (2009).
42. He, H., Yang, T., Terman, J. R. & Zhang, X. Crystal structure of the plexin A3 intracellular region reveals an autoinhibited conformation through active site sequestration. *Proc. Natl. Acad. Sci.* 106, 15610–15615 (2009).
43. Appleton, B. A. *et al.* Structural studies of neuropilin/antibody complexes provide insights into semaphorin and VEGF binding. *EMBO J.* 26, 4902–4912 (2007).
44. Lee, C. C., Kreusch, A., McMullan, D., Ng, K. & Spraggon, G. Crystal Structure of the Human Neuropilin-1 b1 Domain. *Structure* 11, 99–108 (2003).
45. Shang, G. *et al.* Structure analyses reveal a regulated oligomerization mechanism of the PlexinD1/GIPC/myosin VI complex. *Elife* 6, (2017).
46. Kong, Y. *et al.* Structural Basis for Plexin Activation and Regulation. *Neuron* 91, 548–60 (2016).
47. Pascoe, H. G. *et al.* Secondary PDZ domain-binding site on class B plexins enhances the affinity for PDZ–RhoGEF. *Proc. Natl. Acad. Sci.* 112, 14852–14857 (2015).

48. Wang, Y., Pascoe, H. G., Brautigam, C. A., He, H. & Zhang, X. Structural basis for activation and non-canonical catalysis of the Rap GTPase activating protein domain of plexin. *Elife* (2013). doi:10.7554/eLife.01279.001
49. Janssen, B. J. C. *et al.* Neuropilins lock secreted semaphorins onto plexins in a ternary signaling complex. *Nat. Struct. Mol. Biol.* 19, 1293–1299 (2012).
50. Wang, Y. *et al.* Plexins Are GTPase-Activating Proteins for Rap and Are Activated by Induced Dimerization. *Sci. Signal.* 5, ra6-ra6 (2012).
51. Bell, C. H., Aricescu, A. R., Jones, E. Y. & Siebold, C. A Dual Binding Mode for RhoGTPases in Plexin Signalling. *PLoS Biol.* 9, e1001134 (2011).
52. Siebold, C. & Jones, E. Y. Structural insights into semaphorins and their receptors. *Seminars in Cell and Developmental Biology* (2013). doi:10.1016/j.semcdb.2012.11.003
53. Janssen, B. J. C. *et al.* Structural basis of semaphorin–plexin signalling. *Nature* 467, 1118–1122 (2010).
54. Takahashi, T. *et al.* Plexin-neuropilin-1 complexes form functional semaphorin-3A receptors. *Cell* (1999). doi:10.1016/S0092-8674(00)80062-8
55. Gu, C. *et al.* Semaphorin 3E and plexin-D1 control vascular pattern independently of neuropilins. *Science (80-.).* (2005). doi:10.1126/science.1105416
56. Pellet-Many, C., Frankel, P., Jia, H. & Zachary, I. Neuropilins: structure, function and role in disease. *Biochem. J.* 411, 211–226 (2008).
57. Kawakami, a, Kitsukawa, T., Takagi, S. & Fujisawa, H. Developmentally regulated expression of a cell surface protein, neuropilin, in the mouse nervous system. *J. Neurobiol.* (1996). doi:10.1002/(SICI)1097-4695(199601)29:1<1::AID-NEU1>3.0.CO;2-F
58. Andermatt, I. *et al.* Semaphorin 6B acts as a receptor in post-crossing commissural axon guidance. *Development* 141, 3709–3720 (2014).
59. Perez-Branguli, F. *et al.* Reverse Signaling by Semaphorin-6A Regulates Cellular Aggregation and Neuronal Morphology. *PLoS One* 11, e0158686 (2016).
60. Haklai-topper, L., Mlechkovich, G., Savariego, D., Gokhman, I. & Yaron, A. Cis interaction between Semaphorin6A and Plexin-A4 modulates the repulsive response to Sema6A. *EMBO J.* 29, 2635–2645 (2010).
61. Sun, L. O. *et al.* On and Off Retinal Circuit Assembly by Divergent Molecular Mechanisms. *Science (80-.).* 342, 1241974–1241974 (2013).
62. Mizumoto, K. & Shen, K. Interaxonal Interaction Defines Tiled Presynaptic Innervation in C. elegans. *Neuron* (2013). doi:10.1016/j.neuron.2012.12.031
63. Hota, P. K. & Buck, M. Plexin structures are coming: opportunities for multilevel investigations of semaphorin guidance receptors, their cell signaling mechanisms, and functions. *Cell. Mol. Life Sci.* 69, 3765–3805 (2012).
64. Vetter, I. R. & Wittinghofer, A. The guanine nucleotide-binding switch in three dimensions. *Science* (2001). doi:10.1126/science.1062023

65. Hall, A. & Lalli, G. Rho and Ras GTPases in axon growth, guidance, and branching. *Cold Spring Harbor perspectives in biology* (2010). doi:10.1101/cshperspect.a001818
66. Wennerberg, K. Rho-family GTPases: it's not only Rac and Rho (and I like it). *J. Cell Sci.* (2004). doi:10.1242/jcs.01118
67. Bos, J. L., Rehmann, H. & Wittinghofer, A. GEFs and GAPs: critical elements in the control of small G proteins. *Cell* 129, 865–77 (2007).
68. Etienne-Manneville, S. & Hall, A. Rho GTPases in cell biology. *Nature* (2002). doi:10.1038/nature01148
69. Gonzalez-Billault, C. *et al.* The role of small GTPases in neuronal morphogenesis and polarity. *Cytoskeleton* (2012). doi:10.1002/cm.21034
70. Luo, L. RHO GTPASES in neuronal morphogenesis. *Nat. Rev. Neurosci.* (2000). doi:10.1038/35044547
71. Zhao, X.-F. *et al.* PlexinA2 Forward Signaling through Rap1 GTPases Regulates Dentate Gyrus Development and Schizophrenia-like Behaviors. *Cell Rep.* 22, 456–470 (2018).
72. Riccomagno, M. M. *et al.* The RacGAP β2-chimaerin selectively mediates axonal pruning in the hippocampus. *Cell* (2012). doi:10.1016/j.cell.2012.05.018
73. Swiercz, J. M., Kuner, R. & Offermanns, S. Plexin-B1/RhoGEF-mediated RhoA activation involves the receptor tyrosine kinase ErbB-2. *J. Cell Biol.* (2004). doi:10.1083/jcb.200312094
74. Li, X. & Lee, A. Y. W. Semaphorin 5A and plexin-B3 inhibit human glioma cell motility through RhoGDI??-mediated inactivation of Rac1 GTPase. *J. Biol. Chem.* (2010). doi:10.1074/jbc.M110.120451
75. Kuo, Y. C. *et al.* Structural analyses of FERM domain-mediated membrane localization of FARP1. *Sci. Rep.* 8, 1–10 (2018).
76. Toyofuku, T. *et al.* FARP2 triggers signals for Sema3A-mediated axonal repulsion. *Nat. Neurosci.* 8, 1712–1719 (2005).
77. Zhang, Z., Vuori, K., Wang, H. G., Reed, J. C. & Ruoslahti, E. Integrin activation by R-ras. *Cell* (1996). doi:10.1016/S0092-8674(00)81082-X
78. Duan, Y. *et al.* Semaphorin 5A inhibits synaptogenesis in early postnatal- and adult-born hippocampal dentate granule cells. *Elife* (2014). doi:10.7554/eLife.04390
79. Burridge, K. & Wennerberg, K. Rho and Rac Take Center Stage. *Cell* 116, 167–179 (2004).
80. Jaffe, A. B. & Hall, A. RHO GTPASES: Biochemistry and Biology. *Annu. Rev. Cell Dev. Biol.* (2005). doi:10.1146/annurev.cellbio.21.020604.150721
81. Tong, Y. *et al.* Binding of Rac1, Rnd1, and RhoD to a Novel Rho GTPase Interaction Motif Destabilizes Dimerization of the Plexin-B1 Effector Domain. *J. Biol. Chem.* 282, 37215–37224 (2007).

82. Uesugi, K., Oinuma, I., Katoh, H. & Negishi, M. Different requirement for Rnd GTPases of R-Ras GAP activity of Plexin-C1 and Plexin-D1. *J. Biol. Chem.* (2009). doi:10.1074/jbc.M805213200
83. Wylie, T., Garg, R., Ridley, A. J. & Conte, M. R. Analysis of the interaction of Plexin-B1 and Plexin-B2 with Rnd family proteins. *PLoS One* 12, e0185899 (2017).
84. Terman, J. R., Mao, T., Pasterkamp, R. J., Yu, H. H. & Kolodkin, A. L. MICALs, a Family of Conserved Flavoprotein Oxidoreductases, Function in Plexin-Mediated Axonal Repulsion. *Cell* (2002). doi:10.1016/S0092-8674(02)00794-8
85. Hung, R. J. *et al.* Mical links semaphorins to F-actin disassembly. *Nature* (2010). doi:10.1038/nature08724
86. Hung, R. J., Pak, C. W. & Terman, J. R. Direct redox regulation of F-actin assembly and disassembly by Mical. *Science (80-.).* (2011). doi:10.1126/science.1211956
87. Hung, R. J., Spaeth, C. S., Yesilyurt, H. G. & Terman, J. R. Selr Reverses Mical-Mediated Oxidation of Actin to Regulate F-Actin Dynamics. *Nat. Cell Biol.* (2013). doi:10.1038/ncb2871
88. Zhou, Y., Gunput, R. F. & Pasterkamp, R. J. Semaphorin signaling : progress made and promises ahead. 161–170 (2008). doi:10.1016/j.tibs.2008.01.006
89. Godenschwege, T. A., Hu, H., Shan-Crofts, X., Goodman, C. S. & Murphey, R. K. Bi-directional signaling by semaphorin 1a during central synapse formation in Drosophila. *Nat. Neurosci.* (2002). doi:10.1038/nn976
90. Jeong, S., Juhaszova, K. & Kolodkin, A. L. The Control of Semaphorin-1a-Mediated Reverse Signaling by Opposing Pebble and RhoGAPp190 Functions in Drosophila. *Neuron* (2012). doi:10.1016/j.neuron.2012.09.018
91. Jeong, S. *et al.* Varicose and cheerio collaborate with pebble to mediate semaphorin-1a reverse signaling in *Drosophila*. *Proc. Natl. Acad. Sci.* (2017). doi:10.1073/pnas.1713010114
92. Yu, L., Zhou, Y., Cheng, S. & Rao, Y. Plexin A-Semaphorin-1a Reverse Signaling Regulates Photoreceptor Axon Guidance in Drosophila. *J. Neurosci.* (2010). doi:10.1523/JNEUROSCI.1494-10.2010
93. Mauti, O., Domanitskaya, E., Andermatt, I., Sadhu, R. & Stoeckli, E. T. Semaphorin6A acts as a gate keeper between the central and the peripheral nervous system. *Neural Dev.* (2007). doi:10.1186/1749-8104-2-28
94. Bernard, F. *et al.* Role of transmembrane semaphorin Sema6A in oligodendrocyte differentiation and myelination. *Glia* (2012). doi:10.1002/glia.22378
95. Burkhardt, C. *et al.* Semaphorin 4B interacts with the post-synaptic density protein PSD-95/SAP90 and is recruited to synapses through a C-terminal PDZ-binding motif. *FEBS Lett.* 579, 3821–3828 (2005).
96. Leighton, P. A. *et al.* Defining brain wiring patterns and mechanisms through gene trapping in mice. *Nature* (2001). doi:10.1038/35065539

97. Sun, L. O. *et al.* Functional Assembly of Accessory Optic System Circuitry Critical for Compensatory Eye Movements. *Neuron* (2015). doi:10.1016/j.neuron.2015.03.064
98. Toyofuku, T. *et al.* Guidance of myocardial patterning in cardiac development by Sema6D reverse signalling. *Nat. Cell Biol.* (2004). doi:10.1038/ncb1193
99. Hou, T., Chen, K., McLaughlin, W. A., Lu, B. & Wang, W. Computational analysis and prediction of the binding motif and protein interacting partners of the Abl SH3 domain. *PLoS Comput. Biol.* (2006). doi:10.1371/journal.pcbi.0020001
100. Drees, F. & Gertler, F. B. Ena/VASP: proteins at the tip of the nervous system. *Current Opinion in Neurobiology* (2008). doi:10.1016/j.conb.2008.05.007
101. Klostermann, A., Lutz, B., Gertler, F. & Behl, C. The orthologous human and murine semaphorin 6A-1 proteins (SEMA6A-1/Sema6A-1) bind to the enabled/vasodilator-stimulated phosphoprotein-like protein (EVL) via a novel carboxyl-terminal zyxin-like domain. *J. Biol. Chem.* (2000). doi:10.1074/jbc.M006316200
102. Eckhardt, F. *et al.* A Novel Transmembrane Semaphorin Can Bind c-src. *Mol. Cell. Neurosci.* 9, 409–419 (1997).
103. Burkhardt, C. *et al.* Semaphorin 4B interacts with the post-synaptic density protein PSD-95/SAP90 and is recruited to synapses through a C-terminal PDZ-binding motif. *FEBS Lett.* (2005). doi:10.1016/j.febslet.2005.05.079
104. Battistini, C. & Tamagnone, L. Transmembrane semaphorins, forward and reverse signaling: have a look both ways. *Cell. Mol. Life Sci.* 73, 1609–1622 (2016).
105. Huberman, A. D., Clandinin, T. R. & Baier, H. Molecular and cellular mechanisms of lamina-specific axon targeting. *Cold Spring Harbor perspectives in biology* (2010). doi:10.1101/cshperspect.a001743
106. Tawarayama, H., Yoshida, Y., Suto, F., Mitchell, K. J. & Fujisawa, H. Roles of Semaphorin-6B and Plexin-A2 in Lamina-Restricted Projection of Hippocampal Mossy Fibers. *J. Neurosci.* 30, 7049–7060 (2010).
107. Suto, F. *et al.* Article Projection of Hippocampal Mossy Fibers. 535–547 (2007). doi:10.1016/j.neuron.2007.01.028
108. Matsuoka, R. L. *et al.* Class 5 transmembrane semaphorins control selective mammalian retinal lamination and function. *Neuron* (2011). doi:10.1016/j.neuron.2011.06.009
109. Matsuoka, R. L. *et al.* Guidance-Cue Control of Horizontal Cell Morphology, Lamination, and Synapse Formation in the Mammalian Outer Retina. *J. Neurosci.* (2012). doi:10.1523/JNEUROSCI.0267-12.2012
110. Belle, M., Parray, A., Belle, M., Chédotal, A. & Nguyen-Ba-Charvet, K. T. PlexinA2 and Sema6A are required for retinal progenitor cell migration. *Dev. Growth Differ.* 58, 492–502 (2016).
111. Mata, A. *et al.* New functions of Semaphorin 3E and its receptor PlexinD1 during developing and adult hippocampal formation. *Sci. Rep.* 8, 1381 (2018).

112. Chauvet, S. *et al.* Gating of Sema3E/PlexinD1 Signaling by Neuropilin-1 Switches Axonal Repulsion to Attraction during Brain Development. *Neuron* (2007). doi:10.1016/j.neuron.2007.10.019
113. Ding, J. B., Oh, W. J., Sabatini, B. L. & Gu, C. Semaphorin 3Eg-Plexin-D1 signaling controls pathway-specific synapse formation in the striatum. *Nat. Neurosci.* (2012). doi:10.1038/nn.3003
114. Little, G. E. *et al.* Specificity and Plasticity of Thalamocortical Connections in Sema6A Mutant Mice. *PLoS Biol.* 7, e1000098 (2009).
115. Mitsogiannis, M. D., Little, G. E. & Mitchell, K. J. Semaphorin-Plexin signaling influences early ventral telencephalic development and thalamocortical axon guidance. *Neural Dev.* 12, 6 (2017).
116. Watanabe, M. & Kano, M. Climbing fiber synapse elimination in cerebellar Purkinje cells. *European Journal of Neuroscience* (2011). doi:10.1111/j.1460-9568.2011.07894.x
117. Uesaka, N. *et al.* Retrograde semaphorin signaling regulates synapse elimination in the developing mouse brain. *Science (80-.).* 344, 1020–1023 (2014).
118. Uesaka, N. & Kano, M. Presynaptic Mechanisms Mediating Retrograde Semaphorin Signals for Climbing Fiber Synapse Elimination During Postnatal Cerebellar Development. *The Cerebellum* 17, 17–22 (2018).
119. Van Battum, E. Y., Brignani, S. & Pasterkamp, R. J. Axon guidance proteins in neurological disorders. *The Lancet Neurology* (2015). doi:10.1016/S1474-4422(14)70257-1
120. Lin, L., Lesnick, T. G., Maraganore, D. M. & Isacson, O. Axon guidance and synaptic maintenance: preclinical markers for neurodegenerative disease and therapeutics. *Trends in Neurosciences* (2009). doi:10.1016/j.tins.2008.11.006
121. Schmidt, E. R. E., Pasterkamp, R. J. & van den Berg, L. H. Axon guidance proteins: Novel therapeutic targets for ALS? *Progress in Neurobiology* (2009). doi:10.1016/j.pneurobio.2009.05.004
122. Nugent, A. A., Kolpak, A. L. & Engle, E. C. Human disorders of axon guidance. *Current Opinion in Neurobiology* (2012). doi:10.1016/j.conb.2012.02.006
123. Geschwind, D. H. & Levitt, P. Autism spectrum disorders: developmental disconnection syndromes. *Current Opinion in Neurobiology* (2007). doi:10.1016/j.conb.2007.01.009
124. Giger, R. J., Hollis, E. R. & Tuszynski, M. H. Guidance molecules in axon regeneration. *Cold Spring Harbor perspectives in biology* (2010). doi:10.1101/cshperspect.a001867
125. Giacobini, P. & Prevot, V. Semaphorins in the development, homeostasis and disease of hormone systems. *Seminars in Cell and Developmental Biology* (2013). doi:10.1016/j.semcdb.2012.11.005

126. Yaron, A. & Zheng, B. Navigating their way to the clinic: Emerging roles for axon guidance molecules in neurological disorders and injury. *Developmental Neurobiology* (2007). doi:10.1002/dneu.20512
127. Amaral, D. G., Schumann, C. M. & Nordahl, C. W. Neuroanatomy of autism. *Trends in Neurosciences* (2008). doi:10.1016/j.tins.2007.12.005
128. McFadden, K. & Minshew, N. J. Evidence for dysregulation of axonal growth and guidance in the etiology of ASD. *Front. Hum. Neurosci.* (2013). doi:10.3389/fnhum.2013.00671
129. Mosca-Boidron, A.-L. *et al.* A de novo microdeletion of SEMA5A in a boy with autism spectrum disorder and intellectual disability. *Eur. J. Hum. Genet.* 24, 838–843 (2016).
130. Durand, C. M. *et al.* Mutations in the gene encoding the synaptic scaffolding protein SHANK3 are associated with autism spectrum disorders. *Nat. Genet.* (2007). doi:10.1038/ng1933
131. Jiang, Y. hui & Ehlers, M. D. Modeling Autism by SHANK Gene Mutations in Mice. *Neuron* (2013). doi:10.1016/j.neuron.2013.03.016
132. Gauthier, J. *et al.* De novo mutations in the gene encoding the synaptic scaffolding protein *SHANK3* in patients ascertained for schizophrenia. *Proc. Natl. Acad. Sci.* (2010). doi:10.1073/pnas.0906232107
133. Lilja, J. *et al.* SHANK proteins limit integrin activation by directly interacting with Rap1 and R-Ras. *Nat. Cell Biol.* 19, 292–305 (2017).
134. Mei, Y. *et al.* Adult restoration of Shank3 expression rescues selective autistic-like phenotypes. *Nature* (2016). doi:10.1038/nature16971
135. Zhao, X.-F. *et al.* PlexinA2 Forward Signaling through Rap1 GTPases Regulates Dentate Gyrus Development and Schizophrenia-like Behaviors. *Cell Rep.* (2018). doi:10.1016/j.celrep.2017.12.044
136. Cariboni, A. *et al.* Dysfunctional SEMA3E signaling underlies gonadotropin-releasing hormone neuron deficiency in Kallmann syndrome. *J. Clin. Invest.* (2015). doi:10.1172/JCI78448
137. Känsäkoski, J. *et al.* Mutation screening of SEMA3A and SEMA7A in patients with congenital hypogonadotropic hypogonadism. *Pediatr. Res.* (2014). doi:10.1038/pr.2014.23
138. Marcos, S. *et al.* Defective signaling through plexin-A1 compromises the development of the peripheral olfactory system and neuroendocrine reproductive axis in mice. *Hum. Mol. Genet.* (2017). doi:10.1093/hmg/ddx080
139. Hanchate, N. K. *et al.* SEMA3A, a Gene Involved in Axonal Pathfinding, Is Mutated in Patients with Kallmann Syndrome. *PLoS Genet.* (2012). doi:10.1371/journal.pgen.1002896

140. Cariboni, A. *et al.* Defective gonadotropin-releasing hormone neuron migration in mice lacking SEMA3A signalling through NRP1 and NRP2: Implications for the aetiology of hypogonadotropic hypogonadism. *Hum. Mol. Genet.* (2011). doi:10.1093/hmg/ddq468
141. Messina, A. *et al.* Dysregulation of semaphorin7A/β1-integrin signaling leads to defective GnRH-1 cell migration, abnormal gonadal development and altered fertility. *Hum. Mol. Genet.* (2011). doi:10.1093/hmg/ddr403
142. Giacobini, P. *et al.* Semaphorin 4D regulates gonadotropin hormonereleasing hormone-1 neuronal migration through PlexinBl-Met complex. *J. Cell Biol.* (2008). doi:10.1083/jcb.200806160
143. Cariboni, A., Oleari, R., Lettieri, A., Paganoni, A. & Zanieri, L. Semaphorin signalling in GnRH neurons: from development to disease. *Neuroendocrinology* (2018). doi:10.1159/000495916
144. Winter, F. De *et al.* The expression of the chemorepellent Semaphorin 3A is selectively induced in terminal Schwann cells of a subset of neuromuscular synapses that display limited anatomical plasticity and enhanced vulnerability in motor neuron disease. *Mol. Cell. Neurosci.* (2006). doi:10.1016/j.mcn.2006.03.002
145. Venkova, K. *et al.* Semaphorin 3A Signaling Through Neuropilin-1 Is an Early Trigger for Distal Axonopathy in the SOD1 G93A Mouse Model of Amyotrophic Lateral Sclerosis. *J. Neuropathol. Exp. Neurol.* 73, 702–713 (2014).
146. Körner, S. *et al.* The Axon Guidance Protein Semaphorin 3A Is Increased in the Motor Cortex of Patients With Amyotrophic Lateral Sclerosis. *J. Neuropathol. Exp. Neurol.* 75, 326–333 (2016).
147. Shadrach, J. L. & Pierchala, B. A. Sensory and Motor Systems Semaphorin3A Signaling Is Dispensable for Motor Axon Reinnervation of the Adult Neuromuscular Junction. 5, (2018).
148. Maimon, R. *et al.* miR126-5p Downregulation Facilitates Axon Degeneration and NMJ Disruption via a Non–Cell-Autonomous Mechanism in ALS. *J. Neurosci.* 38, 5478–5494 (2018).
149. Hensel, N. & Claus, P. The Actin Cytoskeleton in SMA and ALS: How Does It Contribute to Motoneuron Degeneration? *Neuroscientist* (2018). doi:10.1177/1073858417705059
150. Rademacher, S. *et al.* Metalloprotease-mediated cleavage of PlexinD1 and its sequestration to actin rods in the motoneuron disease spinal muscular atrophy (SMA). *Hum. Mol. Genet.* 26, 3946–3959 (2017).
151. Yu, X., Wang, F., Zhang, J. P. & Zhao, L. Meta analysis of the association of rs7702187 SNP in SEMA5A gene with risk of Parkinson's disease. *Eur. Rev. Med. Pharmacol. Sci.* (2014). doi:10.1039/b306366f

152. Qi, L. *et al.* Role of Rho-mediated ROCK-Semaphorin3A signaling pathway in the pathogenesis of Parkinson's disease in a mouse model. *J. Neurol. Sci.* 370, 21–26 (2016).
153. Van den Heuvel, D. M. A. & Pasterkamp, R. J. Getting connected in the dopamine system. *Progress in Neurobiology* (2008). doi:10.1016/j.pneurobio.2008.01.003
154. Good, P. F. *et al.* A role for semaphorin 3A signaling in the degeneration of hippocampal neurons during Alzheimer's disease. *J. Neurochem.* (2004). doi:10.1111/j.1471-4159.2004.02766.x
155. Cole, A. R. *et al.* GSK-3 phosphorylation of the Alzheimer epitope within collapsin response mediator proteins regulates axon elongation in primary neurons. *J. Biol. Chem.* (2004). doi:10.1074/jbc.C400412200
156. Soutar, M., Thornhill, P., Cole, A. & Sutherland, C. Increased CRMP2 Phosphorylation is Observed in Alzheimers Disease; Does this Tell us Anything About Disease Development? *Curr. Alzheimer Res.* 6, 269–278 (2009).
157. Petratos, S. *et al.* The β-amyloid protein of Alzheimer's disease increases neuronal CRMP-2 phosphorylation by a Rho-GTP mechanism. *Brain* (2008). doi:10.1093/brain/awm260
158. Jun, G. *et al.* PLXNA 4 is associated with Alzheimer disease and modulates tau phosphorylation. *Ann. Neurol.* 76, 379–392 (2014).
159. Vander Kooi, C. W. *et al.* Structural basis for ligand and heparin binding to neuropilin B domains. *Proc. Natl. Acad. Sci.* 104, 6152–6157 (2007).
160. Yelland, T. & Djordjevic, S. Crystal Structure of the Neuropilin-1 MAM Domain: Completing the Neuropilin-1 Ectodomain Picture. *Structure* 24, 2008–2015 (2016).

CHAPTER 3

Generation and characterization of Sema6AΔcyto conditional knockout mice

Marieke G. Verhagen[1], Suzanne Lemstra[1], Aikaterini Koutourlou[1], Klara Jansen[1], Kati Rehberg[1], Christiaan van der Meer[1], Youri Adolfs[1], Geert M. J. Ramakers[1], R. Jeroen Pasterkamp[1]

[1] Department of Translational Neuroscience, UMC Utrecht Brain Center, University Medical Center Utrecht, Utrecht University, The Netherlands

Submitted to BioRxiv

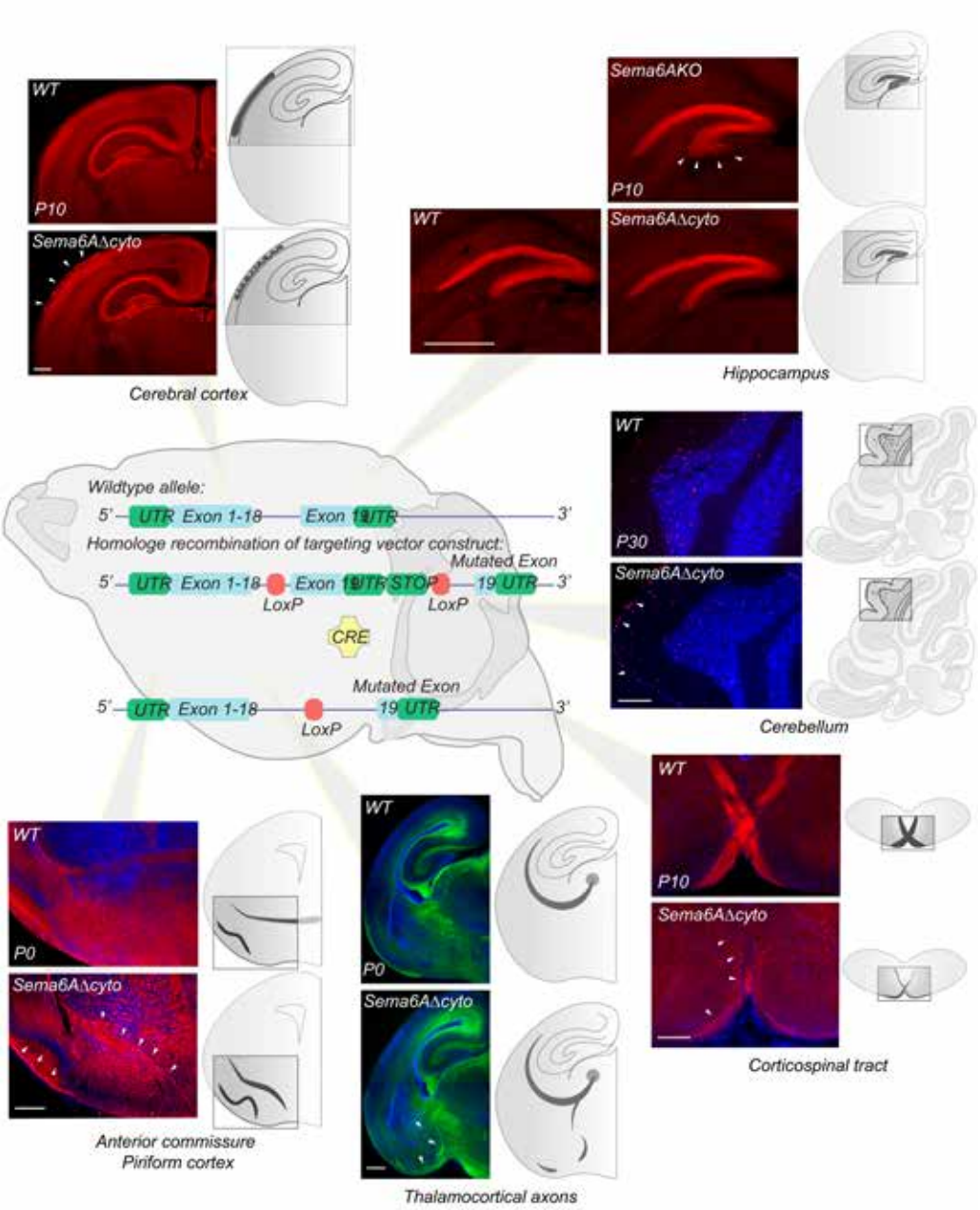

Graphical abstract Chapter 3

Centered image represents Sema6ADcyto mouse brain and genetic strategy used for conditional deletion of the intracellular domain of Sema6A. Surrounding microscopy and schematic images provide an overview of identified developmental defects in Sema6ADcyto mice.

ABSTRACT

The axon guidance molecule Semaphorin6A (Sema6A) plays a key role during the development of the nervous system. Sema6A is a transmembrane protein that, depending on the molecular and cellular context, acts as a ligand inducing forward signaling or as a receptor inducing reverse signaling. When and where Sema6A functions as a ligand and/or as a receptor during development is largely unknown. To study this bidirectional role of Sema6A, we generated a new transgenic mouse model Sema6AΔcyto (referred to as *Sema6AΔcyto*$^{fl/fl}$) lacking the Sema6A intracellular domain, which is essential for its receptor function, using the Cre/Lox system. In this mouse model, Sema6A only acts as a ligand. We performed immunohistochemistry experiments on *Sema6AΔcyto*$^{fl/fl}$ mice using cellular and axonal markers that reveal developmental defects in axon pathfinding and organization of the anterior commissure, piriform cortex, lateral olfactory tract, thalamocortical and corticospinal white matter tracts, and cellular migration in the cerebral cortex and cerebellum. These findings indicate that the intracellular domain of Sema6A is essential for proper development of these brain regions and axonal tracts and provide insight into the importance of the signaling pathways downstream of this transmembrane semaphorin.

INTRODUCTION

Semaphorin6A (Sema6A) is a transmembrane protein that plays a key role during the development of the nervous system. Some transmembrane semaphorins can act in a bidirectional manner as a ligand and/or as a receptor. In forward signaling the semaphorin interacts as a ligand with a receptor. In reverse signaling a ligand interacts with the semaphorin acting as a receptor. While there are many examples of the role of Sema6A ligand interacting with PlexinA2/A4 (PlxnA2/A4) receptors in forward signaling there is limited information of its role as a receptor in reverse signaling. *In vivo* tools to distinguish between Sema6A forward and reverse signaling pathways are not available.

Sema6A knockout mice (*Sema6A*$^{-/-}$) display axonal dysconnectivity and cellular disorganization phenotypes in the neocortex, anterior commissure, lateral olfactory tract, piriform cortex, hippocampus, corticospinal tract, fornix, cerebellum and retina [1–15]. Many of the phenotypes observed cannot be explained by the forward signaling pathway since the affected cells normally express Sema6A themselves, or co-express Sema6A and PlxnA2, suggesting cell-autonomous effects. For example, *Sema6A*$^{-/-}$ mice show abnormal caudal thalamocortical axonal projections that normally express Sema6A. Therefore, it has been suggested that Sema6A acts as a receptor triggering reverse signaling in a cell-autonomous manner [6]. Given the various neurodevelopmental defects that were originally found in *Sema6A*$^{-/-}$ mice, identified deficits were previously discussed in the context of developmental and adult onset nervous system disorders and diseases. This is beyond the scope of this study and therefore we refer to published interpretations [8,13,16].

Our knowledge of Sema6A receptor function and reverse signaling pathway is mostly based on *in vitro* data and *in vivo* evidence for reverse signaling is mostly found in invertebrates for example for Sema1a in *Drosophila* which is a Sema6A orthologue [17–20]. In vertebrates, the strongest support for the receptor function of Sema6A is found in the accessory optic system (AOS) during circuit development between the retina and midbrain nuclei. Axons from Sema6A expressing On direction-selective ganglion cells (On DSGCs) are attracted by PlexinA2 and PlexinA4 ligands expressed in the medial terminal nucleus (MTN) [4,21]. This finding provides proof of the role of Sema6A as a receptor and the possibility to study the underlying mechanisms of reverse signaling in the AOS system. In the spinal cord, Sema6A is found in

boundary cap cells (BCCs) acting as a receptor regulating axonal extension by interacting with PlexinA1 expressed in motoneurons. At the border between the peripheral and central nervous system, Sema6A induces aggregation of BCCs forming the boundary cap and preventing motor neuron mislocalization in the periphery [22]. Information on other potential roles for the Sema6A receptor throughout the development of the nervous system is currently lacking.

Here, we present a conditional transgenic mouse model that lacks the intracellular domain of Sema6A (*Sema6AΔcyto*$^{fl/fl}$) to specifically study the receptor function of this axon guidance molecule *in vivo*. This mouse model permits local genetic manipulation, using Cre/Lox mediated recombination [23], to study nervous system development in the absence of the intracellular domain of Sema6A. The intracellular domain of Sema6A is essential for the receptor function and reverse signaling pathway. Upon Cre recombinase *Sema6AΔcyto*$^{fl/fl}$ mice display multiple brain defects during development. Our results indicate that the Sema6A receptor is required for normal development of the nervous system *in vivo*.

RESULTS

Sema6AΔcyto construct design and mouse model

To study the function of the intracellular domain of Sema6A, we designed a construct were the 19th exon of Sema6A was replaced by a mutated, shorter 19th exon sequence that lacks the region coding for the intracellular domain (Fig. 1A). Sema6A and Sema6AΔcyto sequences were placed under the control of a pCAG promotor sequence and followed by a GFP gene. Upon transcription this results in a 631aa truncated Sema6AΔcyto protein compared to wildtype Sema6A 1031aa and a ±120 kDa and ±160 kDa band, respectively (Fig. S2A) To validate protein expression and localization of Sema6A and Sema6AΔcyto, the pCAG-Sema6AΔcyto-GFP, pCAG-Sema6A-GFP and pCAG-GFP control constructs were overexpressed in primary cortical neurons (Fig. 1B) and neuroblastoma (N2A) cells (Fig. S2B). Sema6AΔcyto-GFP and Sema6A-GFP constructs showed similar Sema6A protein surface expression in relation to GFP cytosolic expression. Expression patterns were determined with immunocytochemistry staining and no accumulation of protein in the cytoplasm was detected (Fig. 1C, Fig. S1B). In addition, to assess the ligand function in forward signaling of Sema6AΔcyto, cortical explants were cultured for 48 hours

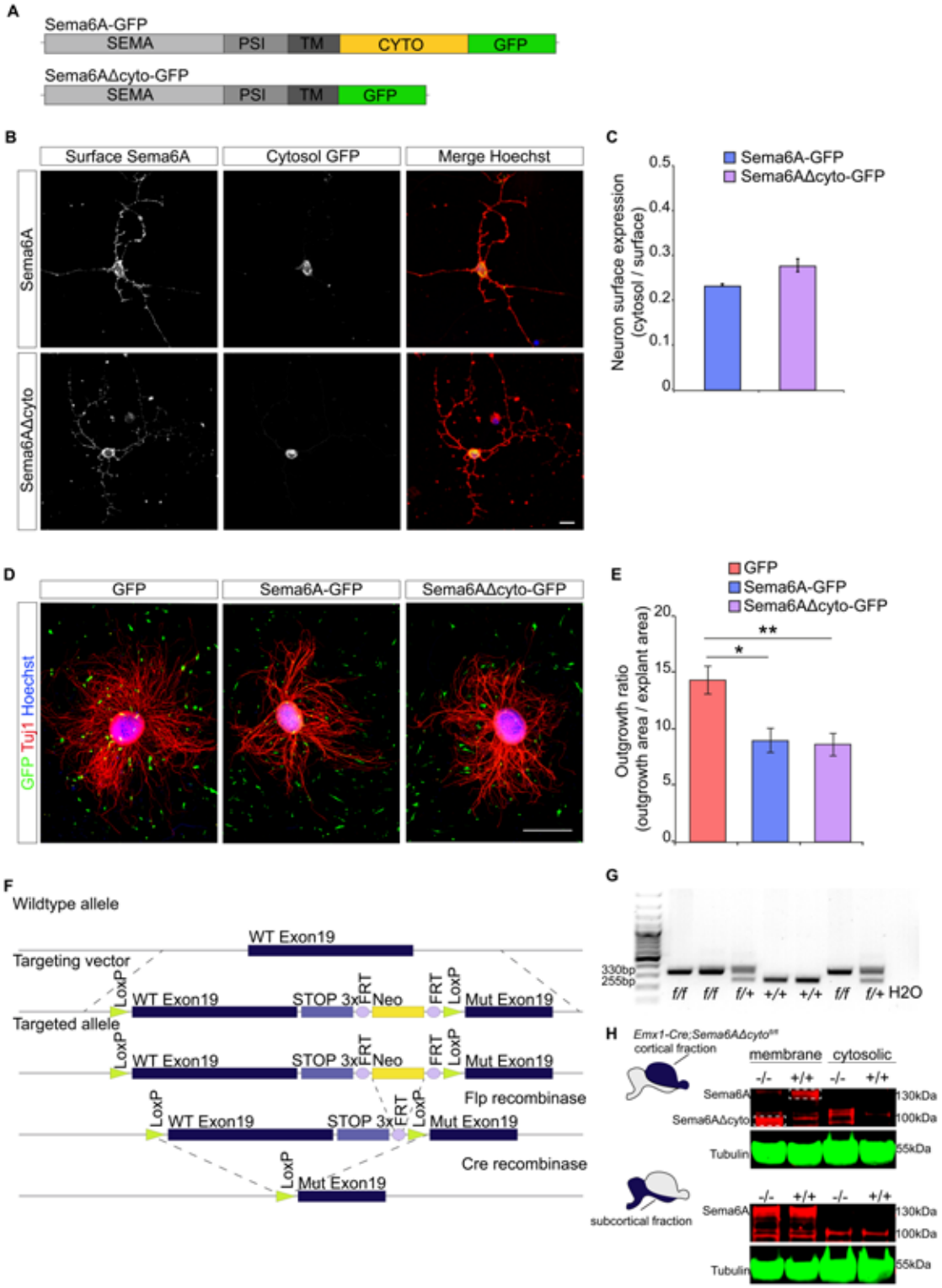
A
Sema6A-GFP
SEMA
PSI
TM
CYTO
GFP
Sema6AΔcyto-GFP
SEMA
PSI
TM
GFP
B
Surface Sema6A
Cytosol GFP
Merge Hoechst
Sema6A
Sema6AΔcyto
C
Sema6A-GFP
Sema6AΔcyto-GFP
Neuron surface expression
(cytosol / surface)
0.5
0.4
0.3
0.2
0.1
0
D
GFP
Sema6A-GFP
Sema6AΔcyto-GFP
GFP Tuj1 Hoechst
E
GFP
Sema6A-GFP
Sema6AΔcyto-GFP
Outgrowth ratio
(outgrowth area / explant area)
20
15
10
5
0
**
*
F
Wildtype allele
WT Exon19
Targeting vector
LoxP
WT Exon19
STOP 3x
FRT
Neo
FRT
LoxP
Mut Exon19
Targeted allele
Flp recombinase
Cre recombinase
G
330bp
255bp
f/f
f/f
f/+
+/+
+/+
f/f
f/+
H2O
H
Emx1-Cre;Sema6AΔcyto
cortical fraction
membrane
cytosolic
-/-
+/+
-/-
+/+
Sema6A
Sema6AΔcyto
Tubulin
130kDa
100kDa
55kDa
subcortical fraction

< Figure 1. Design of Sema6Acyto and *in vitro* and *in vivo* validation experiments. A) Expression validation of Sema6A and Sema6AΔcyto constructs in primary cortical neurons. B) Schematic representation of Sema6A constructs. C) Quantification of surface and cytosolic expression of Sema6A and Sema6AΔcyto showing no significant change. Data presented as means ± SEM, n=3 independent experiments, Student's t-test, p=0.122 surface in relation to cytosol. D) Sema6A ligand function validation in cortical explants co-culture with NIH3T3 cell monolayer expressing Sema6AΔcyto-GFP, Sema6A-GFP or GFP controls. E) Quantification of explant outgrowth for all conditions. Sema6AΔcyto and Sema6A show a, ligand dependent, reduced axonal outgrowth phenotype. The ratio between spanning region and area of the explant was calculated. Bar graphs represent means ± SEM, n=5 experiments, Sema6AΔcyto or Sema6A compared to GFP, p=0.007, p=0.011 respectively, Student's t-test, *p<0.05, **p>0.01. No significant change was detected between Sema6AΔcyto and Sema6A, Student's t-test, p=0.833. F) Schematic representation of transgenic strategy for the conditional knock out mouse model Sema6AΔcyto. Cre-mediated excision of a transcriptional STOP region flanked by *loxP* sites induces the removal of wildtype exon 19. By crossing *Sema6AΔcyto*$^{fl/+}$ with tissue-specific Cre mouse line the floxed region is conditionally removed. Only the 19th exon of a total of 19 exons of the transcript is shown for simplicity. *frt* sites flanking the neomycin cassette. G) Example of PCR analysis using primers against *loxP* sites to determine genotype. H) Cartoon of sagittal mouse brain indicating cortical and subcortical fractions in blue. Cortical tissue shows truncated Sema6AΔcyto protein (97 kDa) located at the membrane in of *Emx1-Cre;Sema6AΔcyto*$^{fl/fl}$ mice. Subcortical tissue shows full length Sema6A (130 kDa) in membrane fractions of *Emx1-Cre;Sema6AΔcyto*$^{fl/fl}$ and control mice. In cytosolic fractions these bands are not detected. Scale bars 20µm (A) 500µm (D).

on transiently transfected NIH3T3 cells. In NIH3T3 cells transfected with Sema6AΔcyto-GFP, the outgrowing axons of the cortical explants show typical repulsive behavior triggered by Sema6A ligand function similar as to NIH3T3 expressing Sema6A-GFP. This effect was compared to NIH3T3 cells transfected with a control construct, expressing GFP only, where no repulsive response was detected in the explants (Fig. 1D). The outgrowth ratio of the explants was decreased for Sema6A and Sema6AΔcyto compared to the GFP control construct (Fig. 1E). Expression levels for Sema6A and Sema6AΔcyto constructs were similar (Fig. S2B, C). GFP was significantly higher expressed compared to Sema6A or Sema6AΔcyto constructs. No difference was found between Sema6A and Sema6AΔcyto constructs (Fig. S2C). Together these results indicate normal processing, expression and ligand function of the Sema6AΔcyto protein.

In order to remove the intracellular domain of Sema6A in mice we further assembled the Sema6A construct in a pcDNA3.1 vector (Invitrogen, Cat #V79020) and designed a construct that contains Sema6A wildtype exon 19 flanked by *loxP* sites and an frt-flanked neomycin cassette inserted at the 5' side followed by a mutated 19th exon (Fig. 1F). The Sema6A cassette was

inserted into a bacterial artificial chromosome (BAC) and electroporated into ES cells. Geomycin (G418) resistant ES cells were selected and checked for correct integration of the construct by PCR and Southern blotting. The transgenic ES cells were subsequently microinjected into pseudo-pregnant females (BALB/c mice) to generate chimeras and bred with C57BL/6 mice to assess germline transmission generating resulting in F1 *Sema6AΔcyto*$^{fl/+}$ mice. Three correctly targeted F1 founder mice were identified and maintained on a *C57BL/6* background. To identify *loxP* sites we obtained tail samples for DNA extraction and PCR analysis resulting in 255bp wildtype and 330bp mutant fragments (Fig. 1G and Supplemental table 1).

Sema6AΔcyto is localized to the cell membrane

Next, we validated that truncated Sema6AΔcyto protein is still expressed on the cell membrane in *Sema6AΔcyto*$^{fl/+}$ mice crossed with *Emx1-Cre* mice. Cortical membrane fractions of *Emx1-Cre;Sema6AΔcyto*$^{fl/fl}$ mice show a truncated Sema6A protein of approximately 97 kDa compared to *Emx1-Cre;Sema6AΔcyto*$^{+/+}$ full length protein of approximately 130 kDa (Fig. 1H, upper panel). In subcortical fractions, full length Sema6A protein is detected in the membrane fractions of *Emx1-Cre;Sema6AΔcyto*$^{fl/fl}$ and control mice (Fig. 1H, lower panel). Cytosolic fractions show a faint signal of residual Sema6A expression.

Neurodevelopmental defects in Sema6AΔcyto mice

Sema6A plays an important role during the development of multiple brain regions. We characterized a new mouse model *Sema6AΔcyto*$^{fl/fl}$ by analyzing multiple neuroanatomical phenotypes that were previously described in *Sema6A*$^{-/-}$ mice [1–15]. We crossed *Sema6AΔcyto*$^{fl/fl}$ with *Ella-Cre* mice to generate *Ella-Cre;Sema6AΔcyto*$^{\Delta/\Delta}$ with germ line deletion of the floxed intracellular domain of Sema6A.

Disturbances in axon pathfinding

In newborn *Ella-Cre;Sema6AΔcyto*$^{\Delta/\Delta}$ and *Sema6A*$^{-/-}$ mice all axons of the posterior limb of the anterior commissure (pAC) fail to project towards the midline and instead growth ventromedially towards the piriform cortex. In wildtype mice, pAC axons cross the midline and establish interhemispheric connectivity patterns (Fig. 2A). The pAC comprises axons of the agranular insular cortex, orbitofrontal cortices and some of the cingulate cortices [24]. We visualized pAC projections with L1CAM-specific antibodies. In this same prefrontal region, 4',6-diamidino-2-fenylindool (DAPI) nuclear staining highlights a change in the morphology of the piriform cortex that

is identified by the high density of pyramidal cell bodies in layer 2. The folding pattern of the piriform cortex is more apparent and exaggerated in *Ella-Cre;Sema6AΔcyto*$^{\Delta/\Delta}$ and *Sema6A*$^{-/-}$ mice. (Fig. 2A). In addition, L1CAM-positive axons from the lateral olfactory tract (LOT), that normally extend superficially in control mice, are displaced in *Ella-Cre;Sema6AΔcyto*$^{\Delta/\Delta}$ and *Sema6A*$^{-/-}$ mice (Fig. 2A).

Another, well described developmental defect in *Sema6A*$^{-/-}$ mice, is found in thalamocortical axon pathfinding [1, 14, 25]. *Ella-Cre;Sema6AΔcyto*$^{\Delta/\Delta}$ and *Sema6A*$^{-/-}$ mice displayed misrouted thalamic axons that fail to project towards the internal capsule and neocortex, but instead grow ventrally. This axonal mislocalization was visualized with anti-L1CAM antibody (Fig. 2B). Lastly, another defect was found in *Ella-Cre;Sema6AΔcyto*$^{\Delta/\Delta}$ and *Sema6A*$^{-/-}$ mice in axon pathfinding during the development of the corticospinal tract [14, 26]. At the border between the medulla and spinal cord, pyramidal tracts normally project dorsally and cross the midline to form the pyramidal decussation and enter the dorsal funiculus. *Ella-Cre;Sema6AΔcyto*$^{\Delta/\Delta}$ and *Sema6A*$^{-/-}$ mice show severe hypoplasia at the level of the pyramidal decussation. Although the few remaining axons cross, the size of the axon bundle is reduced to different degrees from animal to animal and in some instances remains visible as a tight bundle at the ventral surface.

Cellular disturbances in hippocampus, cerebral cortex and cerebellum

Different regions and cell types of the hippocampus are affected by the absence of Sema6A. *Sema6A*$^{-/-}$ mice display a subtle malformation in the molecular layer of the infrapyramidal blade of the dentate gyrus (Fig. 3) [8]. Antibody staining for Prox1 was used to visualize post-mitotic granule cells in the hippocampus. Misplaced prox1-positive granule cells cause a local broadened appearance of the dentate gyrus. This defect was not observed in *Ella-Cre;Sema6AΔcyto*$^{\Delta/\Delta}$ mice (Fig. 3). Further in-depth analysis of the morphology of the dentate gyrus from caudal to rostral regions also did not reveal any disturbances in *Ella-Cre;Sema6AΔcyto*$^{\Delta/\Delta}$ mice (Fig. S3). *PlexinA2*$^{-/-}$ mice display a malformation of the dorsal blade of the dentate gyrus. In addition, granule cell axons, the mossy fibers, form aberrant synaptic connections in the CA3 region of the hippocampus in these mice [13,25,26]. In line with these findings, we detected a severe disturbance in mossy fiber connectivity in the CA3 region in *Emx1-Cre;Sema6AΔcyto*$^{fl/fl}$ mice, suggesting a role for the Sema6A receptor here. *Emx1-Cre;Sema6AΔcyto*$^{fl/}$

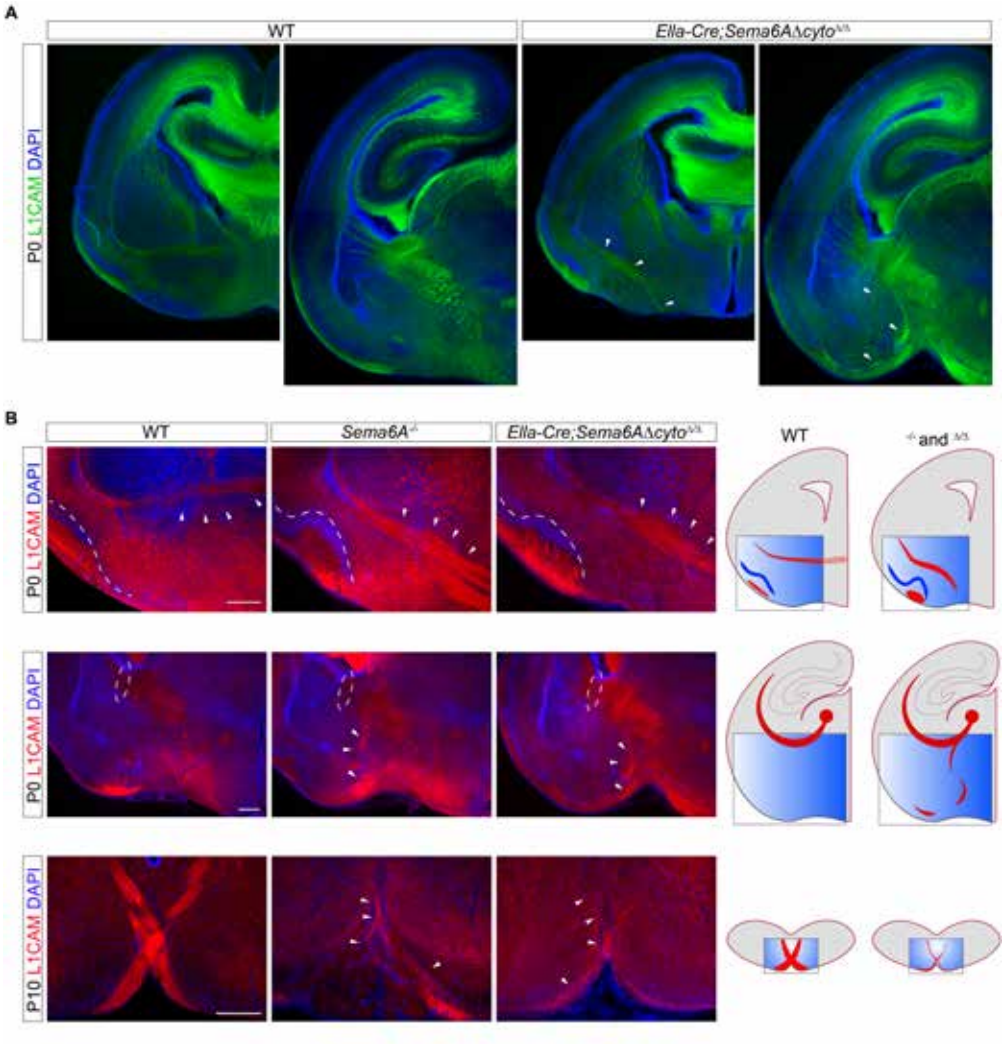

^{fl} mice did not show a malformation of the dorsal blade of the dentate gyrus. For selective labeling of the mossy fibers synaptic boutons, we performed immunohistochemistry using anti-synaptoporin (SPO) and anti-vesicular glutamate transporter 1 (vGLUT1) antibodies. Axons in *Emx1-Cre;Sema6AΔcyto*$^{fl/fl}$ mice fail to innervate the stratum lucidum but instead grow in the stratum pyramidale and oriens (Fig. S4), as described for *PlexinA2*$^{-/-}$ mice [13].

< Figure 2. *Ella-Cre;Sema6AΔcyto*$^{\Delta/\Delta}$ and *Sema6A*$^{-/-}$ mutants have largely overlapping axon guidance defects observed in anterior commissure, piriform cortex, lateral olfactory tract, thalamocortical axon tract and corticospinal tract. A) Anterior commissure axons fail to cross the midline in *Ella-Cre;Sema6AΔcyto*$^{\Delta/\Delta}$ mice. Thalamocortical axons (TCA) fail to grow towards the internal capsule and grow ventrally instead (white arrowheads) in *Ella-Cre;Sema6AΔcyto*$^{\Delta/\Delta}$ mice. B) Representative microscopy images at a higher magnification. In *Ella-Cre;Sema6AΔcyto*$^{\Delta/\Delta}$ and *Sema6A*$^{-/-}$ mice, anterior commissure axons fail to cross the midline and migrate ventrally (white arrowheads indicating axon fibers). Additionally, piriform cortex folding is exaggerated (dotted white line) and the lateral olfactory tract (dotted black line) is no longer superficially located but more in layer 1 in both Sema6A mutants compared to wildtype. B) TCA are misrouted and grow ventrally (white arrowheads) in *Ella-Cre;Sema6AΔcyto*$^{\Delta/\Delta}$ and *Sema6A*$^{-/-}$ compared to wildtype. C) Hypoplasia in the corticospinal tract (CST) at the level of the pyramidal decussation in *Ella-Cre;Sema6AΔcyto*$^{\Delta/\Delta}$ and *Sema6A*$^{-/-}$ (white arrowheads) compared to wildtype. Coronal brain sections show immunohistochemistry experiments with antibodies to visualize rat-anti-L1CAM antibodies (secondary donkey-anti-rat 488 in A, donkey-anti-rat 568 in B) and counterstaining with DAPI (blue) at P0 (A, B) and P10 (B). Schematic representation of AC, TCA and CST defects in *Sema6A*$^{-/-}$ and *Ella-Cre;Sema6AΔcyto*$^{\Delta/\Delta}$ mice. Scale bars 500 µm (A), 100 µm (B), 200 µm (B, CST).

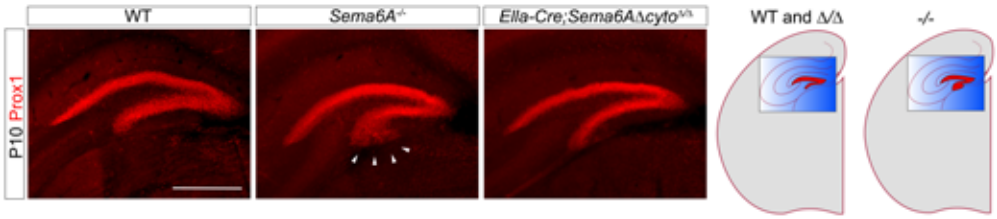

Figure 3. Dentate gyrus malformation found in the absence of Sema6A ligand. Prox1 expression, detected by immunohistochemistry, marking granule cells of the infrapyramidal blade of the dentate gyrus are misplaced in *Sema6A*$^{-/-}$ mice (white arrowheads) but not in *Ella-Cre;Sema6AΔcyto*$^{\Delta/\Delta}$ mice. Coronal sections of the dentate gyrus of P10 *Sema6A*$^{-/-}$, *Ella-Cre;Sema6AΔcyto*$^{\Delta/\Delta}$ and wildtype mice (n=3). Schematic representation of anatomical location in wildtype and Sema6A mutants. Scale bar 500 µm.

In *Sema6A*$^{-/-}$ mice the organization of upper layers of the cerebral cortex was altered [8]. Staining with anti-NeuN antibodies detected a similar defect in the cellular positioning of layer 2/3 neurons in *Ella-Cre;Sema6AΔcyto*$^{\Delta/\Delta}$ mice. The normally distinct border between layer 1 and layer 2/3 was disturbed with increasing severity and cell cluster formation to more lateral regions. Layer 2/3 neurons invaded layer 1, which is normally a cell sparse area devoid of pyramidal neurons [27] (Fig. 4). Previous reports of *Sema6A*$^{-/-}$ mice showed that the defect is detected from developmental timepoint P3 onwards and persists into adulthood. Our data shows that this defect

can be observed earlier, from P2 onwards, and changes dramatically with increasing cell mispositioning and laminar disturbances following the subsequent days and clear ectopic neuronal clusters can be detected at P10 in *Ella-Cre;Sema6AΔcyto*$^{\Delta/\Delta}$ and *Sema6A*$^{-/-}$ mice (Fig. 4) (**Chapter 4**).

Another disturbance in cell migration was found in the cerebellum, which was previously described in *Sema6A*$^{-/-}$ mice [3,10,28]. When Sema6A is absent, cerebellar granule cells, normally switching from tangential migration in the external granule layer (EGL) to radial migration in the molecular layer (ML) stall and remain in the ML of the cerebellum. Only very few cells were able to migrate into the internal granule cell layer (IGL). We repeated and quantified these findings for *Sema6A*$^{-/-}$ mice by injecting bromodeoxyuridine (BrdU) at P15 thereby targeting late-born granule cells [29] and found a similar effect in *Ella-Cre;Sema6AΔcyto*$^{\Delta/\Delta}$ mice at P30 suggesting a role for the Sema6A receptor here (Fig. 5). The cerebellum was subdivided into two zones: the inner zone containing the IGL and the outer zone containing the EGL and ML. In control *Sema6A*$^{+/-}$ and *Ella-Cre;Sema6AΔcyto*$^{\Delta/+}$ mice about 79% of BrdU cells (5690 cells counted, n=5) were detected in the IGL zone. In contrast, 45% of cells reach the IGL in *Sema6A*$^{-/-}$ mice (557 cells counted, n=2) and 48% in *Ella-Cre;Sema6AΔcyto*$^{\Delta/\Delta}$ (1871 cells counted, n=3). In the outer zone, there was a significant increase in BrdU positive cells with 55% in *Sema6A*$^{-/-}$ mice (939 cells counted) and 52% in *Ella-Cre;Sema6AΔcyto*$^{\Delta/\Delta}$ mice (2083 cells counted) compared to 21% in control mice (1667 cells counted) (Kruskal-Wallis test, *p<0.0001).

DISCUSSION

Previous reports show that Sema6A is involved in the development of multiple specific brain areas [1,2,5–14,29]. However, for *Sema6A*$^{-/-}$ mice it is unclear whether these phenotypes are dependent on the ligand and/or the receptor function of Sema6A. The focus of this paper is to distinguish between these two functions by specifically studying the role of the intracellular domain of Sema6A. In order to do this, we designed a Sema6AΔcyto construct in which the intracellular domain of Sema6A is removed while the extracellular domain is retained. *Sema6AΔcyto*$^{fl/fl}$ mice survive embryogenesis, are viable and fertile and show neural developmental defects. Validation experiments show that Sema6AΔcyto protein is still expressed on the cell membrane, due to an intact transmembrane domain. In addition, the ligand function of Sema6A was found to be intact in Sema6AΔcyto constructs and active

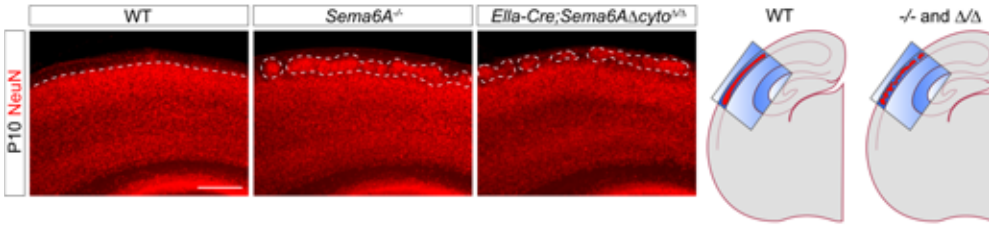

Figure 4 Neuron misplacement found in the neocortex of *Sema6A*$^{-/-}$ and *Ella-Cre;Sema6AΔcyto*$^{Δ/Δ}$ mice. Coronal sections high magnification of misplaced upper cortical layer 2 neurons with increasing severity of cell clustering in lateral cortical regions at P10 (dotted lines). Schematic representation of anatomical location in wildtype and Sema6A mutants. Scale bar 200 µm.

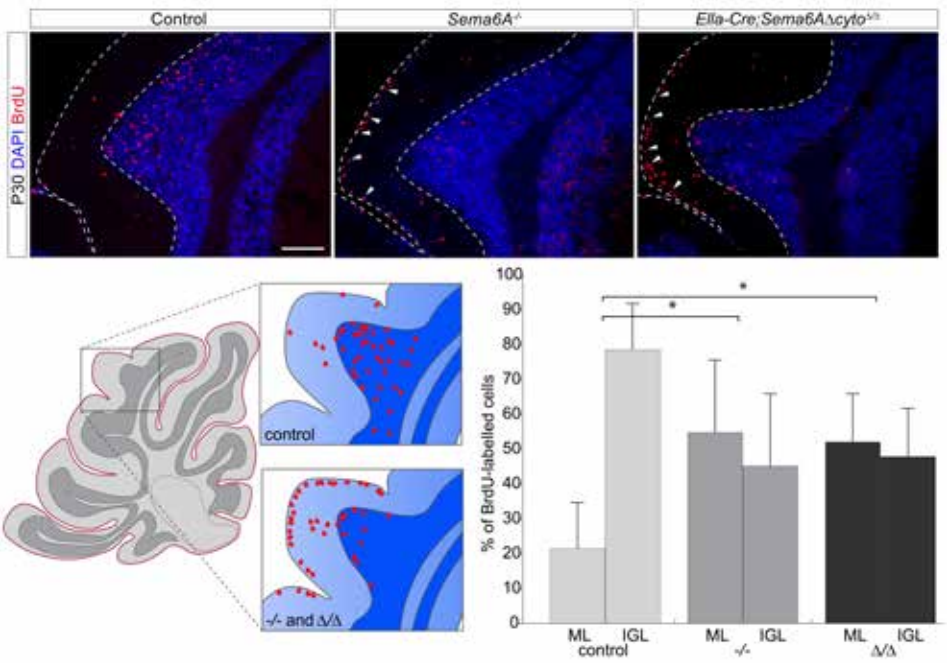

Figure 5. Stalled granule cell migration in external granule layer and the molecular layer of the cerebellum. A) Representative sagittal sections of BrdU immunostaining in the cerebellum of control, *Sema6A*$^{-/-}$ and *Ella-Cre;Sema6AΔcyto*$^{Δ/Δ}$ mice. Outer and inner edge of the external granule layer and molecular layer are marked by the dotted lines. White arrowheads indicate mislocalized BrdU-positive cells. Mice were injected with BrdU (50mg/kg-1) at P15 and processed for immunohistochemistry at P30. B) Schematic representation of the anatomical location within the cerebellum in analyzed tissues. C) Quantification of the distribution of BrdU-positive cells in the ML and IGL corrected for the total area measured at P30. Significant decrease of BrdU-positive cells in the ICL in *Sema6A*$^{-/-}$ and *Ella-Cre;Sema6AΔcyto*$^{Δ/Δ}$ mice. Control animals represent *Sema6A*$^{+/-}$ and *Ella-Cre;Sema6AΔcyto*$^{+/Δ}$ mice. Data are presented as mean percentage ± STDEV, Kruskal-Wallis test *p>0.0001. Control outer zone 21%, inner zone 78%, ± STDEV 13% , *Sema6A*$^{-/-}$ outer zone 54% inner zone 45% ± STDEV 20%, *Ella-Cre;Sema6AΔcyto*$^{Δ/Δ}$ outer zone 52%, inner zone 48%, ± STDEV 13%, Kruskal-Wallis test * p<0.0001. Scale bar 100 µm.

on cortical explants in culture. Outgrowing axons are repelled by Sema6A expressed on NIH3T3 cells and this effect is similar in cells expressing Sema6AΔcyto. Using immunohistochemistry analysis, we provide an overview of observed axon guidance and migration defects in *Sema6AΔcyto*$^{fl/fl}$ mice, that arise during embryonic and early postnatal development of the central nervous system (CNS). The phenotypical changes observed are highly similar to many of the already described defects in *Sema6A*$^{-/-}$ mice [1,2,8,10]. However, in *Sema6A*$^{-/-}$ mice, the development of the infrapyramidal blade of the dentate gyrus was found to be disturbed while *Sema6AΔcyto*$^{fl/fl}$ mice do not display such deficit. This finding suggests that only the ligand function of Sema6A is of importance here to initiate proper development of this structure. In this study, we provide an overview of the anatomical defects found in Sema6AΔcyto mice and show that the intracellular domain of Sema6A is specifically involved in axon pathfinding and organization of the anterior commissure, piriform cortex, lateral olfactory tract, and thalamocortical and corticospinal white matter tracts. Additionally, we found a role in cellular positioning and structural formation in the neocortex and cerebellum.

Interestingly, a previously described defect found in *Sema6A*$^{-/-}$ mice [8] in the dentate gyrus was not detected in *Sema6AΔcyto*$^{fl/fl}$ mice. While the analysis of *Sema6A*$^{-/-}$ mice reveals mispositioning of granule cells in the infrapyramidal blade of the dentate gyrus, *Sema6AΔcyto*$^{fl/fl}$ mice did no display such a deficit suggesting that the intracellular domain of Sema6A is dispensable for proper granule cell distribution. This finding is interesting for two reasons. First, this finding shows the validity of the *Sema6AΔcyto*$^{fl/fl}$ mouse model that while lacking the intracellular domain, the function of the Sema6A ligand through its intact extracellular domain is retained. While other defects previously described for *Sema6A*$^{-/-}$ mice are also found in *Sema6AΔcyto*$^{fl/fl}$ animals, the dentate gyrus develops normally indicating that the Sema6A ligand is functioning normally. Second, the location of the granule cells of the infrapyramidal blade is solely dependent on the Sema6A ligand and not on the receptor. It has been suggested that transmembrane semaphorins can switch between signaling modes in a spatiotemporal dependent manner. For example, Sema6D acts both as a ligand and receptor during heart development or Sema1a showing bidirectional signaling simultaneously [17,18,30]. Depending on the co-expression of interacting molecules, forward or reverse signaling pathways can be activated. These multifunctional and dynamic properties of axon guidance molecules cause an increase in the functional range of axon guidance molecules to

exert multiple functions within one system. However, considering these dynamic and bidirectional properties of Sema6A, these effects seem highly context-dependent since the positioning of granule cells in the dentate gyrus depends on Sema6A ligand without additional roles for its receptor function. In addition to these findings, preliminary data suggest that Sema6A receptor function might be important for the development of the CA3 region of the hippocampus. Previous studies showed that *PlexinA2*$^{-/-}$ mice show a shift and aberrant innervation pattern of mossy fibers growing towards the stratum pyramidale and stratum oriens of the CA3 region [13]. Recently, it was found that and *PlexinA2*$^{R/R}$ mice, that lack PlexinA2 GAP activity and thereby the receptor function of PlexinA2, do not show defects in mossy fiber targeting [26]. Since Sema6A is expressed in the CA3 region, we studied the defect in our *Sema6AΔcyto*$^{fl/fl}$ model. We found that *Emx1-Cre;Sema6AΔcyto*$^{fl/fl}$ mice display a defect in mossy fiber targeting suggesting a role for the Sema6A receptor. Possibly, PlexinA2 and Sema6A interact *in cis* at the same cell surface thereby suppressing the interaction *in trans* between cells [11,31,32]. Alternatively, this interaction may activate the reverse signaling pathway through the Sema6A receptor contributing to the development of the CA3. In support of this idea, commissural/associational fibers, the axons of CA3 pyramidal neurons, express Sema6A that could interact with PlexinA2 *in trans* (Suto et al., 2007). Attenuating these fibers (axons) is necessary for the growth of the mossy fibers in the CA3 region. Activating the reverse signaling pathway could trigger these attenuating and possibly cell-autonomous events that are perhaps not detected as a morphological change but trigger cell intrinsic effects. Alternatively, the Sema6A receptor could affect CA3 pyramidal neuron positioning and area restrictions enabling axon innervation in specific regions (similar to the cortical defect described in **Chapter 4**). These suggestions need to be investigated further.

Thalamocortical axon (TCA) pathfinding was found to be disrupted in *Sema6AΔcyto*$^{fl/fl}$ mice. Normally, Sema6A is expressed on misrouted axons while PlexinA2 and PlexinA4 are expressed in surrounding tissue (Mitosgiannis et al., 2017). This suggest that the mode of action is through the Sema6A receptor. However, since thalamocortical axons migrate over long distances various processes are of influence before the axons reach the cortex. Therefore, it was proposed that guidepost cells that normally express PlexinA2, PlexinA4 and Sema6A are mispositioned which consequently causes the misrouting of the TCAs into the ventral region [6]. Our finding in *Sema6AΔcyto*$^{fl/fl}$ mice supports a direct and cell-autonomous

effect in the axons due to the absence of the intracellular domain. However, we did not study the mispositioning of guidepost cells and therefore an additional defect cannot be excluded and remains to be investigated. Since the initially misrouted TCAs are able to find their target area in the neocortex via alternative routes that run close to the pial surface and the upper layers of the cerebral cortex, we wondered if these anatomical changes could be related to the cortical defect observed in *Sema6A*$^{-/-}$ and *Sema6AΔcyto*$^{fl/fl}$ mouse mutants. The cortical defect and the potential involvement of misrouted TCAs is studied extensively in **Chapter 4**.

Sema6A is widely expressed during development of the nervous system and its loss could therefore affect, in addition to the previously described phenotypes, other systems [33–35]. For example, additional defects in the retina are described for *Sema6A*$^{-/-}$ mice [4,11,12,36]. These defects could be studied in the *Sema6AΔcyto*$^{fl/fl}$ mouse model to determine the role of the intracellular domain in this system. Another defect was previously found in the post-commissural fornix of *Sema6A*$^{-/-}$ mice. However, this phenotype was variable from animal to animal [8]. The fornix was often defasciculated and reduced in size containing fewer axons. These features possibly affect long range connectivity and need to be studied in more detail. Although defects in connectivity patterns in the TCA and CST phenotypes were studied extensively in *Sema6A*$^{-/-}$ mice [6,14], the role for the intracellular domain of Sema6A remains to be determined. The *Sema6AΔcyto*$^{fl/fl}$ mouse model provides an opportunity to explore this and contributes to the information about the role of Sema6A in the nervous system.

Taken together, the *Sema6AΔcyto*$^{fl/fl}$ mouse model provides the possibility to distinguish between ligand and receptor functions of Sema6A through conditional deletion of the intracellular domain of Sema6A. In this study, we have provided an overview of the role of the intracellular domain of Sema6A during nervous system development. To further specify the role of the Sema6A receptor function during development and provide mechanistic insights into the signaling pathway we study the neocortical defect presented in this chapter and in more detail in **Chapter 4**.

METHODS

Mouse lines

All animal use and care were in accordance with institutional guidelines and approved by the Animal Ethics Committee of Utrecht University (Dierexperimenten Ethische Commissie) (CCD licence: AVD115002016532) and conducted in agreement with Dutch laws (Wet op de Dierproeven, 1996, revised 2014) and European regulations. The Sema6A mouse strains used in this study were *Sema6AΔcyto*$^{fl/+}$ and *Sema6A*$^{-/-}$ (Sema6aGt[KST069] Byg)[1] (kindly provided by Keving Mitchell) kept on a *C57BL/6J* background. Timed-pregnant females were 3-6 months of age. The morning on which a vaginal plug was detected was considered embryonic day 0.5 (E0.5). We crossed *Sema6AΔcyto*$^{fl/+}$ with specific Cre lines: *EIIa-Cre* (JAX stock #003800) (Lakso et al., 1996), *Nestin-Cre* (JAX stock #003771) (Tronche et al., 1999) and *Emx1-Cre* (JAX stock #005628) (Gorski et al., 2002) mice obtained from The Jackson Laboratory (see supplemental table for mouse line details) to induce deletion of the *loxP*-flanked intracellular domain of Sema6A in the germ line, CNS or cortex respectively. The specific crosses were referred to as *Ella-Cre;Sema6AΔcyto*$^{\Delta/\Delta}$, *Nestin-Cre;Sema6AΔcyto*$^{\Delta/\Delta}$ and *Emx1-Cre;Sema6AΔcyto*$^{fl/fl}$. To identify *loxP* sites we obtained tail samples for DNA extraction and PCR analysis using primers: Forward, 5′- TGTTGCCACTTCCTCCAAATAGC-3′; Reverse, 5′-GGCACAGCTTGCCAAACATTAAC-3′ resulting in 255bp wildtype and 330bp mutant fragments (Fig. 1G and Supplemental table 1 for program details). Following Cre-specific crosses, excision of the intracellular domain was detected with primers: Forward 5′ - CAGTAGTGCAGCGCAAGGAGAAAGA-3′; Reverse mutant 5′- GGGATTATGTACATGCATCATTGGGCTT-3′; Reverse wildtype 5′- GGGCATTTCACAGTATCTGCGCATAG-3′ resulting in 1000bp wildtype and 1600bp mutant and 600bp recombined mutant fragments (Supplemental table 1). Cre was detected with primers: Forward 5′-GCGGTCTGGCAGTAAAAACTATC-3′; Reverse 5′-GTGAAACA-GCATTGCTGTCACTT-3′. And a wildtype control band with primers: Forward 5′–AAGGTGTGGTTCCAGAATCG-3′; Reverse 5′–CTCTCCACCAGAA-GGCTGAG-3′. Breeding with *C57BL/6* mice expressing Flp-recombinase in the germline produced a heterozygous conditional *Sema6AΔcyto*$^{fl/+}$ line devoid of the neomycin cassette.

Construct design

Sema6A sequences were cloned into the pCAG-GFP vector (Addgene, Cat #11150) to obtain pCAG driven expression of Sema6A and Sema6AΔcyto with a GFP signal sequence located upstream. For assembling the Sema6aΔcyto mouse cassette, Sema6A and *loxP* and *frt* sites were cloned into pcDNA3.1 (Invitrogen, Cat #V79020). The design is based on *Sema6a-transcript 001* (6856bp, 1031aa, ENSMUST00000019791). The integration of a *loxP* site in the large sequence region of intron 18 did not interfere with mRNA splicing. Upon Cre recombinase the cassette is removed and replaced by a mutated exon 19 sequence encoding the transmembrane domain of Sema6A (Fig. 1F).

Cell culture

To assess protein membrane expression, pCAG-GFP, pCAG-Sema6A-GFP or pCAG-Sema6AΔcyto-GFP constructs were studied in both primary cortical neurons and N2A cells. In addition, to assess the ligand function of Sema6A, all three constructs were studied in NIH3T3-cortical explant co-cultures. Cell culture methods were as previously described (van Battum et al., 2014). In short, primary cortical neurons or explants were dissected from P0-P4 *C57BL/6J* mice. Primary neurons were collected in 1x Krebs medium (0.7% NaCl, 0.04% KCl, 0.02% KH_2PO_4, 0.2% $NaHCO_3$ and 0.25% glucose) and dissociated by incubation with 0.25% trypsin in Krebs/EDTA for 10 min at 37°C. The reaction was halted by adding 2 mg soybean trypsin inhibitor, followed by trituration with a fire-polished Pasteur pipette in Krebs medium containing soybean trypsin inhibitor and 20 µg/ml DNAseI. Dissociated cells were resuspended in Neurobasal medium supplemented with B-27, L-glutamine, penicillin/streptomycin and ß-mercaptoethanol. Cells were plated onto poly-L-lysine (20 µg/ml) and laminin (40 µg/ml) coated glass 12mm coverslips in 24 wells plates in a humidified incubator at 37°C and 5% CO_2. Primary cortical neurons were transfected with control, Sema6A and Sema6Acyto constructs using lipofectamine 2000 for 45 minutes. N2A or NIH3T3 cells were plated 1000 cells/well and cultured in DMEM high glucose containing fetal calf serum, L-glutamine and penicillin/streptomycin. Cells reached 70-80% confluency and were switched to DMEM high glucose antibiotics free medium 1 hour prior to transfection with 1ug of control, Sema6A and Sema6Acyto constructs and 1:3 PEI 1 mg/ml (Polyscience) in H2O supplemented with 150mM NaCl. The next day, the transfection medium was replaced by DMEM high glucose without antibiotics. Primary cortical explants were generated by cutting brain slices of 350um with a tissue chopper. The cortex was dissected and cut into small explant pieces

of 100-300um. Explants were plated on NIH3T3 expressing control and Sema6A constructs. Primary neurons or N2A cells and NIH3T3-cortical explant co-cultures were grown for 48 or 72 hours respectively and fixed by adding equal volume of 8% PFA in PBS containing 30% sucrose for 10-30 min at room temperature followed by immunohistochemistry analysis.

BrdU injections

To assess cell proliferation and migration patterns in the cerebellum we used 5-Bromo-2′-deoxyuridine (BrdU) in *Sema6A*$^{-/-}$, *Ella-Cre;Sema6AΔcyto*$^{\Delta/\Delta}$ and control mice. P15 pups where injected intraperitoneal with BrdU (Sigma-Aldrich, 15 mg/ml) 50 mg/kg^{-1} in saline and placed back in the cage with their litter mates and mother. At P30, animals were perfused and processed for immunohistochemistry. Tail tissue was collected for genotyping.

Tissue collection and sectioning

Postnatal pups were euthanized by overdose of Euthanimal (Alfasan) and transcardially perfused with ice-cold phosphate-buffered saline (PBS) followed by 4% paraformaldehyde (PFA). The brains were isolated and incubated overnight in 4% PFA on a slow-speed rocking platform at 4° C. Tissue was washed with PBS, embedded in 4% low melting agarose (Fisher Bioreagents BP165-25) and cut on a vibratome (VT1000S Leica) into 50-60 µm coronal sections, and stored in cryoprotectant solution (30% glycerol, 30% ethyleneglycerol in PBS) at -20 °C or processed for free-floating immunohistochemistry. Brain tissue of BrdU injected animals were incubated in 30% sucrose in PBS and snap-frozen in -40 °C isopentane and stored at -80 °C. For protein fraction analysis dissected brains were directly frozen in isopentane and stored at -80 °C. Frozen brains injected with BrdU were sectioned on a cryostat (Leica CM3050) into 20 µm sagittal sections on superfrost slides.

Immunochemistry

For surface expression analysis, primary neurons and N2A cells were stained using goat anti Sema6A (1:1000, R&D, AF1615) antibodies for 10 minutes at 37C, 5% CO2 incubator. Cells were washed and fixed with 1:1 8% PFA and 30% sucrose for 1 hour at 37C. Cells were blocked in PBS with 5% BSA for 30 min and incubated with Alexa Fluor secondary donkey anti goat 568 (1:1000) in PBS with 2,5% BSA for 1h at RT. Subsequently, cells were treated following immunocytochemistry staining protocol. Cells were fixed with 4% PFA for 10-30 minutes at room temperature and permeabilised

with 0.1% triton in 5% BSA blocking buffer for 30 min at RT. The cytosolic pool of Sema6A-GFP or Sema6AΔcyto-GFP was visualised using rabbit anti GFP (1:1000, A11122 Life Technologies) followed by Alexa Fluor secondary antibody donkey anti rabbit 488 (1:1000) incubation of 1 hour. For primary cortical neurons tubulin was visualized using mouse anti Tuj1 (1:500, MMS-435P Covance) with an Alexa Fluor secondary antibody donkey anti mouse 647 (1:1000) to specifically label neurons. Counterstaining with Hoechst 33258 (#10778843 Fisher) was used to visualize cell nuclei. NIH3T3 expressing cells and primary explants were processed for immunocytochemistry following the same staining protocol described with the exception of blocking for a longer period of time of 1h at RT. For BrdU immunohistochemistry antigen retrieval was required. Sections were incubated in 2N HCL for 30 minutes at 65 °C followed by 10 min incubation in 0.1 M boric acid, ph 8.0. PBS wash and continue IHC normal blocking and antibody incubation protocol using rat anti BrdU (1:500, OBT0030 Accurate) and Alexa Fluor secondary antibody donkey anti rat 568 (1:1000). For tissue sections, immunohistochemistry protocol was as follows. Sections were collected free floating in 12 wells plates or on superfrost slides and washed with PBS. Tissue was blocked in PBS with 5% BSA and 0.1% triton-X in PBS for 1h at RT. Primary antibodies were incubated overnight at 4 °C in 2,5% BSA and 0.1% triton-X in PBS. Hereafter, secondary antibodies were incubated for 2h at RT in 2,5% BSA and 0.1% triton-X in PBS followed by 4',6-diamidino-2-fenylindool (DAPI) (1µg/µl, Sigma, D9564) for 15 minutes at RT. In between steps sections were washed extensively with PBS.

Coverslips and brain sections were mounted using Fluorsave, imaged on an Axioskop EPI-fluorescent microscope (Zeiss) / confocal and processed using FIJI image analysis. For BrdU analysis we used ImageJ ROI and particle analysis plugins to count BrdU positive cells in molecular and inner granule cell layers. To assess BrdU labeling in the cerebellum, the molecular layer and inner granule cell layer were defined as ROIs, followed by particle analysis using FIJI. The number of cells was divided by the area of the ROI to calculate the number of cells/µm and converted into a percentage of cells per region.

Sema6AΔcyto protein expression and localisation

To validate wildtype versus truncated protein expression N2As were transfected with pCAG-Sema6A-GFP and pCAG-Sema6AΔcyto-GFP constructs. 48 hours after transfection, N2As were lysed with RIPA buffer (10mM Tris-buffer pH 7.5, 150mM NaCl, 0.1% SDS, 1% Triton X-100, 1%

Deoxycholate, 0.5mM EDTA, 1mM PMSF and complete protease inhibitor (Roche) and spun down at 12.000 RPM at 4°C for 15 minutes. The protein containing supernatant was isolated and transferred to a new tube. To asses Sema6A localisation to the membrane in *Emx1-Cre;Sema6AΔcyto*$^{fl/fl}$ and *Emx1-Cre;Sema6AΔcyto*$^{fl/+}$ control mice, cytosolic and membrane fractions where prepared using a sucrose buffer (protocol adapted from van Erp et al., 2015). In short, brain tissue was dissected into two samples containing cortices and hippocampi (sample 1) separated from the rest of the brain (sample 2) and snap-frozen in dry ice. Three volumes of fractionation buffer were added to the tissue (0.25M sucrose, 1mM EDTA, 5mM NaCl, 10mM KCL, protease inhibitor 1x and 10mM Tris-HCL pH7.5) followed by homogenization and ultra-centrifugation steps to 1. Nuclei were removed by centrifugation at 1000 g (5000rpm) for 6 min at 4C. 2. Remove cytosolic and membrane fractions from the supernatant after centrifugation at 9.200 g (12500 rpm) at 4C for 15 minutes. And finally, these fractions were separated by centrifugation at 100.000 g at 4C (41000rpm TLA 45 rotor) for 2h, resulting in a cytosol enriched supernatant and a plasma membrane enriched pellet. Cytosol was transferred to a new tube and membrane pellet washed in sucrose buffer and centrifugation at 100.000 g at 4C for 1h. The membrane pellet was resuspended in sucrose buffer (one volumes of original weight starting material). For further analysis, protein samples were supplemented with sample buffer (NuPage, 1:4) and 10% B-mercaptoethanol. Samples were denatured for 10 min at 70 °C and loaded (50 µg) on an 8% gel for SDS-polyacrylamide gel electrophoresis. Protein was transferred from gel to a nitrocellulose membrane (Bio-Rad). For N2A lysates, blots were incubated with the following antibodies: goat anti Sema6A (1:1000, AF1615 R&D), rabbit anti GFP (1:1000, Life Technologies, A11122) followed by the appropriate HRP-conjugated secondary antibody in 1.5% milk in TBS-T. Immunoblots were exposed to Pierce ECL substrate (Thermo Fisher Scientific, 32106) and digitized using an Epson flatbed scanner (Perfection 4990, Epson America). For membrane fractions, blots were incubated with goat anti Sema6A (1:1000, AF1615 R&D) and mouse anti Tuj1 (1:500, MMS-435P Covance) followed by fluorescent secondary antibodies IR800 donkey anti mouse (1:10000) and donkey anti goat 680 (1:10000). Fluorescence was detected using the Odyssey CLx imaging system (Licor).

Acknowledgements

We thank all members of the Pasterkamp laboratory and Department of Translational Neuroscience for assistance and helpful discussions throughout this project. We thank Kevin Mitchell for kindly providing *Sema6A*$^{-/-}$ mice. We thank Roman Giger and the Giger lab for collaborating on the mossy fiber defect. This work was supported by the Netherlands Organization for Health Research and Development (ALW-NOW VICI).

Author Contributions

M.G.V., S.L. and R.J.P. designed all experiments. M.G.V. performed *in vivo* validation experiments. S.L., A.K. and M.G.V. performed to *in vitro* validation experiments. K.J. and M.G.V. performed cerebellar BrdU analysis. C.M. arranged mouse breeding. S.L., K.R., Y.A. and M.G.V. generated Sema6A constructs. M.G.V. and R.J.P. wrote the manuscript with critical feedback from G.M.J.R. and input from all authors.

SUPPLEMENTARY FIGURES

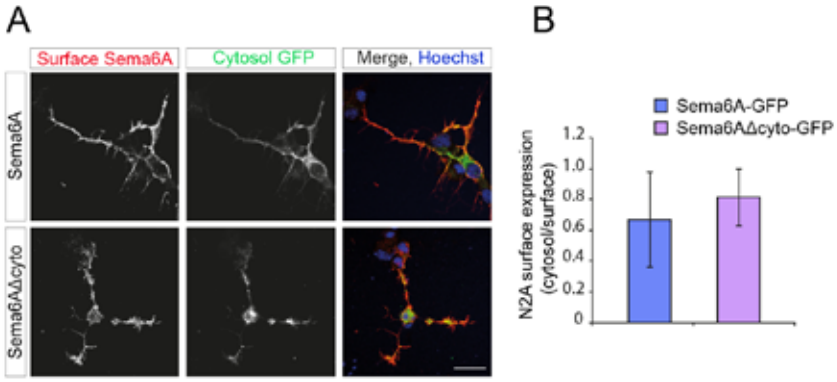

Supplemental figure 1. A) Immunocytochemistry of Sema6A (surface) and GFP (cytosolic) expression of Sema6A-GFP and Sem6AΔcyto-GFP constructs transfected in N2A cells. B) Quantification revealed no differences in cell surface expression in Sema6AΔcyto-GFP compared to Sema6A-GFP calculated as the ratio between surface and cytosolic staining intensity (n=3 experiments, Mean ± SEM, Student's t-test, p=0.293). Scale bar 20 µm.

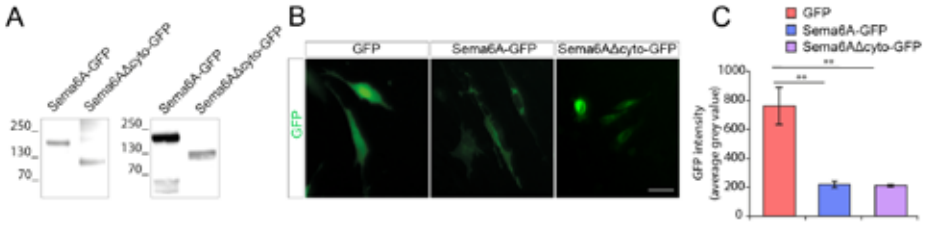

Supplemental figure 2. A. Western blot of Sema6A-GFP and Sem6AΔcyto-GFP overexpressed in N2A cells. Lysates show Sema6A-GFP (160 kDa) and truncated Sem6AΔcyto-GFP (120 kDa) using goat-anti-Sema6A (left panel) and rabbit-anti-GFP (right panel) antibodies. B) NIH3T3 cells transfected with GFP, Sema6A-GFP and Sem6AΔcyto-GFP constructs. C Quantification showed no difference between Sema6A-GFP and Sema6AΔcyto-GFP (n=9 coverslips, Mean ± STDEV, Student's t-test, p=0.770). GFP control construct was significantly higher expressed compared to Sema6A-GFP (**p=0.006) and Sema6AΔcyto-GFP (**p=0.005). Scale bar 40 µm.

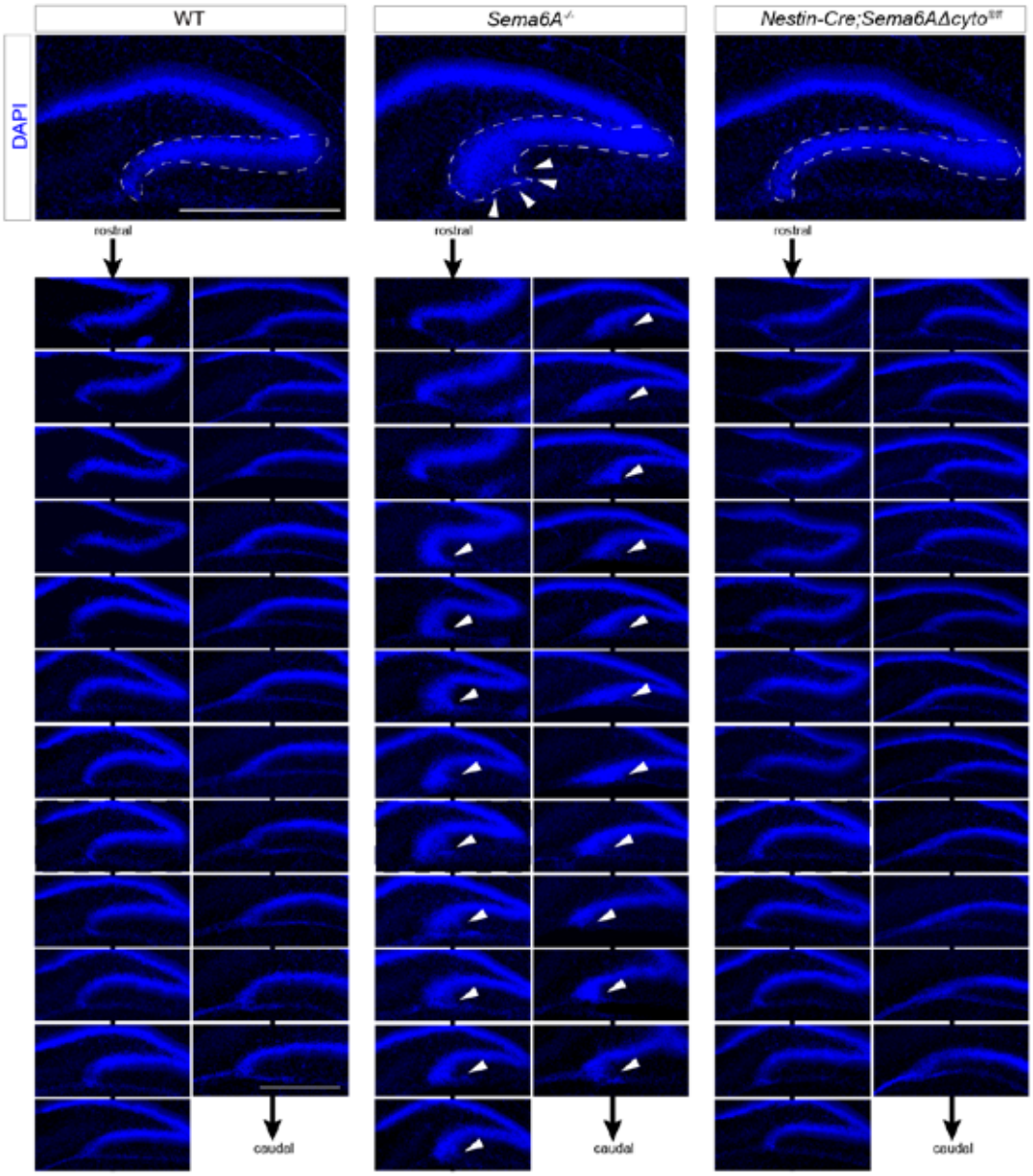

Supplemental figure 3. Extensive overview of the dentate gyrus in the hippocampus showing malformation in *Sema6A*$^{-/-}$ mice. 4',6-diamidino-2-fenylindool (DAPI) nuclear staining showing the dentate gyrus in *Sema6A*$^{-/-}$, *Nestin-Cre;Sema6AΔcyto*$^{fl/fl}$ and control mice at P10. *Sema6A*$^{-/-}$ mice show a broadening of the infrapyramidal blade indicated by the white arrowheads. The entire lower blade of the dentate gyrus is indicated by the dotted line. *Sema6A*$^{-/-}$ mice show malformations indicated by arrowheads from rostral to caudal brain regions shown in 23 coronal sections of 60 µm each. Scale bar 500 µm.

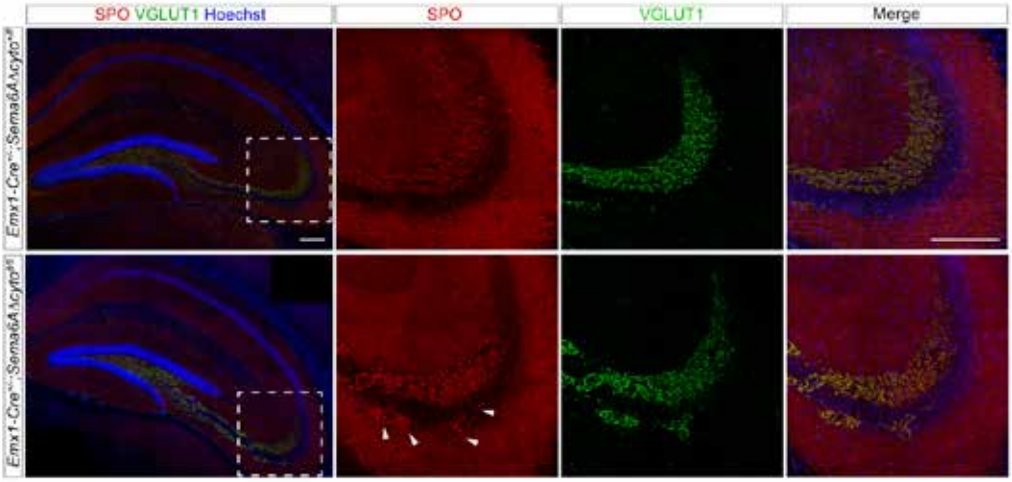

Supplemental figure 4. Sema6A intracellular domain is required for mossy fiber targeting. Immunohistochemistry using anti-SPO and anti-GVLUT1 antibodies to visualize mossy fiber boutons in *Emx1-Cre;Sema6AΔcyto*$^{fl/fl}$ and control at P60. High magnification of the region indicated by the dotted line shows mossy fiber boutons (white arrowheads) in the stratum pyramidale. Scale bar 200 µm.

Supplemental Table 1 PCR programs

Primers from Integrated DNA technology (IDT)	PCR program		Analysis
Aim: identify loxP sites	95˚C	3′	1,5 % agarose gel
Primer 1 forward loxP:	95˚C	30″	
5′-TGTTGCCACTTCCTCCAAATAGC-3′	55˚C	30″	Mutant: ~ 330bp
Primer 2 reverse loxP:	72˚C	30″	Wildtype: ~ 255bp
5′-GGCACAGCTTGCCAAACATTAAC-3′	Repeat 34x		
	72˚C	5′	
	10˚C	∞	
Aim: confirm Cre recombination	95˚C	3′	1 % agarose gel
Primer 1 Forward	95˚C	30″	
5′-CAGTAGTGCAGCGCAAGGAGAAAGA-3′	60˚C	30″	Excised: ~ 600 bp
Primer 2 Reverse mutant	72˚C	2′	Mutant: ~ 1600 bp
5′-GGGATTATGTACATGCATCATTGGGCTT-3′	Repeat 34x		Wildtype: ~ 1000 bp
Primer 3 Reverse wildtype	72˚C	5′	
5′-GGGCATTTCACAGTATCTGCGCATAG-3′	10˚C	∞	
Aim: Cre detection	95˚C	3′	1,5% agarose gel
Primer 1 Forward	95˚C	30″	
5′-GCGGTCTGGCAGTAAAAACTATC-3′	58˚C	30″	Mutant: 100~ bp
Primer 2 Reverse	72˚C	30″	Wildtype: 380~ bp
5′-GTGAAACAGCATTGCTGTCACTT-3′	Repeat 40x		
Primer 3 Forward	72˚C	10′	
5′–AAGGTGTGGTTCCAGAATCG-3′	10˚C	∞	
Primer 4 Reverse			
5′–CTCTCCACCAGAAGGCTGAG-3′			

Supplemental Table 2 Mouse lines

Mouseline	Reference	Source	RRID
EIIa-Cre	The Jackson Laboratory [37]	JAX:003724	IMSR_JAX:003724
ACTB-Flpe	The Jackson Laboratory [38]	JAX: 003800	IMSR_JAX:003800
EMX1-IRES-Cre (Emx1$^{tm1(cre)Krj}$)	The Jackson Laboratory [39]	JAX: 005628	IMSR_JAX:005628
Nestin-Cre (Tg(Nes-cre)1Kln)	The Jackson Laboratory [40]	JAX: 003771	IMSR_JAX: 003771
Sema6A$^{-/-}$ (Sema6aGt[KST069]Byg)	[1]	Provided by Kevin Mitchell	MGI:3037891
Sema6AΔcyto$^{fl/+}$	Biocytogen		
C57BL/6J	Charles Rivers Laboratories		IMSR_JAX:000664

Supplemental Table 3 Primary antibodies and plasmids

Antibody	Dilution	Reference #	RRID
Mouse anti NeuN	1:1000	Abcam, Cat# ab104224	AB_10711040
Rabbit anti Prox1	1:1000	Abcam, Cat# ab101851	AB_10712211
Rat anti L1CAM	1:500	Millipore, Cat# MAB5272	AB_2133200
Rat anti BrdU	1:500	Accurate, Cat# OBT0030	AB_2313756
Goat anti Sema6A	1:1000	R&D, Cat # AF1615	AB_2185995
Mouse anti Tuj1	1:500	Covance, Cat# MMS-435P	AB_2313773
Rabbit anti GFP	1:1000	Life Technologies, Cat# A11122	AB_221569

Construct	Company	Reference #
pCAG-GFP	Addgene	Cat# 11150
Sema6A-GFP	In house cloning	
Sema6AΔcyto-GFP	In house cloning	
Sema6AΔcyto$^{fl/fl}$	In house cloning	

REFERENCES

1. Leighton, P. A. *et al.* Defining brain wiring patterns and mechanisms through gene trapping in mice. *Nature* 410, 174–179 (2001).
2. Rünker, A. E., Little, G. E., Suto, F., Fujisawa, H. & Mitchell, K. J. Semaphorin-6A controls guidance of corticospinal tract axons at multiple choice points. *Neural Dev.* 3, 34 (2008).
3. Renaud, J. & Chédotal, A. Molecular and Cellular Neuroscience Time-lapse analysis of tangential migration in Sema6A and PlexinA2 knockouts. *Mol. Cell. Neurosci.* 63, 49–59 (2014).
4. Lilley, B. N. *et al.* Genetic access to neurons in the accessory optic system reveals a role for Sema6A in midbrain circuitry mediating motion perception. *J. Comp. Neurol.* (2019). doi:10.1002/cne.24507
5. Matsuoka, R. L. *et al.* Transmembrane semaphorin signalling controls laminar stratification in the mammalian retina. *Nature* 470, 259–263 (2011).
6. Mitsogiannis, M. D., Little, G. E. & Mitchell, K. J. Semaphorin-Plexin signaling influences early ventral telencephalic development and thalamocortical axon guidance. *Neural Dev.* 12, 6 (2017).
7. Sun, L. O. *et al.* Functional Assembly of Accessory Optic System Circuitry Critical for Compensatory Eye Movements. *Neuron* 86, 971–984 (2015).
8. Rünker, A. E. *et al.* Mutation of Semaphorin-6A Disrupts Limbic and Cortical Connectivity and Models Neurodevelopmental Psychopathology. *PLoS One* 6, e26488 (2011).
9. Little, G. E. *et al.* Specificity and Plasticity of Thalamocortical Connections in Sema6A Mutant Mice. *PLoS Biol.* 7, e1000098 (2009).
10. Kerjan, G. *et al.* The transmembrane semaphorin Sema6A controls cerebellar granule cell migration. *Nat. Neurosci.* 8, 1516–1524 (2005).
11. Sun, L. O. *et al.* On and Off Retinal Circuit Assembly by Divergent Molecular Mechanisms. *Science (80-.).* 342, 1241974–1241974 (2013).
12. Belle, M., Parray, A., Belle, M., Chédotal, A. & Nguyen-Ba-Charvet, K. T. PlexinA2 and Sema6A are required for retinal progenitor cell migration. *Dev. Growth Differ.* 58, 492–502 (2016).
13. Suto, F. *et al.* Interactions between Plexin-A2, Plexin-A4, and Semaphorin 6A Control Lamina-Restricted Projection of Hippocampal Mossy Fibers. *Neuron* (2007). doi:10.1016/j.neuron.2007.01.028
14. Okada, T., Keino-Masu, K., Suto, F., Mitchell, K. J. & Masu, M. Remarkable complexity and variability of corticospinal tract defects in adult Semaphorin 6A knockout mice. *Brain Res.* (2019). doi:10.1016/j.brainres.2018.12.041
15. Renaud, J. *et al.* Plexin-A2 and its ligand, Sema6A, control nucleus-centrosome coupling in migrating granule cells. *Nat. Neurosci.* (2008). doi:10.1038/nn2064

16. Alto, L. T. & Terman, J. R. Semaphorins and their Signaling Mechanisms. in *Methods in Molecular Biology* 1–25 (2017). doi:10.1007/978-1-4939-6448-2_1
17. Godenschwege, T. A., Hu, H., Shan-Crofts, X., Goodman, C. S. & Murphey, R. K. Bi-directional signaling by semaphorin 1a during central synapse formation in Drosophila. *Nat. Neurosci.* (2002). doi:10.1038/nn976
18. Jeong, S., Juhaszova, K. & Kolodkin, A. L. The Control of Semaphorin-1a-Mediated Reverse Signaling by Opposing Pebble and RhoGAPp190 Functions in Drosophila. *Neuron* (2012). doi:10.1016/j.neuron.2012.09.018
19. Jeong, S. *et al.* Varicose and cheerio collaborate with pebble to mediate semaphorin-1a reverse signaling in *Drosophila*. *Proc. Natl. Acad. Sci.* (2017). doi:10.1073/pnas.1713010114
20. Yu, L., Zhou, Y., Cheng, S. & Rao, Y. Plexin A-Semaphorin-1a Reverse Signaling Regulates Photoreceptor Axon Guidance in Drosophila. *J. Neurosci.* (2010). doi:10.1523/JNEUROSCI.1494-10.2010
21. Sun, L. O. *et al.* Functional Assembly of Accessory Optic System Circuitry Critical for Compensatory Eye Movements. *Neuron* (2015). doi:10.1016/j.neuron.2015.03.064
22. Mauti, O., Domanitskaya, E., Andermatt, I., Sadhu, R. & Stoeckli, E. T. Semaphorin6A acts as a gate keeper between the central and the peripheral nervous system. *Neural Dev.* 2, 28 (2007).
23. Sauer, B. Functional expression of the cre-lox site-specific recombination system in the yeast Saccharomyces cerevisiae. *Mol. Cell. Biol.* (1987). doi:10.1128/MCB.7.6.2087.Updated
24. Wise, S. P. Forward frontal fields: phylogeny and fundamental function. *Trends Neurosci.* (2008). doi:10.1016/j.tins.2008.08.008
25. Tawarayama, H., Yoshida, Y., Suto, F., Mitchell, K. J. & Fujisawa, H. Roles of Semaphorin-6B and Plexin-A2 in Lamina-Restricted Projection of Hippocampal Mossy Fibers. *J. Neurosci.* 30, 7049–7060 (2010).
26. Zhao, X.-F. *et al.* PlexinA2 Forward Signaling through Rap1 GTPases Regulates Dentate Gyrus Development and Schizophrenia-like Behaviors. *Cell Rep.* (2018). doi:10.1016/j.celrep.2017.12.044
27. Ma, J., Yao, X. H., Fu, Y. & Yu, Y. C. Development of layer 1 neurons in the mouse neocortex. *Cereb. Cortex* (2014). doi:10.1093/cercor/bht114
28. Renaud, J. *et al.* Plexin-A2 and its ligand, Sema6A, control nucleus-centrosome coupling in migrating granule cells. *Nat. Neurosci.* 11, 440–449 (2008).
29. Renaud, J. & Chédotal, A. Time-lapse analysis of tangential migration in Sema6A and PlexinA2 knockouts. *Mol. Cell. Neurosci.* 63, 49–59 (2014).
30. Toyofuku, T. *et al.* Guidance of myocardial patterning in cardiac development by Sema6D reverse signalling. *Nat. Cell Biol.* (2004). doi:10.1038/ncb1193

31. Perez-Branguli, F. *et al.* Reverse Signaling by Semaphorin-6A Regulates Cellular Aggregation and Neuronal Morphology. *PLoS One* 11, e0158686 (2016).
32. Haklai-topper, L., Mlechkovich, G., Savariego, D., Gokhman, I. & Yaron, A. Cis interaction between Semaphorin6A and Plexin-A4 modulates the repulsive response to Sema6A. *EMBO J.* 29, 2635–2645 (2010).
33. Xu, X. *et al.* The Transmembrane Protein Semaphorin 6A Repels Embryonic Sympathetic Axons. 20, 2638–2648 (2000).
34. Bernard, F. *et al.* Role of transmembrane semaphorin Sema6A in oligodendrocyte differentiation and myelination. *Glia* 60, 1590–1604 (2012).
35. Okada, A. & Tomooka, Y. A role of Sema6A expressed in oligodendrocyte precursor cells. *Neurosci. Lett.* 539, 48–53 (2013).
36. Matsuoka, R. L. *et al.* Transmembrane semaphorin signalling controls laminar stratification in the mammalian retina. *Nature* 470, 259–263 (2011).
37. Lakso, M. *et al.* Efficient in vivo manipulation of mouse genomic sequences at the zygote stage. *Proc. Natl. Acad. Sci. U. S. A.* (1996). doi:10.1073/pnas.93.12.5860
38. Rodríguez, C. I. *et al.* High-efficiency deleter mice show that FLPe is an alternative to Cre- loxP. *Nature Genetics* (2000). doi:10.1038/75973
39. Gorski, J. a *et al.* Cortical excitatory neurons and glia, but not GABAergic neurons, are produced in the Emx1-expressing lineage. *J. Neurosci.* 22, 6309–6314 (2002).
40. Tronche, F. *et al.* Disruption of the glucocorticoid receptor gene in the nervous system results in reduced anxiety. *Nat. Genet.* (1999). doi:10.1038/12703

CHAPTER 4

Development of cortical layer 2/3 neuron positioning and laminar organization depend on Semaphorin6A reverse signaling

Marieke G. Verhagen[1], Suzanne Lemstra[1], Melissa Zwaan[1], Kati Rehberg[1], Christiaan van der Meer[1], Youri Adolfs[1], Eljo Y. van Battum[1], Josien Beuling[1], Marleen H. van den Munkhof[1], Geert M. J. Ramakers[1], R. Jeroen Pasterkamp[1]

[1] Department of Translational Neuroscience, UMC Utrecht Brain Center, University Medical Center Utrecht, Utrecht University, The Netherlands

Highlights

- Sema6AΔcyto mice show cortical layer 2/3 mispositioning and lamination defects
- Sema6A but not Sema6AΔAbl recues cortical layer 2/3 defects
- PlxnA2/A4-Sema6A reverse signaling regulates layer 2/3 neuron positioning and laminar organization
- Lack of Sema6A receptor function disrupts cortico-cortical connectivity patterns

ABSTRACT

The axon guidance molecule Semaphorin6A (Sema6A) plays key roles during nervous system development. Sema6A is a transmembrane protein that depending on the molecular and cellular context induces forward and/or reverse signaling. To study the receptor and ligand functions of Sema6A, we generated a new conditional mouse model (*Sema6AΔcyto*$^{fl/fl}$) that, when crossed with Cre-specific mouse lines, lacks the Sema6A intracellular domain which is essential for the receptor function. In this mouse model, the Sema6A intracellular domain can be ablated in a spatiotemporally controlled manner. Immunohistochemistry analysis revealed developmental defects in multiple specific brain structures (**Chapter 3**). Here we show that, in the absence of the Sema6A cytoplasmic domain, cortical neuron mispositioning and lamination defects are observed. Following their migration, layer 2/3 pyramidal neurons formed ectopic neuronal clusters in cortical layer 1, displayed altered morphology and were intermingled with neighboring neurons and other cell types. *In utero* electroporation experiments showed that these defects rely on PlexinA2-Sema6A reverse signaling in pyramidal neurons in a non-cell autonomous manner and occur at early postnatal stages to establish final laminar organization. Overall, our findings indicate that the Sema6A cytoplasmic domain is essential for proper development of the cerebral cortex and that Sema6A and PlexinA2 are indispensable for proper positioning of layer 2/3 pyramidal neurons.

INTRODUCTION

During development of the cerebral cortex (corticogenesis), newly born neurons migrate over long distances from their site of origin to a specific target area following highly controlled routes and guideposts. The cortex consists of 6 layers that are gradually structured in an inside-out pattern 1,2. Upper layer neurons pass the early born deeper layers to settle superficially at the pial surface. After this, neurons find the proper target position and start to mature and establish connectivity patterns and complex networks. The proper distribution of cells during development is essential in order to create the 6 layered cytoarchitecture of the cortex. The mechanism behind the cellular distribution and cortical layer formation remains largely unknown.

The final cortical layers to emerge are layer 2/3 which concludes the gradual process of radial migration during late embryonic and early postnatal development [3,4]. Layer 2/3 projection neurons extend a single leading process through the cortical plate (CP) towards the pial surface after which they detach from the radial glia scaffold and execute terminal somal translocation [5,6]. The leading process of the neurons then gives rise to the apical dendrite that branches and expands rapidly into the marginal zone (MZ) [4]. The marginal zone is the predecessor of cortical layer 1. The division between cortical layer 1 and layer 2/3 is unique due to the sharp contrast in cell soma density between the two regions. While most laminar boundaries are not readily detectable, the border between layer 1 and layer 2/3 is clear. Layer 1 is sparsely populated and almost devoid of excitatory neurons while layer 2/3 is densely populated with this cell type. The proper positioning of layer 2/3 neurons during the final stages of cortical migration is essential to maintain the sparsely populated layer 1. After migration, layer 2/3 neurons continue to mature by expanding dendrites thereby contributing to the increase in thickness of the cortex and postnatal brain growth [7]. Layer 1 contains a high density of fibers that represent the projections from the cortical layers below, corticocortical axons, thalamic nuclei projections, subcortical axons, a small population of mostly inhibitory cells, and the intensively studied horizontal cells described by Ramón y Cajal and Retzius [8–13]. The apical dendrites of layer 2/3 neurons are targeted by the short- and long-range axonal projections arriving in layer 1 [13–16]. Proper neuron positioning and laminar organization is essential to prevent disruption of cellular maturation in order to develop functional neuronal circuits [17]. It is unclear how the correct cell distribution and organization of layer 1 and layer 2/3 is established.

Here, we found a novel role for Semaphorin6A (Sema6A), classically known to function as an axon guidance molecule during nervous system development [18], in the proper positioning of layer 2/3 neurons that is essential for cell distribution and laminar organization. Semaphorin6A (Sema6A) is a transmembrane protein that depending on the cellular context can trigger various signaling pathways and plays a key role during the development of the nervous system. It is a bidirectional cue that besides its ligand function, involved in forward signaling, can act as a receptor in the reverse signaling pathway [19–22]. Despite the clear roles for Sema6A as a ligand in forward signaling, the function of the Sema6A receptor and reverse signaling pathway *in vivo* remains unknown. Our findings address this by identifying a specific role for the Sema6A receptor in the organization of layer 2/3 neurons during cortical development. We found that in the absence of the Sema6A intracellular domain, which is essential for its receptor function, multiple developmental defects occur (**Chapter 3**). In *Ella-Cre;Sema6AΔcyto*$^{\Delta/\Delta}$ (**Chapter 3**) and *Sema6A*$^{-/-}$ mice [23], layer 2/3 neurons are mispositioned and form clusters resulting in the disruption of the organization of layer 1 and layer 2/3. In this study, we set out to determine the specific role for Sema6A and its receptor function during the development of layer 2/3 cellular distribution and laminar organization of the cortex. We identified a specific role for one of the main interactors of Sema6A: PlexinA2 (PlxnA2), that shows specific protein expression in the apical dendrites of layer 2/3 neurons. In addition, we study the spatiotemporal development of the cortical defect and confirm the role of the reverse signaling pathway in layer 2/3 neurons by *in utero* electroporation experiments. Lastly, we present multi-omics data that help to understand the mechanism underlying the reverse signaling pathway and to identify novel interactors of Sema6A involved in cortical development.

RESULTS

Cortical defect in *Sema6AΔcyto*$^{fl/fl}$ mice

To study the role of Sema6A during cortical development we studied multiple Sema6A mouse models. The development of the cerebral cortex was affected in *Sema6AΔcyto*$^{fl/fl}$ mice crossed with specific Cre lines to conditionally remove the intracellular domain of Sema6A. *Ella-Cre;Sema6AΔcyto*$^{\Delta/\Delta}$ mice showed a defect in the lamination and cell positioning of cortical layer 2/3 neurons at P10. Neuronal clusters were found in the lateral and caudal brain regions (Fig. 1A, B). The sharp border between layer 1 and layer 2/3 was

also disturbed in the more medial and rostral regions, however, no neuronal clusters were detected (Fig. 1C, B. Heterozygous mice were used as control unless otherwise noted. Structural analysis of cortical layer 2/3 showed a significant increase in intensity fluctuations of anti-neuronal nuclear protein (NeuN) staining in *Ella-Cre;Sema6AΔcyto*$^{\Delta/\Delta}$ mice (Intensity Profile Plot, ImageJ software) reflecting the presence of neuronal clusters (Fig. 1C). Cortical thickness, measured from the ventricular zone up to the pial surface was unchanged (Fig. 1A, C). The mispositioning of layer 2/3 neurons in *Ella-Cre;Sema6AΔcyto*$^{\Delta/\Delta}$ mice, which lack the intracellular domains of Sema6A, suggests a role for the Sema6A reverse signaling pathway during cortical development. The overall integrity of the upper cortical layers of *Ella-Cre;Sema6AΔcyto*$^{\Delta/\Delta}$ mice was analyzed with Golgi-Cox staining and showed disturbances in cellular positioning (Fig. 1D). Besides the mispositioned pyramidal neurons (indicated by red arrows), other cells types seemed to be affected and intermingled with the neurons. Immunohistochemistry staining showed that GFAP-positive astrocytes were located in neuronal clusters suggesting multiple cell types are affected (Fig. S1). A similar defect was found in *Ella-Cre;HASema6A*$^{\Delta/\Delta}$ (full) knockout mice (Fig. 1E). *HASema6A*$^{fl/fl}$ mice were kindly provided by A. Kolodkin. In addition, we repeated the original experiment in *Sema6A*$^{-/-}$ mice, previously described by Rünker et al. [23] and found layer 2/3 mispositioning and neuronal clusters (Fig. 1E). To identify and narrow down the origin of the cortical defect we analyzed *Sema6AΔcyto*$^{fl/fl}$ mice crossed with different Cre lines. To target whole brain, cortex or thalamus we used *Nestin-Cre*, *Emx1-Cre*, and *GBX2-Cre* mice, respectively. *Nestin-Cre; Sema6AΔcyto*$^{fl/fl}$ mice showed neuronal clusters detected at P10 (Fig. 1E). *Emx1-Cre; Sema6AΔcyto*$^{fl/fl}$ mice displayed a somewhat milder, however prevalent defect suggesting a cortical origin (Fig. 1E). Thalamocortical axon (TCA) pathfinding is affected in *Sema6A*$^{-/-}$ mice (Leighton et al., 2001; Little et al., 2009; Mitsogiannis et al., 2017) and *Ella-Cre;Sema6AΔcyto*$^{\Delta/\Delta}$ (**Chapter 3**). Interestingly, misrouted TCAs are able to find their target area in the neocortex via alternative routes that run close to the pial surface and the upper layers of the cerebral cortex. These anatomical changes might consequently affect the neuronal organization of layer 2/3 in the cortex. However, in the absence of Sema6A in the thalamus of *GBX2-Cre; Sema6AΔcyto*$^{fl/fl}$ no neuronal mispositioning was observed suggesting layer 2/3 mispositioning is independent of thalamic input to upper cortical layers (Fig. 1E).

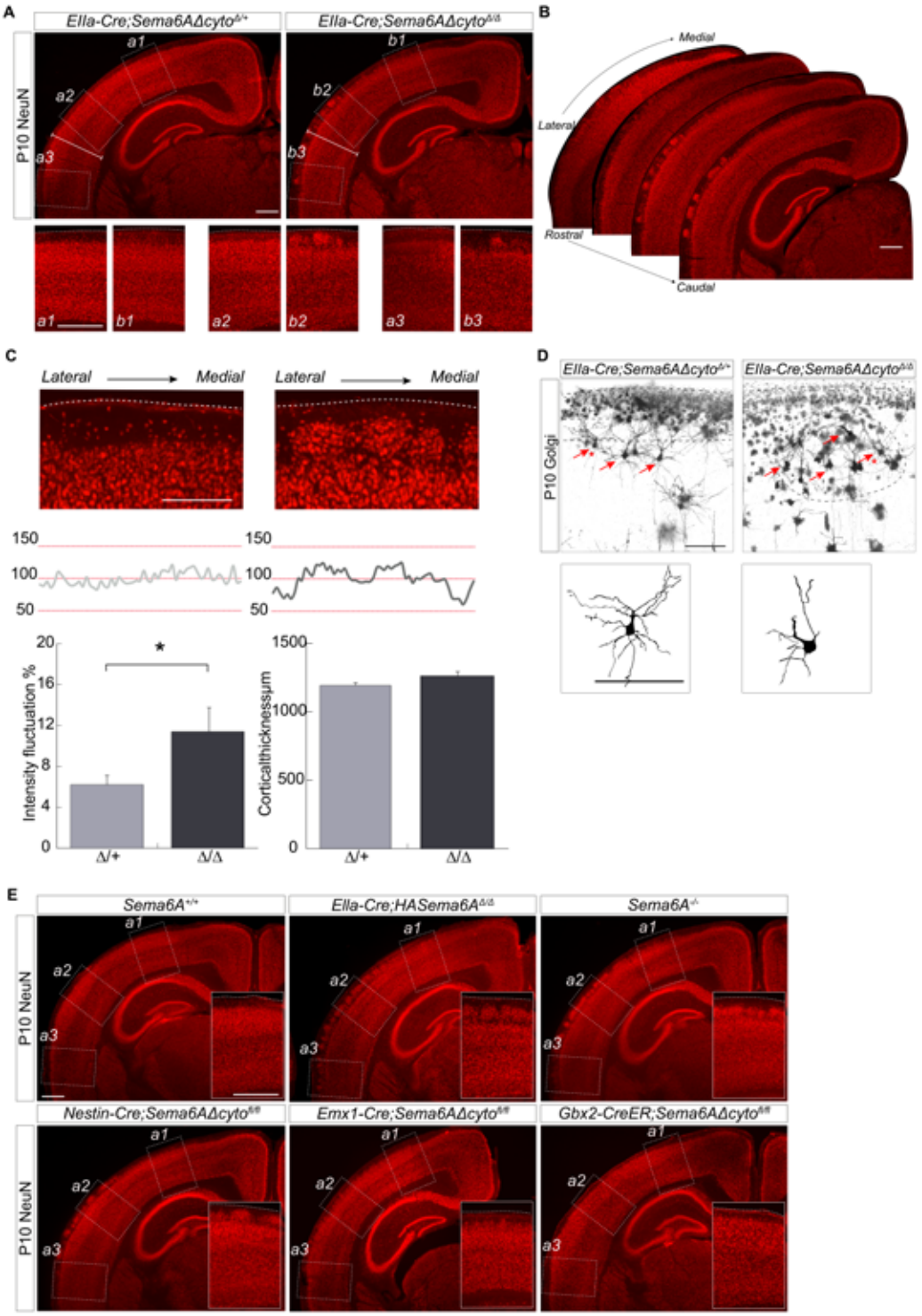
A
Ella-Cre;Sema6AΔcyto$^{\Delta/+}$
Ella-Cre;Sema6AΔcyto$^{\Delta/\Delta}$
P10 NeuN
a1
a2
a3
b1
b2
b3
B
Medial
Lateral
Rostral
Caudal
C
Lateral
Medial
150
100
50
Intensity fluctuation %
20
16
12
8
4
0
Δ/+
Δ/Δ
Corticalthicknessμm
1500
1000
500
D
P10 Golgi
E
Sema6A$^{+/+}$
Ella-Cre;HASema6A$^{\Delta/\Delta}$
Sema6A$^{-/-}$
Nestin-Cre;Sema6AΔcyto$^{fl/fl}$
Emx1-Cre;Sema6AΔcyto$^{fl/fl}$
Gbx2-CreER;Sema6AΔcyto$^{fl/fl}$

< Figure 1. Cortical cytoarchitecture of *Sema6AΔcyto$^{fl/fl}$* mice.
A) Immunohistochemistry staining against NeuN on coronal sections of *Ella-Cre; Sema6AΔcyto$^{\Delta/\Delta}$* mice at P10. Layer 2/3 shows a laminar disturbance with ectopic neuronal clusters invading layer 1. Panels a1-a3 and b1-b3 indicated by the dotted lines specify different areas of the cerebral cortex. Panels are shown at higher magnification directly below comparing control a1-a3 to mutant b1-b3 areas showing a varying degree of neuron mispositioning and clustering. B) Coronal sections showing neuronal clusters that appear in a gradient with low medial-rostral and high lateral-caudal occurrence. C) Intensity plot profile showing intensity fluctuation measurement of NeuN staining (ranging between 50-150 pixel values for 8-bit epifluorescent microscopy images) in layer 1 and layer 2/3 of the cortex. Bar histogram showing average intensity fluctuation percentage with a significant increase in *Ella-Cre;Sema6AΔcyto$^{\Delta/\Delta}$* compared to control (Mean ± SEM, Student's t-test *p<0.00.01). Cortical thickness is unchanged (Mean ± SEM, Student's t-test p=0.38). D) Golgi-Cox staining of *Ella-Cre;Sema6AΔcyto$^{\Delta/\Delta}$* and control coronal sections at P10. Example images showing cell soma's located in layer 2/3 in control and located in layer 1 and layer 2/3 in *Ella-Cre;Sema6AΔcyto$^{\Delta/\Delta}$* (red arrows). Dotted line indicates the border between layer 1 and layer 2/3 in control and the area with mispositioned neurons in *Ella-Cre;Sema6AΔcyto$^{\Delta/\Delta}$*. Representative neurons indicated by the red asterisks are shown at a higher magnification. E) Cortical cytoarchitecture of *Sema6A$^{-/-}$*, *Ella-Cre;HASema6A$^{\Delta/\Delta}$*, *Emx1-Cre;Sema6AΔcyto$^{fl/fl}$*, *Nestin-Cre;Sema6AΔcyto$^{fl/fl}$*, *Gbx2-CreER;Sema6AΔcyto$^{fl/fl}$* and control mice. All lines display layer 2/3 laminar disturbance except *Gbx2-Cre;Sema6AΔcyto$^{fl/fl}$*. Higher magnification showing panel a2 for each genotype. Scale bars 500 µm (A, B, C, E), 100 µm (D).

3D analysis reveals clustering in functionally distinct regions

To provide a clear view of the extent and anatomical position of the cortical defect, we used whole-mount immunohistochemistry iDISCO staining and tissue clearing methods [24] followed by fluorescent lightsheet microscopy [25] and data visualization using Imaris software (Bitplane). We used immunostaining for Special AT-rich sequence-binding protein 2 (SATB2) as a marker to label the upper layers of the cerebral cortex (Fig 2.A) [26–31]. Intact brain tissue samples of *Ella-Cre;Sema6AΔcyto$^{\Delta/\Delta}$* mice at P10 consistently showed a gradual cellular mispositioning phenotype (area indicated by the dotted lines, Fig. 2C, movies Table S4) with the highest disturbance and clustering effect of SATB2-positive cells in the lateral to caudal brain regions and low disturbance in the medial to rostral areas. SATB2-positive neuronal clusters were detected in both hemispheres and in multiple functionally distinct cortical regions that were determined using the Allen Developing Mouse Brain Atlas [32] (Fig 2B). Neuronal clusters were observed in the somatosensory cortex (SS), auditory cortex (AUD) and temporal association cortex (TEa) (Fig. 2B).

Onset and development of the cortical defect in Sema6A mutant mice

To determine the initial developmental event that is causing the mispositioning in cortical layer 2/3 we analyzed a timed series of *Emx1-Cre;Sema6AΔcyto*$^{fl/fl}$ and *Ella-Cre;HASema6A*$^{\Delta/\Delta}$ mice using immunohistochemistry staining against SATB2. To validate Emx1-Cre specificity we crossed this mouse line with Ai14-tdtom reporter. *Emx1-Cre;Sema6AΔcyto*$^{fl/fl}$ animals show specific cre recombination in the cerebral cortex and hippocampus (Fig. 3A) [33]. Layer 2/3 neurons start to arrive at the pial surface from embryonic day 18.5 (E18.5) onwards and most of the neurons have arrived at the pial surface at postnatal day 0 (P0) [4,34]. At timepoint E18.5 no change in cell positioning was detected in *Emx1-Cre;Sema6AΔcyto*$^{fl/fl}$ mice (Fig. 3B). At P0 and P1 few SATB2-positive cells were mispositioned in layer 1 (Fig. 3B, white arrow heads). At P2, the disturbance became clear with mispositioned SATB2-positive cells spread out into layer 1 in *Emx1-Cre;Sema6AΔcyto*$^{fl/fl}$ and *Ella-Cre;HASema6A*$^{\Delta/\Delta}$ mice. The boundary between layer 1 and layer 2/3 was nonexistent. By P4, the first neuronal clusters started to appear. At P6, most layer 2/3 SATB2-positive cells disintegrated from the layers below and formed multiple neuronal clusters (Fig 3B, C). *Emx1-Cre;Sema6AΔcyto*$^{+/+}$ and *Ella-Cre;HASema6A*$^{+/+}$ mice were used as control animals. In conclusion, the mispositioning of layer 2/3 neurons was observed from P2 onwards (Fig. 3B, C) and fully displayed at P10 (Fig. 1, Fig. 2). At P2 *Emx1-Cre;Sema6AΔcyto*$^{fl/fl}$ and *Ella-Cre;HASema6A*$^{\Delta/\Delta}$ initially showed displacement of layer 2/3 neurons into layer 1 but no clustering effect (Fig. 3B, C). Cellular clustering increased over time from P4 onwards (Fig. 3B, C). Additional developmental timepoints for *Emx1-Cre;Sema6AΔcyto*$^{fl/fl}$ and *Ella-Cre;HASema6A*$^{\Delta/\Delta}$ mice can be found in supplemental figure 2 (Fig. S2).

PlxnA2 is expressed in apical dendrites of layer 2/3 neurons marking the border between layer 1 and layer 2/3 in the cortex

In *Emx1-Cre;Sema6AΔcyto*$^{fl/fl}$ mice, PLXNA2 was found in neuronal clusters (Fig. 4A). In addition, PLXNA2 expression was detected at the border between layer 1 and layer 2/3 (Fig. 4A, B). At higher magnification, PLXNA2 expression was detected in the apical dendrites of layer 2/3 neurons extending into layer 1 at P0 (Fig. 4C, D). Dendrites of cortical neurons form after radial migration ends [35]. This suggests that the mispositioning of layer 2/3 neurons gradually increases after radial migration is completed from P2 onwards (Fig. 3B, C). Interestingly, PLXNA2 expression seems gradual and coincides with the occurrence of a structural change and shift in the

location of the border between layer 2/3 and layer 1. In the presence of PLXNA2, layer 1 seemed broader (Fig. 4B, D). These findings suggest that PLXNA2 is important for the border formation between layer 1 and layer 2/3 during early postnatal development. In the absence of the intracellular domain of Sema6A, layer 2/3 neurons no longer respond to PLXNA2 and are mispositioned in layer 1 (Fig. 4E).

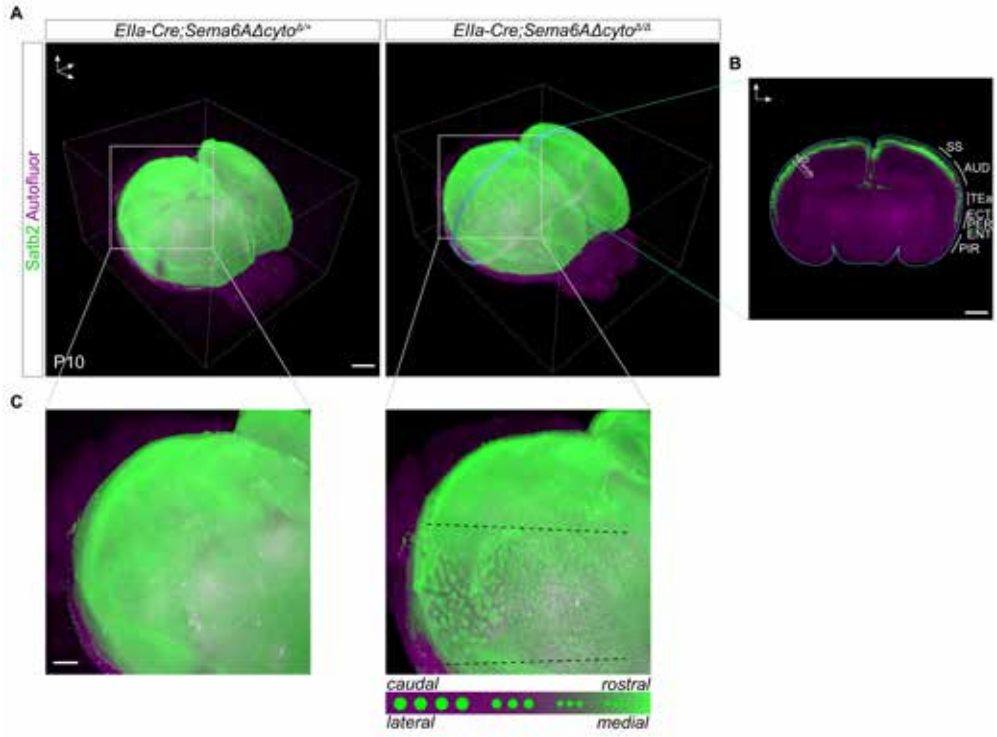

Figure 2. iDISCO 3D analysis showing neuron mispositioning in *Ella-Cre;Sema6AΔcyto*$^{\Delta/\Delta}$ mice.
A) iDISCO staining using primary antibody rabbit anti-SATB2 followed by secondary antibody donkey anti-rabbit 750 in green in *Ella-Cre;Sema6AΔcyto*$^{\Delta/\Delta}$ and control mice at P10. Autofluor signal was used as a reference (magenta). B) Coronal section showing anti-SATB2 in upper cortical layers. Neuronal clusters are predominantly detected in somatosensory cortex (SS), auditory cortex (AUD) and temporal association area (TEa). C) High magnification showing high lateral-rostral and low medial-caudal occurrence of neuronal clusters in *Ella-Cre;Sema6Acyto*$^{\Delta/\Delta}$. Control mice show an even distribution of SATB2-positive neurons. Scale bars 1000 µm (A, B) 500 µm (C).

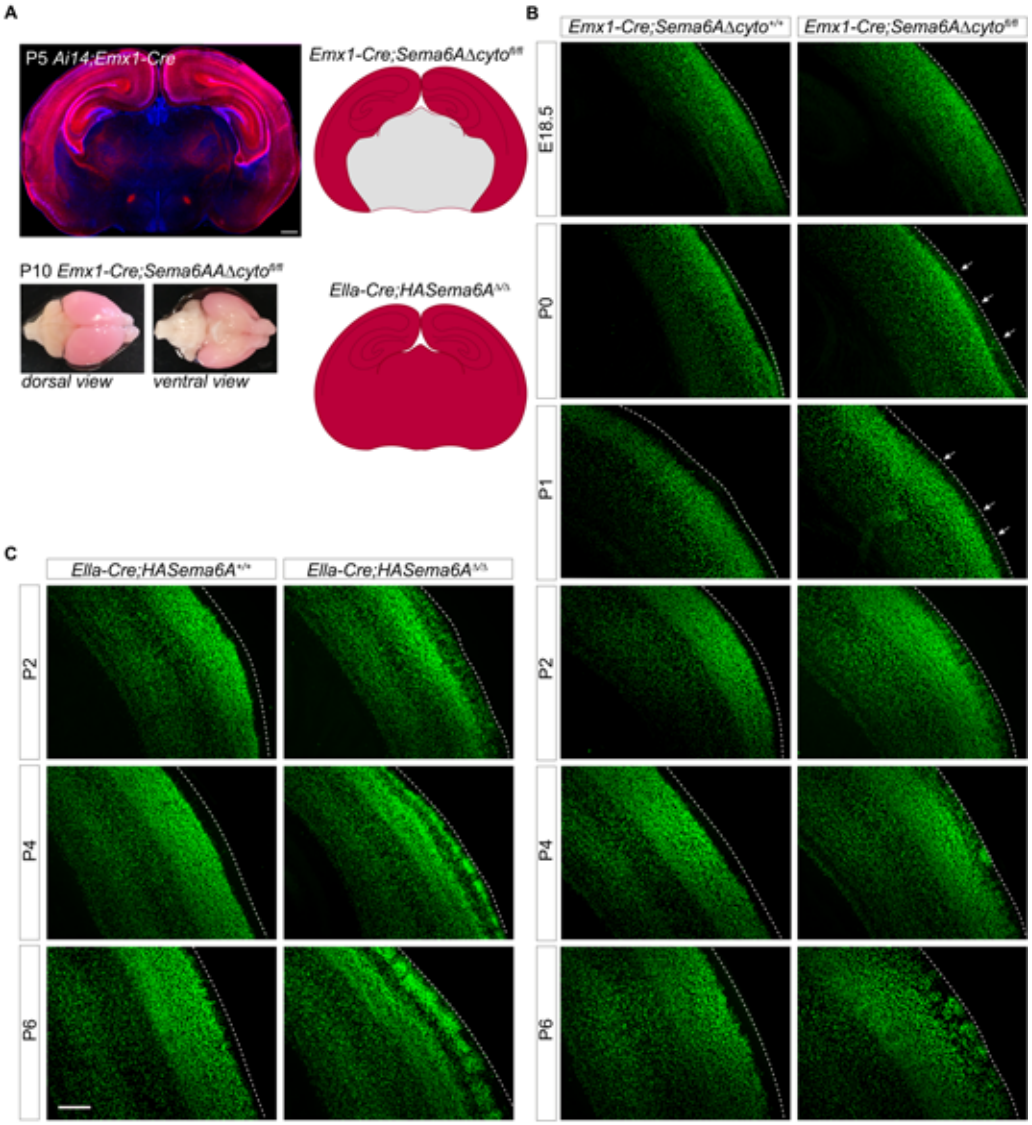

Figure 3. Developmental onset of layer 2/3 neuron mispositioning in *Emx1-Cre;Sema6AΔcyto*$^{fl/fl}$ and *Ella-Cre;HA-Sema6A*$^{\Delta/\Delta}$ mice.

A) Coronal section of *Emx1-Cre* crossed with *Ai14-tdtom* reporter mice showing specificity of Cre recombination in cortex and hippocampus at P5. Dorsal and ventral views of *Ai14; Emx1-Cre;Sema6AΔcyto*$^{fl/fl}$ showing strong tdtomato expression at P10. Schematics showing *Emx1-Cre;Sema6AΔcyto*$^{fl/fl}$ and *Ella-Cre;HASema6A*$^{\Delta/\Delta}$ mouse lines with cre excision sites indicated in red. B) *Emx1-Cre;Sema6AΔcyto*$^{fl/fl}$ coronal sections at developmental time-points E18.5, P0, P1, P2, P4 and P6. Immunostaining using anti-SATB2 antibodies labeling cortical neurons. Few mispositioned SATB2-positive cells are observed at P0 and P1 (white arrows). Neuron mispositioning is observed from P2 onwards and neuronal clusters arise at P4. C) *Ella-Cre;HASema6A*$^{\Delta/\Delta}$ coronal sections at developmental timepoints P2, P4 and P6 showing defect onset at P2 and cluster formation from P4 onwards. Scale bars 500 µm (A), 200 µm (B, C).

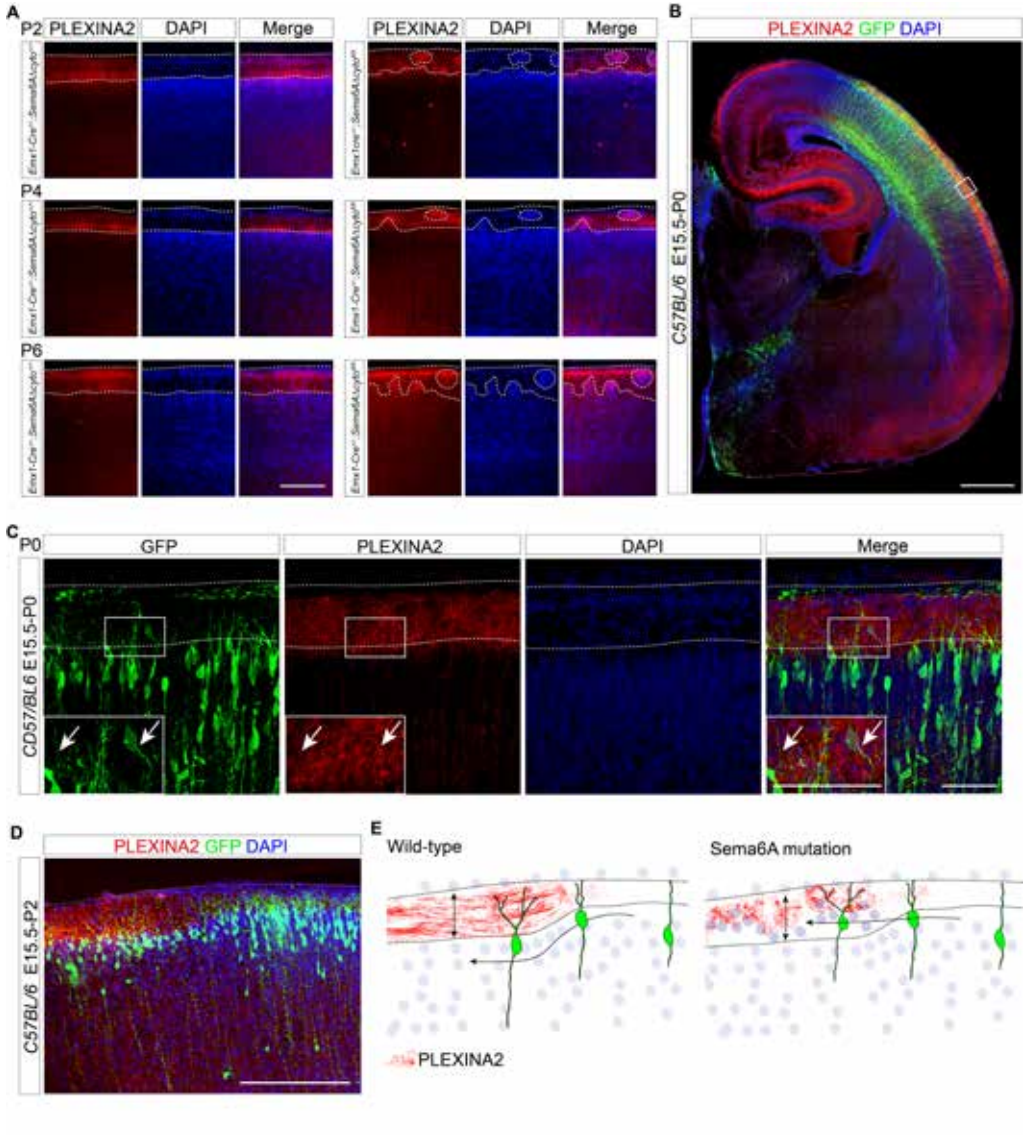

Figure 4. Spatiotemporal expression of PLXNA2 in the developing cortex.
A) PLXNA2 expression at developmental timepoints P2, P4 and P6. *Emx1-Cre;Sema6AΔcyto*$^{fl/fl}$ mice show PLXNA2 in neuronal clusters indicated by dotted areas. Dotted linea indicate the border between layer 1 and layer 2/3 and the outer edge of the cortex. B) PLXNA2 is detected at P0 and overlaps with layer 2/3 neurons labeled with GFP by *in utero* electroporation (IUE). C) Apical dendrites of layer 2/3 neurons labeled with GFP by IUE show strong PLXNA2 expression. D) PLXNA2 expression coincides with broadening of layer 1 and a shift in layer 2/3 cell positioning. E) Schematic representation of PLXNA2 expression in wild-type mice and Sema6A mutants. In wild-type, PLXNA2 expression coincides with a broadening of layer 1, causing a shift in GFP-positive layer 2/3 neuron positioning and results in a strict border between layer 1 and layer 2/3. In the absence of the intracellular domain of Sema6A, GFP-positive layer 2/3 neurons no longer respond to PLXNA2 and reside in layer 1. Scale bars 200 µm (A, D), 500 µm (B) 50 µm (C).

PlexinA2 and PlexinA4 single mutants do not show cortical defect and compensate for the loss of each other

The two main interactors of SEMA6A are PLXNA2 and PLXNA4. To explore their potential involvement in the cortical defect we analyzed knockout tissue from both *PlexinA2*$^{-/-}$ and *PlexinA4*$^{-/-}$ mice [36,37]. *PlexinA2*$^{-/-}$ mice, kindly provided by R. Giger, did not display neuronal clusters at P10 (Fig. 5A). No neuronal clusters where detected at developmental timepoints P2, P4 and P8 (Fig. 5B, C). However, the sharp border between layer 1 and 2 was not clearly detectable with SATB2-positive cells positioned in a somewhat curved pattern at P8. This tendency was completely gone at P10 which suggests that this effect might be compensated (Fig. 5C). Immunohistochemistry using anti-PLXNA2 antibodies confirmed the complete absence of PLXNA2 in the cortex of *PlexinA2*$^{-/-}$ mice (Fig. 5B). At the outer edge of layer 2/3, strong PLXNA2 expression was detected from P0 until P6 that coincides with the border between layer 1 and layer 2/3 (Fig. 5B and Fig. 4). Additional crosses of *PlexinA2*$^{+/-}$;*Ella-Cre-Sema6AΔcyto*$^{\Delta/+}$ and *PlexinA2*$^{+/-}$; *Ella-Cre;HASema6A*$^{\Delta/+}$ double heterozygous mice showed no cortical defect (Fig. S3). *PlexinA4*$^{-/-}$ mouse tissue, kindly provided by A. Chédotal, did not display neuronal clusters at P10 (Fig. 5D). Anti-NeuN and anti-SATB2 antibodies showed no laminar disturbance or mispositioning of layer 2/3 neurons in medial or lateral regions of the cortex (Fig. 5A, B). In conclusion, we found that *PlexinA2*$^{-/-}$ and *PlexinA4*$^{-/-}$ do not show mispositioning of layer 2/3 neurons. Literature shows that *PlxnA2/A4* double knockout (dKO) mutants show layer 2/3 neuron mispositioning and laminar disturbance at P15 (Hatanaka et al., 2019). This suggests that PLXNA2 and PLXNA4 compensate each other and redundantly regulate layer 2/3 neuron positioning during cortical development.

Cortical layer 2/3 is specifically affected, while other cortical layers are intact

To study the identity of the mispositioned cells in the affected upper layers of the cerebral cortex we used *in utero* electroporation (IUE) and immunohistochemistry experiments (Fig. 6A). We used a pCAG-GFP construct to label post-mitotic neurons and other cell types located in the ventricular zone of the developing cortex. IUE at developmental timepoint E15.5 showed GFP-positive neurons in layer 2/3 in *C57Bl6* mice at P10 (Fig. 6A). Following IUE of *EIIa-Cre;Sema6AΔcyto*$^{\Delta/\Delta}$ mice at E14.5 we detected few GFP-positive neurons located in the neuronal clusters. Instead, almost all GFP-positive neurons were located below the clusters (Fig. 6B). On the contrary, IUE at E15.5 showed that all GFP-positive neurons were

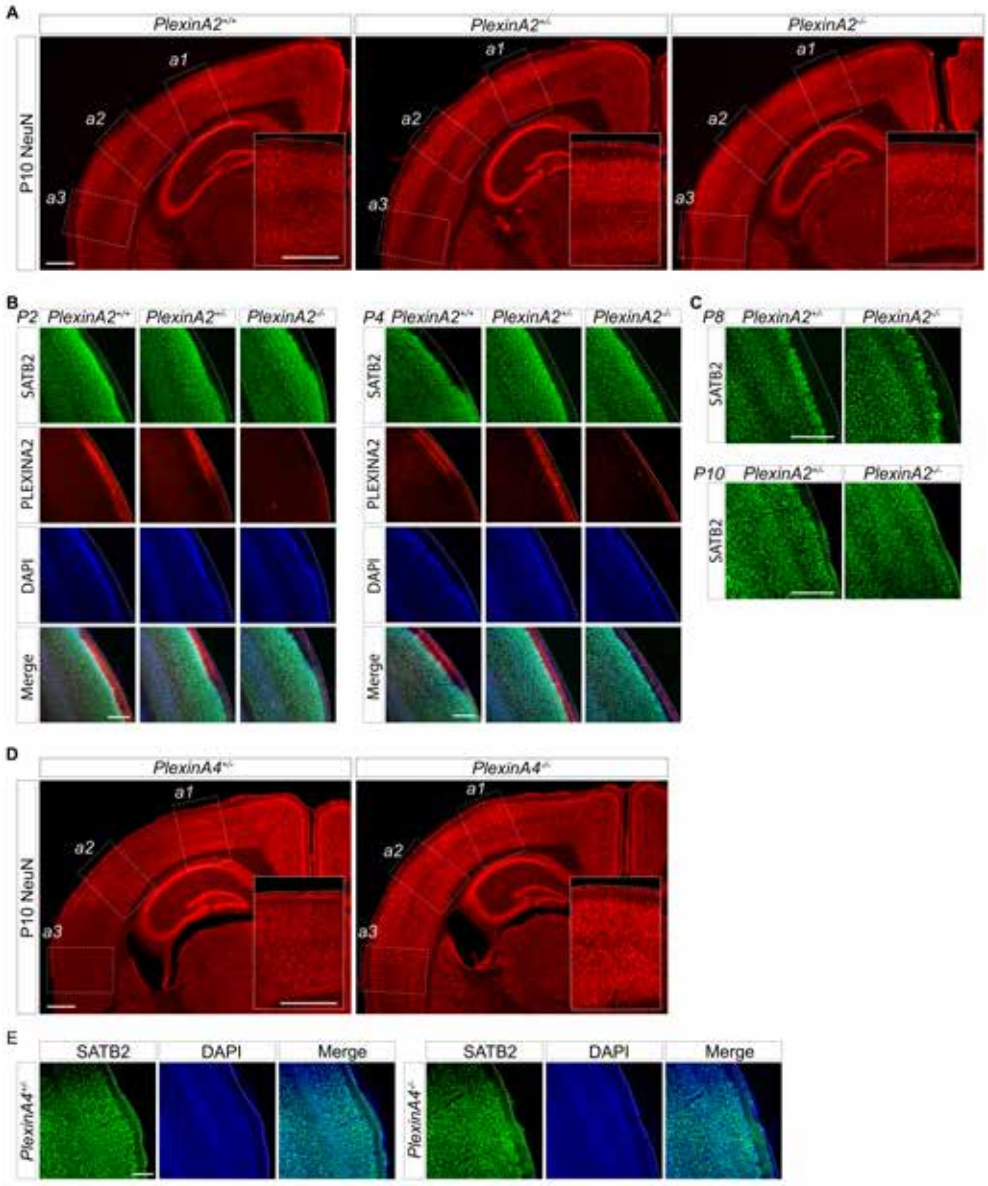

Figure 5. Cortical cytoarchitecture of *PlexinA2*$^{-/-}$ mice and *PlexinA4*$^{-/-}$ mice.
A) Immunohistochemistry using anti-NeuN antibodies on coronal sections of *PlexinA2*$^{-/-}$ and control mice showing no neuron mispositioning or lamination defects in layer 2/3 of the cortex. Higher magnification showing panel a2. B) SATB2-positive neurons show no neuron mispositioning at developmental timepoints P2 and P4. PLXNA2 expression is not detected in *PlexinA2*$^{-/-}$ mice. C) At P8, SATB2-positive neurons show a mild laminar disturbance of the border between layer 2/3 and layer 1. At P10, SATB2-positive neurons show no neuron mispositioning or laminar disturbance. D) Immunohistochemistry using anti-NeuN antibodies on coronal sections of *PlexinA4*$^{-/-}$ and control mice showing no neuron mispositioning or lamination defects in layer 2/3 of the cortex. Higher magnification showing panel a2. E) SATB2-positive neurons show no neuron mispositioning at P10. Scale bars 500 µm (A, D) 200 µm (B, C, E) .

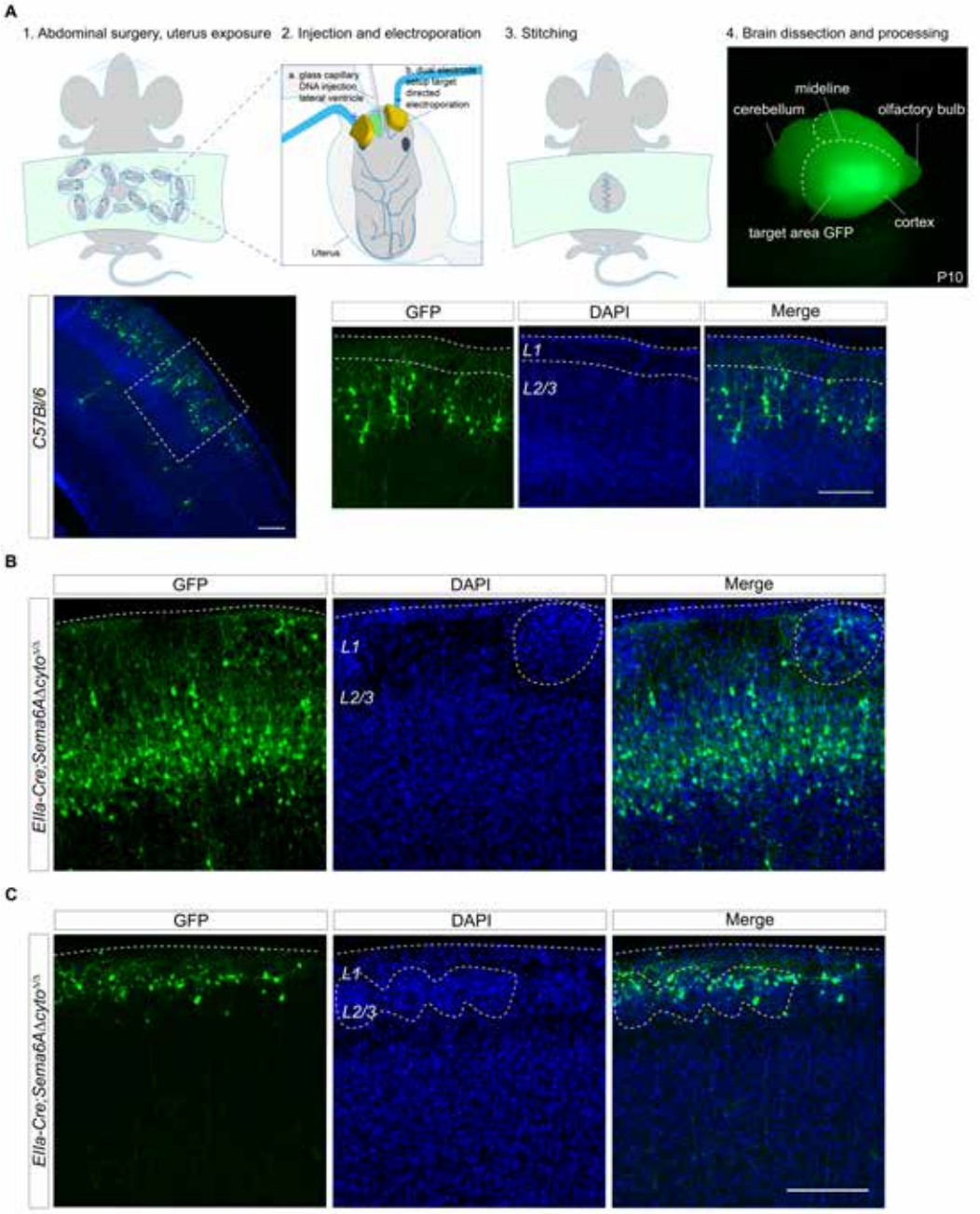
A
1. Abdominal surgery, uterus exposure
2. Injection and electroporation
3. Stitching
4. Brain dissection and processing
a. glass capillary DNA injection lateral ventricle
b. Pt/Ir electrode cortical target directed electroporation
Uterus
midline
cerebellum
olfactory bulb
cortex
target area GFP
P10
C57Bl/6
GFP
DAPI
Merge
L1
L2/3
B
Ella-Cre;Sema6AΔcyto^3/3
C
Ella-Cre;Sema6AΔcyto^3/3

< Figure 6. Layer 2/3 neurons are mispositioned in layer 1 of the cerebral cortex in *Ella-Cre;Sema6AΔcyto*$^{\Delta/\Delta}$ mice.
A) Schematic representation of IUE of layer 2/3 neurons in the lateral cerebral cortex at E15.5 using a pCAG-GFP plasmid. Timed pregnant females were anesthetized and subjected to abdominal surgery to expose the uterus (1). Embryos were injected with pCAG-GFP in the lateral ventricle and electroporated using a dual electrode setup targeting the lateral region of the cortex (2). Embryos are placed back to continue development (3). Brains were dissected and checked for correct GFP targeting. Tissue was processed for immunohistochemistry using anti-GFP antibodies (4). IUE at E15.5 shows GFP-positive neurons in layer 2/3 of the cortex in *C57Bl6* mice. B) IUE at E14.5 shows few GFP-positive neurons in neuronal clusters in *Ella-Cre;Sema6AΔcyto*$^{\Delta/\Delta}$ mice at P9. IUE at E15.5 shows all GFP-positive neurons are located in neuronal clusters in *Ella-Cre;Sema6AΔcyto*$^{\Delta/\Delta}$ mice at P6. Scale bars 200 µm.

mispositioned and located in the clusters at P6 (Fig. 6C). In conclusion, mispositioned neurons are layer 2/3 specific and can be specifically targeted at developmental timepoint E15.5.

Previous reports show that *PlxnA2/A4* dKO animals display a similar defect in layer 2/3 and that deeper cortical layers are unaffected [27]. No differences were found in layer marker expression patterns and the number of cleaved caspase 3-positive cells (Hatanaka et al., 2019). In our study, we confirmed no overall change in the organization of the cortical layers below layer 2/3 in *Ella-Cre;HASema6A*$^{\Delta/\Delta}$ (Fig. S4) and *Emx1-Cre;Sema6AΔcyto*$^{fl/fl}$ (Fig. S5) mice using the layer-specific marker CTIP2 and cell-type specific marker Reelin, supporting previously published results [27]. We did detect a tendency of an upward shift the location of homeodomain transcription factor PROX1-positive cells in *Ella-Cre;HASema6A*$^{\Delta/\Delta}$ and *Emx1-Cre;Sema6AΔcyto*$^{fl/fl}$ mice. PROX1 is a specific marker for post-mitotic caudal ganglionic eminence (CGE)-derived cortical interneurons that are normally located in the different layers of the cortex (Miyoshi et al., 2015). PROX1-positive cells were detected inside the neuronal clusters similar to the previously mentioned GFAP-positive neurons (Fig. S1) supporting the observation that in layer 2/3 not only pyramidal neurons are affected. To conclude, together with previously published data [27] and the additional markers used in our study, deeper layer neurons are not found in the neuronal clusters, while various cell types normally located in layer 2/3 are, including pyramidal neurons, interneurons and glia. In addition, we used L1 cell adhesion molecule (L1CAM) as marker to study axonal fibers in the upper cortical layers. L1CAM is expressed throughout the nervous system at the cell surface and involved in different processes including axon growth and guidance during development, neuronal cell migration and myelination [38–40]. *Emx1-Cre;Sema6AΔcyto*$^{fl/fl}$ and *Ella-*

Cre;HASema6A$^{\Delta/\Delta}$ mice compared to controls showed a displacement of L1CAM-positive fibers located around the neuronal clusters (Fig. S3, S4). This suggests that axon bundles, that are normally located in the cell sparse area of layer 1, follow alternative routes around the neuronal clusters.

In vivo anatomy of mispositioned layer 2/3 neurons at P2

Layer 2/3 neurons mispositioning was detected from P2 onwards. Therefore, we performed IUE of *Ella-Cre;HASema6A*$^{\Delta/\Delta}$ mice at E15.5 and analyzed the tissue at time of defect onset. GFP-positive layer 2/3 neurons were observed in the medial to lateral regions of the cortex. *Ella-Cre;HA-Sema6A*$^{\Delta/\Delta}$ mice display an overall shift and mispositioning of layer 2/3 cells towards the pial surface invading layer 1 (Fig. 7A). The distinct boundary between layer 1 and layer 2/3, visualized using 4', 6-diamidino-2-phenylindole (DAPI), was not detected. Control mice showed a clear border between layer 1 and layer 2/3 in both medial and lateral regions (Fig. 7A). GFP-positive neurons were located in layer 2/3 and displayed initial local branching of apical dendrites extending into layer 1 (Fig. 7B) further supporting the finding that radial migration is terminated in these cells (Fig. 4C). The medial region of *Ella-Cre;HASema6A*$^{\Delta/\Delta}$ mice also displayed a diffuse border and gradual shift of layer 2/3 into layer 1. However, the difference in cell density between layer 1 and layer 2/3 was still detectable and most GFP-positive neurons displayed extending apical dendrites into layer 1 (Fig. 7A). The lateral, most severely affected region showed an altered cell soma orientation of the mispositioned GFP-positive cells (white arrows) in layer 1 and disorganization of the apical dendrites (Fig. 7B).

Spatiotemporal development of layer 2/3 neurons

Since the mispositioned cells in Sema6A IUE experiments were identified as layer 2/3 neurons we set out to determine the spatiotemporal developmental trajectory of layer 2/3 neurons in a normal developing brain of *C57Bl6* wildtype animals. Layer 2/3 neurons are produced between E14-E17 with the highest birth peak at E15 [41]. We used birth dating experiments injecting bromodeoxyuridine (BrdU), as a marker for proliferating cells, at E15.5 or E16.5 in combination with IUE of a pCAG-GFP construct to label future layer 2/3 neurons in the ventricular zone. BrdU injection at E15.5 followed by tissue analysis at P0 showed a large proportion of proliferating layer 2/3 cells (Fig. 8A) compared to injection at E16.5 (Fig. 8C). In combination with IUE at E15.5 we found that a large proportion of layer 2/3 neurons arrived from P0 onwards (Fig. 8A) and at P2 almost all targeted cells had arrived in upper compartment of layer 2/3 with few cells still on route towards the

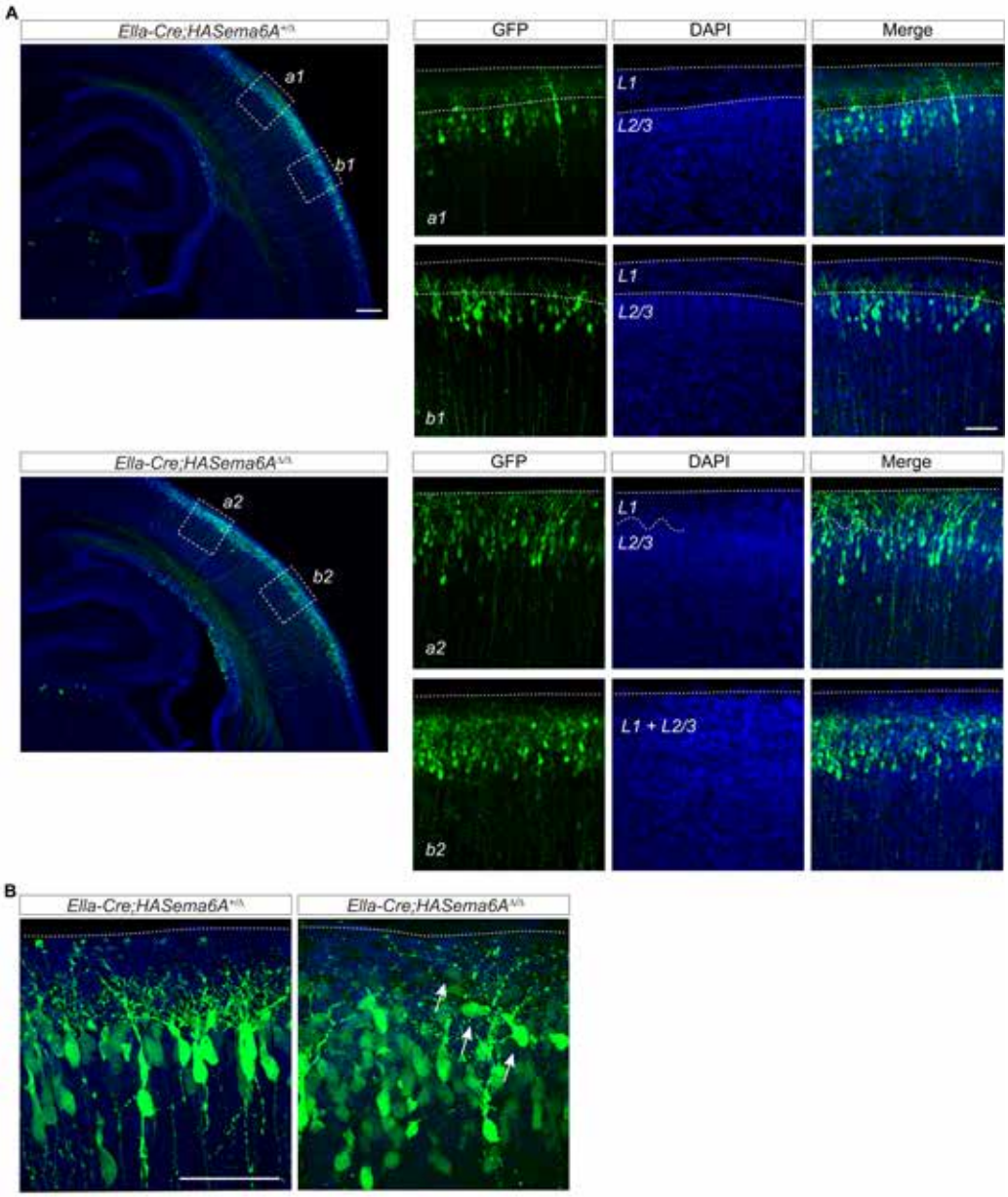

Figure 7. Mispositioned neurons are identified as layer 2/3 pyramidal neurons.
A) IUE at E15.5 using pCAG-GFP shows layer 2/3 neurons mispositioning in *Ella-Cre;HASema6A*$^{\Delta/\Delta}$ mice at P2. Coronal sections show neuron mispositioning increases from medial (a2) to lateral (b2) regions of the cortex. The sharp border between layer 2/3 and layer 1 (visualized using DAPI) is not observed in *Ella-Cre;HASema6A*$^{\Delta/\Delta}$ mice. B) *Ella-Cre;HASema6A*$^{\Delta/\Delta}$ mice show mispositioning of GFP-positive neurons (white arrow showing examples) towards the pial surface indicate by the dotted line. Control mice show GFP-positive neurons with branching apical dendrites extending in layer 1. Scale bars 200 µm (A), high magnifications 50 µm (A, B).

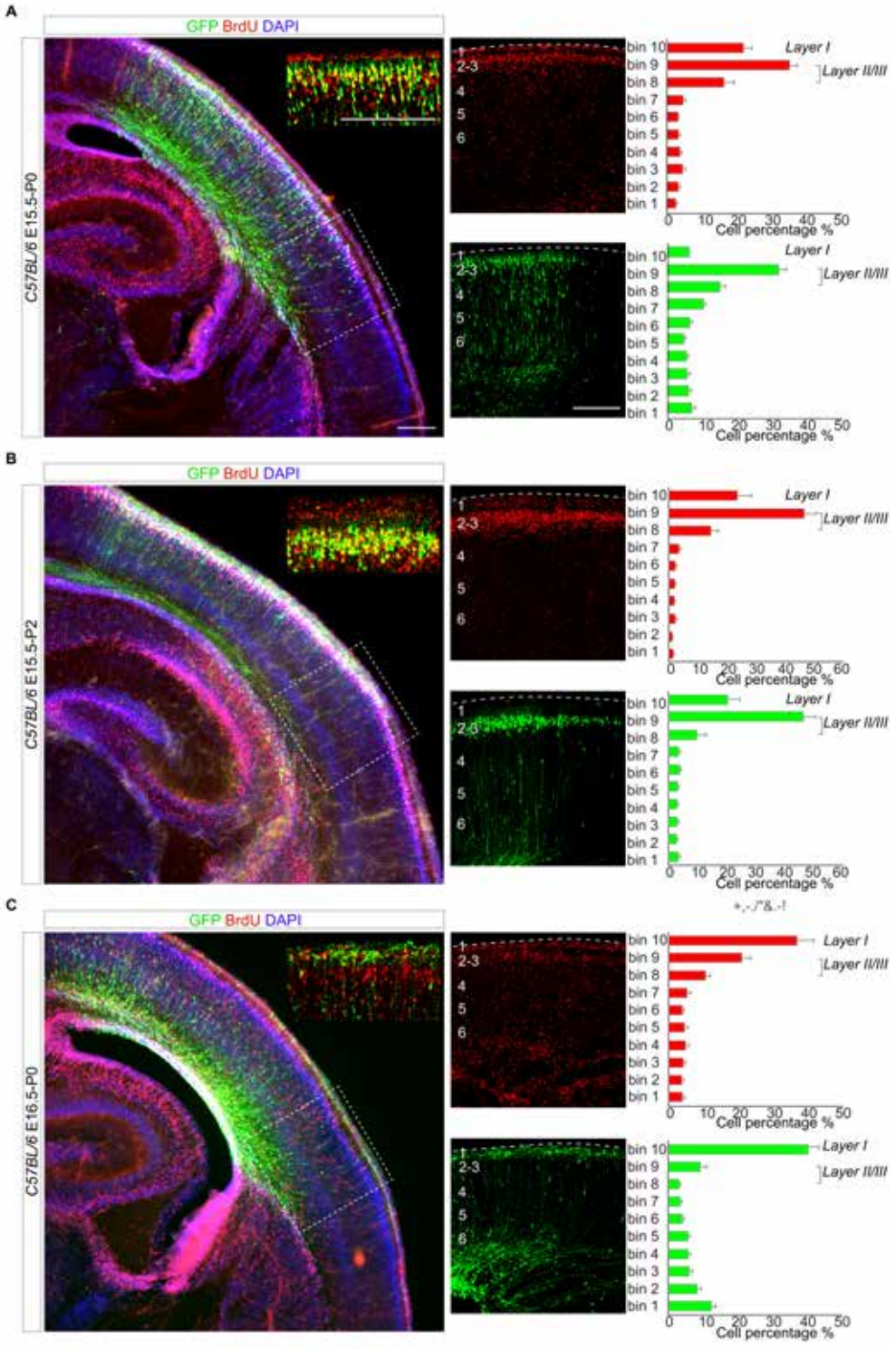
A
GFP BrdU DAPI
C57BL/6 E15.5-P0
1
2-3
4
5
6
bin 10
bin 9
bin 8
bin 7
bin 6
bin 5
bin 4
bin 3
bin 2
bin 1
Layer I
Layer II/III
0 10 20 30 40 50
Cell percentage %
B
GFP BrdU DAPI
C57BL/6 E15.5-P2
0 10 20 30 40 50 60
Cell percentage %
C
GFP BrdU DAPI
C57BL/6 E16.5-P0

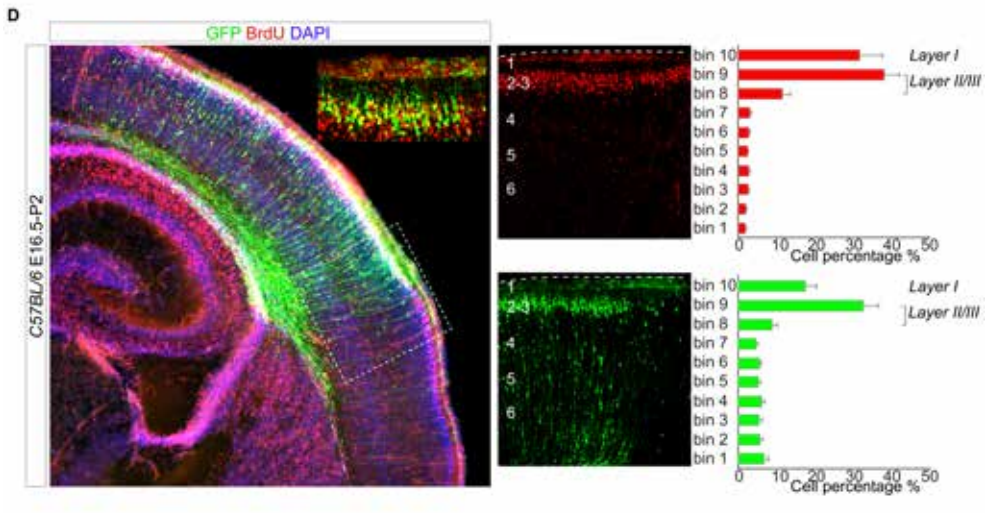

Figure 8. Spatiotemporal overview of layer 2/3 neuron migration and proliferation.
A-D) Representative images of IUE at E15.5 or E16.5 analyzed at P0 or P2. Double immunohistochemistry for GFP and BrdU on coronal sections of the cerebral cortex. High magnification in the upper right corner shows overlapping (yellow) GFP-positive (green) and BrdU-positive (red) signal. Analyzed region indicated by the dotted line and separate channels showing BrdU and GFP distribution in the cortical layers. Graphs show cell percentage calculated from the total amount of cell somas (GFP) or nuclei (BrdU) counted using ImageJ software. Cortical layers 1-6 were divided in 10 bins with bin 10 corresponding to layer 1 and bin 9 and 8 corresponding to layer 2/3. A) IUE and BrdU injection at E15.5 analyzed at P0. B) IUE and BrdU injection at E15.5 analyzed at P2. C) IUE and BrdU injection at E16.5 analyzed at P0. D) IUE and BrdU injection at E16.5 analyzed at P2. Data represented as mean ± SEM. Scale bars 200 µm.

cortex (Fig. 8B). Electroporation at E16.5 resulted in a low contribution of GFP-positive neurons to layer 2/3 at P0 (Fig. 8C). However, at P2 some late arriving neurons were found in layer 2/3 (Fig. 8D). These findings show that layer 2/3 neurons arrive gradually with a large proportion arriving between P0 and P2. This suggests that the majority of layer 2/3 neurons arrives in layer 2/3 before the onset of the cortical defect.

Conditional deletion Sema6A

To study the Sema6A signaling pathway that is causing the mispositioning of layer 2/3 neurons we used a conditional approach to induce Cre recombination in a population of cells at specific developmental timepoints. Layer 2/3 neurons were targeted at the previously determined timepoint E15.5 via IUE using a pCAG-IRES2-Cre-GFP construct in *HASema6A*$^{fl/fl}$ mice. Interestingly, these mice displayed neuronal clusters that were detected in the lateral

regions of the cortex using anti-NeuN antibodies at P10 (Fig. 9A). Intensity profile analysis showed a significant increase in intensity fluctuations in *HASema6A*$^{fl/fl}$ mice (Fig. 9B). The neuronal clusters contained electroporated and non-electroporated cells suggesting a non-cell-autonomous effect in the absence of Sema6A (Fig. 9C). Hatanaka and authors suggest a role for Sema6A in radial glia cells during the process of migration [27]. To test this hypothesis, we used IUE experiments to determine the role of radial glia in the cortical defect. At E17.5, most post-mitotic neurons have left the ventricular zone and migrate through the cortical plate towards their target destination [4]. At this stage, radial glia cells reside in the ventricular zone, extending up to the pial surface [42] and can be targeted by IUE [4]. IUE of pCAG-Cre-IRES2-GFP at E17.5 resulted in the conditional deletion of Sema6A from radial glia cells (Fig. 10A). No neuronal mispositioning or clusters were detected in the lateral regions of the cortex at P10 (Fig. 10B, C). This finding suggests no apparent role for radial glia cells in the formation of neuronal clusters in layer 2/3. Also, it provides support for a post-migratory effect in the mispositioning of layer 2/3 neurons. Interestingly, some neurons were targeted at E17.5 and were found in layer 2/3 in the medial region of the cortex analyzed at P10. These neurons displayed non-cell-autonomous clustering in layer 1 (Fig. 11A, B). Control animals showed a clear border between layer 1 and layer 2/3 and GFP-positive neurons extending apical dendrites into layer 1 (Fig. 11C). Radial glial cells diminish during postnatal stages and retract their processes to become GFAP-positive astrocytes that start to appear after the first postnatal week [42–44]. To control for the loss of radial glia, we confirmed our findings at an earlier developmental timepoint P3 (Fig. 12A). At this stage the lateral region of the cortex showed GFP-positive radial glia fibers up to the pial surface. No layer 2/3 neurons were targeted at E17.5 in this region. Therefore, no mispositioning of layer 2/3 neurons was detected after the conditional deletion of Sema6A from radial glia cells in the lateral cortex (Fig. 12B). However, mispositioned SATB2-positive neurons were detected in the medial region of the cortex showing GFP-positive layer 2/3 neurons targeted at E17.5 (Fig. 12A, white arrows indicate mispositioned neurons) through IUE of pCAG-Cre-IRES2-GFP.

Sema6A expression is detected in cortical layer 2/3

Previously published work shows *in* situ hybridization (ISH) of *Sema6A* in the mouse cortex with strong expression in layer 2/3 at P0 [45]. We found *Sema6A* expression in all cortical layers at the onset of the cortical defect (P2) (Fig. S6A). Similar profiles were found for *PlenxinA2* and

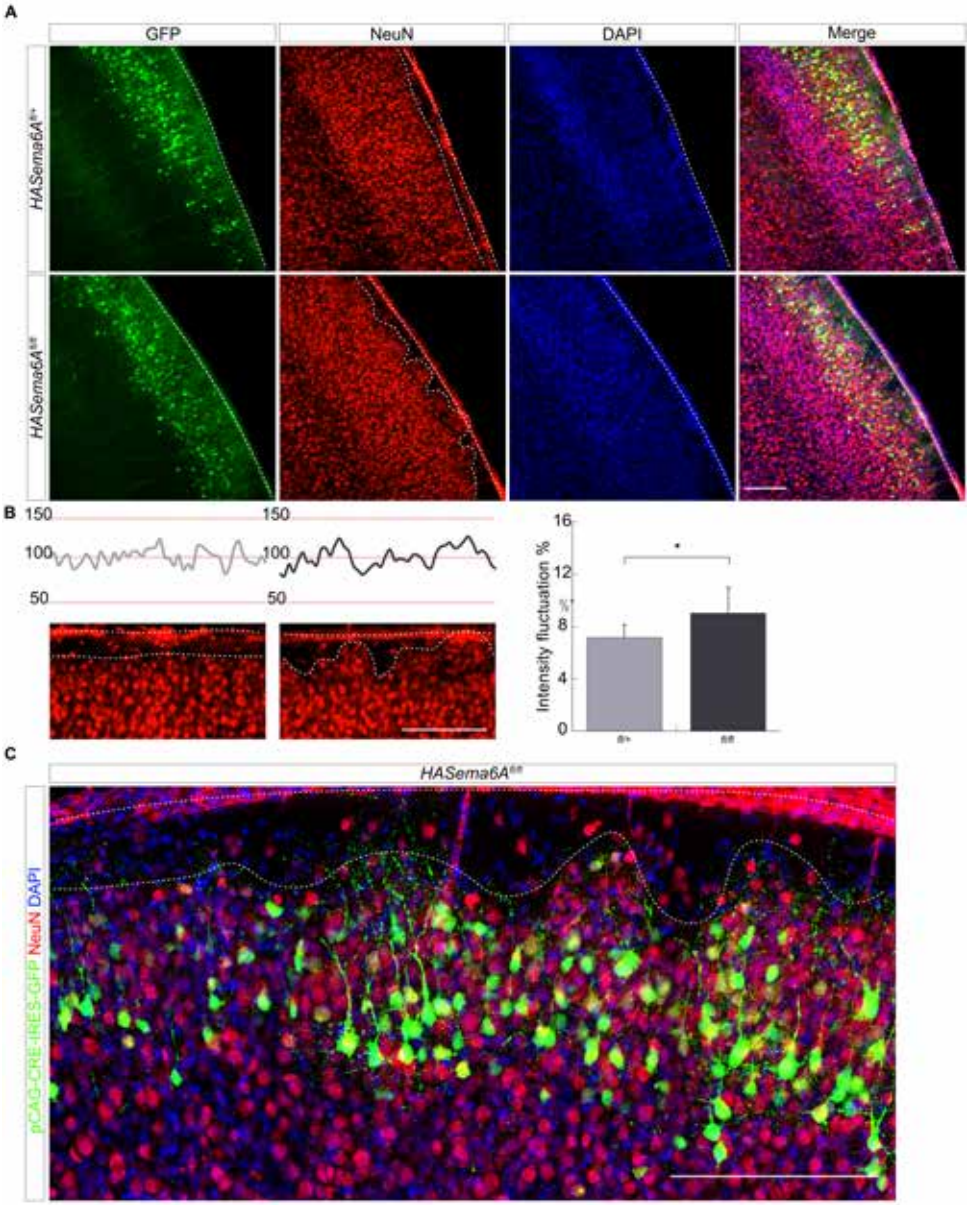

Figure 9. IUE of Cre in layer 2/3 neurons targeted at E15.5 in *HASema6A*$^{fl/fl}$ mice induces layer 2/3 mispositioning.

A) IUE with pCAG-Cre-IRES2-GFP in *HASema6A*$^{fl/fl}$ and control mice at E15.5 and brain analysis at P10. B) Higher magnification views of the regions analyzed for intensity profile plots. Bar graph showing the percentage of intensity fluctuations. Data represented as mean ± SEM, Student's t-test, *p<0.05. C) Higher magnification view of GFP fluorescence and NeuN staining after IUE with pCAG-Cre-IRES2-GFP in *HASema6A*$^{fl/fl}$ mice. Dotted lines indicate the border between layer 1 and layer 2/3 and the outer edge of the pial surface. Note that GFP-positive cells are located in neuronal clusters together with neighboring GFP-negative cells. Scale bars 200 µm.

PlexinA4 at this stage of development (Fig. S6A). In combination with immunohistochemistry, *Sema6A* was observed to co-localize with mouse anti-NeuN and rabbit anti-BLBP antibodies suggesting expression in pyramidal neurons and glia (Fig. S6B). Immunohistochemistry using SEMA6A antibodies showed a diffuse expression pattern however, the signal was consistent and detectable throughout the layers of the cortex at P2, P4 and P6 (Fig. 13). Oligodendrocytes and regions of the cerebellum known to express SEMA6A [46,47] were used as a reference to control for antibody specificity (Fig. S6C). In the cortex, SEMA6A was located at the membrane of the cell soma. SEMA6A was detected in cells located in neuronal clusters in *Emx1-Cre;Sema6AΔcyto*$^{fl/fl}$ mice. We observed SEMA6A expression due to the intact extracellular domain. In addition to this, preliminary data of ISH on *Emx1-Cre;Sema6AΔcyto*$^{fl/fl}$ P3 mouse tissue showed *Sema6A* expression only when using a probe designed against the extracellular domain (Fig. S7).

The Sema6A reverse signaling pathway is involved in laminar organization of layer 2/3 neurons

To understand how Sema6A instructs layer 2/3 pyramidal neurons to find their appropriate target location, we studied the function of the Sema6A receptor that is essential for the initiation of the reverse signaling pathway. Computational analysis predicts binding of Sema6A and the cytoplasmic tyrosine kinase ABL [48]. In addition, *in vitro* studies find evidence for a direct interaction between Sema6A and ABL during reverse signaling [21]. ABL recruits additional cytoskeletal regulators that affect cellular morphology, adhesion and migration [49]. To study the role of ABL and the reverse signaling pathway during the development of layer 2/3 neuron positioning, we electroporated a pEF1-myc-Sema6AΔABL construct, kindly provided by Alain Chédotal, *in utero* in *Ella-Cre;HASema6A*$^{\Delta/\Delta}$ mice at E15.5. At P10, GFP-positive layer 2/3 neurons lacking the ABL binding domain were mispositioned and neuronal clusters were detected in *Ella-Cre;HASema6A*$^{\Delta/\Delta}$ mice (Fig. 14). Intensity profile analysis showed no change in neuronal clustering between conditions (Fig. 14B). In contrast, when restoring the ABL binding domain by IUE of a full length Sema6A construct (pCAG-Sema6A-GFP), the defect was partially rescued (Fig. 15). The intensity fluctuation using anti-NeuN as a neuronal marker was significantly reduced in *Ella-Cre;HASema6A*$^{\Delta/\Delta}$ mice (Fig. 15B). These findings suggest that the ABL binding domain is essential for the activation of the Sema6A reverse signaling pathway involved in layer 2/3 neuron positioning.

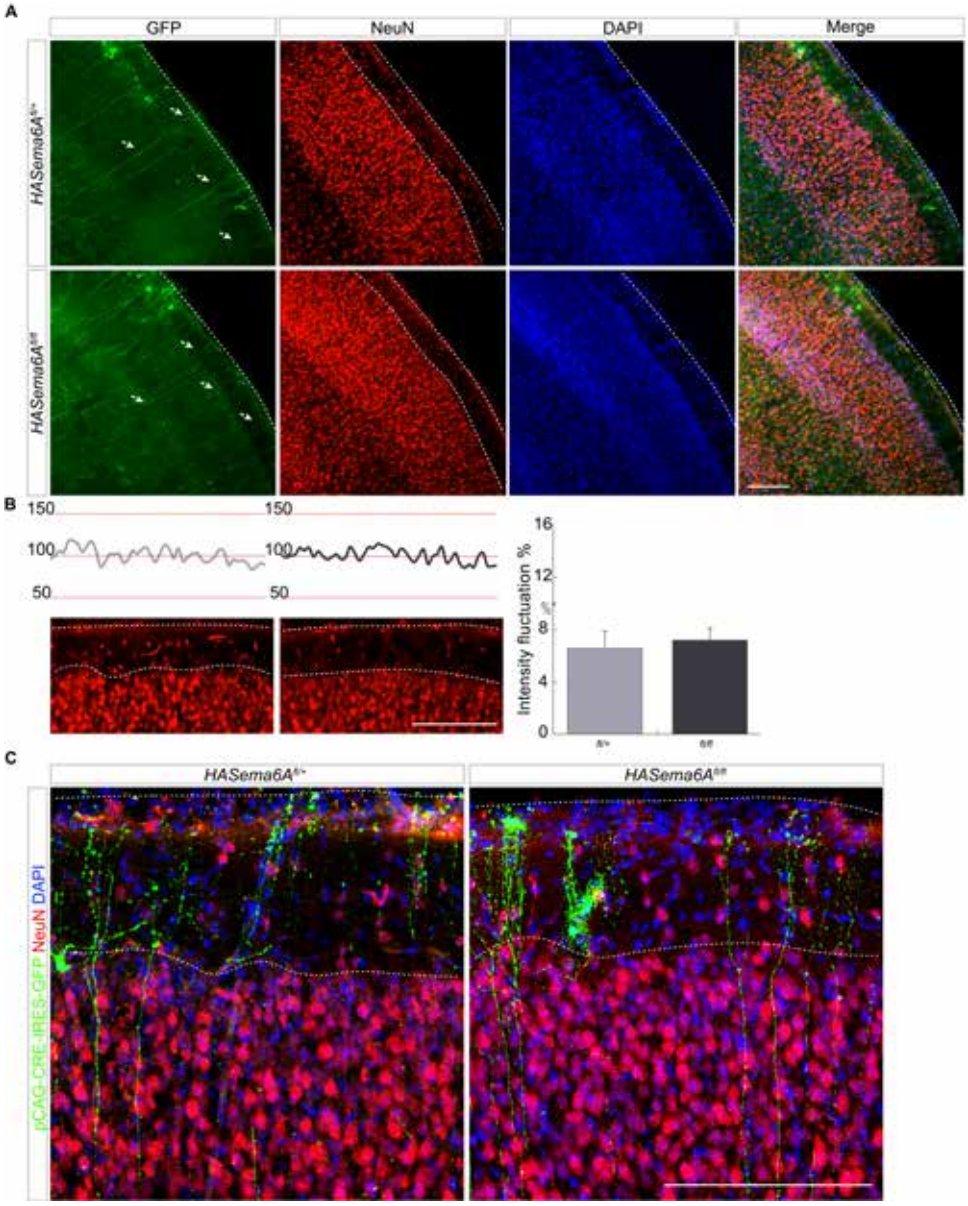

Figure 10. IUE of Cre in radial glia targeted at E17.5 in *HASema6A*$^{fl/fl}$ mice does not affect layer 2/3 positioning.

A) IUE with pCAG-Cre-IRES2-GFP in *HASema6A*$^{fl/fl}$ and control mice at E17.5 and brain analysis at P10. B) Higher magnification views of the regions analyzed for intensity profile plots. Bar graph showing the percentage of intensity fluctuations. Data represented as mean ± SEM, Student's t-test, p=0.13. C) Higher magnification view of GFP fluorescence and NeuN staining after IUE with pCAG-Cre-IRES2-GFP in *HASema6A*$^{fl/fl}$ and control mice. Dotted lines indicate the border between layer 1 and layer 2/3 and the outer edge of the pial surface. Scale bars 200 µm.

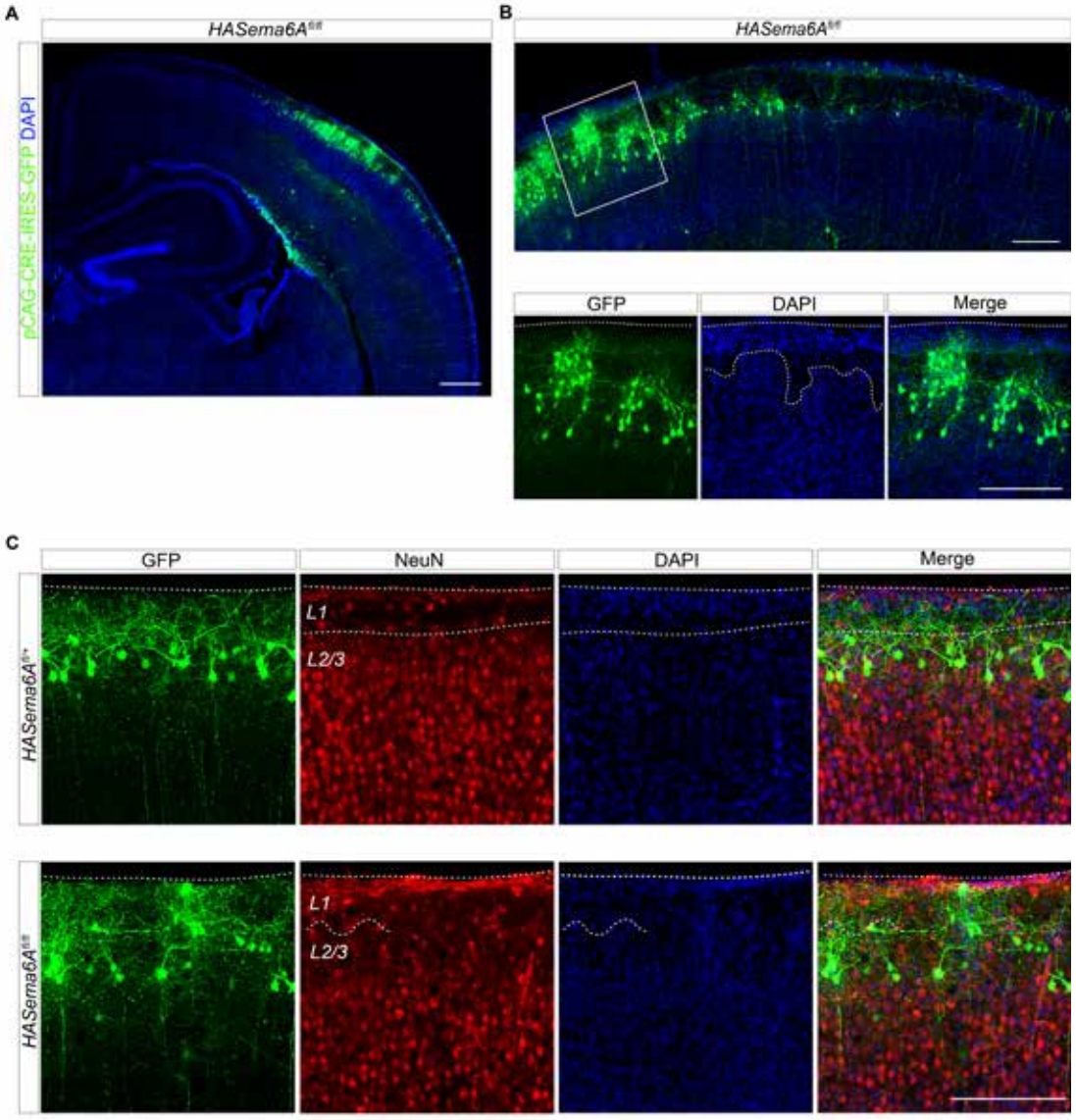

Figure 11. IUE of Cre in layer 2/3 neurons targeted at E17.5 in *HASema6A*$^{fl/fl}$ mice induces layer 2/3 mispositioning.

A) IUE with pCAG-Cre-IRES2-GFP in *HASema6A*$^{fl/fl}$ mice at E17.5 and brain analysis at P10. Note that in lateral cortical regions radial glia fibers are transfected showing no neuronal mispositioning. In medial cortical regions transfected layer 2/3 neurons and neighboring cells are mispositioned and form clusters. B) Higher magnification views of layer 2/3 neuron mispositioning. C) IUE with pCAG-Cre-IRES2-GFP in *HASema6A*$^{fl/fl}$ and control mice at E17.5 and brain analysis at P10. Immunohistochemistry showing GFP and NeuN staining. Dotted lines indicate the border between layer 1 and layer 2/3 and the outer edge of the pial surface. Scale bar 500 µm (A), 200 µm (B, C).

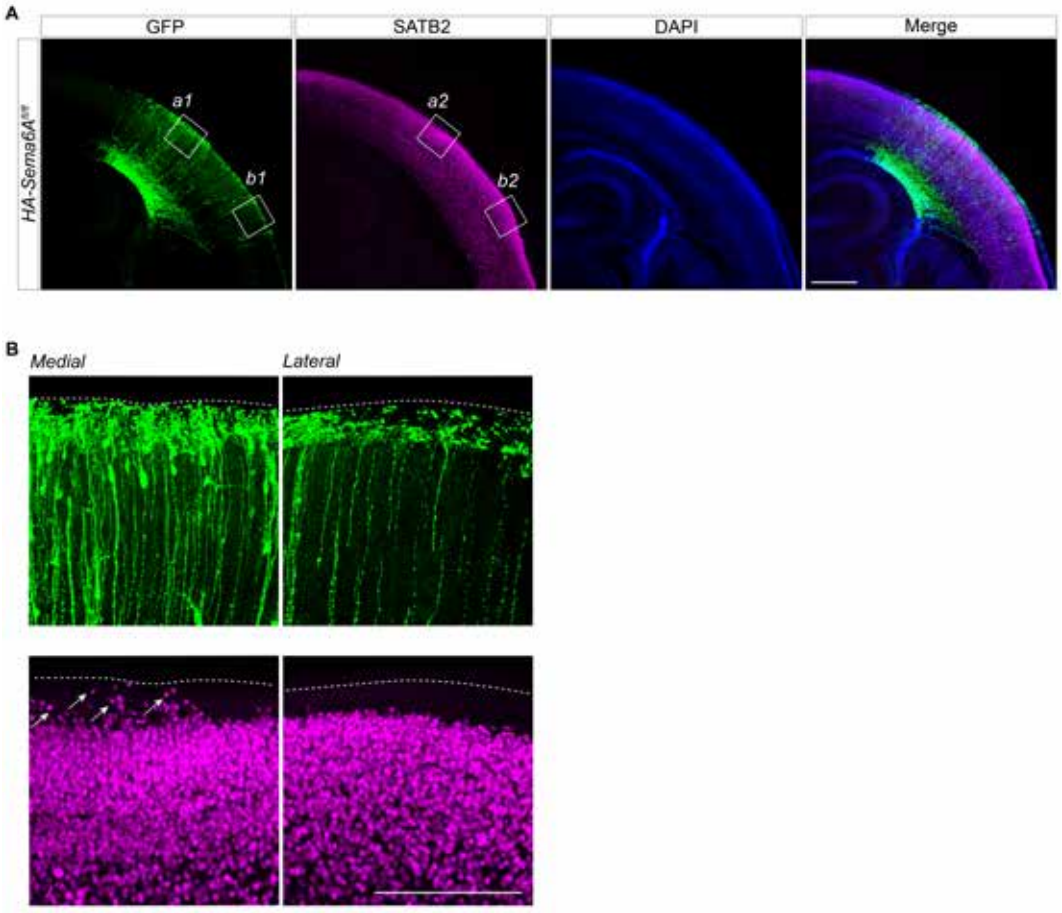

Figure 12. IUE of Cre at E17.5 in *HASema6A*$^{fl/fl}$ mice targets radial glia and layer 2/3 neurons.
A) IUE of pCAG-CRE-IRES2-GFP at E17.5 in *HASema6A*$^{fl/fl}$ mice analyzed at P3. Immunohistochemistry showing GFP, SATB2 and DAPI staining. GFP-positive radial glia fibers are detected in medial (a1,2) and lateral (b1,2) regions of the cortex. B) High magnification of indicated regions (a1,2 and b1,2). Note that in the medial region (a1) layer 2/3 neurons are targeted and SATB2-positive neurons are found in layer 1 (white arrows). Dotted line indicates the outer edge of the pial surface. Scale bar 500 µm (A), 200 µm (B).

Identification of novel regulators involved in cortical development using a multi-omics approach

The Sema6A reverse signaling pathway involves multiple proteins with functions in cytoskeletal regulation including the previously described protein ABL [21]. To study these and identify other proteins involved in the positioning and lamination of layer 2/3 neurons we used a multi-omics approach. We used mass spectrometry (MS) to assess the differential expression of proteins and phosphorylation events, that affect protein functions, activity, localization and interaction, of *Emx1-Cre;Sema6AΔcyto*$^{fl/fl}$ and *Emx1-Cre;Sema6AΔcyto*$^{fl/+}$ control mice. Upper cortical layers were manually dissected and processed to generate two datasets (Fig. 16A). One containing the global proteome and the second, following phosphopeptide enrichment to detect phosphorylation sites, resulted in a phospho-proteome dataset (Fig. 16A). We found more than 1,700 expressed proteins in the global proteome and over 8,000 unique sequences in the phospho-proteome. To analyze the overall functional distribution of targets found in both datasets, we used the functional classification tool in the Panther Classification System (http://www.pantherdb.org/) [50]. Both datasets include categorically similar hits, within major cellular functional classes (Fig. 16B). Identified members include adhesion molecules, regulatory proteins and axon guidance families such as Ephrins and Ephs. Gene ontology (GO) analysis using the statistical overrepresentation test (Panther Overrepresentation Test, released 20200728) showing the top ten over- or underrepresented molecular functions are shown in supplementary table 3. Remarkably, for a high number of phosphorylation sites identified (128) we found a statistically significant difference between the two genotypes (Fig. 16C) while global protein expression revealed only few (3) differentially expressed targets (Fig. 16D). We manually searched Uniprot (https://www.uniprot.org) and Pubmed (https://pubmed.ncbi.nlm.nih.govdatabases) for published data describing protein localization data and characterized functions of our identified targets.

In the global proteome, we found 3 statistically significant hits: Putative RNA-binding protein Luc7-like 1 (Luc7l), 40S ribosomal protein S28 (Rps28) and receptor expression-enhancing protein 5 (Reep5) (Fig. 16D). None of these 3 differentially expressed proteins have been previously linked to the development of the cerebral cortex. Rps28 was upregulated in *Emx1-Cre;Sema6AΔcyto*$^{fl/fl}$ mice and is known to play an essential role in ribosome assembly and protein translation [51]. Reep5 was upregulated in *Emx1-Cre;Sema6AΔcyto*$^{fl/fl}$ mice and its altered expression is known to be involved in the development of cardiac disease [52]. Luc7l was found

to be downregulated in the defective upper cortical layers of *Emx1-Cre;Sema6AΔcyto*$^{fl/fl}$ mice. This protein is broadly expressed with low region-specificity and known to be involved in the regulation of alternative splicing events and muscle differentiation [53]. Among non-significant hits we detected PLXNA2 and PLXNA4 in the upper layers of the cerebral cortex (Fig. 16D).

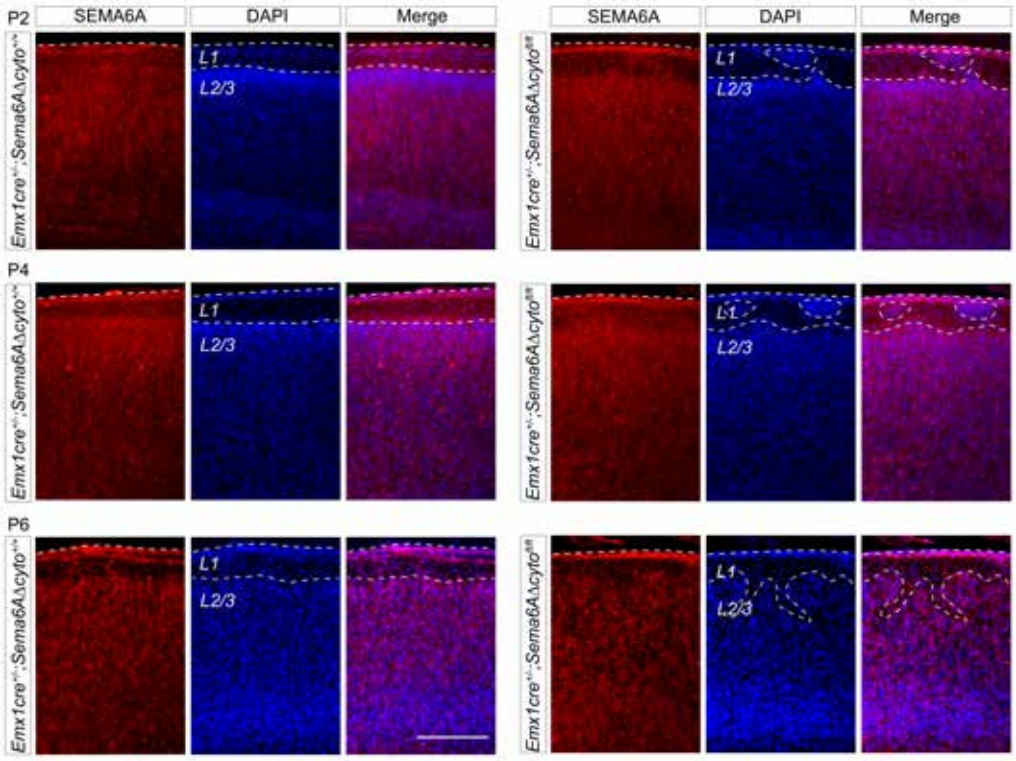

Figure 13. Immunohistochemistry with anti-Sema6A antibodies showing protein expression in the cortex.
Sema6A staining of coronal sections in *Emx1-Cre;Sema6AΔcyto* $^{fl/fl}$ and control mice at P2, P4 and P6. Scale bar 200 µm. Dotted lines indicate the border between layer 1 and layer 2/3 and the outer edge of the pial surface. In *Emx1-Cre;Sema6AΔcyto* $^{fl/fl}$ mice laminar disturbance and neuronal clusters are indicated by the dotted line. Note that Sema6A staining is detected in the clusters.

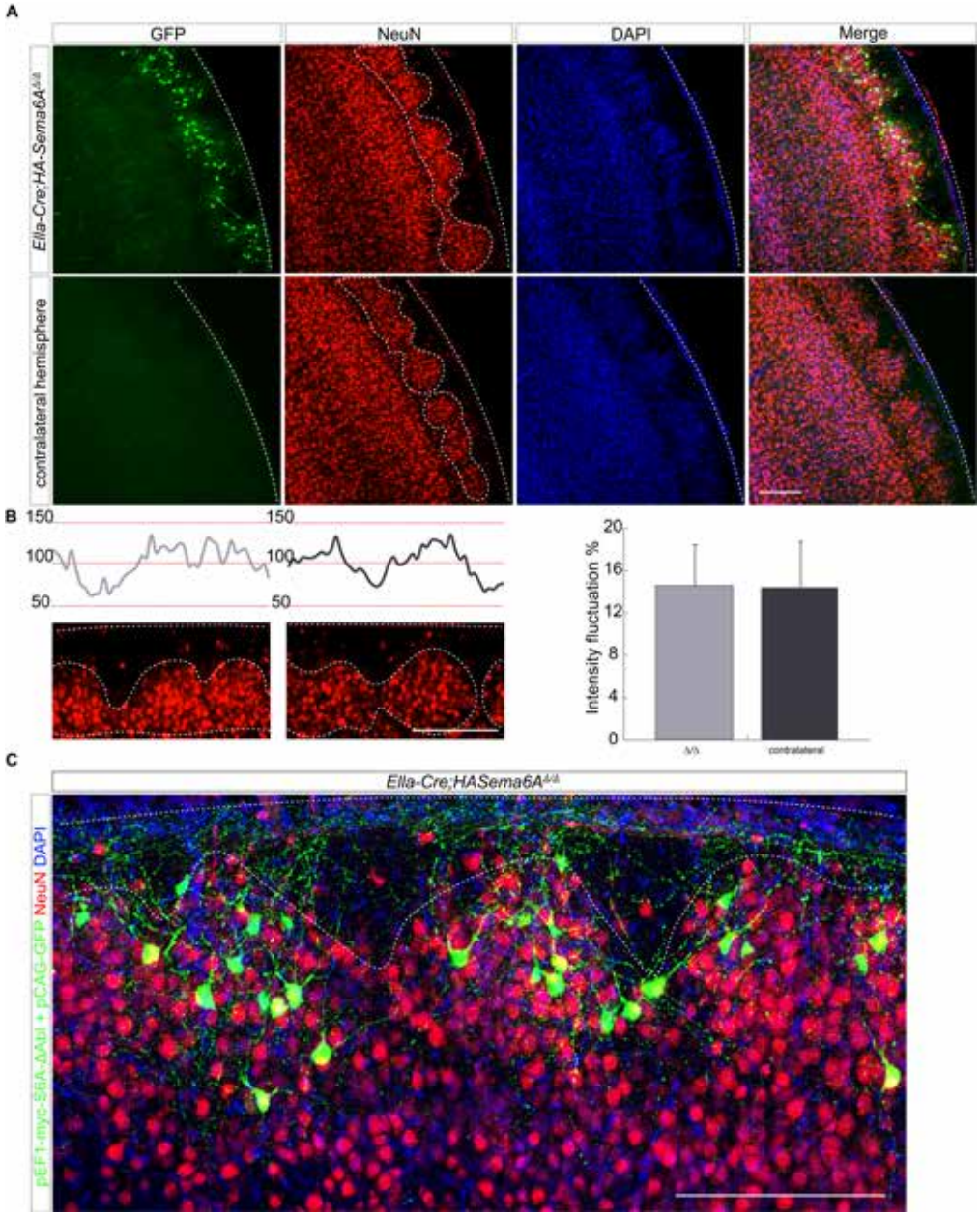

Figure 14. IUE of Sema6AΔAbl in layer 2/3 neurons targeted at E15.5 in *Ella-Cre; HASema6A*$^{\Delta/\Delta}$ mice shows no rescue effect.

A) IUE with pEF1-myc-S6AΔAbl in *Ella-Cre;HASema6A*$^{\Delta/\Delta}$ and control mice at E15.5 and brain analysis at P10. B) Higher magnification views of the regions analyzed for intensity profile plots. Bar graph showing the percentage of intensity fluctuations. Data represented as mean ± SEM, Student's t-test, p=0.44. C) Higher magnification view of GFP fluorescence and NeuN staining. Dotted lines indicate the border between layer 1 and layer 2/3 and the outer edge of the pial surface. Scale bars 200 µm (A, B, C).

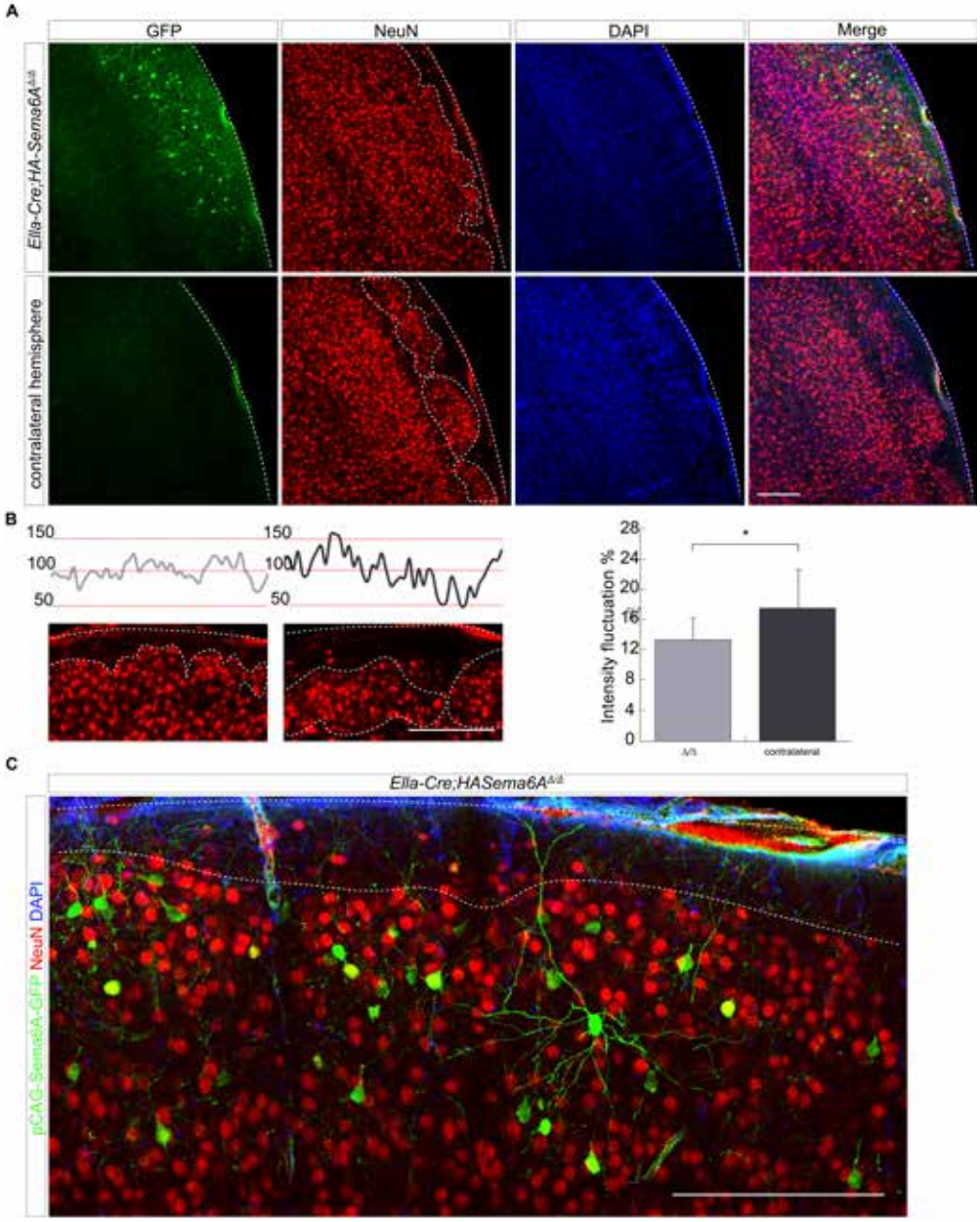

Figure 15. IUE of Sema6A in layer 2/3 neurons targeted at E15.5 in *Ella-Cre;HASema6A*$^{\Delta/\Delta}$ mice recues mispositioning of layer 2/3 neurons.

A) IUE with pCAG-S6A-GFP in *Ella-Cre;HASema6A*$^{\Delta/\Delta}$ and control mice at E15.5 and brain analysis at P15. B) Higher magnification views of the regions analyzed for intensity profile plots. Bar graph showing the percentage of intensity fluctuations. Data represented as mean ± SEM, Student's t-test, *p<0.001. C) Higher magnification view of GFP fluorescence and NeuN staining. Dotted lines indicate the border between layer 1 and layer 2/3 and the outer edge of the pial surface. Scale bars 200 µm (A, B, C).

The phospho-proteome showed a significant differential expression of phosphorylated SATB2. Interestingly, previously published data showed that downregulation of SATB2 in layer 2/3 pyramidal neurons using a short hairpin construct results in neuronal clustering and laminar disturbance of layer 2/3 in the cortex [54]. SATB2 is a transcription factor originally identified as a gene expression regulator by chromatin rearrangement to activate or repress transcription. In addition, it is frequently used as a marker and determines neuron identity of upper layer neurons that project contralaterally to form the corpus callosum [26,29]. *Emx1-Cre;Sema6AΔcyto*$^{fl/fl}$ mice showed a decrease in phosphorylation of a SATB2 peptide sequence. SATB2 directly binds to the *Ctip2* locus [26,29], together with a histone deacetylase (HDAC)-containing repressor complex recruited by Ski, to repress expression of this gene [55]. CTIP2 is a transcription factor and marker for deeper layer neurons. In *Satb2*$^{-/-}$ mice CTIP2 is upregulated in upper layer neurons that take on a deeper layer neuron identity and projection to subcortical regions [26,29]. In our dataset we found an increase of phosphorylated CTIP2 in *Emx1-Cre;Sema6AΔcyto*$^{fl/fl}$ mice suggesting altered phosphorylation of SATB2 might affect its activity here that could consequently affect the regulation and activity of CTIP2. In conclusion, SATB2 and CTIP2 phosphorylation motifs were significantly altered in *Emx1-Cre;Sema6AΔcyto*$^{fl/fl}$ mice suggesting a potential change in protein activity and function that could affect developmental programs involved in neuronal identity. Laminar disturbance and neuron mispositioning significantly affected the phosphorylation pattern of multiple other proteins including adhesion molecules, GTPases, kinases, RNA binding proteins. Protein phosphorylation at serine, threonine and tyrosine residues result in motifs that correspond to protein kinases and phosphatases. We used the online motifeR tool [56] and identified 187 enriched phosphorylation motifs (Fig. S8). The enrichment of certain amino acid motifs found here could help to identify the modifying enzyme and biological processes involved. MotifeR currently uses NetworKIN database to determine kinase signaling networks for human phospho-proteomics datasets [56]. Future studies and novel tools are needed to identify kinase signaling networks for the mouse phospho-proteome.

Previous work suggested actin regulatory proteins as potential interactors of Sema6A [57]. In this study, Sema6A and Sema6AΔcyto immunoprecipitation *in vitro* revealed strong enrichment for proteins of the actin-related proteins (Arp) 2/3 complex involved in the regulation of the actin cytoskeleton. All three datasets combined showed 49 shared protein hits (Fig. 16D). 9 out of 10 enriched IP hits, associated with actin regulation and organization or the

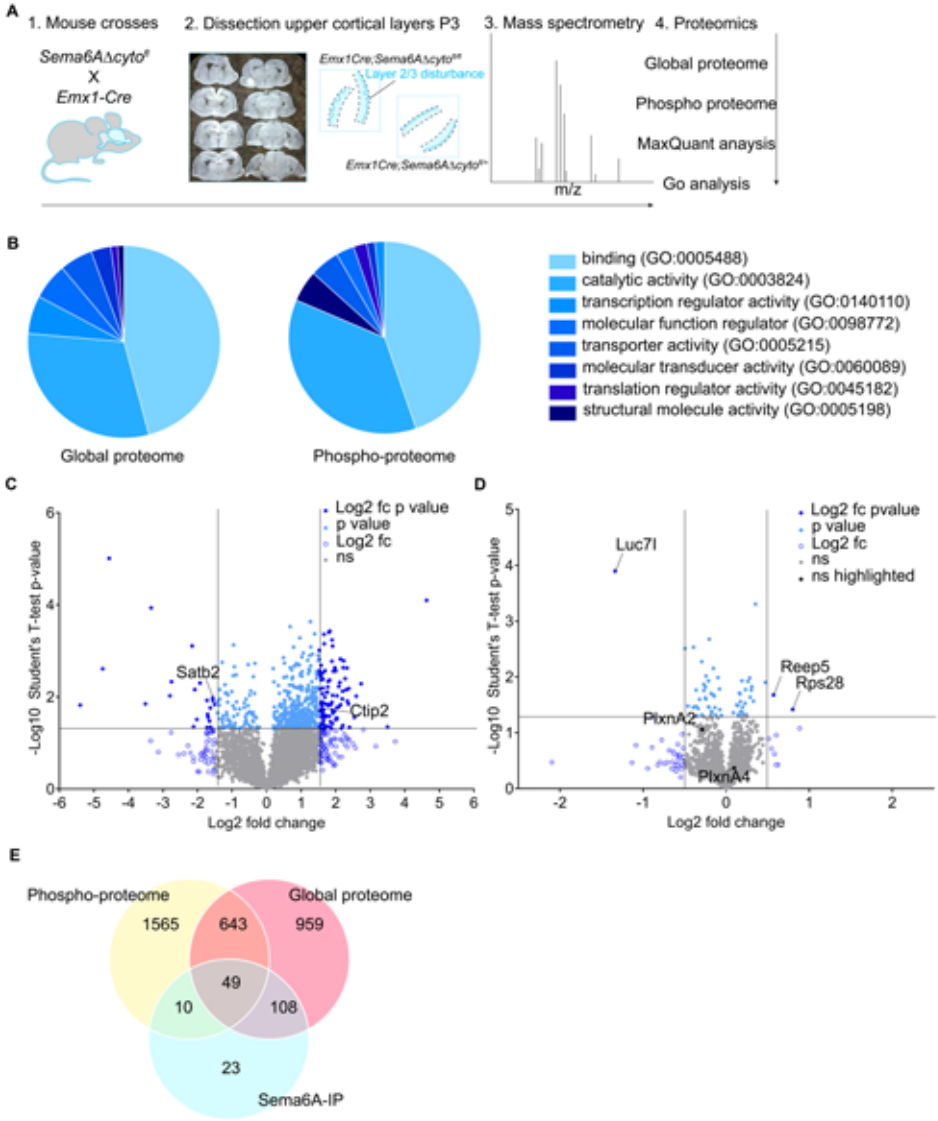

Figure 16. Isolation and proteomic profiling of layer 2/3 neuron mispositioning.
A) Cartoon illustrating experimental procedures. *Emx1-Cre;Sema6AΔcyto*$^{fl/fl}$ and control mice at P3 (1). Upper cortical layer dissection (n= 3-5 animals per sample) (2) followed by mass-spectrometry (3) to generate two datasets: global proteome and phospho-proteome (4). B) Protein functional classes represented in the upper cortical layers of *Emx1-Cre;Sema6AΔcyto*$^{fl/fl}$ and control mice in global and phospho-proteome. C) Distribution of proteins detected in phospho-proteome of *Emx1-Cre;Sema6AΔcyto*$^{fl/fl}$ versus control mice. D) Distribution of proteins detected in the global proteome of *Emx1-Cre;Sema6AΔcyto*$^{fl/fl}$ versus control mice. C, D) Significant proteins are highlighted as closed circles in blue (p value <0.05, Student's t-test). Significant measurements with differential expression are shown as closed circles with dark blue showing a log2 fold change >1.5 and light blue log2 fold change <1.5 (q value < 0.05, Benjamini-Hochberg correction). Open circles represent non-significant measurements with log2 fold change >1.5. D) Venn diagram capturing number and distribution of overlapping proteins detected in proteome, phosphor-proteome and IP experiments.

Arp2/3 complex directly [57], were also found in our global protein expression dataset. However, only 2 out of 9 hits, ARPC2 and CPSF6 proteins, were statistically significant measurements with no differential expression between conditions. Previously identified Sema6A-interacting proteins are mammalian enabled (Mena), vasodilator stimulated phosphoprotein (VASP), Ena-VASP like (EVL) and Tyrosine-protein kinase Abl (ABL) [21,58]. Enah (alias Mena), EVL and ABL were found in our global proteome and phospho-proteome datasets. However, these findings were not significant or showed no differential expression between groups and future studies are needed to determine their role. Mena, EVL and ABL are members of the Ena/VASP pathway involved in actin remodeling [21,58]. Future studies are needed to validate global and phospho-proteome findings and to determine the specific role for Arp2/3 complex and Ena/VASP pathway proteins in neuron positioning and cortical lamination.

RNAseq

As a final approach, we crossed *Emx1-Cre;Sema6AΔcyto*$^{fl/fl}$ with an *Ai14-stop-tdtom* reporter mouse line and sorted upper cortical layer cells including glutamatergic neurons, Cajal Retzius cells and glia at P2 (Fig. 17A, E) [33]. Sorted cells were processed for RNAseq to study RNA expression profiles of *Ai14;Emx1-Cre;Sema6AΔcyto*$^{fl/fl}$ and control animals. RNAseq transcript hits for exon 19 of *Sema6A* were visualized using the Integrative Genomics Viewer (IGV) [59] showing *Ai14;Emx1-Cre;Sema6AΔcyto*$^{fl/fl}$ mice lack most of exon 19 upon Cre recombination (Fig. 17B) (**Chapter 3**, Fig. 1F). Principle component analysis (PCA) did not demonstrate a clear separation of groups into clusters (Fig. 17C). Gene ontology (GO) analysis using the statistical overrepresentation test (Panther Overrepresentation Test, released 20200728) showing the top ten over- or underrepresented molecular functions are shown in supplementary table 3. We identified *PlexinA2, PlexinA4* and *Sema6A* in the dataset (Fig. 17D) suggesting that all three are expressed in upper cortical layers at P2. In total, 3 genes: ATP Binding Cassette Subfamily B Member 9 (ABCB9), 2-Oxoglutarate And Iron Dependent Oxygenase Domain Containing 2 (OGFOD2) and ADP Ribosylation Factor Like GTPase 6 Interacting Protein 4 (ARL6iP4), were found statistically differentially expressed between groups (Fig. 17D). None of these were previously linked to cortical lamination or neuron positioning. However, all three are associated with and shared between schizophrenia and cardiometabolic disease [60]. Taken together, we revealed a wide range of potential proteins involved in the Sema6A defect using a multi-omics approach. The interpretation of the combined omics data together with

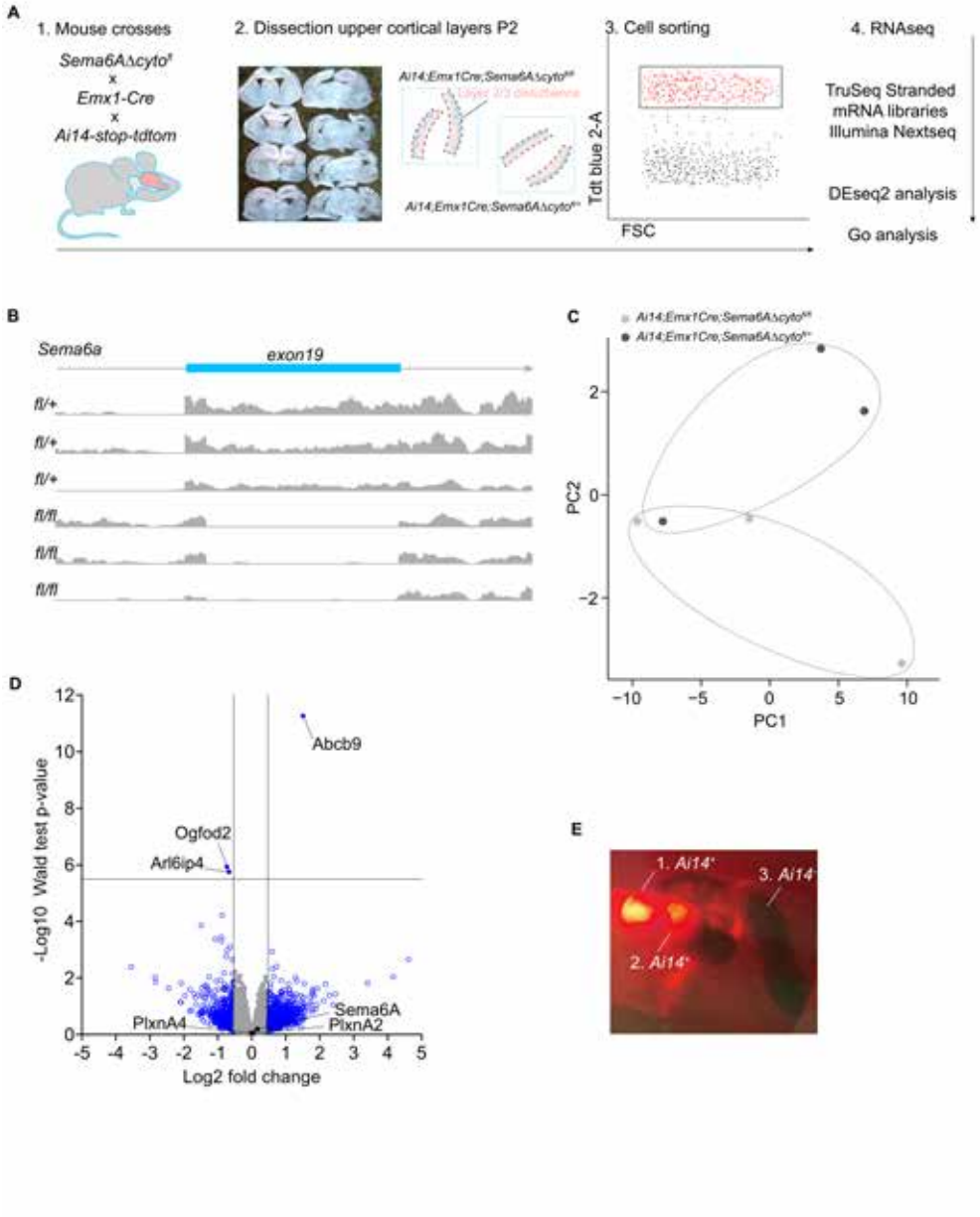

Figure 17. Bulk RNA-seq of *Ai14;Emx1-Cre;Sema6AΔcyto$^{fl/fl}$*.
A) Schematic overview of experimental process for bulk RNA-seq. *Ai14;Emx1-Cre;Sema6AΔcyto$^{fl/fl}$* and control mice at P2 (1). Upper cortical layer dissection (n= 3-5 animals per sample) (2) followed by Fluorescence-activated cell sorting (FACS) (3) and bulk RNA-seq (4). B) Schematic of Sema6A transcript hits for exon 19 . C) Principal component analysis of analyzed tissue samples. D) Blue closed dots represent significant DE genes in *Ai14;Emx1-Cre;Sema6AΔcyto$^{fl/fl}$* versus control mice (p value <0.05, Wald test) with a log2 fold change of >0.5 (q value <0.05, Benjamini-Hochberg correction). E) *Ai14;Emx1-Cre;Sema6AΔcyto$^{fl/fl}$* mice showing tdTom-positive fluorescence in the cortex.

functional studies to validate the role of identified proteins and their corresponding pathways provides an extensive dataset to understand the interplay of molecules at the level of the transcriptome, proteome and phospho-proteome during cortical development.

DISCUSSION

The cerebral cortex consists of 6 layers that are gradually formed and continue to grow and expand during postnatal development. The development of the 6 layered structure is a highly organized and complex process and its disruption has consequences for cortical function. How the precise organization of the layered structure is established and maintained during early postnatal development remains poorly understood. Here, we find a specific role for Sema6A reverse signaling in the organization of layer 2/3 neurons during early postnatal development. This signaling pathway is required to maintain the highly organized border between the cell sparse layer 1 and the densely populated layer 2/3 directly below. These findings show for the first time that Sema6A acts as a receptor in reverse signaling during cortical development *in vivo*. In addition, the reverse signaling pathway is essential for a novel principle of local structural organization during the development of the cerebral cortex.

Sema6A reverse signaling in layer 2/3 neurons

Previously published *PlxnA2/A4* dKO mice display neuronal mispositioning and laminar disturbance in layer 2/3 of the cortex [27]. To a similar extent, we found that the depletion of the intracellular domain of Sema6A from layer 2/3 pyramidal neurons specifically affects the positioning of these neurons and their neighboring cells. The proposed model by Hatanaka and authors suggests a role for SEMA6A in radial glia cells where it interacts with PLXNA2 and PLXNA4 expressed on the apical dendrites of layer 2/3 neurons during radial migration [27]. We set out to test this hypothesis, and to study how these molecules together are responsible for the organization of upper cortical laminae. We demonstrate that upon conditional deletion of Sema6A from radial glia cells, no neuronal mispositioning or laminar disturbance is detected. Instead, conditional deletion of Sema6A from layer 2/3 neurons specifically results in mispositioning and cluster formation. This effect has non-cell autonomous consequences for neighboring, unaffected cells located in the neuronal clusters as well. The non-cell autonomous effect can be explained due to the mispositioned neurons that have grown into

layer 1 and express PLXNA2 on their apical dendrites. This signal enhances the mispositioning for neighboring neurons that still express SEMA6A and interact with the mispositioned neurons and their apical dendrites expressing PLXNA2. In addition, before the defect onset, layer 2/3 neurons display a branched phenotype with dendrites innervating layer 1 that suggests a post-migratory effect since dendrites in cortical neurons form after migration ends [35]. Also, early arrived layer 2/3 neurons settle around E18.5-P0 (Chai et al. 2015; Ignacio et al. 1995 and Fig. 9) and do not display a 'build-up' of over-migrating cells towards the pial surface as hypothesized by Hanatanaka et al. [27]. We did not detect such a phenotype in the absence of the intracellular domain or in the complete absence of SEMA6A. Instead, spatiotemporal analysis showed that when most layer 2/3 neurons have settled at the pial surface the initial neuron mispositioning is characterized by an overall shift of layer 2/3 invading the cell sparse layer 1 at P2. At this time, the brain is expanding rapidly and our findings suggest that the normally sharp border between layer 2/3 and layer 1 is no longer controlled in the absence of SEMA6A intracellular domain.

Neuronal cluster formation in *Sema6AΔcyto*$^{fl/fl}$ mice

The correct positioning of neurons and organization of cortical layers during development is essential for the establishment of neuronal circuits [17]. *Sema6AΔcyto*$^{fl/fl}$ mice display neuronal clusters in multiple sensory brain regions including somatosensory cortex, auditory cortex and the temporal association area (Fig. 2). Recently, the differences in migratory behavior of neurons in multiple sensory regions were described in detail [61]. Neurons generated on the same day during embryonic ages, position more superficial in the auditory cortex compared somatosensory or visual cortical regions during early postnatal development [34]. The timing difference in these areas could contribute to the number of cells affected per region in *Sema6AΔcyto*$^{fl/fl}$ mice and consequently the formation of clusters that vary in size. In addition, previous reports have shown that the laminar thickness and cortical boundaries between the different layers in the primary sensory cortexes are different for the auditory (A1), somatosensory (S1) and visual (V1) cortical regions that become apparent during postnatal development [62]. For example, layer 5 in the A1 is larger compared to layer 5 in the S1 and V1. In the A1, layer 5 increases during early postnatal development and becomes mature at P10 while S1 and V1 continue to mature until P15 (Chang et al., 2018). Layer 5 neurons project to layer 1 that is increasingly innervated to establish connections and form functional microcircuits [62]. Consequently, mispositioned neurons that are located in layer 1 become

confined to an increasingly smaller space and form clusters. In conclusion, neuron mispositioning is detected with increasing severity and cluster formation, from low in medial to high in lateral regions. We hypothesize that the formation of the clusters is a secondary effect triggered by the region-specific migratory behavior and timing of neurons followed by an increase in layer 1 innervation during postnatal development.

The increased innervation and growth of layer 1 during at stages seem to coincide with PLXNA2 expression on apical dendrites that creates a non-permissive zone for neurons in layer 2/3 that change their position accordingly. Interestingly, a change in position of layer 2/3 neurons that shift to a slightly deeper position was observed previously (Yoshinaga et al., 2020). This was found in the lateral cortex specifically while it was not observed in the medial cortex (Yoshinaga et al., 2020). Since the shift is normally more dramatic in the lateral region of the cortex it could explain why the mispositioning and the largest clusters are found in the lateral cortical regions in the absence of SEMA6A. Also, rescue experiments by Hanataka et al. (Hatanaka et al. 2019 and Fig. 5C') showed that overexpression of PLXNA2 in neurons located in the middle and lower compartment of layer 2/3 creates a cell sparse zone right above. This finding contributes to the idea that the high increase in PLXNA2 acts as a non-permissive zone for neurons irrespective of their location.

The clustering effect potentially further compromises the organization of layer 2/3 neurons that show altered cell soma orientation in *Sema6AΔcyto*$^{fl/fl}$ mice. Mispositioned layer 2/3 neurons might also be morphologically affected and therefore future *in vivo* experiments are important to study the neuronal morphology that potentially influences their functions in the circuitry. Although there is no clear architectonic boundary between layer 2 and layer 3, neurons at the border of layer 2 have a distinct morphology, compared to layer 3, with apical and basal dendrites that invade layer 1 extensively [63]. These neurons have oblique apical dendrites or no obvious apical dendrites which is not a typical pyramidal neuron morphology [63]. Interestingly, PLXNA2 shows high expression at the border of layer 2 were this type of morphologically distinct cell is located. In addition, in *Emx1-Cre;Sema6AΔcyto*$^{fl/fl}$ mice, mispositioned neuronal clusters within layer 1 seem to keep their original horizontal organization with PLXNA2 found closest to the pial surface. Future studies are needed to confirm the importance of this morphologically distinct subset of neurons in the positioning of layer 2/3.

Based on our proteomics data, we hypothesize that SATB2 is a potential candidate involved in layer 2/3 mispositioning and formation of neuronal clusters. SATB2 was previously suggested to be involved in the regulation of genes that are required for adhesion and/or repulsion of cortical pyramidal neurons [54]. Layer 2/3 neurons that lack SATB2 showed reduced dendritic expansion and fascicle formation. Interestingly, not only Satb2-deficient neurons but also neighboring neurons were affected which was also observed in our studies for SEMA6A deficient layer 2/3 neurons that display a non-cell autonomous effect. Morphological analysis of affected neurons in *Sema6AΔcyto*$^{fl/fl}$ mice is essential to explore the role of SEMA6A on dendrite morphology and to study a potential link with SATB2. This idea could be studied by using IUE to overexpress SATB2 (pCAG-SATB2 plasmid) in *Sema6AΔcyto*$^{fl/fl}$ mice and determine if this treatment might rescue mispositioning defects. If so, this would suggest that SATB2 has a downstream effect in Sema6A reverse signaling.

Ena/VASP proteins were detected in our proteomics datasets and have been previously linked to Sema6A reverse signaling [21,58,64]. Ena/VASP proteins are a family of actin-associated proteins known to influence actin dynamics. This pathway is required for the process of neuritogenesis in the developing cortex found to be involved in regulating cortical positioning [65]. Ena/VASP deficient neurons show aberrant targeting to more superficial layers and formation of neuronal ectopias [65,66]. To what extent the Ena/VASP pathway is involved in specific processes affected here, for example, radial migration, termination of migration or post-migratory sorting, remains unknown. In general, many not previously associated hits or candidates with uncharacterized functions were identified in our dataset. Future studies are needed to validate the biological relevance of the identified hits.

Neuronal circuit development in *Sema6AΔcyto*$^{fl/fl}$ mice

Proper neuron positioning and laminar organization might be important for the formation of microcircuits within the cortex [17,67-69]. The precise pattern of laminar connectivity generates characteristic response properties of cortical neurons [70,71]. The question remains how the neuronal clusters found in *Sema6AΔcyto*$^{fl/fl}$ mice affect the functional connectivity of mispositioned neurons. One way to study this is to determine the electrophysiological properties of layer 2/3 neurons located in neuronal clusters and to specify their role and activity within the circuit. Long-range projections and inputs might be preserved as was found for Reeler mice where the cortex is still innervated by thalamic inputs although cortical laminae are severely

disturbed [72]. However, local connectivity patterns might be affected. Network disorganization in layer 1 and lamination problems causing an imbalance in excitation and inhibition are associated with neurodevelopmental disorders such as autism spectrum disorder (ASD) [73,74]. It is therefore important to study the electrophysiological properties and for example excitability of layer 2/3 neurons in order to determine the consequences of their mispositioning and cluster formation for neuronal circuitry formation and function.

Model

Based on our results we propose the following model (Fig. 18). Layer 2/3 neuron terminate glia-guided radial migration and somal translocation at the pial surface (Fig. 18.1). Apical dendrites branch and start to express PLXNA2 at the border between layer 2/3 and layer 1. PLXNA2 expressing apical dendrites interact with SEMA6A expressing layer 2/3 neurons and occupy their final target position in layer 2/3 through the reverse signaling pathway (Fig. 18.2a) In the absence of the intracellular domain of Sema6A, this signaling pathway is lost which causes mispositioning of layer 2/3 neurons into layer 1 and neuronal cluster formation (Fig. 18.2b). The question remains how this defect influences neuronal maturation and circuitry development (Fig. 18.3). In conclusion, Sema6A-PlexinA2/A4 reverse signaling in cortical layer 2/3 neurons is important for layer 2/3 neuron positioning and laminar organization. Normally, the Sema6A-PlexinA2/A4 interaction creates a non-permissive zone in layer 1 to orchestrate cell positioning and laminar organization in a non-cell autonomous manner. Consequently, layer 2/3 neurons create space for increasing local and long-range innervation in layer 1 to establish functional neuronal circuitry during development.

METHODS

Mouse lines

All animal use and care were in accordance with institutional guidelines and approved by the Animal Ethics Committee of Utrecht University (Dierexperimenten Ethische Commissie) (CCD licence: AVD115002016532) and conducted in agreement with Dutch laws (Wet op de Dierproeven, 1996, revised 2014) and European regulations. The different Sema6A mouse strains used in this study were *Sema6AΔcyto*$^{fl/+}$ (**Chapter 3**), *HASema6A* $^{fl/+}$ (unpublished, kindly provided by Alex Kolodkin) and

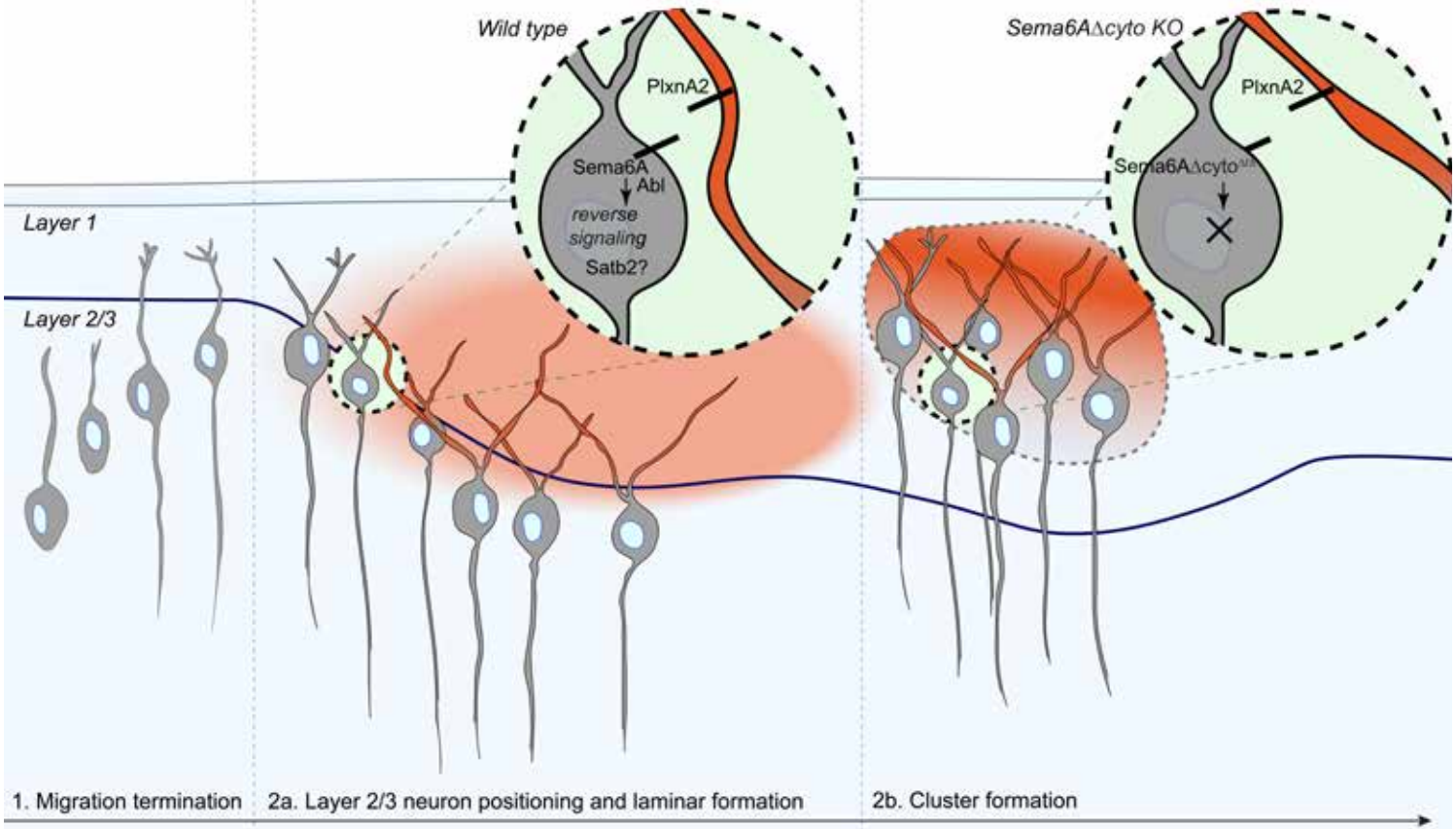

Figure 18. Proposed model of Sema6A reverse signaling in cortical neurons regulating neuron positioning and laminar organization.
During early postnatal development layer 2/3 neurons settle at the pial surface and start to mature and branch into layer 1 with apical dendrites expressing PlxnA2. Sema6A expressing neurons interact with apical dendrites in a non-cell autonomous manner and settle slightly deeper into the cortex to maintain a strict border between layer 1 and layer 2/3. In the absence of the intracellular domain of Sema6A (*Sema6AΔcyto*$^{fl/fl}$), neurons fail to move to their proper position and instead stay close to the pial surface with extending apical dendrites expressing PlxnA2. Layer 1 innervation increases rapidly and consequently neuronal clusters are formed.

Sema6A$^{-/-}$ (Sema6aGt[KST069]Byg) [75]. In addition, we used *PlexinA2*$^{-/-}$ mice (Suto et al. 2007, kindly provided by Roman Giger) and brain tissue from *PlexinA4*$^{-/-}$ *mice* (Suto et al. 2005, kindly provided by Alain Chédotal) mice. Timed-pregnant females were 3-6 months of age. The morning on which a vaginal plug was detected was considered embryonic day 0.5 (E0.5). We crossed *Sema6AΔcyto*$^{fl/+}$ with specific Cre lines: *Ella-Cre* (JAX stock #003800) [76], *Nestin-Cre* (JAX stock #003771) [77], *Emx1-Cre* (JAX stock #005628) [33] or *GBX2-CreEr-IRES-EGFP* (JAX stock #022135) [78] (kindly provided by Peter Burbach). *HASema6A* $^{fl/+}$ mice were crossed with *Ella-Cre*. The specific crosses were referred to as *Ella-Cre;Sema6AΔcyto*$^{\Delta/\Delta}$, *Nestin-Cre;Sema6AΔcyto*$^{fl/fl,}$ *Emx1-Cre;Sema6AΔcyto*$^{fl/fl}$ and *Gbx2-Cre;Sema 6AΔcyto*$^{fl/fl}$ and *Ella-Cre;HASema6A*$^{\Delta/\Delta}$*. Emx1-cre;Sema6AΔcyto*$^{fl/fl}$ mice were then crossed with Ai14 reporter mice (JAX stock #007914) containing a floxed-stop cassette followed by tdTomato fluorescent protein (tdTom) in the ROSA26 gene locus [79]. All mice were maintained on a *C57Bl/6* background and housed under a 12 h light/dark cycle and were given food and water ad libitum. For genotyping, we obtained tail samples for DNA extraction and PCR analysis (**Chapter 3**, supplemental table 1 for program details).

In Utero Electroporation

For *in utero* electroporation (IUE) experiments, timed-pregnant *C57BL/6* mothers were injected with 0.05 mg/kg buprenorfinhydrochloride in saline and deeply anesthetized with isoflurane. The abdominal cavity was opened under sterile surgical conditions, uterine horns exposed and 1.7 µl of DNA mixture containing 0.4 µg/µl pCAG-GFP (Addgene, Cat #11150), 2,0 µg/µl pCAG-Cre-IRES2-GFP (Addgene, Cat# 26646) (Woodhead et al., 2006), pCAG-Sema6A-GFP (in house cloning, adaptation of pCAG-GFP) or pEF1-myc-Sema6AΔABL (kindly provided by Alain Chédotal) vectors dissolved in MQ with 0.05% Fast Green (Sigma-Aldrich) was injected in the lateral ventricles of the embryo's using glass micropipettes (Harvard Apparatus) and a PLI-100 Pico-injector (Harvard Apparatus). Brains were electroporated using an ECM 830 Electro-Square-Porator (Harvard Apparatus) set to five unipolar pulses of 35 V (50 ms pulse length, 950 ms interval). The lateral cortex was targeted by two gold-plated Genepaddles placed on the head diagonally in the coronal plane, with one positive pole placed on the lateral cortex and one negative pole on the medial cortex on the contralateral side (Fig. 6A). Brain tissue was collected at multiple timepoints ranging from P0-P15. After birth, pups were perfused and processed for immunohistochemistry.

BrdU injections

To assess cell proliferation and migration patterns in the cortex we used 5-Bromo-2'-deoxyuridine (BrdU) in *C57Bl/6* mice. IUE pregnant mice were injected intraperitoneal with BrdU (Sigma-Aldrich, 15 mg/ml) 50 mg/kg^{-1} in saline. After birth, pups were perfused and processed for immunohistochemistry. For analysis of IUE combined with BrdU experiments, the location of the cells was determined using a field of 10 bins corresponding to different cortical areas. Bin 10 corresponds to layer 1, bin 9, 8 to layer 2/3, bin 7 to layer 4, bin 6, 5 to layer 5, bin 4 to layer 6 and bin 3, 2, 1 to ventricular and intermediate zones.

Tamoxifen administration

At E10.5 *Gbx2-CreER;Sema6AΔcyto$^{fl/+}$* pregnant mothers were treated with 0.1 mg/gr body weight tamoxifen (Sigma-Aldrich) in corn oil (Sigma-Aldrich) through oral gavage as described previously [80]. After birth, brain tissue was collected at P10 and processed for immunohistochemistry.

Tissue collection and sectioning followed by immunohistochemistry

Tissue collection and sectioning was done as described previously (**Chapter 3**). Immunohistochemistry was done as described previously (**Chapter 3**) with the following adjustments. Anti-Sema6A staining required blocking buffer without triton. Brain sections were mounted using Fluorsave, imaged on an Axioskop EPI-fluorescent microscope (Zeiss) or LSM laser-scanning confocal microscope (Zeiss) and processed using FIJI image analysis software.

iDISCO tissue clearing

Brains were perfused, fixed in 4% PFA overnight and washed in PBS. The iDISCO+ procedure was performed as described by Reinier et al. (protocol version december 2016) [24]. In short, brains were permeabilized following gradual dehydration in methanol/H2O (20%-40%-60%-80%-100%; 1 h each) followed by overnight incubation in 66% dichloromethane (DCM)/33% methanol at RT. The next day, samples were washed in 100% methanol and kept at 4 °C for overnight bleaching with a 1:5 ratio (hydrogen peroxide:methanol) followed by rehydration in methanol/PBS (80%-60%-40%-20%-PBS-PBS, 1 h each) and one final wash with PBS and 2% TritonX-100 (PTx.2). Samples were permeabilized (PTx.2, 2,3% Glycine, 20% DMSO) for 2 days at 37 °C and blocked (84% PTx.2, 6% donkey serum, 10% DMSO) for 2 days at 37 °C. After washing with PBS, supplemented with

2% Tween-20 and 1% Heparin (10mg/ml) (PTwH) (4-5 times, 1 h each), samples were incubated with primary antibody anti-SATB2 (1:500) in PTwH, supplemented with 5% DMSO and 3% donkey serum, for 14 days at 37 °C on a rocking platform. After washing in PTwH (4-5 times, 1h each) samples were incubated with filtered (45 µm filter) secondary antibodies donkey anti rabbit 750 (Alexa, 1:1000) in PTwH, supplemented with 3% donkey serum, for 7 days at 37 °C. After, samples were washed with (PtwH) (4-5 times, 1 h each) and processed for tissue clearing [24]. Tissue was gradually dehydrated by incubation with methanol in H2O (20%-40%-60%-80%-100%-100%, 1 h each). Samples were incubated with 66% DCM (Sigma, 270997) and 33% methanol for 3 h at RT, and two times with 100% DCM for 15 min. each to wash the methanol. Brains were transferred to a new tube containing 100% DBE (Sigma, Cat# 108014) kept in the dark for 1 day before imaging.

Lightsheet microscopy

3D imaging of whole brain samples was performed with an Ultramicroscope II lightsheet microscope (LaVision Biotec GmbH) equipped an MVX-10 Zoom Body (Olympus), MVPLAPO 2x Objective lens (Olympus), Neo sCMOS camera (Andor) (2560 x 2160 pixels, pixel size: 6.5 x 6.5 μm^2). Samples were placed in a DBE containing reservoir. The samples were illuminating with sheets of light, a sheet numerical aperture (NA) of 0.7 µm, in combination with a 730 nm emission filter (Coherent OBIS 730-30 LX Laser (30mW)). As a reference the 488nm emission filter (Coherent OBIS 488-50 LX Laser (50mW)) was used to image auto-fluorescence signal. ImpectorPro software (version 7.1, LaVision BioTech GmbH) was used for image acquisition with a minimal step size of 2.5 µm and horizontal focus scanning method with the suggested optimal number of steps, using the blending mode algorithm and zoom factor 0.8x for P10 brains. Image analysis was done using Imaris software (version 9.6, Bitplane). Images were processed to remove debris and antibody aggregates. Snapshots and movies (Supplementary Table 4) were generated.

Golgi-Cox staining

Brain tissue processed for Golgi-Cox staining using the FD rapid-Golgi staining kit (FD Neurotechnologies USA, Cat# PK401). In short, brains were dissected, quickly rinsed in double distilled Milli-Q to remove blood and immersed with mercury chromate-based solution for 14 days in the dark. 200 µm coronal sections were cut on a vibratome (VT1000S Leica) and collected on gelatin-coated microscope slides (FD Neurotechnologies USA, #PO101). Slides were stained, dehydrated and embedded in Permount

mounting medium (Thermo Fisher Scientific, #SP15-100). Samples were imaged on a digital slide scanner (Hamamatsu Nanozoomer) using a 40x objective and 4 µm z-axis step size. Lateral and caudal cortical brain regions were selected using NDP.view software (version 2.5.14).

RNA *in situ* hybridization

Brains were isolated and fixed in 4% PFA over night, cryoprotected in 30% sucrose in PBS, frozen in isopentane and stored in -80 °C for later use. Brain tissue was cut on a cryostat (Leica) in 20 µm thick sections and mounted on superfrost slides. RNA probes were produced as described previously [81]. T3 or T7 promotor sequences were introduced at the 5′ end of gene-specific oligonucleotide reverse and or forward primers respectively. *In situ* hybridization (ISH) was performed as described previously by Pasterkamp et al. (Pasterkamp et al. 1998a). For *Emx1-Cre;Sema6AΔcyto*$^{fl/fl}$, *Ella-Cre;HASema6A*$^{\Delta/\Delta}$ and control mouse tissue DNA-templates were transcribed from PCAG-Sema6A, pCAG-PlexinA2 and pCAG-PlexinA4 plasmids using the following primers: *PlxnA2*: 5′-TAATACGACTCACTATAGGGGAGAGTGTCTAAGCTCAGGGG-3′ 5′-AATTAACCCTCACTAAAGGGGGTACGAGCTGTTTTGGCAC-3′ *PlxnA4*: 5′-TAATACGACTCACTATAGGGCAAGGACCACGAGCAACTCT-3′ 5′-AATTAACCCTCACTAAAGGGCTCAGGTAGCTTCACTCGGC-3′ *Sema6A*: exon 3 5′-TAATACGACTCACTATAGGGCCCAGAAGATTCCGAGCCAA-3′ 5′-AATTAACCCTCACTAAAGGGTCTGTGTGGGATGTGTCTATATCA-3′ *Sema6A*: intracellular sequence 5′-TAATACGACTCACTATAGGGCCAGCATCACCTAGACCTCACC-3′ 5′-AATTAACCCTCACTAAAGGGCTTCATGGATGTGGAAAGGGGA-3′. Following gel electrophoresis, PCR fragments were purified using Quick-spin columns (Qiagen). 50 ng of purified fragments were transcribed using T3 or T7 RNA polymerase (Roche) and Digoxigenin-labeled nucleotide mix using Dig-labeling kit (Roche) to produce cRNA probes. Digoxigenin was detected with anti-digoxigenin FAB fragments conjugated to alkaline phosphatase (Roche) and NBT/BCIP staining (Roche). ISH was combined with immunohistochemistry as described previously with the following adaptations. Blocking buffer used was PBS/GT 0.25% (0.2% gelatin, o.25% triton-X in PBS) and secondary antibody mixtures were filtered (45 µm filter) before use. Sections were mounting using Mowiol and images were acquired using epifluorescent illumination on a Zeiss Axioskop A1 or by confocal laser scanning microscopy (LSM880, Carl Zeiss).

Dissection of *Emx1-Cre;Sema6AΔcyto$^{fl/fl}$* upper cortical layers and mass spectrometry

Brain tissue of P3 *Emx1-Cre;Sema6AΔcyto$^{fl/fl}$* and control mice were cut into 300 µm coronal sections using the tissue chopper (McIllwain). Upper cortical layers were dissected in Leibovitz's L-15 medium (Thermo Fisher Scientific, Cat #21083027) and isolated tissue comprised approximately cortical layers 1-4 (Fig. 16A, 17A). Tissue was collected in an Eppendorf tube and quickly frozen in isopentane and stored at -80 °C for later use. Three samples of each n=4 pups for each condition were subjected to mass spectrometry analysis (Erasmus Proteomics Center Rotterdam).

Mass Spectrometry

Sample preparation

Brain tissue was lysed in 0.25 ml 50 mM Tris/HCl pH 8.2, 2 % sodium deoxycholate (SDC) using a Bioruptor ultasonicator (Diagenode). Protein concentrations were measured using the BCA assay (Thermo Scientific). 0.5 mg protein in 0.25 ml were reduced with 5 mM DTT and cysteine residues were alkylated with 10 mM iodoacetamide. Proteins were digested with LysC (1:200 enzyme:protein ratio) for 4 h at 37 °C. Next, trypsin was added (1:100 enzyme:protein ratio) and the digestion proceeded overnight at 37 °C.

Phosphopeptide enrichment

Phosphopeptide enrichment was carried out according to the protocol of Humphrey et al. [83] with some modifications. To the tryptic digest 400 µl isopropanol, 100 µl 48% TFA and 6 mg TiO_2 beads (GL Sciences) were added and this was incubated on a rotator at room temperature for 30 min. The TiO_2 beads were spun down and washed four times with 5% TFA in 60 % isopropanol. Next, the TiO_2 beads were transferred to a C8 Stagetip and washed once with 60 % isopropanol. The phosphopeptides were eluted with two times 50 µl ammonia in 40% acetonitrile and the eluate was dried in a vacuum centrifuge.

LC-MS

(Phospho)peptides were analyzed by nanoflow LC-MS/MS on an EASY-nLC 1200 coupled to an Orbitrap Lumos Tribid mass spectrometer (Thermo) operating in positive mode and equipped with a nanospray source as described earlier [84]. Peptides were separated on a 1.9 µm ReproSil C18 reversed phase column (Dr Maisch GmbH; column dimensions 25 cm × 75 µm, packed in-house) using a linear gradient from 0 to 40% B (A = 0.1 % FA; B = 80% (v/v) AcN, 0.1 % FA) in 120 min and at a constant flow rate of

250 nl/min. The column eluent was directly sprayed into the ESI source of the mass spectrometer. Mass spectra were acquired in continuum mode; fragmentation of the peptides was performed in data-dependent mode.

Data analysis

Raw mass spectrometry data were analyzed with the MaxQuant software suite (version 1.6.6.0) [85] with the additional options 'LFQ' and 'iBAQ' selected. A false discovery rate (FDR) of 0.01 for proteins and peptides and a minimum peptide length of 7 amino acids were set. The Andromeda search engine was used to search the MS/MS spectra against the Uniprot database (taxonomy: *Mus musculus*, release April 2019) concatenated with the reversed versions of all sequences. A maximum of two missed cleavages was allowed. The peptide tolerance was set to 10 ppm and the fragment ion tolerance was set to 0.6 Da for HCD spectra. The enzyme specificity was set to trypsin and carbamidomethylation (C) was set as a fixed modification, while phosphorylation (STY) and oxidation (M) were set as variable modifications. Both the PSM and protein target FDR were set to 0.01. In case the identified peptides of two proteins were the same or the identified peptides of one protein included all peptides of another protein, these proteins were combined by MaxQuant and reported as one protein group. Before further statistical analysis, known contaminants and reverse hits were removed.

For the identification of significantly changed proteins in the global proteome or phosphopeptides in the phospho-proteome, t-test-based statistics was applied on LFQ data in Perseus. First, the logarithm (log2) of the LFQ values were taken, resulting in a Gaussian distribution of the data. This allowed imputation of missing values by normal distribution (width=0.3, shift=1.8), assuming these proteins were close to the detection limit. Statistical outliers for *Emx1-Cre;Sema6AΔcyto*$^{fl/fl}$ compared to control were then determined using two-tailed t-test. Multiple testing correction was applied by using a permutation-based false discovery rate (FDR) method. As a final step, we filtered our protein list based on the following criteria. Identified proteins had to have at least three peptide identifications in one of the two conditions. The log2 fold change was set on the basis of the normalized value of 0.5 for global proteome and 1.5 for phospho-proteome. Proteins were determined significant if the student's t test p-value was <0.05.

MotifeR

To identify enriched phosphorylation motifs in the phospho-proteome dataset we used a novel online tool MotifeR [56]. In short, in our dataset we found 19783 (unfiltered) phosphopeptides that we used as the foreground dataset and compared it to a background dataset of mouse proteome from UniProt database (Proteome ID: UP000000589, https://www.uniprot.org). Analysis identified patterns of amino acids that are overrepresented in the foreground dataset relative to the background dataset.

Fluorescence-activated sorting and RNAseq of *Ai14;Emx1-Cre;Sema6AΔcyto*$^{fl/fl}$ and RNAseq

Dissection of upper cortical layers was done as described previously. Isolated cortical tissue from P2 *Ai14;Emx1-Cre;Sema6AΔcyto*$^{fl/fl}$ was transferred to a collection tube and processed for fluorescence-activated cell sorting (FACS). We used trehalose enhanced isolation methods described by Saxena et al. [86] and papain dissociation (Papain Dissociation Kit, Worthington Biochemical Corporation, Cat # LK003176). Cortical tissue was trypsinized, dissociated into single cells and transferred to a BSA column (30% BSA) and centrifuged for 5 min at 4 °C to collect the cellular fraction. Cells were resuspended in HBSS medium (Fisher Scientific, Cat #14185045) supplemented with 1.5% trehalose (MP Biomedicals Cat #103087) and 0.6% Hepes (1M, Sigma-Aldrich Cat #54457). In addition, 20% deoxyribonuclease I (dnaseI) (1 mg/ml) and 0.25% EDTA (0.5M) were added and total suspension was filtered (70 µm) to prevent clotting. Just before running the samples in the cytometer, DAPI was added (1mg/ml). TdTomato positive cells were sorted on a BD FACS Aria III flow cytometer using an 85 µm nozzle at 45 psi. TdTomato was excited using a 488 nm laser and detected with a 575/26 nm band-pass filter. Unstained cells were analysed to calculate the percentage of positive versus negative cells expected at a balance of approximately 85%-15% respectively for cortical tissue of *Ai14;Emx1-Cre;Sema6AΔcyto*$^{fl/fl}$ and gates were set accordingly. To prevent RNA degradation, sorted cells were collected directly in Qiazole (Qiagen) and snap frozen on dry ice and stored at -80 °C for later use. Samples were processed for RNA isolation using miRNAeasy kit (Qiagen) according to the manufacturer's protocol and stored at -80 °C for later use. Samples were pooled from n=4-6 pups to create three samples for each condition and were subjected to RNA sequencing (RNAseq) (USEQ, University Utrecht).

RNAseq

RNA quantity was measured with the Invitrogen™ Qubit™ 3.0 Fluorometer using the Qubit RNA HS Assay Kit (Cat. Q32855). And RNA quality was checked with Agilent Bioanalyzer2100 RNA Pico chip (Cat# 5067-1513). 50 ng of total RNA was used to prepare TruSeq Stranded mRNA libraries (Cat# 20020594) following the manufacturers protocol. After the library preparation, libraries were checked with a Bioanalyzer2100 DNA 1000 chip (Cat# 5067-1504) and with Qubit dsDNA HS Assay Kit (Cat# Q32854). Libraries were equimolar pooled and 0,9 pM of library pool was sequenced in a Illumina Nextseq 1 x 75 bp high output (Cat. 20024906) run.

Data analysis

Data analysis was carried out according to standardized USEQ (Univerisity Utrecht) protocols (https://github.com/UMCUGenetics/RNASeq). In short, RNAseq data were checked for overall quality and yield using FastQC. The reads were mapped to the *Mus musculus* reference genome (Mus_musculus.GRCm38.70.gtf) available on ENSEMBL (https://www.ensembl.org/) using STAR alignment (85%-90% uniquely mapped reads per sample) to generate BAM files. Unique gene hits within exon regions were counted. Gene ontology analysis based on the molecular function was performed on all unique hits using the Panther Classification System (http://www.pantherdb.org) [50]. Differentially expressed gene analysis was carried out using DESeq2 [87] to compare gene expression between the two groups of samples. A PCA plot of the samples was generated within the DESeq2 package. The Wald test was used to generate p-values and log2 fold changes. An adjusted p-value was calculated based on Benjamin-Hochberg procedure. Genes with adjusted p-values of <0.05 and log2 fold change >0.5 were considered statistically differentially expressed genes.

Gene ontology analysis

To find molecular functions overrepresented in the upper cortical layers of P3 *Emx1-Cre;Sema6AΔcyto*$^{fl/fl}$ mice, we used the statistical overrepresentation test in the Panther Classification System (http://www.pantherdb.org) [50]. The functional classification tool was used to analyze the overall distribution without major cellular components. We used the *Mus musculus* genome as a reference (http://www.pantherdb.org).

Acknowledgements

We thank all members of the Pasterkamp laboratory and Department of Translational Neuroscience for assistance and helpful discussions throughout this project. We thank Kevin Mitchell for providing *Sema6A*$^{-/-}$ mice; Roman Giger for providing *PlexinA2*$^{-/-}$ mice; Alain Chédotal for providing the pEF1-myc-Sema6AΔABL plasmid; Jeroen Demmers, Karel Bezstarosti and Erikjan Rijkers for mass spectrometry experiments and data analysis; Roland van Dijk for FACS experiments; USEQ Utrecht for help with RNAseq and data analysis. This work was supported by the Netherlands Organization for Health Research and Development (ALW-VICI).

Author Contributions

M.G.V. and R.J.P. designed all experiments. M.G.V. performed all experiments together with Y.A. for iDISCO experiments; C.M. for IUE experiments and tamoxifen administration; M.Z. for immunohistochemistry; E.Y.B. and J.B. for ISH. C.M. arranged mouse breeding. M.G.V. and R.J.P. wrote the manuscript with critical feedback from G.M.J.R. and input from all authors.

SUPPLEMENTAL FIGURES

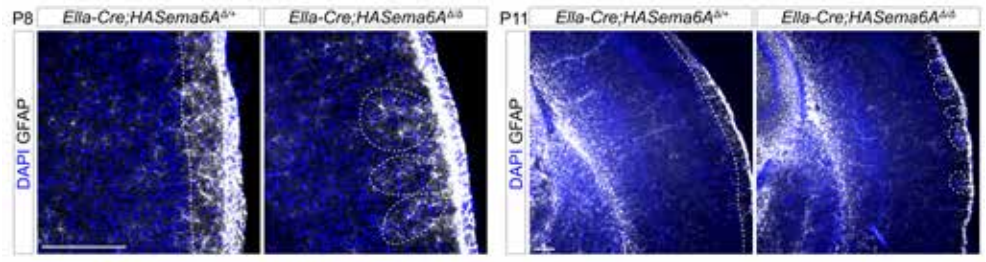

Figure S1. Astrocytes positive for GFAP found in neuronal clusters in *Ella-Cre;HASema6A*$^{\Delta/\Delta}$ mice. Immunohistochemistry using rabbit anti-GFAP antibodies at P8 (left) and P11 (right). Neuronal clusters visualized using DAPI and indicated by the dotted circles. Dotted lines indicate the border between layer 1 and layer 2/3. Scale bar 200 µm.

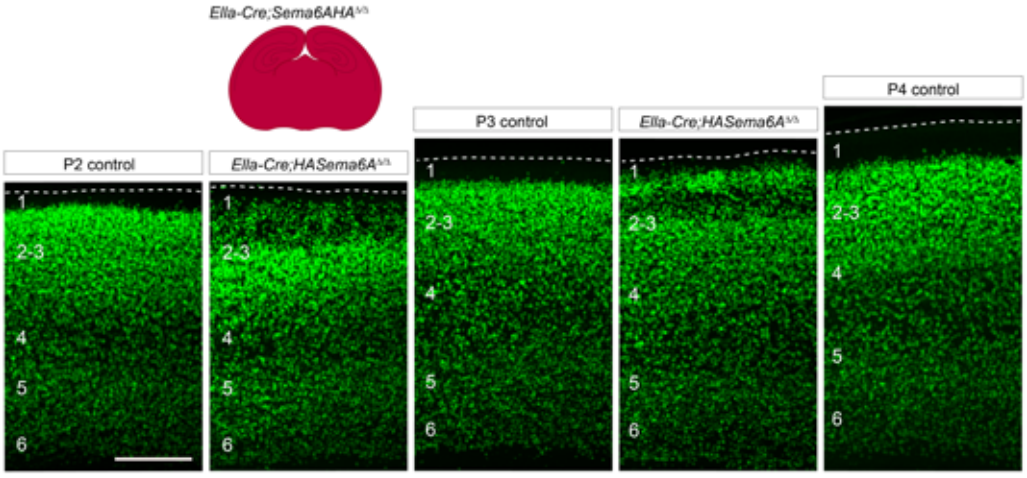
Ella-Cre;Sema6AHA$^{lx/lx}$
P2 control
Ella-Cre;HASema6A$^{lx/lx}$
P3 control
Ella-Cre;HASema6A$^{lx/lx}$
P4 control
1
2-3
4
5
6

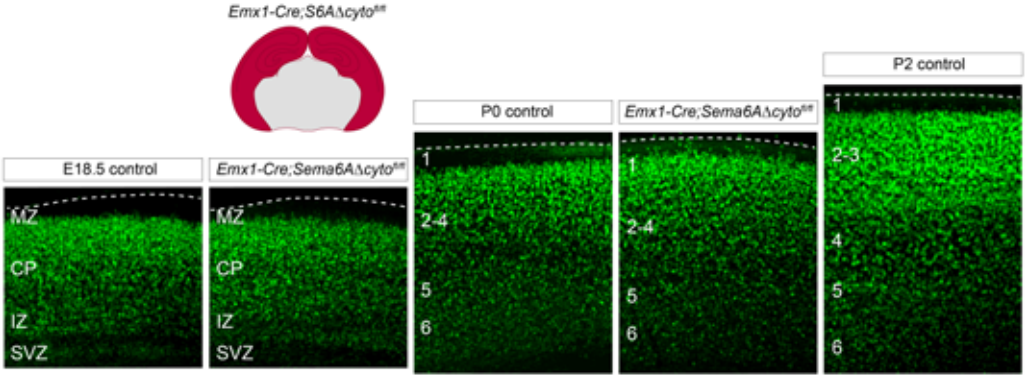
Emx1-Cre;S6AΔcyto$^{fl/fl}$
E18.5 control
Emx1-Cre;Sema6AΔcyto$^{fl/fl}$
P0 control
Emx1-Cre;Sema6AΔcyto$^{fl/fl}$
P2 control
MZ
CP
IZ
SVZ
1
2-4
2-3
4
5
6

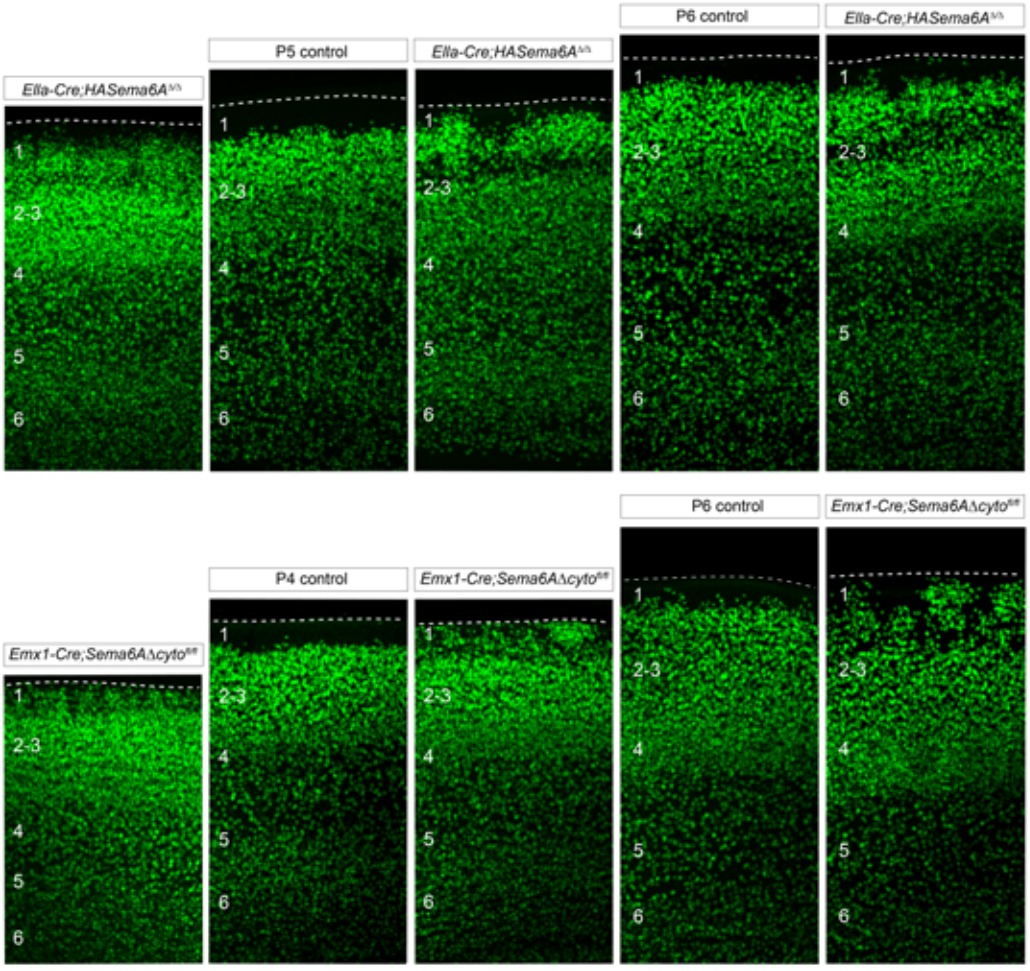

Figure S2. Extended developmental overview of cortical defect at multiple timepoints in *Emx1-Cre;Sem6AΔcyto*$^{fl/fl}$ and *Ella-Cre;HASema6A*$^{\Delta/\Delta}$, related to figure 3.
Cartoon of coronal section indicating Cre line specificity. Coronal sections of Satb2 expression detected by immunohistochemistry showing development of cortical neuron mispositioning and cluster formation. Cortical layers are indicated and the other edge of the cortex is indicated by the dotted line. Scale bar 200 µm

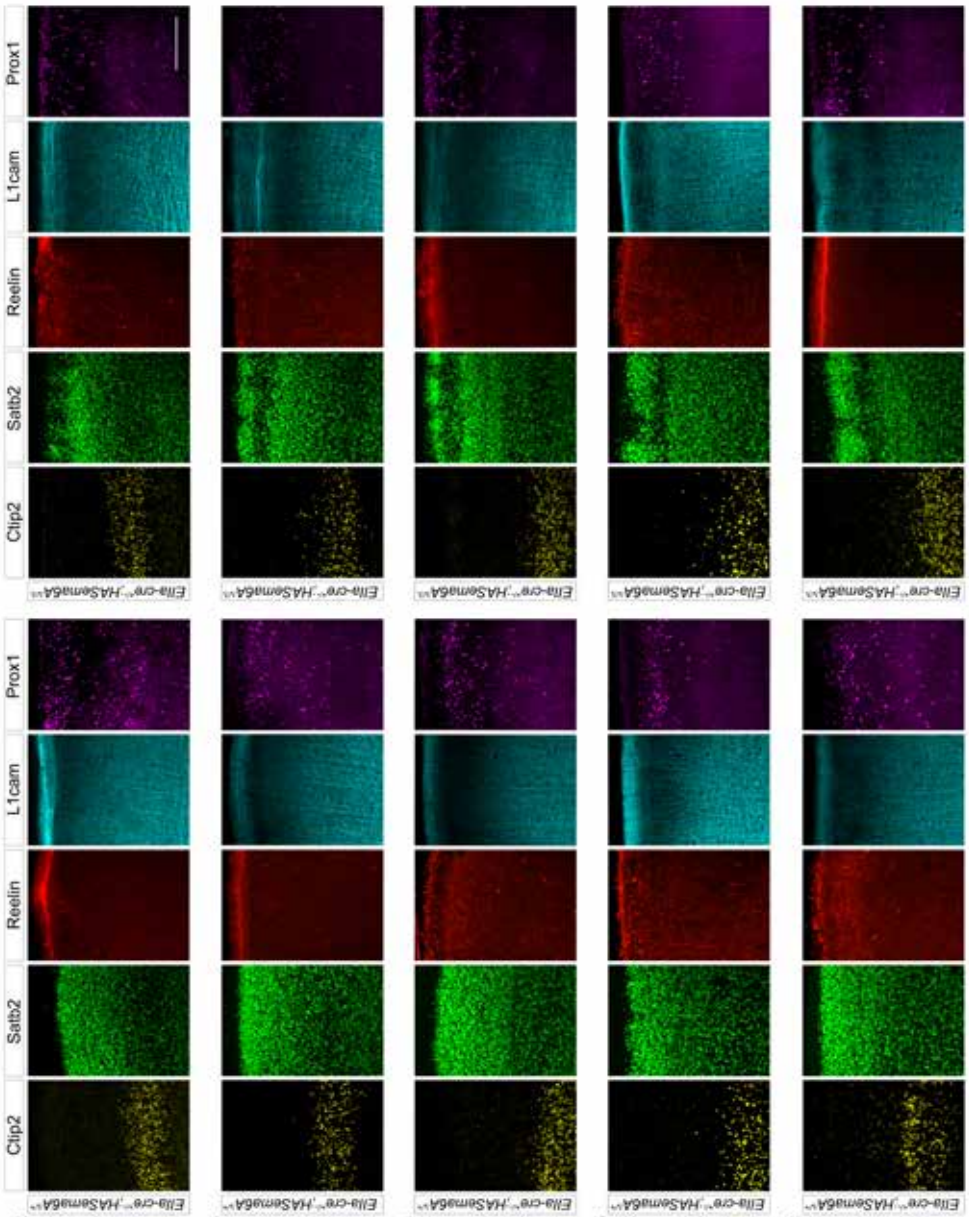

Figure S3. Cortical layer structure of *Ella-Cre;HASema6A*$^{\Delta/\Delta}$ mice at early postnatal stages.
Immunohistochemistry on coronal sections of *Ella-Cre;HASema6A*$^{\Delta/\Delta}$ and control mice at P2, P3, P4, P5 and P6. Cortical markers are indicated. There was no apparent difference in the deeper cortical region. In the superficial region Prox1-positive and L1cam-positive cells show a potential mispositioning phenotype that corresponds to the area containing neuronal clusters. Scale bar 200 µm.

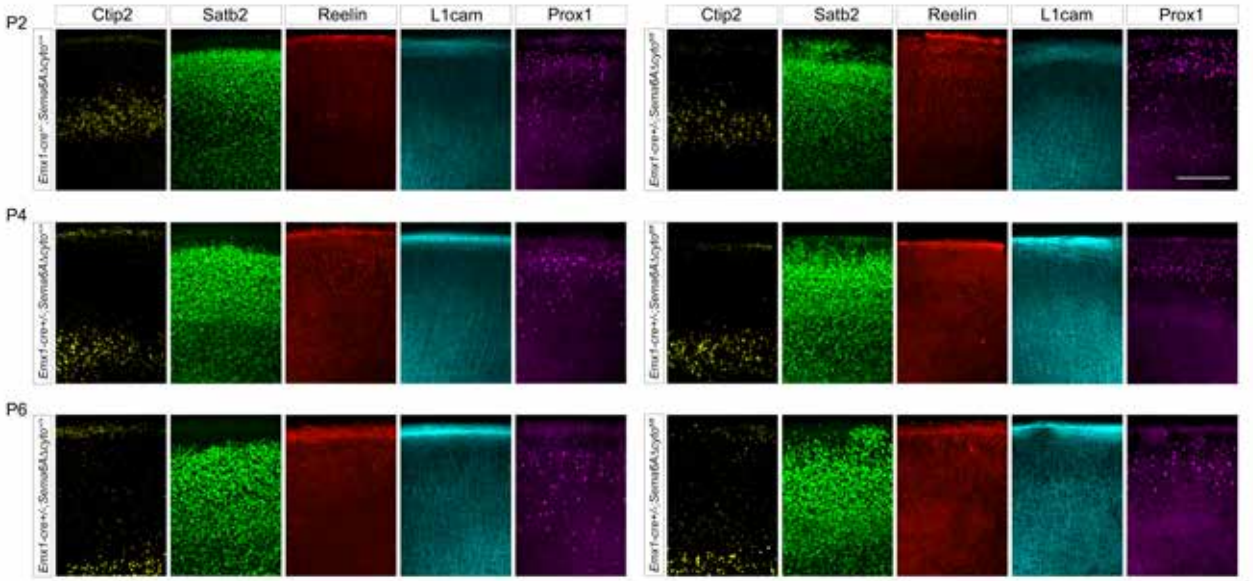

Figure S4. Cortical layer structure of *Emx1-Cre;Sem6AΔcyto*$^{fl/fl}$ mice at early postnatal stages.
Immunohistochemistry on coronal sections of *Emx1-Cre;Sem6AΔcyto*$^{fl/fl}$ and control mice at P2, P4 and P6. Cortical markers are indicated. There was no apparent difference in the deeper cortical region. In the superficial region Prox1-positive and L1cam-positive cells show a potential mispositioning phenotype that corresponds to the area containing neuronal clusters. Scale bar 200 µm.

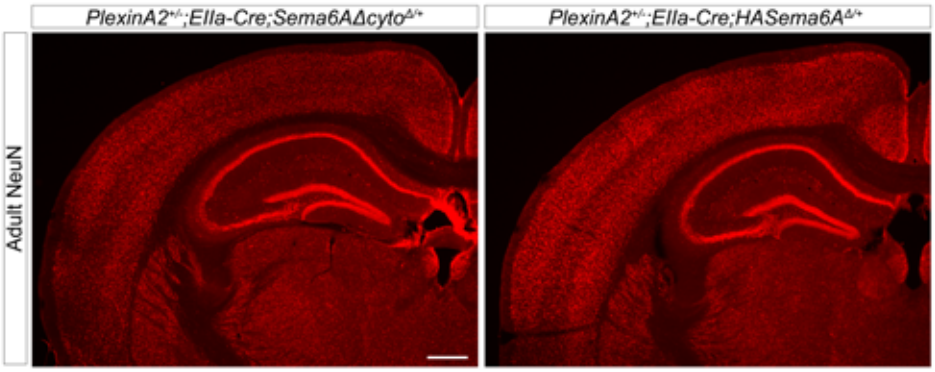

Figure S5. Cortical cytoarchitecture of *PlexinA2$^{+/-}$;Ella-Cre;Sema6AΔcyto $^{Δ/+}$* and *PlexinA2$^{+/-}$;Ella-Cre;HASema6A$^{Δ/+}$* double heterozygous adult mice.
NeuN staining of coronal sections from *PlexinA2$^{+/-}$;Ella-Cre;Sema6AΔcyto$^{Δ/+}$* and *PlexinA2;Ella-Cre;HASema6A$^{Δ/+}$* mice showing no neuron mispositioning or layer 2/3 laminar disturbance. Scale bar 500 µm.

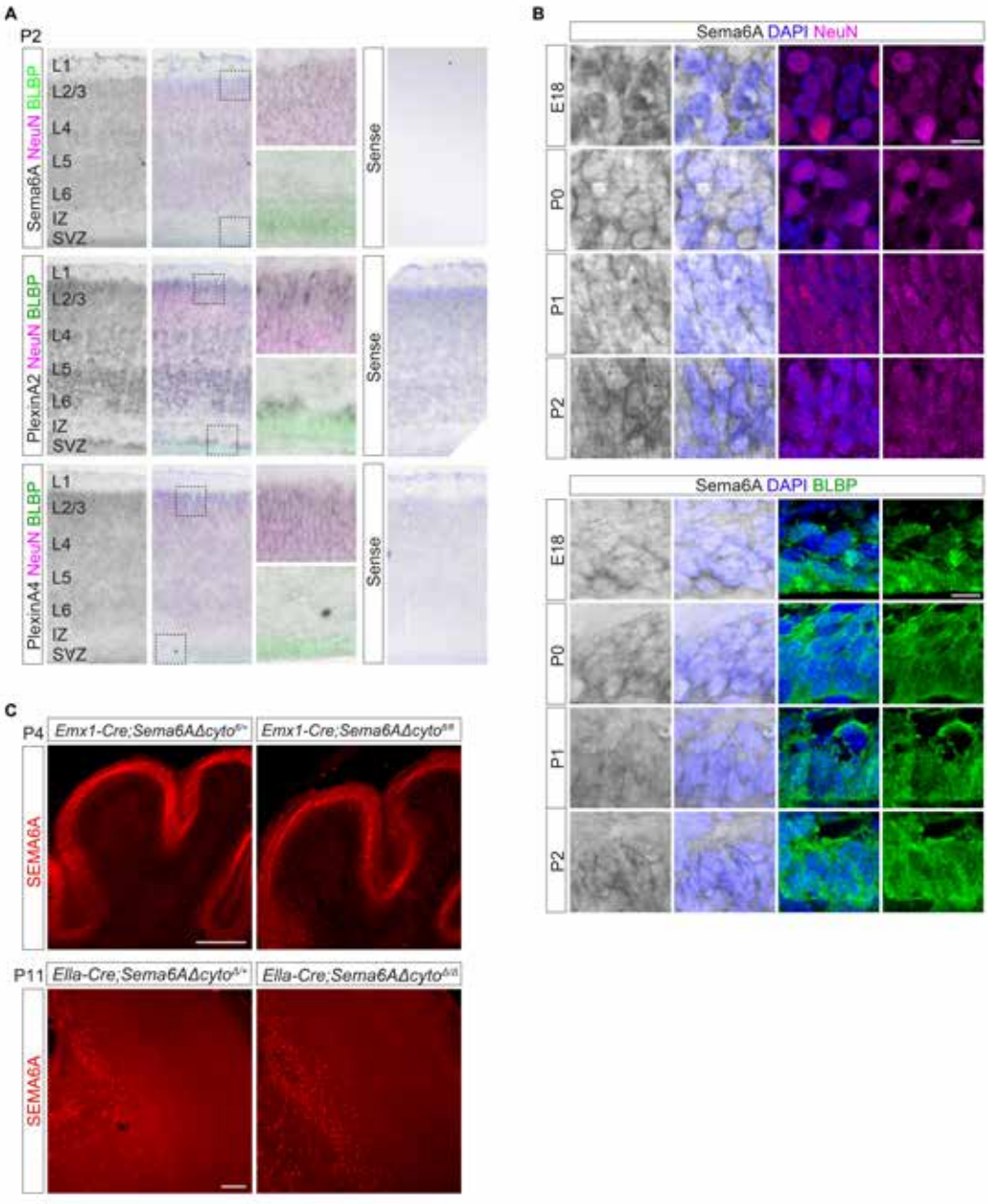

Figure S6. *Sema6A* expression is detected in the cortex at the onset of the cortical defect, related to figure 13.

A) ISH on *C57Bl/6* brain tissue shows *Sema6A, PlexinA2* and *PlexinA4* expression throughout the cortical layers at P2. B) High magnification images show *Sema6A* expression in combined with mouse anti-NeuN and rabbit anti-BLBP antibodies at E18, P0, P1 and P2 in *C57Bl/6* mice.

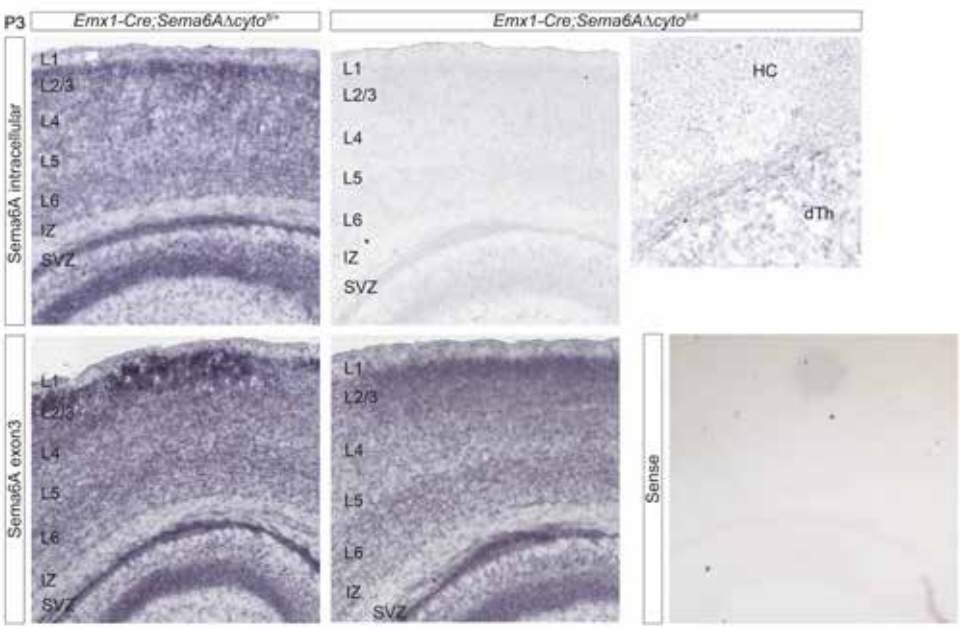

C) Immunohistochemistry using anti-Sema6A antibodies on coronal sections in *Emx1-Cre;Sema6AΔcyto*$^{fl/fl}$ mice at P4 and *Ella-Cre; Sema6AΔcyto*$^{\Delta/\Delta}$ mice at P11. Scale bars 10 µm (B) 200 µm (C).

Figure S7. *Sema6A* expression is absent when using an intracellular probe for ISH, related to figure 13.
Emx1-Cre;Sema6AΔcyto$^{fl/fl}$ show *Sema6A* expression throughout the cortical layers only when using an extracellular probe (designed against exon3). Control mice show *Sema6A* expression for both intracellular and extracellular probes. Sense probes did not show specific signals.

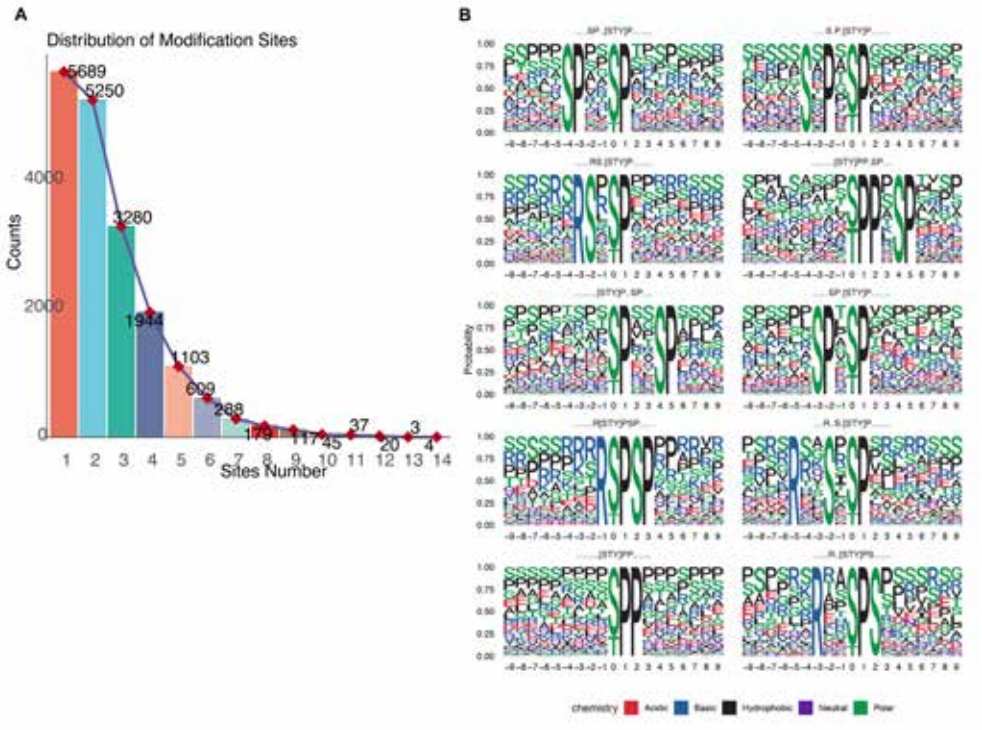

Figure S8. MotifeR analysis showing top 10 enriched motifs in the phospho-proteome of *Emx1-Cre;Sem6AΔcyto*$^{fl/fl}$ mice.

A) Distribution of original peptide modification site number using the mouse proteome (Uniprot, ID UP000000589) as background dataset. B) Phospho-peptide motif visualization after enrichment using motifeR.

Supplemental Table 1 Mouse lines

Mouse strain	Reference	Stock #	RRID
EIIa-Cre	The Jackson Laboratory [76]	JAX:003724	IMSR_JAX:003724
EMX1-IRES-Cre (Emx1$^{tm1(cre)Krj}$)	The Jackson Laboratory [33]	JAX: 005628	IMSR_JAX:005628
Nestin-Cre (Tg(Nes-cre)1Kln)	The Jackson Laboratory [77]	JAX: 003771	IMSR_JAX:003771
GBX2-CreEr-IRES-EGFP	The Jackson Laboratory [78]	JAX: 022135 Provided by Peter Burbach	IMSR_JAX:022135
STOP-tdTomato	The Jackson Laboratory [79]	JAX stock #007914	IMSR_JAX:007914
Sema6A$^{-/-}$ (Sema6aGt[KST069]Byg)	[18]	Provided by Kevin Mitchell	MGI:3795751
Sema6AΔcyto$^{fl/+}$	Chapter 3		
HASema6A$^{fl/+}$	unpublished	Provided by Alex Kolodkin	
C57BL/6J	Charles Rivers Laboratories		IMSR_JAX:000664
PlexinA2$^{-/-}$	[37]	Provided by Roman Giger	

Supplementary Table 2 Primary antibodies and plasmids

Antibody	Dilution	Reference #	RRID
Mouse anti-NeuN	1:1000	Abcam, Cat# ab104224	AB_10711040
Rabbit anti-Prox1	1:1000	Abcam, Cat# ab101851	AB_10712211
Rat anti-L1CAM	1:500	Millipore, Cat# MAB5272	AB_2133200
Rat anti-BrdU	1:500	Accurate , Cat# OBT0030	AB_2313756
Goat anti-Sema6A	1:1000	R&D, Cat # AF1615	AB_2185995
Rabbit anti-GFP	1:1000	Life Technologies, Cat# A11122	AB_221569
Rabbit anti-GFAP	1:1000	Abcam, Cat# ab7260	AB_305808
Rabbit anti-BLBP	1:2000	Abcam, Cat# ab32423	AB_880078
Mouse anti-Reelin	1:200	Millipore, Cat# MAB5364	AB_2179313
Rabbit anti-Satb2	1:500	Abcam, Cat# AB34735	AB_2301417
Rat anti-Ctip2	1:1000	Abcam, Cat# AB18465	AB_2064130
Goat anti-PlexinA2	1:200	R&D, Cat# AF5486	AB_10573285

Construct	Company	Reference #
pCAG-GFP	Addgene	Cat# 11150
pCAG-IRES2-Cre-GFP	Addgene	Cat #26646
pCAG-Sema6A-GFP	In house cloning	
pEF1-Sema6ADABL		Provided by Alain Chédotal

Supplementary Table 3 Gene ontology analysis

Gene ontology analysis of global proteome (A), phospho-proteome (B) and RNAseq (C) datasets. All identified hits in mass spectrometry and RNAseq datasets were analyzed using Panther overrepresentation test showing top ten over- and underrepresented molecular functions. FDR > 0.01.

A

Molecular function	GO term	*Mus musculus*	Dataset	Expected	Under/Over	Fold enrichment	Raw p-value	FDR
Binding	GO:0005488	13767	1538	1093.82	+	1.41	2.62E-114	1.22E-110
Protein binding	GO:0005515	9327	1214	741.05	+	1.64	1.62E-105	3.75E-102
RNA binding	GO:0003723	1107	333	87.95	+	3.79	1.20E-85	1.85E-82
Heterocyclic compound binding	GO:1901363	5313	766	422.13	+	1.81	5.70E-66	6.62E-63
Organic cyclic compound binding	GO:0097159	5415	774	430.23	+	1.8	2.18E-65	2.03E-62
Enzyme binding	GO:0019899	2372	446	188.46	+	2.37	1.16E-60	8.95E-58
Protein-containing complex binding	GO:0044877	1470	334	116.76	+	2.86	5.13E-60	3.41E-57
Small molecule binding	GO:0036094	2438	426	193.7	+	2.2	6.35E-50	3.69E-47
Nucleotide binding	GO:0000166	2034	379	161.61	+	2.35	1.21E-49	5.61E-47
Nucleoside phosphate binding	GO:1901265	2034	379	161.61	+	2.35	1.21E-49	6.23E-47
Transmembrane signaling receptor activity	GO:0004888	2148	21	170.66	-	0.12	6.02E-48	2.54E-45
Signaling receptor activity	GO:0038023	2344	30	186.24	-	0.16	2.02E-46	6.72E-44
Molecular transducer activity	GO:0060089	2344	30	186.24	-	0.16	2.02E-46	7.23E-44
Olfactory receptor activity	GO:0004984	1138	0	90.42	-	<0.01	2.74E-39	6.71E-37
Unclassified	Unclassified	1962	42	155.88	-	0.27	3.19E-27	4.95E-25
G protein-coupled receptor activity	GO:0004930	755	5	59.99	-	0.08	3.73E-19	4.03E-17
DNA-binding transcription factor activity. RNA polymerase II-specific	GO:0000981	1295	26	102.89	-	0.25	4.64E-19	4.90E-17
DNA-binding transcription factor activity	GO:0003700	1370	30	108.85	-	0.28	1.04E-18	1.05E-16
Odorant binding	GO:0005549	527	0	41.87	-	<0.01	3.06E-18	3.02E-16
RNA polymerase II transcription regulatory region sequence-specific DNA binding	GO:0000977	1378	57	109.48	-	0.52	6.69E-08	3.58E-06

B)

Molecular function	GO term	*Mus musculus*	Dataset	Expected	Under/Over	Fold enrichment	Raw p-value	FDR
Protein binding	GO:0005515	9327	1482	938.77	+	1.58	2.45E-170	1.14E-103
Binding	GO:0005488	13767	1860	1385067	+	1.34	2.00E-97	4.65E-94
Enzyme binding	GO:0019899	2372	548	238.74	+	2.3	8.77E-68	1.36E-64
RNA binding	GO:0003723	1107	317	111.42	+	2.85	1.19E-53	1.38E-50
Heterocyclic compound binding	GO:1901363	5313	858	534.76	+	1.6	5.68E-47	2.94E-44
Organic cyclic compound binding	GO:0097159	5415	867	545.03	+	1.59	4.09E-46	1.90E-43
Nucleic acid binding	GO:0003676	3386	605	340.81	+	1.78	1.05E-41	4.44E-39
Cytoskeletal protein binding	GO:0008092	981	255	98.74	+	2.58	7.48E-37	2.90E-34
Transcription coregulator activity	GO:0003712	451	149	45.39	+	3.28	1.73E-30	6.19E-28
Kinase binding	GO:0019900	836	211	84.14	+	2.51	6.62E-29	2.20E-26
Transmembrane signaling receptor activity	GO:0004888	2148	36	216.2	-	0.17	8.15E-52	7.58E-49
Signaling receptor activity	GO:0038023	2344	48	235.93	-	0.2	2.51E-50	1.67E-47
Molecular transducer activity	GO:0060089	2344	48	235.93	-	0.2	2.51E-50	1.94E-47
Olfactory receptor activity	GO:0004984	1138	0	114.54	-	<0.01	4.14E-49	2.41E-46
Odorant binding	GO:0005549	527	0	53.04	-	<0.01	1.48E-22	3.27E-20
Unclassified	Unclassified	1962	91	197.48	-	0.46	3.84E-17	5.10E-15
G protein-coupled receptor activity	GO:0004930	755	17	75.99	-	0.22	3.25E-15	3.21E-13
Oxidoreductase activity	GO:0016491	800	28	80.52	-	0.35	7.42E-11	5.39E-09
Immunoglobulin receptor binding	GO:0034987	195	0	19.63	-	<0.01	1.17E-08	7.17E-07
Receptor ligand activity	GO:0048018	467	15	50.02	-	0.3	2.65E-08	1.58E-06

C)

Molecular function	GO term	*Mus musculus*	Dataset	Expected	Under/Over	Fold enrichment	Raw p-value	FDR
Binding	GO:0005488	13767	10058	8463.63	+	1.19	6.95E-116	1.08E-112
Protein binding	GO:0005515	9327	7200	5734.02	+	1.26	4.60E-87	3.05E-84
Molecular function	GO:003674	20303	13118	12481.81	+	1.05	4.15E-67	2.41E-64
Ion binding	GO:0043167	5519	4501	3392.95	+	1.33	2.60E-61	1.21E-58
Heterocyclic compound binding	GO:1901363	5313	4289	3266.31	+	1.31	7.57E-54	3.20E-51
Organic cyclic compound binding	GO:0097159	5415	4343	3329.02	+	1.3	1.70E-52	6.59E-50
Catalytic activity	GO:0003824	5696	4492	3501.77	+	1.28	5.92E-49	2.12E-46
Enzyme binding	GO:19899	2372	2078	1458.25	+	1.42	5.15E-36	1.71E-33
Cation binding	GO:0043169	3619	2934	2224.88	+	1.32	1.57E-34	4.56E-32
Metal ion binding	GO:0046872	3530	2864	2170.16	+	1.32	1.01E-33	2.77E-31
Olfactory receptor activity	GO:0004984	1138	4	699.62	-	<0.01	4.92E-233	2.29E-229
Transmembrane signaling receptor activity	GO:0004888	2148	467	1320.54	-	0.35	1.36E-119	3.15E-116
Odorant binding	GO:0005549	527	1	323.99	-	<0.01	5.20E-1.09	6.05E-106
Signaling receptor activity	GO:0038023	2344	583	1441.04	-	0.4	1.74E-107	1.34E-104
Molecular transducer activity	GO:0060089	2344	583	1441.04	-	0.4	1.74E-107	1.61E-104
Unclassified	Unclassified	1962	570	1206.19	-	0.47	4.15E-67	2.14E-64
Immunoglobulin receptor binding	GO:0034987	195	4	119.88	-	0.03	5.46E-35	1.69E-32
Antigen binding	GO:003823	253	30	155.54	-	0.19	1.93E-25	3.32E-23
G protein-coupled receptor activity	GO:0004930	755	231	464.1	-	0.5	3.42E-23	4.96E-21
Pheromone receptor activity	GO:0016503	99	0	60.86	-	<0.01	3.42E-21	4.43E-19

Supplementary Table 4 QR codes 3D sample movies and raw data

1. Movie iDISCO movie control mice

2. Movie iDISCO *Ella-Cre;Sema6AΔcyto*$^{\Delta/\Delta}$ mice

3. Global proteome

4. Phospho-proteome

5. RNAseq

REFERENCES

1. Angevine, J. B. & Sidman, R. L. Autoradiographic study of cell migration during histogenesis of cerebral cortex in the mouse. *Nature* (1961). doi:10.1038/192766b0
2. Rakic, P. Neurons in rhesus monkey visual cortex: Systematic relation between time of origin and eventual disposition. *Science (80-.).* (1974). doi:10.1126/science.183.4123.425
3. Rakic, P. Mode of cell migration to the superficial layers of fetal monkey neocortex. *J. Comp. Neurol.* (1972). doi:10.1002/cne.901450105
4. Chai, X. *et al.* Reelin induces branching of neurons and radial glial cells during corticogenesis. *Cereb. Cortex* (2015). doi:10.1093/cercor/bhu216
5. Nadarajah, B., Brunstrom, J. E., Grutzendler, J., Wong, R. O. L. & Pearlman, A. L. Two modes of radial migration in early development of the cerebral cortex. *Nat. Neurosci.* (2001). doi:10.1038/83967
6. Nadarajah, B., Alifragis, P., Wong, R. O. L. & Parnavelas, J. G. Neuronal migration in the developing cerebral cortex: Observations based on real-time imaging. *Cerebral Cortex* (2003). doi:10.1093/cercor/13.6.607
7. Puram, S. V. & Bonni, A. Cell-intrinsic drivers of dendrite morphogenesis. *Development (Cambridge)* (2013). doi:10.1242/dev.087676
8. y Cajal, S. R. *Sobre la existencia de células nerviosas especiales en la primera capa de las circunvoluciones cerebrales*. (1890).
9. Retzius, G. Weitere beitrage zur kenntniss der Cajal'schen Zellen der grosshirnrinde des menschen. Biol. Unters 6, 29–34 (1894).
10. Multiple, A. *Cerebral Cortex: Normal and Altered States of Function*. *Cerebral Cortex* (1991).
11. Rubio-Garrido, P., Pérez-De-Manzo, F., Porrero, C., Galazo, M. J. & Clascá, F. Thalamic input to distal apical dendrites in neocortical layer 1 is massive and highly convergent. *Cereb. Cortex* (2009). doi:10.1093/cercor/bhn259
12. Murray Sherman, S. & Guillery, R. W. Distinct functions for direct and transthalamic corticocortical connections. *J. Neurophysiol.* (2011). doi:10.1152/jn.00429.2011
13. D'Souza, R. D. & Burkhalter, A. A laminar organization for selective cortico-cortical communication. *Front. Neuroanat.* (2017). doi:10.3389/fnana.2017.00071
14. Cauller, L. Layer I of primary sensory neocortex: where top-down converges upon bottom-up. *Behav. Brain Res.* (1995). doi:10.1016/0166-4328(95)00032-1
15. Larkum, M. A cellular mechanism for cortical associations: An organizing principle for the cerebral cortex. *Trends in Neurosciences* (2013). doi:10.1016/j.tins.2012.11.006

16. Garcia-Munoz, M. & Arbuthnott, G. W. Basal ganglia–thalamus and the "crowning enigma". *Frontiers in Neural Circuits* (2015). doi:10.3389/fncir.2015.00071
17. Martineau, F. S. *et al.* Correct Laminar Positioning in the Neocortex Influences Proper Dendritic and Synaptic Development. *Cereb. Cortex* (2018). doi:10.1093/cercor/bhy113
18. Leighton, P. A. et al. Defining brain wiring patterns and mechanisms through gene trapping in mice. 410, (2001).
19. Toyofuku, T. *et al.* Guidance of myocardial patterning in cardiac development by Sema6D reverse signalling. *Nat. Cell Biol.* (2004). doi:10.1038/ncb1193
20. Mauti, O., Domanitskaya, E., Andermatt, I., Sadhu, R. & Stoeckli, E. T. Semaphorin6A acts as a gate keeper between the central and the peripheral nervous system. *Neural Dev.* (2007). doi:10.1186/1749-8104-2-28
21. Perez-Branguli, F. et al. Reverse Signaling by Semaphorin-6A Regulates Cellular Aggregation and Neuronal Morphology. PLoS One 11, e0158686 (2016).
22. Sun, T. et al. A reverse signaling pathway downstream of Sema4A controls cell migration via Scrib. J. Cell Biol. 216, 199–215 (2017).
23. Rünker, A. E. et al. Mutation of Semaphorin-6A Disrupts Limbic and Cortical Connectivity and Models Neurodevelopmental Psychopathology. PLoS One 6, e26488 (2011).
24. Renier, N. *et al.* IDISCO: A simple, rapid method to immunolabel large tissue samples for volume imaging. *Cell* (2014). doi:10.1016/j.cell.2014.10.010
25. Belle, M. et al. A Simple Method for 3D Analysis of Immunolabeled Axonal Tracts in a Transparent Nervous System. Cell Rep. 9, (2014).
26. Alcamo, E. A. *et al.* Satb2 Regulates Callosal Projection Neuron Identity in the Developing Cerebral Cortex. *Neuron* (2008). doi:10.1016/j.neuron.2007.12.012
27. Hatanaka, Y. *et al.* Semaphorin 6A–Plexin A2/A4 Interactions with Radial Glia Regulate Migration Termination of Superficial Layer Cortical Neurons. *iScience* (2019). doi:10.1016/j.isci.2019.10.034
28. Szemes, M., Gyorgy, A., Paweletz, C., Dobi, A. & Agoston, D. V. Isolation and characterization of SATB2, a novel AT-rich DNA binding protein expressed in development- and cell-specific manner in the rat brain. *Neurochem. Res.* (2006). doi:10.1007/s11064-005-9012-8
29. Britanova, O. *et al.* Satb2 Is a Postmitotic Determinant for Upper-Layer Neuron Specification in the Neocortex. *Neuron* (2008). doi:10.1016/j.neuron.2007.12.028
30. Franco, S. J. *et al.* Fate-restricted neural progenitors in the mammalian cerebral cortex. *Science (80-.).* (2012). doi:10.1126/science.1223616
31. Huang, Y. *et al.* Expression of Transcription Factor Satb2 in Adult Mouse Brain. *Anat. Rec.* (2013). doi:10.1002/ar.22656
32. Lein, E. S. *et al.* Genome-wide atlas of gene expression in the adult mouse brain. *Nature* (2007). doi:10.1038/nature05453

33. Gorski, J. a et al. Cortical excitatory neurons and glia, but not GABAergic neurons, are produced in the Emx1-expressing lineage. J. Neurosci. 22, 6309–6314 (2002).
34. Ignacio, M. P. D., Kimm, E. J., Kageyama, G. H., Yu, J. & Robertson, R. T. Postnatal migration of neurons and formation of laminae in rat cerebral cortex. *Anat. Embryol. (Berl).* (1995). doi:10.1007/BF00186782
35. Whitford, K. L., Dijkhuizen, P., Polleux, F. & Ghosh, A. Molecular control of cortical dendrite development. *Annual Review of Neuroscience* (2002). doi:10.1146/annurev.neuro.25.112701.142932
36. Suto, F. *et al.* Plexin-A4 mediates axon-repulsive activities of both secreted and transmembrane semaphorins and plays roles in nerve fiber guidance. *J. Neurosci.* (2005). doi:10.1523/JNEUROSCI.4480-04.2005
37. Suto, F. *et al.* Interactions between Plexin-A2, Plexin-A4, and Semaphorin 6A Control Lamina-Restricted Projection of Hippocampal Mossy Fibers. *Neuron* (2007). doi:10.1016/j.neuron.2007.01.028
38. Hlavin, M. L. & Lemmon, V. Molecular structure and functional testing of human L1CAM: An interspecies comparison. *Genomics* (1991). doi:10.1016/0888-7543(91)90150-D
39. Lindner, J., Rathjen, F. G. & Schachner, M. L1 mono- And polyclonal antibodies modify cell migration in early postnatal mouse cerebellum. *Nature* (1983). doi:10.1038/305427a0
40. Bixby, J. L., Lilien, J. & Reichardt, L. F. Identification of the major proteins that promote neuronal process outgrowth on Schwann cells in vitro. *J. Cell Biol.* (1988). doi:10.1083/jcb.107.1.353
41. Toma, K. & Hanashima, C. Switching modes in corticogenesis: mechanisms of neuronal subtype transitions and integration in the cerebral cortex. Front. Neurosci. 9, (2015).
42. Schmechel, D. E. & Rakic, P. A golgi study of radial glial cells in developing monkey telencephalon: Morphogenesis and transformation into astrocytes. *Anat. Embryol. (Berl).* (1979). doi:10.1007/BF00300010
43. Voigt, T. Development of glial cells in the cerebral wall of ferrets: Direct tracing of their transformation from radial glia into astrocytes. *J. Comp. Neurol.* (1989). doi:10.1002/cne.902890106
44. Tramontin, A. D. Postnatal Development of Radial Glia and the Ventricular Zone (VZ): a Continuum of the Neural Stem Cell Compartment. Cereb. Cortex 13, 580–587 (2003).
45. Peter, C. J. et al. In vivo epigenetic editing of Sema6a promoter reverses transcallosal dysconnectivity caused by C11orf46/Arl14ep risk gene. Nat. Commun. 10, 4112 (2019).
46. Bernard, F. *et al.* Role of transmembrane semaphorin Sema6A in oligodendrocyte differentiation and myelination. *Glia* (2012). doi:10.1002/glia.22378

47. Kerjan, G. et al. The transmembrane semaphorin Sema6A controls cerebellar granule cell migration. Nat. Neurosci. 8, 1516–1524 (2005).
48. Hou, T., Chen, K., McLaughlin, W. A., Lu, B. & Wang, W. Computational analysis and prediction of the binding motif and protein interacting partners of the Abl SH3 domain. *PLoS Comput. Biol.* (2006). doi:10.1371/journal.pcbi.0020001
49. Bradley, W. D. & Koleske, A. J. Regulation of cell migration and morphogenesis by Abl-family kinases: Emerging mechanisms and physiological contexts. *J. Cell Sci.* (2009). doi:10.1242/jcs.039859
50. Mi, H. *et al.* Protocol Update for large-scale genome and gene function analysis with the PANTHER classification system (v.14.0). *Nat. Protoc.* (2019). doi:10.1038/s41596-019-0128-8
51. Robledo, S. *et al.* The role of human ribosomal proteins in the maturation of rRNA and ribosome production. *RNA* (2008). doi:10.1261/rna.1132008
52. Lee, S. H. *et al.* REEP5 depletion causes sarco-endoplasmic reticulum vacuolization and cardiac functional defects. *Nat. Commun.* (2020). doi:10.1038/s41467-019-14143-9
53. Kimura, E. *et al.* Serine-arginine-rich nuclear protein Luc7l regulates myogenesis in mice. *Gene* (2004). doi:10.1016/j.gene.2004.07.035
54. Zhang, L. et al. Satb2 Is Required for Dendritic Arborization and Soma Spacing in Mouse Cerebral Cortex. Cereb. Cortex 22, 1510–1519 (2012).
55. Baranek, C. *et al.* Protooncogene Ski cooperates with the chromatin-remodeling factor Satb2 in specifying callosal neurons. *Proc. Natl. Acad. Sci. U. S. A.* (2012). doi:10.1073/pnas.1108718109
56. Wang, S. *et al.* motifeR: An Integrated Web Software for Identification and Visualization of Protein Posttranslational Modification Motifs. *Proteomics* (2019). doi:10.1002/pmic.201900245
57. Lemstra, S. The Complexity of Semaphorin and Plexin Signalling in the Healthy and Diseased Brain. (University Utrecht, 2019).
58. Klostermann, A., Lutz, B., Gertler, F. & Behl, C. The orthologous human and murine semaphorin 6A-1 proteins (SEMA6A-1/Sema6A-1) bind to the enabled/vasodilator-stimulated phosphoprotein-like protein (EVL) via a novel carboxyl-terminal zyxin-like domain. *J. Biol. Chem.* (2000). doi:10.1074/jbc.M006316200
59. Robinson, J. T. *et al.* Integrative genomics viewer. *Nature Biotechnology* (2011). doi:10.1038/nbt.1754
60. Liu, H. *et al.* Integrated Analysis of Summary Statistics to Identify Pleiotropic Genes and Pathways for the Comorbidity of Schizophrenia and Cardiometabolic Disease. *Front. Psychiatry* (2020). doi:10.3389/fpsyt.2020.00256
61. Yoshinaga, S. *et al.* Comprehensive Characterization of Migration Profiles of Murine Cerebral Cortical Neurons During Development Using FlashTag Labeling. *SSRN Electron. J.* (2020). doi:10.2139/ssrn.3696753

62. Chang, M. & Kawai, H. D. A characterization of laminar architecture in mouse primary auditory cortex. *Brain Struct. Funct.* (2018). doi:10.1007/s00429-018-1744-8
63. Luo, H., Hasegawa, K., Liu, M. & Song, W.-J. Comparison of the Upper Marginal Neurons of Cortical Layer 2 with Layer 2/3 Pyramidal Neurons in Mouse Temporal Cortex. Front. Neuroanat. 11, (2017).
64. Prislei, S. et al. From plasma membrane to cytoskeleton : a novel function for semaphorin 6A. 7, 233–242 (2008).
65. Kwiatkowski, A. V. *et al.* Ena/VASP Is Required for Neuritogenesis in the Developing Cortex. *Neuron* (2007). doi:10.1016/j.neuron.2007.09.008
66. Goh, K. L., Cai, L., Cepko, C. L. & Gertler, F. B. Ena/VASP proteins regulate cortical neuronal positioning. *Curr. Biol.* (2002). doi:10.1016/S0960-9822(02)00725-X
67. Meng, X., Winkowski, D. E., Kao, J. P. Y. & Kanold, P. O. Sublaminar Subdivision of Mouse Auditory Cortex Layer 2/3 Based on Functional Translaminar Connections. J. Neurosci. 37, 10200–10214 (2017).
68. Schuman, B. *et al.* Four unique interneuron populations reside in neocortical layer 1. *J. Neurosci.* (2019). doi:10.1523/JNEUROSCI.1613-18.2018
69. Jabaudon, D. Fate and freedom in developing neocortical circuits. *Nature Communications* (2017). doi:10.1038/ncomms16042
70. Bolz, J. & Gilbert, C. D. Generation of end-inhibition in the visual cortex via interlaminar connections. *Nature* (1986). doi:10.1038/320362a0
71. Schwarz, C. & Bolz, J. Functional specificity of a long-range horizontal connection in cat visual cortex: A cross-correlation study. *J. Neurosci.* (1991). doi:10.1523/jneurosci.11-10-02995.1991
72. Caviness, V. S. & Rakic, P. Mechanisms of cortical development: a view from mutations in mice. *Annual review of neuroscience* (1978). doi:10.1146/annurev.ne.01.030178.001501
73. Trutzer, I. M., García-Cabezas, M. Á. & Zikopoulos, B. Postnatal development and maturation of layer 1 in the lateral prefrontal cortex and its disruption in autism. Acta Neuropathol. Commun. 7, 40 (2019).
74. Bailey, A. *et al.* A clinicopathological study of autism. *Brain* (1998). doi:10.1093/brain/121.5.889
75. Leighton, P. A. et al. Defining brain wiring patterns and mechanisms through gene trapping in mice. Nature 410, 174–179 (2001).
76. Lakso, M. *et al.* Efficient in vivo manipulation of mouse genomic sequences at the zygote stage. *Proc. Natl. Acad. Sci. U. S. A.* (1996). doi:10.1073/pnas.93.12.5860
77. Tronche, F. *et al.* Disruption of the glucocorticoid receptor gene in the nervous system results in reduced anxiety. *Nat. Genet.* (1999). doi:10.1038/12703

78. Chen, L., Guo, Q. & Li, J. Y. H. Transcription factor Gbx2 acts cell-nonautonomously to regulate the formation of lineage-restriction boundaries ofthe thalamus. *Development* (2009). doi:10.1242/dev.030510
79. Madisen, L. *et al.* A robust and high-throughput Cre reporting and characterization system for the whole mouse brain. *Nat. Neurosci.* (2010). doi:10.1038/nn.2467
80. Kleijer, K. T. E. Neurobiological properties of two autism-risk genes: Pten and Cntn5. (Utrecht University, 2017).
81. David, R. & Wedlich, D. PCR-based RNA probes: A quick and sensitive method to improve whole mount embryo in situ hybridizations. *Biotechniques* (2001). doi:10.2144/01304st02
82. Pasterkamp, R. J., De Winter, F., Giger, R. J. & Verhaagen, J. Role for semaphorin III and its receptor neuropilin-1 in neuronal regeneration and scar formation? in *Progress in Brain Research* (1998). doi:10.1016/s0079-6123(08)64014-5
83. Humphrey, S. J., Karayel, O., James, D. E. & Mann, M. High-throughput and high-sensitivity phosphoproteomics with the EasyPhos platform. *Nat. Protoc.* (2018). doi:10.1038/s41596-018-0014-9
84. Bezstarosti, K., van der Wal, L. & Demmers, J. A. A. Detection of Protein Ubiquitination Sites by Peptide Enrichment and Mass Spectrometry. *JoVE (Journal Vis. Exp.* e59079 (2020).
85. Cox, J. *et al.* A practical guide to the maxquant computational platform for silac-based quantitative proteomics. *Nat. Protoc.* (2009). doi:10.1038/nprot.2009.36
86. Saxena, A. *et al.* Trehalose-enhanced isolation of neuronal sub-types from adult mouse brain. *Biotechniques* (2012). doi:10.2144/0000113878
87. Love, M. I., Huber, W. & Anders, S. Moderated estimation of fold change and dispersion for RNA-seq data with DESeq2. *Genome Biol.* (2014). doi:10.1186/s13059-014-0550-8

CHAPTER 5

Structural basis of semaphorin-plexin *cis* interaction

Daniel Rozbesky[1], Marieke G. Verhagen[2], Dimple Karia[1], Gergely N. Nagy[1], Luis Alvarez[3], Ross A. Robinson[1,4], Karl Harlos[1], Sergi Padilla-Parra[1,3,5,6], R. Jeroen Pasterkamp[2*], and E. Yvonne Jones[1,*]

[1] Division of Structural Biology, Wellcome Centre for Human Genetics, University of Oxford, Oxford, OX3 7BN, United Kingdom

[2] Department of Translational Neuroscience, UMC Utrecht Brain Center, University Medical Center Utrecht, Utrecht University, 3584 CG Utrecht, The Netherlands

[3] Cellular imaging, Wellcome Centre for Human Genetics, University of Oxford, Oxford, OX3 7BN, United Kingdom

[4] Present address: Immunocore Ltd, Milton Park, Abingdon, OX14 4RY, United Kingdom

[5] Present address: Department of Infectious Diseases, King's College London, Faculty of Life Sciences & Medicine, London SE1 9RT, UK

[6] Present address: Randall Centre for Cell and Molecular Biology, King's College London, London SE1 1UL, UK

*Correspondence: yvonne@strubi.ox.ac.uk, r.j.pasterkamp@umcutrecht.nl

EMBO journal 2020; 39:e102926, https://doi.org/10.15252/embj.2019102926

ABSTRACT

Semaphorin ligands interact with plexin receptors to contribute to functions in the development of myriad tissues including neurite guidance and synaptic organization within the nervous system. Cell attached semaphorins interact in *trans* with plexins on opposing cells, but also in *cis* on the same cell. The interplay between *trans* and *cis* interactions is crucial for the regulated development of complex neural circuitry, but the underlying molecular mechanisms are uncharacterised. We have discovered a distinct mode of interaction through which the *Drosophila* semaphorin Sema1b and mouse Sema6A mediate binding in *cis* to their cognate plexin receptors. Our high-resolution structural, biophysical and *in vitro* analyses demonstrate that monomeric semaphorins can mediate a distinctive plexin binding mode. These findings suggest the interplay between monomeric *vs* dimeric states has a hereto unappreciated role in semaphorin biology, providing a mechanism by which Sema6s may balance *cis* and *trans* functionalities.

INTRODUCTION

Semaphorins and plexins are one of the classical cell guidance ligand-receptor families first characterised by their ability to steer axon growth cones in the developing nervous system [1-4]. Beyond axon guidance, semaphorin-plexin signalling is implicated in a plethora of physiological functions including other aspects of neural development, angiogenesis, vascularization, organogenesis, and regulation of immune responses [5-7]. Conversely, deregulation of semaphorin-plexin signalling is associated with tumour progression and other diseases [8]. Exquisite control of the local level and biological consequence of signalling is characteristic of the semaphorin-plexin system and essential for many of its functions.

Semaphorins are secreted, transmembrane or GPI-anchored proteins [2]. Membrane-attached semaphorins and plexins commonly function through cell-to-cell *trans* interactions in which the semaphorin ligands and plexin receptors are presented on opposing cells. However, when ligand and receptor are present on the same cell surface there is potential for ligand-receptor binding in *cis* at the same plasma membrane. An increasing body of evidence points to the importance of *cis* interactions in the regulation of diverse cell guidance signalling systems [9]. In the semaphorin-plexin signalling system, *cis* interactions were first described between class 6 semaphorins (Sema6s) and their cognate plexin class A (PlxnA) receptors. Studies in migrating granule cells suggest that binding of Sema6A and PlxnA2 in *cis* inhibits the binding of PlxnA2 by Sema6A in *trans* as the absence of Sema6A in *cis* causes over-activation of PlxnA2 [10]. The *cis* interaction of Sema6A-PlxnA2 has been further reported to be essential for proper development of lamina-restricted projection of hippocampal mossy fibers [11,12]. Finally, the inhibitory effect of *cis* interaction has been demonstrated between Sema6A and PlxnA4 [13], and Sema6B and PlxnA2 [14]. Contrary to these inhibition effects, the *cis* interaction between semaphorin SMP-1 and the PlxnA4 homolog, PLX-1, in *C. elegans* has been shown to result in plexin activation [15]. Similarly, mouse Sema5A signals through PlxnA2 co-expressed on hippocampal dentate granule cells to regulate synaptogenesis [16]. Perhaps the most exquisite interplay of semaphorin-plexin *cis* and *trans* interactions reported to date is that of Sema6A and PlxnA2 in the elaboration of dendritic arbors during retinal circuit assembly Sun 2013. Intriguingly, it has been suggested that the *cis* and *trans* interaction modes of semaphorins and plexins require distinct binding sites [13,17].

The first crystal structures of semaphorins revealed that the hallmark N-terminal sema domain is a seven-bladed β-propeller with a propensity to dimerise [18,19] and the homodimeric architecture has long been reported as essential for semaphorins to function as repulsive guidance cues [20,21]. In a recent study, we have demonstrated that semaphorins can also form heterodimers and monomers, and thus their architecture is not restricted to homodimers [22]. Plexins are type I transmembrane proteins containing an N-terminal sema domain followed by multiple PSI and IPT domains in their extracellular segment [23,24]. The plexin intracellular region has a distinctive GAP domain architecture [25–28], which structural and functional studies suggest is activated by dimerization [26–29]. Recent crystal structures of full length mouse PlxnA ectodomains (comprising ten domains) revealed a ring-like overall shape, which is presumably orientated parallel to the plane of the plasma membrane at the cell surface Kong 2016. The ring-like structure is consistent with an observed PlxnA-to-PlxnA 'head-to-stalk' *cis* interaction being able to maintain pre-ligand bound plexins in a clustered, but autoinhibited, state on the cell surface, presumably by favouring separation, and thus preventing spontaneous dimerization, of the transmembrane and intracellular regions [30]. The existence of inactive dimers of pre-ligand bound plexin is further supported by data from fluorescence cross-correlation spectroscopy experiments on mouse PlxnA4 [31]. Crystal structures have been reported for complexes formed between semaphorin ectodomains and fragments comprising up to four of the N-terminal domains of the cognate plexin ectodomain. These semaphorin-plexin complexes all show a bivalent 2:2 architecture that comprises a semaphorin dimer interacting with two copies of the plexin consistent with receptor activation by ligand-mediated dimerization, a conclusion supported by structure-guided biophysical and cell-based assays [32–34]. In all semaphorin-plexin complexes analysed to date, the semaphorins and plexins bind in a head-to-head (semaphorin sema domain-to-plexin sema domain) orientation suitable for a *trans* interaction between ligands and receptors attached to opposing cell surfaces triggering receptor activation [30]. No molecular interaction surfaces have been characterised in terms of their ability to mediate semaphorin-plexin binding modes in *cis*, thus the structural basis and molecular mechanism(s) governing the divergent outcomes of *cis* and *trans* binding remain elusive.

The ectodomain of Sema6A forms a weak dimer with monomeric and dimeric forms present in solution [32,34]. The interplay of monomeric and dimeric Sema6 at the plasma membrane is likely relevant to *cis* interactions with

the cognate PlxnA receptors. Structural and biophysical analyses at high concentrations have provided detailed insight into the interaction of dimeric Sema6A with PlxnA2, however, because of the monomer-dimer equilibrium, the binding properties of wild-type monomeric Sema6A have eluded direct analysis. In structural and biophysical studies of the *Drosophila* semaphorin system we recently discovered a wild-type monomeric semaphorin, Sema1b [22]. This unexpected discovery provided us with a system in which we could dissect the interaction surfaces, and contributions to plexin binding in *cis*, of a semaphorin that is purely in the monomeric state.

The class 1 (Sema1a and Sema1b) and class 2 (Sema2a and Sema2b) *Drosophila* semaphorins are membrane-attached and secreted, respectively. Sema1a and Sema1b are most closely related to the mammalian class 6 semaphorins and interact with the sole *Drosophila* class A plexin, PlexA [5]. In previous studies we have shown that the secreted *Drosophila* semaphorins, Sema2a and Sema2b, and also the ectodomain of membrane-attached $Sema1a_{ecto}$ are disulfide-linked dimers. All three of these semaphorins contain an intermolecular sema-to-sema disulfide bridge. Conversely, we found the ectodomain of membrane-attached $Sema1b_{ecto}$ to be a monomer in solution due to an amino acid substitution in the intermolecular disulfide bridge at position 254 [22]. Here we show that *Drosophila* Sema1b is a monomer on the cell surface and can interact in *cis* with PlexA. We further report two crystal structures of Sema1b complexed with the semaphorin-binding region of PlexA. The crystal structures, along with biophysical and cell-based assays, show that monomeric Sema1b binds PlexA at two independent binding sites. One interaction mode corresponds to the canonical head-to-head orientation described previously for semaphorin-plexin binding. The second mode uses an interactive surface on Sema1b that is occluded in dimeric semaphorins. We were able to demonstrate that this novel 'side-on' binding mode perturbs the ring-like structure of the PlexA ectodomain. In cell collapse assays we found that the side-on mode of monomeric Sema1b-PlexA binding in *cis* was sufficient to inhibit PlexA signalling by dimeric Sema1a binding *in trans*. In dorsal root ganglia neurons, we also confirmed that mouse Sema6A utilises the same molecular mechanism for *cis* interaction with its cognate plexin receptor as its *Drosophila* homolog, Sema1b. Based on our findings we propose models for semaphorin-plexin *cis* interactions which incorporate a distinctive role for monomeric semaphorin binding in the regulation of plexin signalling.

RESULTS

Sema1b is a monomer on the cell surface and fails to mediate PlexA dimerization

We considered the oligomeric state of Sema1b on the membrane of live cells. COS-7 cells were transiently transfected with Sema1b-F254C-mClover (a mutant which provides Sema1a-like disulfide-linked dimer formation) or with the wild-type Sema1b-mClover. Both constructs encompassed the ectodomain followed by a native transmembrane segment, short cytoplasmic linker and the C-terminal fluorescent protein mClover. mClover is a monomeric bright yellow-green fluorescent protein commonly used for the analysis of dimerization or protein-protein interactions in live cells [35]. Using Number and Brightness analysis we determined a molecular brightness (ε) in live cells, which is directly related to the oligomeric state. Number and Brightness analysis is a fluorescence fluctuation spectroscopy technique to measure the average number and oligomeric state of labeled entities in each pixel of a stack of fluorescently labeled images [36]. We have recently developed the method further by implementing a novel detrending algorithm to detect monomers and dimers in live cells [37–39] or *in vitro* [40]. Here, we calculated the molecular brightness of Sema1b-F254C-mClover to be double that of the molecular brightness of Sema1b-mClover consistent with Sema1b-mClover molecules being present on the membrane of COS-7 cells as monomers (Fig EV1A and EV1B).

Our previous studies have shown that although monomeric, $Sema1b_{ecto}$ maintains PlexA binding in the nanomolar range [22]. To investigate whether $Sema1b_{ecto}$ dimerizes or clusters PlexA on live cell surfaces, we probed the molecular brightness of PlexA-mClover on the membrane of COS-7 cells before and after stimulation with purified wild-type $Sema1b_{ecto}$ or the disulfide-linked dimer $Sema1b_{ecto}$-F254C. The PlexA-mClover construct contained the ectodomain followed by a transmembrane segment and the C-terminal fluorescent protein mClover. The addition of $Sema1b_{ecto}$-F254C resulted in a significant 3.0±1.8 fold increase of the average molecular brightness which is likely related to a change of the PlexA-mClover oligomeric state. Conversely, the addition of wild-type $Sema1b_{ecto}$ at the same concentration had no noticeable effect on the average molecular brightness (1.2±0.7 fold increase) (Fig EV1C and EV1D). Thus, though Sema1b binds PlexA in the nanomolar range, it fails to mediate PlexA dimerization on the cell surface, presumably due to its monomeric state.

A novel binding mode revealed by the crystal structure of the PlexA-Sema1b complex

We next determined crystal structures of the $PlexA_{1-4}$-$Sema1b_{1-2}$ complex from two different crystal forms (1:1 complex and 2:2 complex) at 3.0 and 4.8 Å resolution (Fig 1A-C, Table 1). The 1:1 complex crystal lattice contains one $PlexA_{1-4}$ monomer and one $Sema1b_{1-2}$ monomer per asymmetric unit. The crystal packing provides no $Sema1b_{1-2}$ dimerization resembling that of the generic homodimeric architecture. The $Sema1b_{1-2}$ bound in the 1:1 complex with $PlexA_{1-4}$ is very similar to the unbound $Sema1b_{1-2}$ with the Cα rmsd of 0.81 Å indicating no large conformational changes upon complex formation. Only small differences in loop orientations at the ligand-receptor interface are apparent. The ectodomain of *Drosophila* PlexA has not been structurally characterized previously. The $PlexA_{1-4}$ structure in the 1:1 complex contains a sema domain composed of a seven-bladed β-propeller fold, which is followed by a PSI domain, however, we were not able to locate the IPT1-PSI2 domain segment. The sema domain of PlexA is most similar to mouse PlxnA2 with an rmsd of 1.43 Å over 424 matched Cα positions. In the 1:1 complex crystal structure, $PlexA_{1-4}$ and $Sema1b_{1-2}$ interact through their sema domains in a head-to-head orientation similar to the generic architecture shared by all reported structures of semaphorin-plexin complexes [32–34]. The $PlexA_{1-4}$-$Sema1b_{1-2}$ interface buries a total solvent-accessible area of 1837 $Å^2$. This extensive interface is composed of a mixture of hydrophobic and hydrophilic interactions similar to that of PlxnA2-Sema6A.

In the crystal of 2:2 complex, two pairs of 1:1 complexes are packed together in the asymmetric unit with a relative orientation of 168.8° to form a pseudo tetramer. Each Sema1b molecule binds to both PlexA molecules in the pseudo tetramer. There are therefore two independent interaction sites, A and B (Fig 1C), involving two different Sema1b-PlexA orientations. The first, head-to-head orientation is equivalent to that observed in the 1:1 complex (interaction site A; Fig 1B). In the second interaction mode, termed side-on (Fig 1D), $Sema1b_{1-2}$ and $PlexA_{1-4}$ bind through the site B or B′ with their carboxy-terminal PSI domains oriented in parallel. The B and B′ binding sites are not identical within the pseudo tetramer. Whilst the B interaction site is extensive, the B′ interaction site is formed through distant contacts between three residues only. Although the two PlexA molecules in the pseudo tetramer form a substantial interface, we did not observe any propensity for $PlexA_{1-4}$ to dimerize in solution to a concentration at least of 33 μM (Fig EV1E and EV1F).

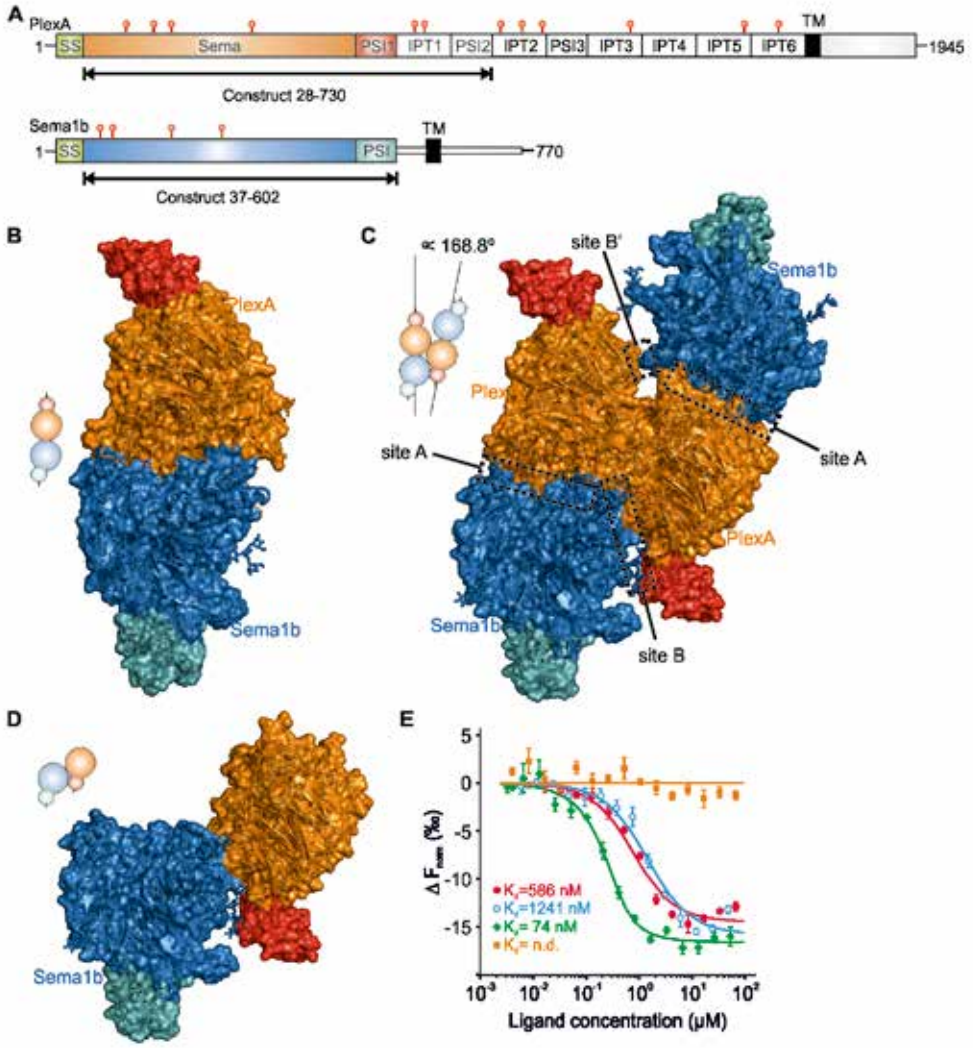

Figure 1. Sema1b binds PlexA at two independent sites, A and B, indicating two independent Sema1b-PlexA orientations: head-to-head and side-on

A. Schematic domain organization of *Drosophila* PlexA and Sema1b (SS, signal sequence; TM, transmembrane region, red symbols represent the position of N-linked glycosylation sites). B, C. Ribbon representation of the $PlexA_{1-4}$-$Sema1b_{1-2}$ 1:1 (C) and 2:2 (D) complexes. N-glycans are shown in stick representation. D. Ribbon representation of the side-on orientation derived from the 2:2 complex. E. Microscale thermophoresis binding experiment for $PlexA_{1-4}$-mVenus and $Sema1b_{ecto}$ (red) or $Sema1b_{ecto}$-mutA (blue) or $Sema1b_{ecto}$-mutB (green,) or $Sema1b_{ecto}$-mutA+B (orange). The $Sema1b_{ecto}$ wild-type binding results are as reported previously [22]. All data were collected at the same time, error bars represent s.d. of three technical replicates.

Table 1. Data collection and refinement statistics.

	$PlexA_{1-4}$-$Sema1b_{1-2}$ 1:1 complex	$PlexA_{1-4}$-$Sema1b_{1-2}$ 2:2 complex
Data collection		
Space group	C 2 2 2_1	P 6_5 2 2
Cell dimensions		
a, b, c (Å)	130.9, 195.1, 124.8	153.6, 153.6, 425.4
α, β, γ (°)	90, 90, 90	90, 90, 120
Resolution (Å)	76.86 - 2.96 (3.07 - 2.96)	127 - 4.80 (4.97 - 4.80)
Unique reflections	31584 (2791)	15309 (1485)
Multiplicity	4.6 (2.2)	20.9 (19.8)
Completeness (%)	93.78 (83.79)	99.90 (100.00)
I/σ(I)	8.86 (1.75)	7.41 (1.19)
Wilson B-factor ($Å^2$)	69.89	217.35
R-merge (%)	17.4 (63.4)	33.9 (224.1)
CC1/2	0.99 (0.548)	0.998 (0.492)
CC*	0.997 (0.841)	1 (0.812)
Refinement		
Resolution (Å)	76.86 - 2.96 (3.06 - 2.96)	127 - 4.80 (4.97 - 4.80)
Reflections used in refinement	31582	15303
Rwork/Rfree (%)	18.62/24.63	28.66/30.68
Number of atoms	8119	15728
Protein	7941	15350
Ligands	178	378
B-factor ($Å^2$)		
Protein	73.66	260.8
Ligand	129.39	297.52
R.m.s. deviations		
Bond lengths (Å)	0.005	0.01
Bond angles (°)	0.76	1.43
Ramachandran		
Favored (%)	95.28	95.31
Allowed (%)	4.72	4.69
Outliers (%)	0	0

*Highest resolution shell is shown in parenthesis

The structure of individual Sema1b$_{1-2}$ and PlexA$_{1-4}$ molecules in the 2:2 complex is very similar to those observed in the 1:1 complex, showing no significant conformational changes with the exception of the Exβ1-β2 loop in the extrusion of Sema1b$_{1-2}$, which adopts a different orientation in order to avoid steric clashes with PlexA$_{1-4}$. Unfortunately, we were not able to model the Exβ1-β2 loop completely because of fragmentary electron density, however, the loop's position is consistent with it making interactions to the PlexA$_{1-4}$. As well as undergoing this large-scale reorientation to accommodate PlexA$_{1-4}$ the Exβ1-β2 loop may also stabilize the complex.

In the side-on orientation, the sema domains of Sema1b$_{1-2}$ and PlexA$_{1-4}$ are bound in a configuration in which the bottom face of PlexA$_{1-4}$ is oriented perpendicularly to the side edge of Sema1b$_{1-2}$ (Fig 1D). The position of the B binding site between Sema1b and PlexA in the 2:2 complex is different to the binding site of the co-receptor neuropilin in the previously reported mouse Sema3A-PlexinA2-Nrp1 ternary complex [41], however, they are positioned in very close proximity (Fig EV2A-C). Interface B can be divided into three main binding sites (Fig EV1G). The most prominent, site 1, is formed by the extrusion of Sema1b and blade 6 of PlexA. Site 2 is composed of the β4B-β4C loop of Sema1b and the β4D-β5A loop of PlexA. In site 3 the N-linked glycan at residue N289 of Sema1b forms contacts with the PSI1 domain of PlexA. The Exβ1-β2 and β4B-β4C loops are involved in semaphorin homodimerization [42], however, for Sema1b$_{1-2}$ in the 2:2 complex these loops mediate interaction with PlexA suggesting that a B-type interaction can only be mediated by a monomeric semaphorin molecule (Fig EV1H).

To confirm both interaction interfaces observed in the 2:2 complex, we produced three mutants of Sema1b$_{ecto}$, termed A, B or A+B, and analyzed plexin binding using microscale thermophoresis (MST). In Sema1b-mutA, we mutated interface residues F203E, Q219R and K223E in order to disrupt the head-to-head interaction at site A. The single point mutations were designed to introduce electrostatic repulsions or reduction of surface hydrophobicity. Given the low resolution of the 2:2 complex and consequent lack of detailed information on residue-to-residue interactions, we decided to test the side-on interface by replacing each residue in the Exβ1-β2 loop by alanine rather than simple point mutations. Sema1b-mutA+B combined the modifications to potentially abolish both head-to-head and side-on interactions. All three Sema1b mutants were expressed and secreted at similar levels to the Sema1b wild-type. Furthermore, wild-type and all mutants were eluted at the same time from the size-exclusion column

suggesting there is no problem with folding. We found using MST that both Sema1b-mutA and Sema1b-mutB maintained $PlexA_{1-4}$ binding while Sema1b-mutA+B did not provide any measurable indication of $PlexA_{1-4}$ binding at concentrations up to 66.3 μM (Fig 1E and EV2D-L). These data indicate that in solution $Sema1b_{ecto}$ can interact with $PlexA_{1-4}$ using either the head-to-head (site A) or side-on (site B) binding modes. We further assessed the stoichiometry of interaction between $Sema1b_{1-2}$ and $PlexA_{1-4}$ in solution using SEC-MALS. The unliganded $Sema1b_{1-2}$ or $PlexA_{1-4}$ eluted as a single peak corresponding to monomer (Fig EV2M, N); no propensity to dimerize was observed. SEC-MALS analysis of a sample containing an equimolar mixture of $Sema1b_{1-2}$ and $PlexA_{1-4}$ revealed three peaks corresponding to unliganded $Sema1b_{1-2}$ and $PlexA_{1-4}$ and a $Sema1b_{1-2}$-$PlexA_{1-4}$ complex in 1:1 stoichiometry (Fig EV2O).

Sema1b binds PlexA in *cis*

We then investigated whether Sema1b binds PlexA in *cis* on live cell surfaces by FRET-FLIM [30,43,44]. COS-7 cells were transiently co-transfected with PlexA-mClover and Sema1b-mRuby2. For cells co-expressing PlexA-mClover and Sema1b-mRuby2, we observed an average lifetime (τ_{av}) of 2.51±0.06 ns, while τ_{av} of 2.72±0.03 was detected for cells expressing PlexA-mClover alone (Fig 2A and EV3A-B). The average fraction of the interacting donor (f_D) for cells co-expressing PlexA-mClover and Sema1b-mRuby2 was 0.26±0.09 (Fig EV3C). This result clearly demonstrates that Sema1b indeed binds PlexA in *cis*.

Based on the architecture of our 2:2 complex, the *cis* interaction may be mediated by the head-to-head or side-on orientation between PlexA and Sema1b. Thus, to elucidate the structural basis for the PlexA-Sema1b *cis* interaction, we measured τ_{av} for FRET-FLIM between PlexA-mClover and Sema1b-mRuby2 mutants, (site A, B and A+B mutants as described in the previous section). In order to assay the level of surface expression of the wild-type and mutant proteins we measured fluorescence intensity on the membrane of COS-7 cells by TIRF microscopy. We observed comparable intensities for all constructs (**Fig EV3D-E**) indicating that Sema1b wild-type and all three mutants are expressed at similar levels on the cell surface. As a negative control, we used COS-7 cells co-expressing PlexA-mClover and Sema1b-mutA+B-mRuby2 because Sema1b-mutA+B abolished both the head-to-head and side-on interactions in MST. These cells showed a τ_{av} of 2.65±0.03 ns, which is similar to the lifetime of donor alone with τ_{av} of 2.72±0.03 ns indicating no or very low FRET. A statistically significant

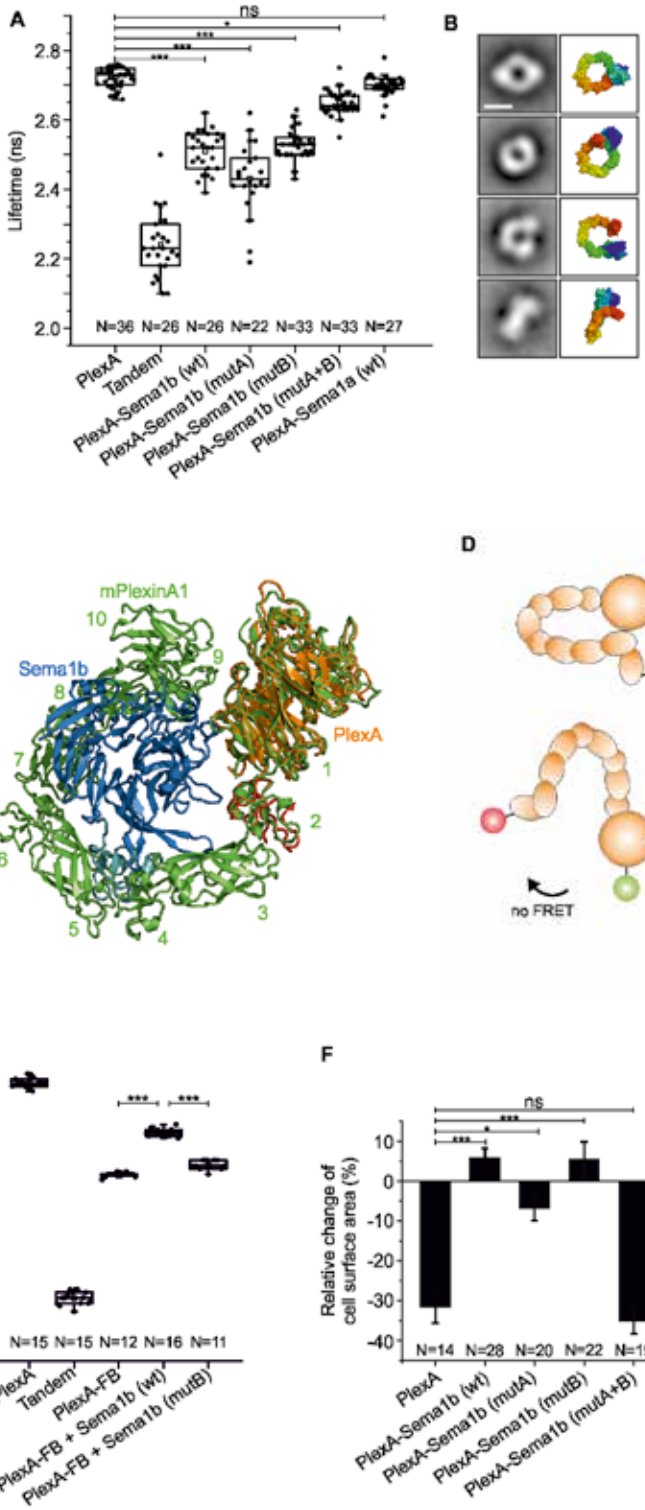
A
B
C
D
E
F
ns
Lifetime (ns)
N=36 N=26 N=26 N=22 N=33 N=33 N=27
PlexA
Tandem
PlexA-Sema1b (wt)
PlexA-Sema1b (mutA)
PlexA-Sema1b (mutB)
PlexA-Sema1b (mutA+B)
PlexA-Sema1a (wt)
mPlexinA1
Sema1b
PlexA
sema domain
FRET
no FRET
N=15 N=15 N=12 N=16 N=11
PlexA-FB
PlexA-FB + Sema1b (wt)
PlexA-FB + Sema1b (mutB)
Relative change of cell surface area (%)
N=14 N=28 N=20 N=22 N=19

Figure 2. Binding of Sema1b to PlexA in *cis* perturbs the PlexA ring-like conformation

A. FRET-FLIM in live COS-7 cells shows cell surface PlexA-Sema1b *cis* interaction. Sema1b mutants reveal that both head-to-head and side-on orientations of the PlexA-Sema1b complex are involved in the *cis* interaction. The *cis* interaction between Sema1a and PlexA is not observed. The boxcharts represent the average lifetime. Box limits indicate the 25th and 75th percentiles, centred lines show the median, squares represent sample means, whiskers extend 1.5-fold the interquartile range from the 25th and 75th percentiles, p-value was calculated by one-way analysis of variance (ANOVA). *P<0.05, ***P<0.001. B. Representative negative stain class averages of $PlexA_{ecto}$ correlate well with the ring-like conformation of mouse PlxnA1. The ring-like conformation of mouse PlxnA1 is shown in surface representation rainbow colour ramped from blue (N terminus) to red (C terminus). Scale bar, 10 nm. All class averages of $PlexA_{ecto}$ are shown in Fig EV3H. C. Superposition of the side-on orientation derived from the 2:2 complex with the mouse PlexinA1 (pdb 5l56) ring structure (green) based on the *Drosophila* and mouse PlexinA1 sema domains. D. Design of $PlexA_{ecto}$-FRET Biosensor for monitoring conformational changes. In the ring-like conformation, the fluorescent protein mClover and mRuby2 at N- and C- termini, respectively, are in close proximity generating FRET. Opening the ring-like conformation results in a FRET decrease. E. *In vitro* FRET-FLIM measurement of the PlexA-FRET Biosensor shows that the PlexA ectodomain undergoes a conformational change upon treatment with Sema1b resulting in more open conformation. The boxcharts represent the average lifetime. Box limits indicate the 25th and 75th percentiles, centred lines show the median, squares represent sample means, whiskers extend 1.5-fold the interquartile range from the 25th and 75th percentiles, p-value was calculated by one-way analysis of variance (ANOVA). ***P<0.001. F. Relative change of COS-7 cells surface area upon treatment with Sema1a-Fc. Cells expressing $PlexA_{FL}$-mClover or $PlexA_{FL}$-mCover and Sema1b-mRuby2 wild-type or mutants were treated with purified Sema1a-Fc at a final concentration of 5.8 μM. Images were acquired every minute for 30 minutes. Cell surface area was calculated using ImageJ before and after stimulation. Data are presented as means ± sem. *P<0.05, ***P<0.001, p-value calculated by one-way analysis of variance (ANOVA).

(calculated by ANOVA test) shortening of the average lifetime due to FRET was observed for cells co-expressing PlexA-mClover and Sema1b-mutA-mRuby2 (τ_{av} =2.43±0.10 ns) as well as for cells co-expressing PlexA-mClover and Sema1b-mutB-mRuby2 (τ_{av} =2.53±0.04 ns) indicating that both head-to-head and side-on orientations can mediate *cis* interactions (Fig 2A). The side-on orientation appears to be more populated than the head-to-head as the average fraction of the interacting donor for cells co-expressing PlexA-mClover and Sema1b-mutA-mRuby2 (f_D=0.37±0.15) is higher than for cells co-expressing PlexA-mClover and Sema1b-mutB-mRuby2 (f_D=0.21±0.07) (Fig EV3C). Intriguingly, FRET-FLIM data indicate that the side-on orientation dominates over the canonical head-to-head orientation in the Sema1b-PlexA *cis* interaction on the cell surface. This observation appears to be counterintuitive to the structural data suggesting the side-on interface is weaker than the head-to-head interface. One

possible explanation might be that partial deglycosylation of $Sema1b_{1-2}$ weakened the interaction mediated by the N-linked glycan at residue N289 of Sema1b in the 2:2 complex.

We then interrogated whether *cis* interaction occurs between PlexA and dimeric Sema1a, which has also been shown to bind PlexA [45]. Cells co-expressing PlexA-mClover and Sema1a-mRuby2 showed τ_{av} of 2.70±0.03 ns, which is similar to the lifetime of donor alone indicating no *cis* interaction (Fig 2A). Sema1a is tethered, from PSI domain to the membrane, by a linker that is some 35 residues shorter than in Sema1b, which is possibly insufficient to allow site A (head-to-head) mediated binding in *cis*. The lack of the PlexA-Sema1a *cis* interaction through an interaction site B on Sema1a is consistent with the inaccessibility of the sema domain loop Exβ1-β2 in dimeric semaphorins. Indeed, in all previously reported semaphorin crystal structures apart from Sema7A and the viral semaphorin A39R, the Exβ1-β2 loop is involved in the homodimerization and is therefore not accessible for the side-on interaction with plexin (Fig EV3F). Thus, semaphorin-plexin binding through site B appears to be a unique feature of monomeric semaphorin molecules.

PlexA ectodomain architecture and interactions

How does site B mediated interaction sit in the context of the structure and binding characteristics of full length PlexA ectodomain? Recently, it has been shown that the ectodomains of human and mouse PlxnAs can adopt two distinct conformations: a preferred ring-like conformation and a less frequent chair-like conformation. In the ring-like conformation, the ectodomain forms a ring, which is nearly or fully closed by an intramolecular head-to-tail interaction [30,46]. In light of the mammalian PlxnA ring-like conformation, we set out to assess the possible conformations of the *Drosophila* PlexA full ectodomain ($PlexA_{ecto}$) using negative stain EM. In the micrographs, $PlexA_{ecto}$ was monomeric. Single particle 2D class averages showed PlexA in the ring-like conformation with overall shapes ranging from the nearly closed to the predominant, fully closed ring, which matches the mouse PlxnA ectodomain crystal structures and major 2D class averages (Fig 2B and EV3G-H).

The intermolecular head-to-stalk interaction previously reported to occur for mouse PlxnA ectodomains involves sema domain and domain 4 and 5 residues that are conserved across the A class plexins in vertebrates [30]. This conservation extends to *Drosophila* PlexA. We therefore used analytical

ultracentrifugation sedimentation velocity experiments to examine whether *Drosophila* $PlexA_{ecto}$ forms a dimer in solution. As seen in the equivalent experiments for mouse PlxnA1 [30], *Drosophila* $PlexA_{ecto}$ exists in a heterogeneous mixture encompassing monomer up to tetramer (Fig EV3I). Since *Drosophila* $PlexA_{1-4}$ is a monomer in solution (Fig EV1E and EV1F), these data suggest that, similar to mammalian class A plexins, $PlexA_{ecto}$ can form an intermolecular head-to-stalk interaction on the cell membrane to provide pre-ligand bound autoinhibition.

PlexA-Sema1b *cis* interaction leads to opening of the PlexA ring-like conformation

In the mouse $PlxnA1_{1-10}$ ring-like conformation, the ring is closed by the intramolecular head-to-tail interaction between the sema domain (domain 1) and IPT5 domain (domain 9) [30]. Structural superposition of the mouse $PlxnA1_{1-10}$ ring-like crystal structure and *Drosophila* $PlexA_{1-4}$ in the 2:2 complex (Fig 2C) revealed that the position of the head-to-tail interaction site in the mouse $PlxnA1_{1-10}$ is very close to that used for the side-on interaction in the 2:2 complex between PlexA and Sema1b. Sema1b-PlexA interaction through site B binding appears sterically incompatible with the PlexA ectodomain maintaining a fully closed ring-like conformation. This observation suggests that a side-on interaction with monomeric semaphorin in *cis* may provide a mechanism for opening the plexin ectodomain ring.

We hypothesized that Sema1b and the IPT5 domain of PlexA compete for PlexA sema domain binding. Thus interaction between PlexA and Sema1b in *cis* might move the IPT5 domain out to open the ring and make the binding site on the PlexA sema domain accessible for the side-on interaction with Sema1b. To test our hypothesis, we constructed a PlexA-FRET-Biosensor (PlexA-FB) containing the $PlexA_{1-10}$ ectodomain fused with the fluorescent proteins mClover and mRuby2 at N- and C-termini, respectively. In PlexA-FB, ring opening of the $PlexA_{1-10}$ ectodomain would lead to a change of FRET efficiency between donor and acceptor (Fig 2D). Apart from PlexA-FB, we expressed and purified PlexA-mClover and tandem mClover-mRuby2 protein as control samples. *In vitro* measurement of PlexA-mClover by FRET-FLIM revealed the average lifetime (τ_{av}) of donor alone of 3.01±0.02 ns. For the PlexA-FB we observed a τ_{av} of 2.68±0.01 ns indicating FRET consistent with mClover and mRuby2 being held in close proximity by the PlexA ring-like conformation (Fig 2E). The calculated apparent inter-fluorophore distance in the PlexA-FB was 80.8 Å assuming random inter-fluorophore orientation. Addition of $Sema1b_{ecto}$ led to an increase of τ_{av}

to 2.83±0.01 ns, however, this effect was not observed when using the Sema1b$_{ecto}$-mutantB that is unable to bind PlexA by side-on interaction. The increase of the average lifetime upon Sema1b$_{ecto}$ treatment is likely a result of lower FRET efficiency because, on average, the distance between the mClover and mRuby2 has lengthened. Assuming random inter-fluorophore orientation the calculated apparent inter-fluorophore distance in the PlexA-FB was 90.2 Å upon Sema1b$_{ecto}$ treatment. These data are consistent with Sema1b side-on binding to PlexA perturbing the ring-like PlexA ectodomain to a more open conformation.

PlexA-Sema1b *cis* interaction prevents *cis*-engaged PlexA from interacting with Sema1a in *trans*

Drosophila Sema1a has been shown to bind PlexA and their interaction in *trans* has been reported to be crucial for controlling axon guidance [45]. Therefore, we next investigated whether the PlexA-Sema1b *cis* interaction can serve as a competitive inhibitor for Sema1a binding in *trans*. We used a COS-7 cell-based assay as a heterologous system that can mimic growth cone collapse [47]. COS-7 cells transiently expressing full-length PlexA$_{FL}$-mClover showed a typical well-spread morphology. Incubation of these cells with recombinant Sema1a-Fc induced a robust morphological collapse (Fig 2F and EV3J-O). Conversely, this effect was not observed when using COS-7 cells co-expressing PlexA$_{FL}$-mClover and Sema1b-mRuby2, indicating that dimeric Sema1a-Fc binding to PlexA in *trans* is blocked by the monovalent PlexA-Sema1b *cis* interaction. We also examined the ability of Sema1b mutants to inhibit collapse. Incubation with Sema1a-Fc did not significantly alter the morphology of COS-7 cells that co-expressed PlexA$_{FL}$-mClover and Sema1b-mutA-mRuby2 or Sema1b-mutB-mRuby2. Conversely, co-expression of PlexA$_{FL}$-mClover and Sema1b-mutA+B-mRuby2 resulted in COS-7 cells showing collapse on incubation with Sema1a-Fc similar to that observed for COS-7 cells expressing PlexA$_{FL}$-mClover alone. Taken together, these results show that the interaction of monomeric Sema1b with PlexA in *cis* can inhibit dimeric Sema1a signalling through PlexA in *trans.* Furthermore, our data support a model in which monovalent Sema1b-PlexA *cis* interaction can be mediated by two distinct binding sites, A and B, using head-to-head or side-on orientations respectively.

Mouse Sema6A and *Drosophila* Sema1b utilise the same head-to-head and side-on binding modes to interact with plexins in *cis*

We next addressed whether this model was of relevance to vertebrate semaphorin function. Based on our results for Sema1b, we designed three mutants of mouse Sema6A, termed A, B or A+B, and analyzed their PlxnA2 binding using FRET-FLIM. Instead of point mutations, we introduced N-linked glycosylation sites at binding sites A and B, to provide substantial steric hindrance to interface formation. In Sema6A-mutA, we introduced the N-linked glycosylation site Sema6A H212N in order to disrupt the head-to-head interaction at site A. In Sema6A-mutB, we designed the N-linked glycosylation site Sema6A E345N, K347T to target the putative side-on interaction through site B. Sema6A-mutA+B combined both N-linked glycosylation sites to potentially abolish both head-to-head and side-on interactions.

For FRET-FLIM we used mouse PlxnA2 fused with mClover while Sema6A wild-type or mutants were fused with mRuby2. We observed statistically significant (calculated by ANOVA test) shortening of the average lifetime due to FRET for cells co-expressing mouse PlxnA2 and Sema6A wild-type or Sema6A-mutA or Sema6A-mutB (Fig EV4A and Fig EV4B). Cells co-expressing mouse PlxnA2 and Sema6A-mutaA+B revealed a lifetime statistically similar to the lifetime of donor alone. Sema6A and its three mutants showed similar fluorescence intensities as measured in TIRF microscopy (Fig EV4C-D) confirming that they had comparable expression levels on the surface of live COS7 cells. Consistent with our findings for *Drosophila* Sema1b, these data suggest that mouse Sema6A can bind PlxnA2 in *cis* using both head-to-head and side-on interaction. For mouse PlxnA2 and Sema6A, we did not observe such dramatic changes in the average lifetime as those observed for their *Drosophila* counterparts, presumably because Sema6A potentially exists on the cell surface as a mixture of monomers and non-covalent dimers while Sema1b is present exclusively as the monomer.

Cis interaction between mouse Sema6A and PlxnA4 serves as an inhibitory mechanism to signalling in *trans*

We further investigated whether mouse Sema6A and *Drosophila* Sema1b utilise the same molecular mechanism to inhibit plexin function using a growth cone collapse assay. Here we used dorsal root ganglia (DRG) neurons, which have been previously reported to endogenously express

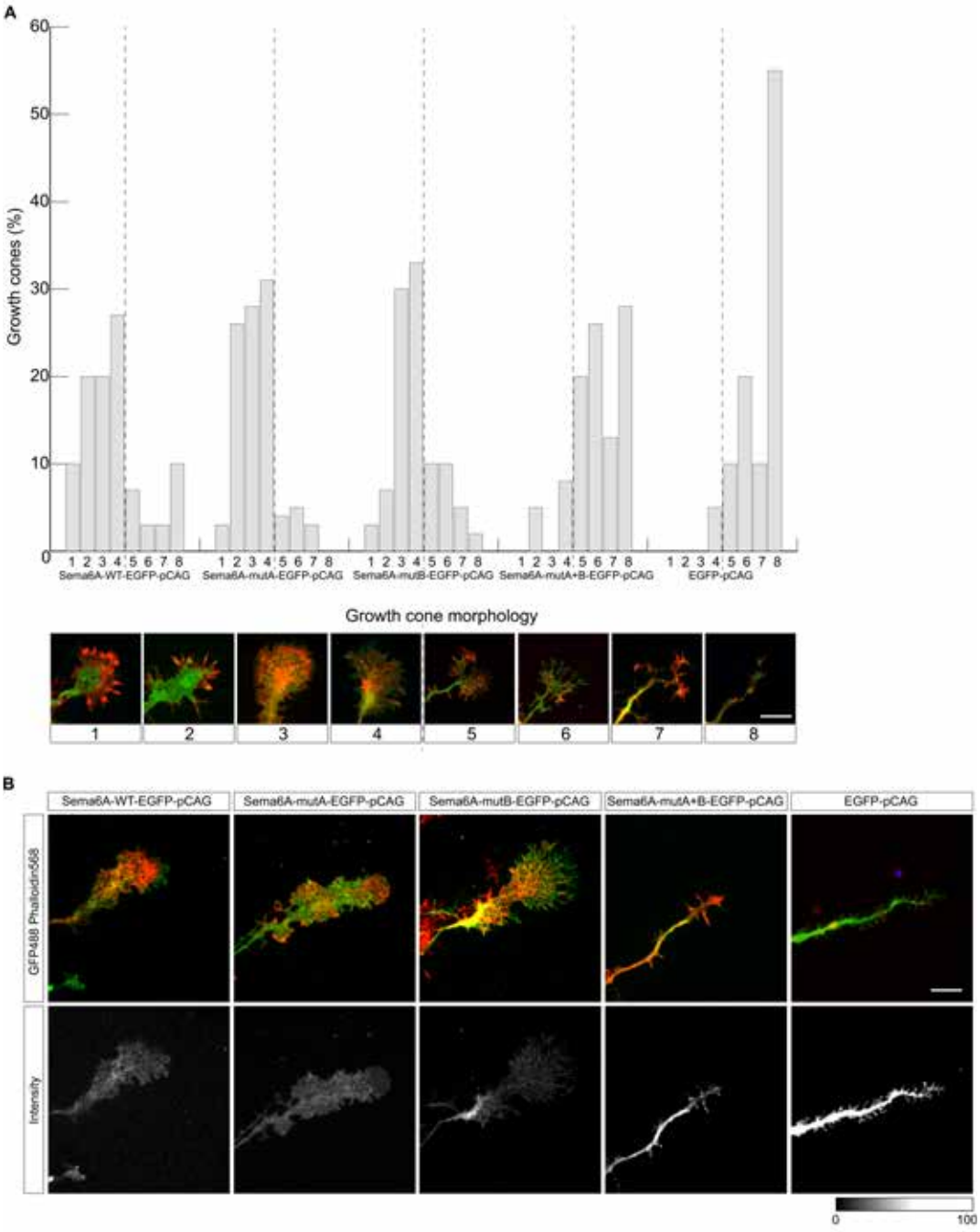
A
Growth cones (%)
60
50
40
30
20
10
0
1 2 3 4 5 6 7 8
Sema6A-WT-EGFP-pCAG
Sema6A-mutA-EGFP-pCAG
Sema6A-mutB-EGFP-pCAG
Sema6A-mutA+B-EGFP-pCAG
EGFP-pCAG
Growth cone morphology
1
2
3
4
5
6
7
8
B
Sema6A-WT-EGFP-pCAG
Sema6A-mutA-EGFP-pCAG
Sema6A-mutB-EGFP-pCAG
Sema6A-mutA+B-EGFP-pCAG
EGFP-pCAG
GFP488 Phalloidin568
Intensity
0
100

< Figure 3. Mouse Sema6A utilises the same molecular mechanism to inhibit plexin function as that observed for *Drosophila* Sema1b

A. Cultured dorsal root ganglion (DRG) neurons from E12.5 *Sema6*A knockout (KO) embryos were transfected with EGFP, EGFP-tagged wild-type (WT) Sema6A (Sema6A-WT) or different EGFP-tagged Sema6A mutants (Sema6A-mutA, Sema6A-mutB, and Sema6A-mutA+B) at 1 day *in vitro* (DIV1) and treated with purified Sema6A-Fc at a concentration of 75 nM for 1 hour at 37°C at DIV4. Transfection of EGFP was used as a control (full collapse). DRG neurons from *Sema6A* KO embryos acquired sensitivity to Sema6A and growth cone collapse was observed in three independent experiments. Transfection of Sema6A-WT, Sema6A-mutA and Sema6A-mutB but not of EGFP or Sema6A-mutantA+B prevented Sema6A-mediated growth cone collapse (Fisher's exact test $p<0.0001$). Quantification of growth cone collapse was performed using a growth cone morphology matrix (lower part panel A). Data are presented as percentage of morphologically distinct growth cones, divided (represented by the dotted line) in two categories, from uncollapsed (1-4) to fully collapsed (5-8). Totally, 20-40 growth cones were analysed for each condition per experiment (n=3 experiments). Scale bar 20 μm. B. Representative images of growth cones of mouse DRG neurons transfected with WT or mutant constructs treated with 75 nM Sema6A-Fc and visualised with immunofluorescent staining to detect GFP (green) and phalloidin (red). Average intensity images for all different constructs are shown in grey color. Scale bar 20 μm.

Sema6A and PlxnA4 [13,48]. Further, binding of Sema6A to PlxnA4 *in cis* has been shown to inhibit growth cone collapse induced by Sema6A presented *in trans* in DRG neurons [13]. We transfected cultured DRG neurons from *Sema6A* knockout embryos with Sema6A-EGFP wild-type or Sema6A-EGFP mutants (mutA, mutB or mutA+B) or EGFP alone. Three days post-transfection DRG neurons were treated with purified Sema6A-Fc, and growth cone collapse was scaled from one (uncollapsed) to eight (fully collapsed) using a previously established growth cone morphology matrix (Fig 3A, B) [30,49].

In a pilot study, GFP control transfection and treatment with different concentrations of Sema6A-Fc were tested. Following treatment with 75 nM purified Sema6A-Fc, we observed a robust growth cone collapse for cells expressing EGFP, as compared to a low level of collapse in control treated growth cones (0 nM; Fig EV5). In contrast, *Sema6A* knockout cells transfected with a Sema6A wild-type construct were unresponsive to addition of purified Sema6A-Fc (at 1, 10 and 75 nM) indicating that interaction of Sema6A with its PlxnA4 receptor in *cis* serves as a competitive inhibitor for Sema6A-Fc binding in *trans*. A similar effect was observed for cells expressing Sema6A-mutA or Sema6A-mutB suggesting that both mutants maintained PlxnA4 binding in *cis* using the side-on or head-to-head sites, respectively. Conversely, cells expressing Sema6A-mutA+B showed modest (10 nM) or robust (75 nM) growth cone collapse similar

to that observed for cells expressing EGFP alone (as shown for 75 nM). On basis of these data a larger number of growth cones was analysed in 3 independent experiments using 75 nM Sema6A-Fc (Fig. 3A, B). This analysis confirmed the pilot data showing strong Sema6A-Fc-induced growth cone collapse in EGFP-transfected Sema6A knockout neurons, a rescue effect by transfection of Sema6A wildtype, and a failure to rescue by Sema6A-mutA+B. These findings are in agreement with the Sema1b cell-based assay. Overall, these results support our model that Sema6A-PlxnA4 *cis* interaction can be mediated by two distinct binding sites and also demonstrate that Sema6A-PlxnA4 *cis* interaction directly inhibits the plexin receptor's ability to respond to ligand binding in *trans.*

DISCUSSION

In the immune system *cis* interactions provide a mechanism to fine tune the level of signalling at which a biological response is triggered [50]. Similarly, *cis* interactions have been proposed to act as threshold-generating mechanisms for semaphorin-plexin, ephrin-Eph and Notch-Delta signalling during the development of the nervous system [51]. For semaphorin-plexin signalling there is particular abundance of evidence for *cis* interactions between vertebrate class 6 semaphorins and their plexin A receptors. Inhibitory *cis* interactions between Sema6s and PlxnAs have been reported to modulate repulsive cell guidance signalling in a number of neuronal cell types: dorsal root ganglion neurons, spinal cord, star burst amacrine cells in the retina and granule cell axons (mossy fibers) in the hippocampus [10–14,52]. In these examples either *cis* interaction with a semaphorin ligand directly inhibits the plexin receptor's ability to respond to ligand binding in *trans* or plexin binding in *cis* sequesters the semaphorin ligand so that it cannot interact with a plexin receptor in *trans*. Both these scenarios require that the *cis* interaction between ligand and receptor does not activate the receptor. This poses a conundrum; how does the inhibitory interaction between ligand and receptor in *cis* differ from the activating interaction in *trans*? To date, research into the molecular mechanism underlying plexin activation by semaphorin binding in *trans* has highlighted the role of the dimeric ligand in crosslinking two receptors [42,53]. In this paper we present structural, biophysical and cell-based analyses that delineate the distinctive properties of monomeric semaphorins interacting in *cis* with their plexin receptors. Our data suggest a mechanism by which cell-attached semaphorin molecules in the monomeric state can contribute to the inhibition of *trans* interactions

through a side-on interaction in *cis*. This side-on interaction requires the semaphorin to be in the monomeric state, causes conformational change in the ectodomain of the plexin receptor and, independent of the well-established head-to-head semaphorin-plexin binding mode, can inhibit the activation of plexin receptor by dimeric semaphorin. Below we discuss these data and based on them propose molecular mechanisms that can provide distinct functional outcomes for *cis* and *trans* binding between a semaphorin ligand and plexin receptor.

Monomeric semaphorins with distinctive side-on binding properties

We showed that *Drosophila* Sema1b exists on the cell surface in a monomeric state. Whereas *Drosophila* Sema1a, Sema2a and Sema2b can be locked into a dimeric state through formation of a sema-to-sema domain disulfide bond, Sema1b lacks this bond [22]. Some, but not all, of the mammalian semaphorins can form inter-chain disulfide bonds at various points in their ectodomains, however, we are not aware of any wild-type semaphorin that lacks a measureable propensity for sema-to-sema domain dimerization other than Sema1b. In particular the ectodomains of Sema6s, the vertebrate homologues of the class 1 semaphorins, do not form covalently stabilized dimers, and we and others have reported secreted forms of Sema6A to be in monomer-dimer equilibrium [32,34].

We analysed the atomic level determinants of Sema1b-PlexA binding in crystal structures of the complex to address whether the monomeric state of Sema1b per se provides this semaphorin ligand with distinctive properties promoting *cis* interaction. In addition to the head-to-head interaction, which for dimeric semaphorin binding has been shown to mediate receptor activation in *trans* [32–34], our x-ray crystallographic analysis revealed a putative side-on binding mode. This side-on binding mode only becomes possible if a semaphorin is in the monomeric state, because the interaction site is otherwise occluded by the dimer interface. Notably, all previously reported crystal structures of semaphorin-plexin complexes have involved semaphorin dimers, presumably because, even when a monomer-dimer equilibrium is present in solution, crystallization favours the dimeric state. We were able to use structure-guided mutants of Sema1b and Sema6A in FRET-FLIM experiments to reveal that *cis* interactions between the semaphorins and their cognate plexins can be mediated by either the, more favoured, side-on orientation or, less frequently, the head-to-head orientation. These findings were supported by the results

from collapse assays, which confirmed that both interaction modes were inhibitory. Thus, monomeric Sema1b and Sema6A can utilise a side-on mode of interaction to inhibit plexin activation. Interestingly, side-on *cis* interaction with plexin could also serve to sequester semaphorin from monomer-dimer equilibrium into an 'inert' monomeric state, inhibiting dimeric engagement and activation of plexin in *trans*. This mechanism would be consistent with the observation that interaction of PlxnA2 and Sema6A in *cis* functions to inhibit activation of PlxnA4 in *trans* [11]. In previous work, ectopic expression of Sema1b in muscle subsets revealed that Sema1b can act as a repulsive guidance cue [45]. Although elegant, a caveat of this study is that for this Sema1b gain-of-function experiment, Sema1b was expressed at high levels. It is possible that such high expression may lead to Sema1b dimerization or multimerization and thereby allow this semaphorin to act as a ligand. Evidence to support the idea that Sema1b acts as a repellent under physiological conditions is currently lacking.

Mechanisms for inhibition in *cis* resulting from the monomeric side-on interaction

Previous studies on PlxnA4-Sema6A [13] and PlxnA2-Sema6A [17] have suggested that *cis* and *trans* interactions are mediated by two distinct modes. In Fig 4 we propose models for the molecular mechanisms underlying inhibitory semaphorin-plexin *cis* interactions that are consistent with the data we report in this paper. First, we consider the likely conformation and interactive state of the PlexA in isolation at the cell surface. Our results show that, similar to PlxnA ectodomains [30], the PlexA ectodomain forms a ring-like structure and exists as a heterogeneous mixture of oligomeric states encompassing monomer up to tetramer in solution. As the PlexA ectodomain has high sequence similarity to the mammalian PlxnA ectodomains and shares the same structural and biophysical characteristics, it appears plausible that the PlexA ectodomain can also maintain a level of pre-ligand bound autoinhibition using the inter-molecular head-to-stalk interaction reported for the PlxnAs [30]. Bivalent ligand binding in *trans* overcomes receptor autoinhibition. The *trans* interaction between PlexA and dimeric Sema1a can be expected to conform to the canonical semaphorin-plexin architecture resulting in dimerization and activation of the PlexA (Fig 4A).

Inhibitory interactions between ligand and receptor in *cis* provide a mechanism for modulating the threshold for activation of signalling by the *trans* interaction. However, this modulatory mechanism requires that the ligand interact with the receptor without activating it. Our results suggest

that this can be achieved in two ways. In mode A, the sema domain of monomeric Sema1b binds the sema domain of PlexA in the canonical head-to-head mode to directly inhibit head-to-head binding in *trans* (Fig 4B). This mode requires that the semaphorin ligand has sufficient flexibility in its ectodomain to position its sema domain at the requisite height and orientation relative to the plexin receptor. If a dimeric semaphorin is able to make mode A interactions with both its sema domains this form of *cis* interaction could presumably serve to activate the plexin receptor, consistent with the reports of *cis* activation for the semaphorin SMP-1 and plexin PLX-1 in *C.elegans* [15] and for mouse Sema5A signalling through PlxnA2 co-expressed on hippocampal dentate granule cells [16].

Mode B is the previously unobserved side-on interaction mode revealed in our studies of Sema1b. Interestingly, FRET-FLIM measurements suggest that this side-on interaction mode is more populated than the head-to-head *cis* interaction of mode A. The side-on interaction does not directly involve the head-to-head ligand binding site on PlexA, but it is inhibitory in cell collapse assays. We propose that side-on binding by monomeric semaphorin prevents formation of the 2:2 arrangement of semaphorin dimer complexed with two ring-like plexin ectodomains required to trigger a repulsive signal (**Fig 4C**). One subunit of the dimeric Sema1a could form a 2:1 complex with PlexA by head-to-head *trans* binding, but side-on Sema1b binding in *cis* would sterically hinder the engagement of a second PlexA in the orientation seen for canonical 2:2 complexes. Furthermore, our PlexA-FRET biosensor data suggest that *cis* binding of monomeric Sema1b to PlexA through the side-on interaction forces the ring-like structure of the PlexA ectodomain into more open conformation. It is possible that this altered PlexA ectodomain conformation may itself prevent activation of signalling for cell collapse.

Our studies on Sema1b have provided the first insights into the *cis* binding modes of monomeric semaphorins. Furthermore, our biophysical and cellular assays have demonstrated that Sema6A utilises the same molecular mechanism to occlude plexin function. The molecular mechanisms for semaphorin-plexin *cis* interaction we propose here suggest that the balance between monomeric and dimeric states is central to the biological functions of the Sema6s. Further investigation will be required to tease out how the interplay between monomeric and dimeric states of Sema6 ligands, expression levels of Sema6s and their PlxnA receptors, and *cis* and *trans* binding affinities in the context of cell membranes, combine to set signalling thresholds.

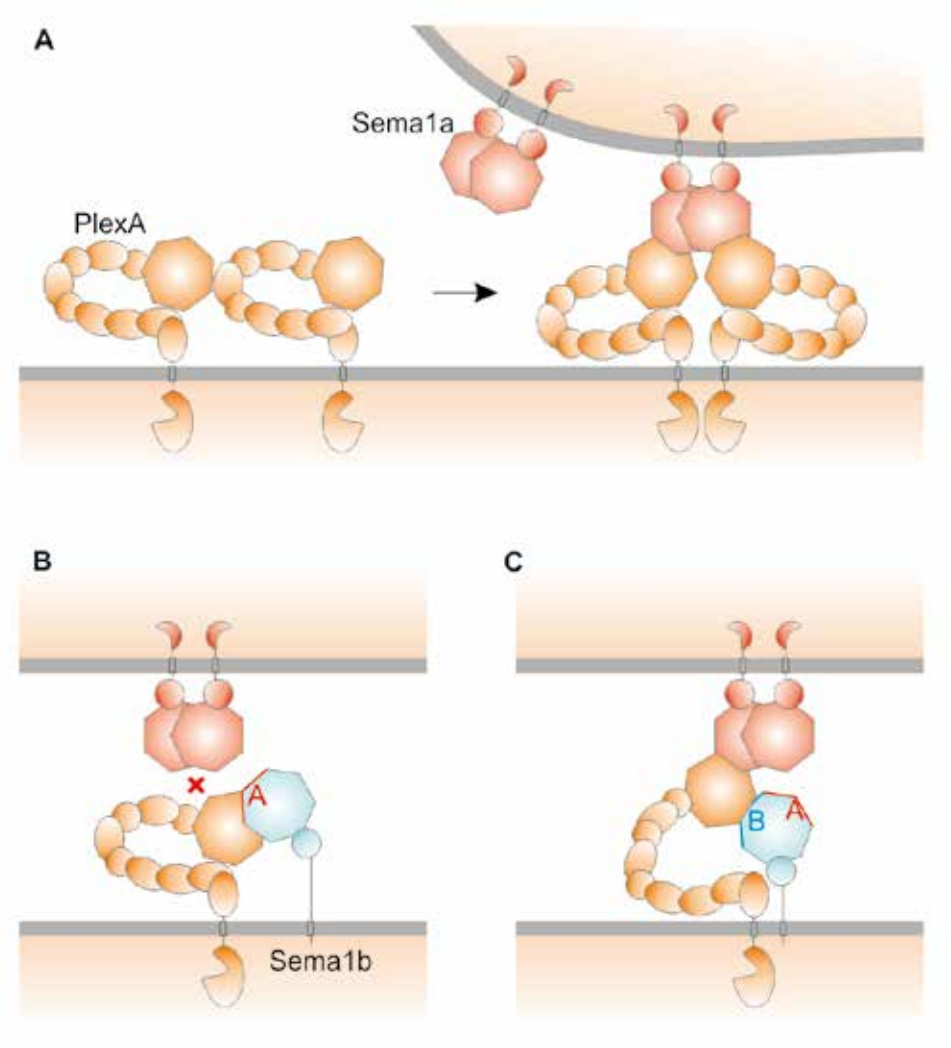

Figure 4. Model for the PlexA-Sema1b *cis* interaction

A. The ring-like ectodomain of PlexA imposes a pre-signalling autoinhibition. Engagement of dimeric Sema1a with PlexA possibly disrupt the PlexA autoinhibitory dimer and switch it to the active dimer. B. A structural model for the PlexA-Sema1b *cis* interaction. Monomeric Sema1b binds PlexA in the head-to-head orientation through site A without disruption of the PlexA ring-like. C. In another model of the PlexA-Sema1b *cis* interaction, the monomeric state of Sema1b allows binding PlexA through the side-on binding site (site B) which may cause the PlexA ectodomain to be in a more open conformation. Possibly, the conformational change in the PlexA ectodomain makes the binding site on the PlexA more accessible for interaction with Sema1a presented in *trans*, however, Sema1a fails to dimerize PlexA because of steric clashes.

MATERIAL AND METHODS

Protein Production

Constructs encoding *Drosophila melanogaster* Sema1b$_{ecto}$, Sema1b$_{1-2}$, PlexA$_{1-4}$ and PlexA$_{ecto}$ (residues 37-659, 37-602, 28-730 and 28-1272, respectively) were cloned into pHLsec vector [54] in-frame with a C-terminal hexahistidine (His6) tag. A human IgGγ1 hinge and Fc-fusion construct of Sema1a (residues 21-602) or mouse Sema6A (residues 19-571) was constructed using pHL-FcHis vector [54]. For MST experiments, PlexA$_{1-4}$ was cloned in frame with a C-terminal monoVenus (mVenus) followed by a C-terminal (His6) tag in pHLsec [54].

For crystallization experiments, proteins were produced by transient transfection in HEK 293T cells (ATCC CRL-3216) in the presence of the αmannosidase inhibitor kifunensine [55]. For all other experiments, proteins were produced in HEK 293T cells without kifunensine. Five days post-transfection, the conditioned medium was collected and buffer exchanged using a QuixStand diafiltration system (GE Healthcare) and subjected to immobilized metal-affinity chromatography using a HisTrap FF column (GE Healthcare) and further purified by size-exclusion chromatography using a Superdex 200 16/60 column (GE Healthcare).

To investigate conformational changes of PlexA ectodomain, we produced a PlexA-FRET-Biosensor (PlexA-FB). First, based on pHLsec vector, we developed a novel pHLsec-FRET-Biosensor vector (pHLsec-FB), in which inserts can be cloned between AgeI and KpnI sites allowing the protein to be secreted with the fluorescent proteins mClover and mRuby2, at the N-terminus and the C-terminus, respectively, followed by the C-terminal octahistidine-tag. We produced PlexA-FB, PlexA-mClover and tandem mClover-mRuby2 by transient transfection in HEK 293T cells as described above. PlexA-mClover and tandem mClover-mRuby2 were used as control samples. For PlexA-FB, a construct encoding *Drosophila* PlexA$_{1-10}$ (residues 67-1274) was cloned into pHLsec-FB. For the tandem mClover-mRuby2, an insert containing GGGGGA sequence encoding Gly-Gly was cloned into pHLsec-FB. For PlexA-mClover, a construct encoding PlexA$_{1-10}$ (residues 67-1274) was C-terminally tagged with mClover followed by the C-terminal His6-tag.

Site-directed mutagenesis

Site-directed mutagenesis of Sema1b was carried out by overlap-extension PCR and the resulting PCR products were cloned into the pHLsec vector as described above. In Sema1b-mutant A (mutA), we mutated interface residues F203E, Q219R and K223E. For Sema1b-mutant B (mutB), in which the loop 350-367 was replaced with 18 alanine residues, a synthetic clone was commercially synthesized (Invitrogen-GeneArt). Sema1b mutant A+B (mutA+B) combined the previous modifications. All mutant Sema1b proteins were secreted at similar levels to the wild-type protein.

Crystallization and data collection

Proteins for crystallization were prepared in a buffer consisting of 15 mM Tris-HCl (pH 8.0) and 50 mM NaCl. For the $Sema1b_{1-2}$-$PlexA_{1-4}$ complex crystallization, proteins were mixed at a 1:1 molar ratio and concentrated to 7.6 mg/ml. Prior to complex formation $Sema1b_{1-2}$ was treated with endoglycosidase F1 (1:100 w/w) for 1 h at 37°C, whereas $PlexA_{1-4}$ was not deglycosylated. Sitting drop vapour diffusion crystallization trials were set up using a Cartesian Technologies pipetting robot and consisted of 100 nl protein solution and 100 nl reservoir solution [56]. Plates were maintained at 20°C in a Formulatrix storage and imaging system. The $Sema1b_{1-2}$-$PlexA_{1-4}$ complex crystallized in two different crystal forms. One crystal form, with space group C2221, was grown in 0.1 M HEPES (pH 7.0) and 8% (w/v) PEG 8000, the other crystal form, with space group P6555, crystallized in 0.1 M MES (pH 6.5) and 12% (w/v) PEG 20 000. Crystals were cryoprotected by soaking in reservoir solution supplemented with 25% (v/v) glycerol, and then flash-cooled in liquid nitrogen. Diffraction data were collected at 100K at Diamond Light Source beamlines I03 and I24 and indexed, integrated and scaled using the automated XIA2 expert system [57]. For $PlexA_{1-4}$-$Sema1b_{1-2}$ 1:1 complex, due to radiation sensitivity, diffraction data from two separate isomorphic crystals were merged together to increase completeness.

Structure determination and refinement

The structure of the $PlexA_{1-4}$-$Sema1b_{1-2}$ 1:1 complex was solved by molecular replacement in PHASER with the $Sema1b_{1-2}$ structure (PDB 6FKK) and the $PlexinA2_{1-4}$ structure (PDB 3OKY) [32] as search models. This solution was re-built automatically by BUCCANEER and completed by several cycles of manual rebuilding in COOT and refinement in PHENIX. PlexA domains IPT1-PSI2 were omitted from the model due to disorder. The structure of the $PlexA_{1-4}$-$Sema1b_{1-2}$ 2:2 complex was solved by molecular replacement in PHASER with the $Sema1b_{1-2}$ and $PlexA_{1-2}$ structures as search models.

This solution was refined by Rosetta [58] and rigid-body in PHENIX with each domain as a rigid group and a single *B* factor per domain and using global NCS restraints. Structure validation was performed using MolProbity [59]. Refinement statistics are given in Table 1.

Buried surface areas of protein–protein interactions were calculated using PISA [60], alignments were generated with Clustal Omega [61], structural alignment was performed using PDBeFold [60], electrostatics potentials were generated using APBS [62]. Figures were produced with PyMOL (Schrodinger, LLC), ESPRIPT [63] and Corel Draw (Corel Corporation).

Microscale thermophoresis (MST)

MST experiments were performed using a Nanotemper Monolith NT.115 instrument (Nanotemper) at 28°C in 15 mM HEPES (pH 7.4), 150 mM NaCl, 2 mM $CaCl_2$ and 0.05% (v/v) Tween-20. A dilution series was prepared and a concentration of the fluorescent $PlexA_{1-4}$-mVenus was kept constant in all samples and the unlabeled $Sema1b_{ecto}$ mutants were varied in 1:1 dilution to give a titration. The samples were equilibrated 1 hour at room temperature before filling into the standard capillaries (Nanotemper). To find the best thermophoretic setting, a measurement at 20, 40, 60 and 80% MST power was performed and the best signal to noise ratio was obtained by using 80% MST power. The LED power was set to 40%. The overall measurement time consisted of 5 s of cold fluorescence followed by IR-laser on and off times set at 30 and 5 s. Data were analysed using the MO Affinity Analysis v2.1.3 software (Nanotemper). The experiments were performed with three independent replicates.

Analytical ultracentrifugation

Sedimentation velocity experiments were performed using an Optima XL-I analytical ultracentrifuge (Beckman). $PlexA_{1-4}$ and $PlexA_{ecto}$ samples in 15 mM HEPES (pH 7.4) and 150 mM NaCl were centrifuged in double sector 12 mm centerpieces in an An-60 Ti rotor (Beckman) at 40000 rpm. Protein sedimentation was monitored by an absorption optical system and Rayleigh interference system. Data were analysed using SEDFIT [64]. Expected sedimentation coefficients of the structural models were predicted using WinHydroPRO [65].

Size-exclusion chromatography with multi-angle light scattering (SEC-MALS)

SEC-MALS experiments were carried out with the Superdex 200 10/300 column (GE Healthcare) connected online with a static light-scattering (DAWN HELEOS II, Wyatt Technology), differential refractive index (Optilab rEX, Wyatt Technology) and Agilent 1200 UV (Agilent Technologies) detectors. $PlexA_{1-4}$ were injected into the column at flow rate of 0.5 ml/min in 15 mM HEPES (pH 7.8) and 150 mM NaCl. The molecular mass of glycoproteins containing N-linked oligomannose-type sugars was determined using an adapted RI increment value (dn/dc standard value, 0.185 ml/g). Data were analysed using the ASTRA software (Wyatt Technology).

Single particle negative stain electron microscopy

A freshly purified $PlexA_{ecto}$ (3.5 µg/ml) was stained with 0.75% uranyl formate using the conventional negative staining protocol [66]. Images were recorded using a Tecnai T12 transmission electron microscope operated at 120 kV on a 4000×4000 high-sensitivity FEI Eagle at magnification of 67,000, which corresponds to 1.68 Å/pixel sampling of the specimen. A defocus value of about -1.5 µm was used. Particles were manually selected and processed using the Eman2 [67] and Imagic [68] software.

Fluorescence Resonance Energy Transfer – Fluorescence Lifetime Imaging microscopy (FRET-FLIM) in live cells

Drosophila melanogaster PlexA (residues 28-1311) or Sema1b (residues 37-686) and Sema1a (residues 21-633) were cloned into pHLsec vector in-frame with C-terminal fluorescent proteins mClover or mRuby2, respectively. For FRET-FLIM analysis of mouse Sema6A and PlxnA2, genes encoding mouse Sema6A (residues 19-675) and PlxnA2 (residues 36-1263) were cloned into pHR-CMV-TetO2 vector in frame with C-terminal fluorescent proteins mClover and mRuby2, respectively [69]. All constructs encompassed the ectodomain followed by a transmembrane segment and the C-terminal fluorescent protein. The same constructs were used for Number and Brightness analysis. COS-7 cells (ATCC CRL-1651) grown on glass-bottom 35 mm Petri dishes (Mattek) were transiently co-transfected with *Drosophila* PlexA-mClover and Sema1b-mRuby2 or a donor-only sample (PlexA-mClover) or a fusion construct of mClover-mRuby2, which was used as a positive control. For mouse Sema6A and PlxnA2, we used lentiviral transduction of COS-7 cells followed by FACS to enrich subpopulations of transduced cells [69].

Before imaging, a Dulbecco's modified eagle medium was replaced with PBS equilibrated at 37°C. Multicolour images were acquired two days post-transfection using a Leica SP8-X-SMD confocal microscope (Leica Microsystems) with a 63×/1.40 numerical aperture oil immersion objective. mClover and mRuby2 were excited at 488 and 561 nm, respectively, and the fluorescence emission was detected using two hybrid detectors in photon counting mode at 498-551 and 573-625 nm, respectively. FRET detection was based on the time domain FLIM experiments which were performed using a Time-Correlated Single Photon Counting (TCSPC) system operated by a PicoHarp 300 module (PicoQuant) attached to the Leica SP8-X-SMD confocal microscope (Leica Microsystems) with a 63×/1.40 numerical aperture oil immersion objective at 37°C. A 488 nm picosecond pulsed diode laser PDL 800-B (PicoQuant) tuned at 80 MHz was used to excite the donor and the emitted photons passing through the 500-550 nm emission filter were detected using an external hybrid detector in photon counting mode. At least 600 photon events per pixel were collected in all cases and the lifetime analysis was carried out using a Symphotime (PicoQuant). The acquired fluorescent decays *i(t)* were fitted by mono- (equation 1) or bi-exponential (equation 2) model.

$$i(t) = Ae^{-t/\tau_1} \quad (1)$$

$$i(t) = A_1 e^{-t/\tau_1} + A_2 e^{-t/\tau_2} \quad (2)$$

In equation 1 and 2, τ_1 is the lifetime of the donor alone, τ_2 is the lifetime of the donor in the presence of the acceptor, A, A_1 and A_2 are amplitudes. The average donor lifetime obtained from a mono-exponential fit from the cells expressing the donor only (PlexA-mClover) was fixed in the bi-exponential model to calculate the remaining two amplitudes and the second lifetime [43,44]. The amplitude weighted average lifetime of donor (τ_{av}) was calculated using equation 3:

$$\tau_{av} = \sum_i A_i \tau_i / \sum_i A_i \quad (3)$$

The fraction of the interacting donor (f_D) was calculated using equation 4:

$$f_{D=} A_2/(A_1 + A_2) \quad (4)$$

The fraction of the interacting donor was normalized by multiplying by a factor of 2 because we were able to detect just ~50% of the real interaction [70].

Fluorescence Resonance Energy Transfer – Fluorescence Lifetime Imaging microscopy (FRET-FLIM) in solution

For FLIM measurements *in vitro*, the purified fluorescent proteins were diluted to a concentration of 106 nM in 15 mM HEPES (pH 7.6) and 150 mM NaCl and 30 µl of the protein sample was loaded onto the µ-Slide with 18 wells (Ibidi). FRET was measured using the time domain FLIM experiments which were performed using a Time-Correlated Single Photon Counting (TCSPC) system operated by a PicoHarp 300 module (PicoQuant) attached to the Leica SP8-X-SMD confocal microscope (Leica Microsystems) with a 63×/1.40 numerical aperture oil immersion objective at room temperature.

A 488 nm picosecond pulsed diode laser PDL 800-B (PicoQuant) tuned at 40 MHz was used to excite the donor and the emitted photons passing through the 500-550 emission filter were detected using an external hybrid detector in photon counting mode for a period of 350 s. The lifetime analysis was carried out using a Symphotime (PicoQuant). The acquired fluorescent decays were fitted by mono- or bi-exponential model as described above. The apparent interfluorophore distance *r* was calculated from equation 5:

$$E_{app} = 1 - \tau_{DA,av}/\tau_{D,av} = R_0^6/(R_0^6 + r^6) \quad (5)$$

In equation 5, τ_D is the lifetime of the donor alone, τ_{DA} is the lifetime of the donor in the presence of the acceptor and R_0 is the Förster radius. The R_0 for the mClover/mRuby2 pair was calculated by the following equation:

$$R_0 = \left(\frac{9000\ ln10\ \Phi_D\ \kappa^2\ J}{128\ \pi^5\ N_A\ n^4}\right)^{1/6} \quad (6)$$

where Φ_D is the fluorescence quantum yield of the donor in the absence of the acceptor, κ is the dipole orientation factor, *n* is the refractive index of the medium, N_A is Avogadro's number, and *J* is the spectral overlap integral calculated as

$$J = \int F_D(\lambda)\ \varepsilon_A(\lambda)\ \lambda^4\ d\lambda / \int F_D(\lambda)\ d\lambda \quad (7)$$

Where F_D is the donor emission spectrum, and ε_A is the acceptor molar extinction coefficient. To calculate the apparent interfluorophore distance, we used the Förster radius of 57 Å for the mClover-mRuby2 assuming random interfluorophore orientation. The spectral overlap integral of the mClover/mRuby2 pair was calculated using the Simpson method utilizing the normalized excitation spectrum of the donor and the acceptor corrected for the published extinction coefficient [71]. Knowing the value of J we calculated R_0 assuming random interfluorophore orientation ($\kappa^2=2/3$).

Number & Brightness analysis

COS-7 cells grown on µ-Slides (chambered coverslips) with 8 wells (Ibidi) were transiently transfected with *Drosophila melanogaster* PlexA-mClover (residues 28-1311), Sema1b-mClover (residues 37-686) or Sema1b-F254C-mClover (residues 37-686). Before imaging, the cells were washed with PBS and Dulbecco's modified eagle medium was replaced with a phenol red free Dulbecco's modified eagle medium equilibrated at 37°C.

Images were acquired using a Leica SP8-X-SMD confocal microscope (Leica Microsystems) with a 63×/1.40 numerical aperture oil immersion objective at 37°C. For each studied cell, a single plane stack of 500 images was acquired at a resolution of 256 × 256 pixels and pixel size of 481 nm, with a pixel dwell time 2.43 µs. mClover was excited at 488 nm with the same laser power for each cell and the fluorescence emission was detected using a hybrid detector in photon counting mode at 498-551 nm. The data were analyzed using a nandb – an R package for performing N&B analysis [39].

Total Internal Reflection Microscopy

COS-7 cells grown on glass-bottom 35 mm Petri dishes (Mattek) were transiently co-transfected with PlexA-mClover, wild-type Sema1b-mRuby2 and all three Sema1b mutants. The same constructs were used for FRET-FLIM or Number and Brightness analysis. Two days post-transfection, the cells were washed with PBS and Dulbecco's modified eagle medium was replaced with a phenol red-free Dulbecco's modified eagle medium equilibrated at 37°C. For mouse Sema6A and PlxnA2, we used the same stable COS-7 cell lines as we used for FRET-FLIM. The images were acquired by a Zeiss Elyra TIRF microscope equipped with a 100x oil objective (1.46 NA). mRuby2 was excited at 561 nm, and the images were acquired at a resolution of 512 × 512 pixels (image size 49.7 × 49.7 um). The average fluorescence intensity was calculated using ImageJ [72]. In particular, TIRF micrographs were background subtracted to get rid of the EM-CCD camera

noise. After this, each cell was profiled utilizing a mask that only contained the signal coming from each cell and non-attributed-numbers for the background. The average grey value per each profiled cell was obtained and plotted as a box plot for each condition.

Collapse assay of COS-7 cells

COS-7 cells grown on µ-Slides (chambered coverslips) with 8 wells (Ibidi) were transiently transfected with *Drosophila melanogaster* full length PlexA-mClover (residues 28-1945), wild-type Sema1b-mRuby2 (residues 37-686) or Sema1b-mutA-mRuby2 (residues 37-686) or Sema1b-mutB-mRuby2 (residues 37-686) or Sema1b-mutA+B-mRuby2 (residues 37-686). Two days post-transfection, the cells were washed with PBS and Dulbecco's modified eagle medium was replaced with a phenol red free Dulbecco's modified eagle medium equilibrated at 37°C.

Images were acquired using a Leica SP8-X-SMD confocal microscope (Leica Microsystems) with a 63×/1.40 numerical aperture oil immersion objective at 37°C. mClover and mRuby2 were excited at 488 and 561 nm, respectively, and the fluorescence emission was detected using two hybrid detectors in photon counting mode at 498-551 and 573-625 nm, respectively. Tiled positions (3×3) were scanned in 512×512 format every minute for 30 minutes. The pinhole was set at 3.0 Airy units, and an automatic adaptive autofocus was used to prevent z-drifting while imaging. After 2 minutes of imaging, a recombinant Sema1a-Fc was added to a final concentration of 5.8 µM. Cell surface area was calculated using ImageJ [72] before and after stimulation with recombinant Sema1a-Fc.

DRG cultures

Culture methods were as previously described [73]. In short, DRG neurons were dissected from E12.5 *Sema6A* knockout mouse embryos [74]. DRGs were collected in 1x Krebs medium (0.7% NaCl, 0.04% KCl, 0.02% KH_2PO_4, 0.2% $NaHCO_3$ and 0.25% glucose) and dissociated by incubation with 0.25% trypsin in Krebs/EDTA for 10 min at 37°C. The reaction was halted by adding 2 mg soybean trypsin inhibitor, followed by trituration with a fire-polished Pasteur pipette in Krebs medium containing soybean trypsin inhibitor and 20 µg/ml DNAseI. Dissociated cells were resuspended in neurobasal medium supplemented with B-27, L-glutamine, penicillin/streptomycin, ß-mercaptoethanol and nerve growth factor 2.5S (50 ng/ml, Alomone labs). Cells were plated onto poly-D-lysine (20 µg/ml) and laminin (10 µg/ml)

coated glass coverslips in 12 wells plates in a humidified incubator at 37°C and 5% CO_2. Cultures were fixed by adding equal volume of 8% PFA in PBS containing 30% sucrose for 10-30 min at room temperature.

Growth cone collapse assay

For growth cone collapse assays, DRG neurons were transfected at 1 day *in vitro* (DIV1) with Sema6A-WT-EGFP-pCAG, Sema6A-mutA-EGFP-pCAG, Sema6A-mutB-EGFP-pCAG or Sema6A-mutA+B-EGFP-pCAG mutant constructs or empty EGFP-pCAG vector using lipofectamine 2000 for 45 minutes at 37°C. At DIV4, vehicle (medium) or purified Sema6A-Fc was added to the cultures at a concentration of 1, 10 or 75 nM for 1 hour at 37°C. Cultures were fixed and processed for immunocytochemistry with anti-GFP antibodies and counterstained with phalloidin to visualize F-actin in filopodia and lamellipodia to determine growth cone morphology. The following antibodies were used in this experiment: Rabbit anti GFP (Thermo Fisher Scientific, catalog # A-11122), Donkey anti-Rabbit IgG (H+L) Alexa Fluor 488 (Thermo Fisher Scientific, catalog # A-21206) and Alexa Fluor 568 Phalloidin (Invitrogen, catalog # A-12380). Coverslips were mounted and scored for growth cone morphology using a scale from one to four (uncollapsed) and five to eight (fully collapsed) according to a matrix of growth cones with different morphologies, allowing the detection of even subtle changes in growth cone morphology [30,49]. Assigning each growth cone to its appropriate category was based on the following criteria: Categories 1-4 show uncollapsed growth cones, with category 1 showing multiple extending filopodia that are reduced in number in category 2. Category 3 and 4 growth cones both lack filopodia with category 4 growth cones additionally showing F-actin reduction. Categories 5-8 show collapsed growth cones, with growth cone size and shape reducing to no discernible growth cone at all in category 8. Images were acquired on an epifluorescence miscroscope (Zeiss Axioskop A1). A categorial analysis using Fisher's exact test was used to test for statistical significance of uncollapsed or fully collapsed growth cones for each mutant or control construct. Statistical tests were performed using IBM SPSS Statistics 23.

Animals

All animal use and care was in accordance with institutional guidelines and approved by the animal experimentation committee (DEC). The mouse strain was Sema6A (Sema6aGt[KST069]Byg) kept on a C57/B6J background. Timed-pregnant females were 3-6 months of age. Timed-pregnant mice were euthanized by means of cervical dislocation. The morning on which a vaginal plug was detected was considered embryonic day 0.5 (E0.5).

Data availability

Structure factors and coordinates have been deposited in the Protein Data Bank with identification numbers PDB: 6FKM and 6FKN.

Acknowledgements

We thank the staff of Diamond Light Source for support and access to beamlines I03 and I24; Weixian Lu for help with tissue culture; Thomas Walter for crystallization technical support; David Staunton for assistance with biophysical experiments. The work was funded by Cancer Research UK and Medical Research Council Programme Grants (to E.Y.J., C375/A17721 and MR/M000141/1) and the Netherlands Organization for Scientific Research (to R.J.P., ALW-VICI). The Wellcome Centre for Human Genetics is supported by Wellcome Trust Centre grant 203141/Z/16/Z. D.R. was supported by EMBO Long-Term Fellowship (ALTF 604-2014) and S. P. P. by the Nuffield Department of Medicine Leadership Fellowship.

Author Contributions

Conceptualization, D.R., R.J.P. and E.Y.J.; Methodology, D.R., R.A.R, L.A., S.P.-P. and E.Y.J.; Investigation, D.R., M.G.V, D.K., G.N., L.A. and K.H., Writing, D.R. and E.Y.J., Funding acquisition, D.R., S.P.-P., R.J.P. and E.Y.J; Supervision, S.P.-P., R.J.P. and E.Y.J.

Conflict of interests

The authors declare that they have no conflict of interest.

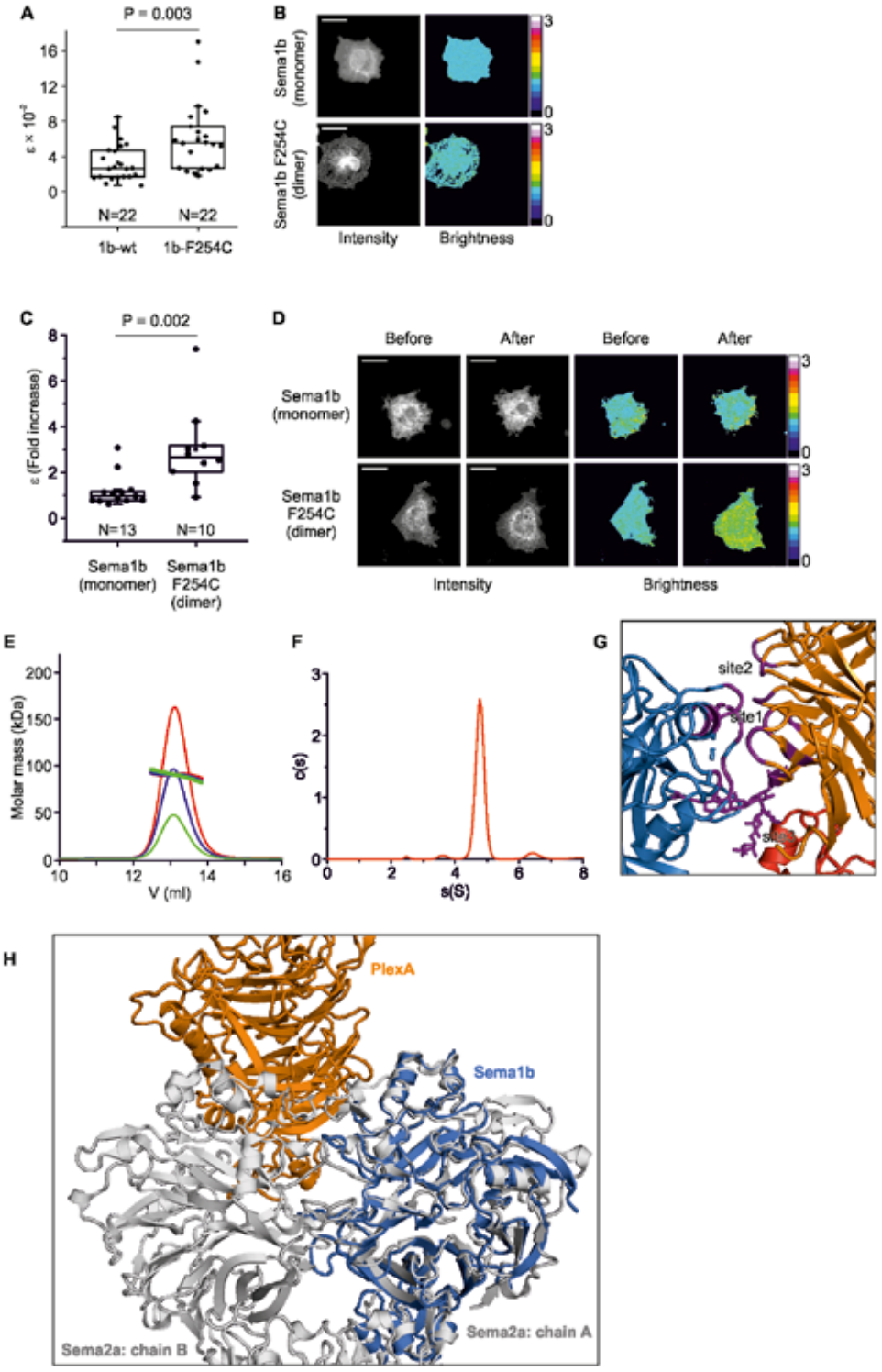
A
P = 0.003
ε × 10²
16
12
8
4
0
N=22
N=22
1b-wt
1b-F254C
B
Sema1b (monomer)
Sema1b F254C (dimer)
3
0
Intensity
Brightness
C
P = 0.002
ε (Fold increase)
8
6
4
2
0
N=13
N=10
Sema1b (monomer)
Sema1b F254C (dimer)
D
Before
After
Before
After
Sema1b (monomer)
Sema1b F254C (dimer)
Intensity
Brightness
E
Molar mass (kDa)
200
150
100
50
0
10
12
14
16
V (ml)
F
c(s)
3
2
1
0
0
2
4
6
8
s(S)
G
site2
site1
site3
H
PlexA
Sema1b
Sema2a: chain B
Sema2a: chain A

< Figure EV1. Sema1b is a monomer on the cell surface

A. Number and Brightness analysis was used to determine the molecular brightness (ε) of Sema1b-mClover or Sema1b-F254C-mClover in live COS-7 cells. Sema1b seems to be a monomer on the cell surface as the average ε value for Sema1b-mClover (ε_{av}=0.033) is half of the dimeric Sema1b-F254C-mClover (ε_{av}=0.061). The box limits indicate the 25th and 75th percentiles, centred lines show the median, squares represent sample means, whiskers extend 1.5-fold the interquartile range from the 25th and 75th percentiles, p-value was calculated by one-way analysis of variance (ANOVA). B. Representative images of COS-7 cells transiently expressing Sema1b-mClover or Sema1b-F254C-mClover in the Number and Brightness experiment. The average intensity images (first column from the left, grey color) are shown along with the brightness images (second column from the left, rainbow pseudocolor). Scale bar, 40 μm. C. Number and Brightness analysis shows that Sema1b$_{ecto}$ fails to dimerize PlexA-mClover on the cell surface of COS-7 cells contrary to the dimeric Sema1b$_{ecto}$-F254C. The PlexA-mClover construct contained the ectodomain followed by a transmembrane segment and the C-terminal fluorescent protein mClover. The box limits indicate the 25th and 75th percentiles, centred lines show the median, squares represent sample means, whiskers extend 1.5-fold the interquartile range from the 25th and 75th percentiles, p-value was calculated by one-way analysis of variance (ANOVA). D. Dimerization of PlexA analysed by Number and Brightness assay. Representative images of COS-7 cells transiently expressing PlexA-mClover before and after treatment with monomeric Sema1b$_{ecto}$ or dimeric Sema1b$_{ecto}$-F254C. The average intensity images (first and second column from the left, grey color) are shown along with the brightness images (third and fourth column from the left, rainbow pseudocolor). Scale bar, 40 μm. E. Size exclusion chromatography with multi-angle light scattering of PlexA$_{1-4}$ showing the molar mass and elution profiles at three initial PlexA$_{1-4}$ concentrations of 2.0 (red), 1.0 (blue) and 0.5 mg/ml (green). Experimental mass of 75 kDa indicates that PlexA$_{1-4}$ is a monomer.

F. Sedimentation coefficient distribution of PlexA$_{1-4}$ determined by sedimentation velocity analytical ultracentrifugation at a concentration of 33 μM. Calculated sedimentation coefficient (s_w(20,w)=5.0 S) corresponds to the predicted sedimentation coefficient for the monomer. G. Zoomed-in view of the side-on interface showing three main binding sites. Interacting residues are shown in purple. H. Superposition showing the side-on Sema1b-PlexA (blue-orange) interaction from the 2:2 complex overlayed onto the *Drosophila* Sema2a dimer (pdb 6qp7) structure (grey). The superposition is based on the Sema1b and Sema2a (chain A) sema domains. The clashes between PlexA and Sema2a (chain B) indicate that the side-on binding mode only becomes possible if a semaphorin is in the monomeric state, because the interaction site is otherwise occluded by the dimer interface.

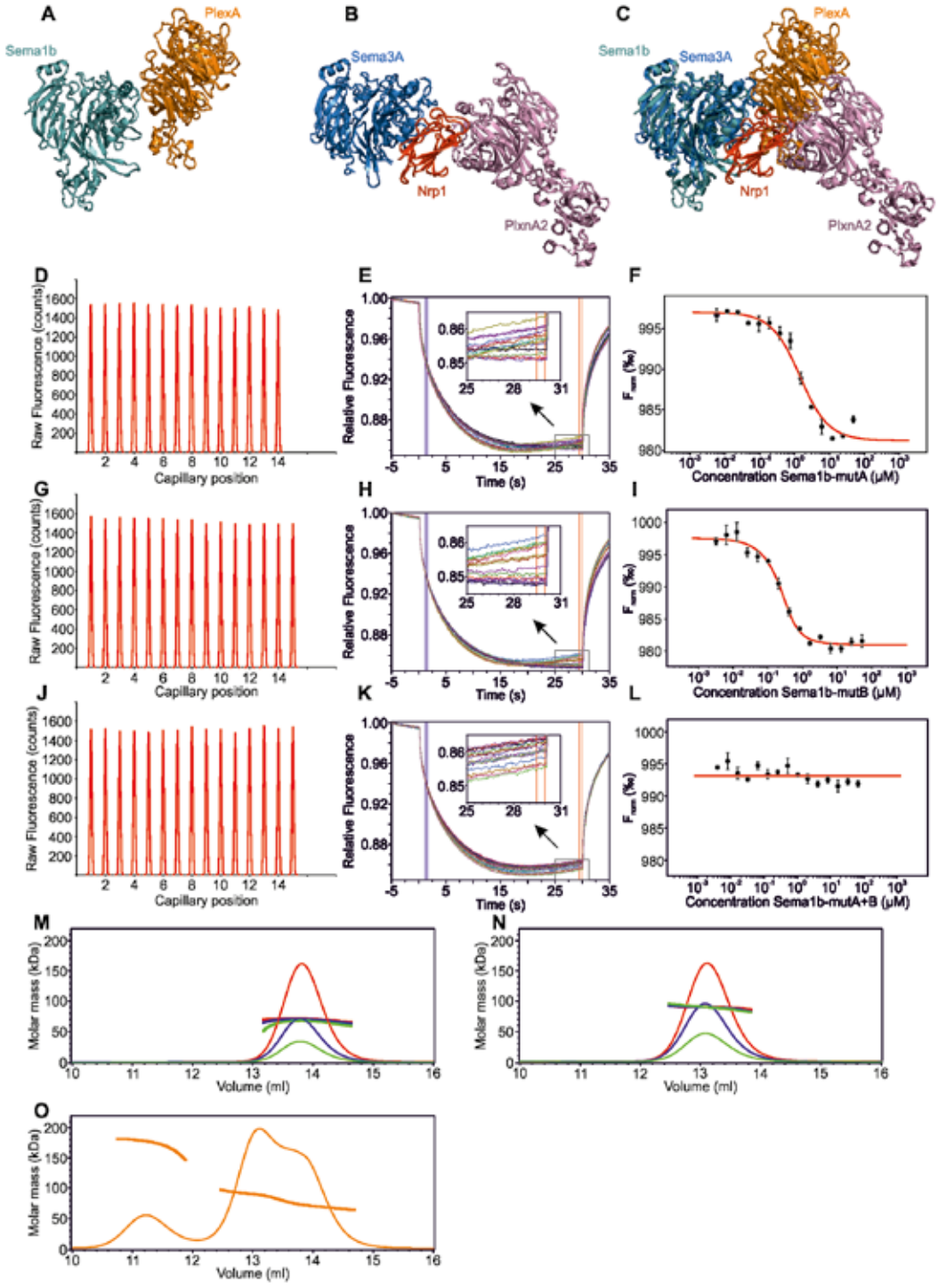
A
PlexA
Sema1b
B
Sema3A
Nrp1
PlxnA2
C
PlexA
Sema1b
Sema3A
Nrp1
PlxnA2
D
Raw Fluorescence (counts)
Capillary position
E
Relative Fluorescence
Time (s)
F
Concentration Sema1b-mutA (μM)
G
Raw Fluorescence (counts)
Capillary position
H
Relative Fluorescence
Time (s)
I
Concentration Sema1b-mutB (μM)
J
Raw Fluorescence (counts)
Capillary position
K
Relative Fluorescence
Time (s)
L
Concentration Sema1b-mutA+B (μM)
M
Molar mass (kDa)
Volume (ml)
N
Molar mass (kDa)
Volume (ml)
O
Molar mass (kDa)
Volume (ml)

< Figure EV2. Sema1b binds PlexA at two independent sites

A. Ribbon representation of the PlexA-Sema1b side-on orientation. B. The positioning of Nrp1, which is wedged between the sema domains of semaphorin and plexin, in the Sema3A-PlxnA2-Nrp1 ternary complex (pdb 4gza) in ribbon representation. C. Superposition of (A) and (B) on the basis of the sema domains of Sema1b and Sema3A. Superposition shows that the neuropilin binding site and the interaction site B in the side-on orientation are in very close proximity without any significant steric clashes. D-L. Microscale thermophoresis binding experiment for $PlexA_{1-4}$-mVenus and $Sema1b_{ecto}$-mutA (D-F) or $Sema1b_{ecto}$-mutB (G-I) or $Sema1b_{ecto}$-mutA+B (J-L). (D, G, J) Capillary scans of $PlexA_{1-4}$-mVenus in standard capillaries. (E, H, K) Fluorescence time traces recorded by MST instrument. The cold and hot regions used for fitting are shown by blue and red vertical lines, respectively. Close-up views of the hot regions are shown in the middle. (F, I, L) The binding curves of $Sema1b_{ecto}$ to $PlexA_{1-4}$-mVenus. Error bars represent s.d. of three technical replicates. M-O. Size exclusion chromatography with multi-angle light scattering of $Sema1b_{1-2}$ (M), $PlexA_{1-4}$ (N), and an equimolar mixture of $Sema1b_{1-2}$ and $PlexA_{1-4}$ (O). Panels (M) and (N) show the molar mass and elution profiles at three initial concentrations of 2.0 (red), 1.0 (blue) and 0.5 mg/ml (green). Experimental mass of 75 kDa for $PlexA_{1-4}$ and experimental mass of 60 kDa for $Sema1b_{1-2}$ indicate that both $PlexA_{1-4}$ and $Sema1b_{1-2}$ are monomers in solution. The sample containing the equimolar mixture of $Sema1b_{1-2}$ and $PlexA_{1-4}$ (O) revealed three peaks corresponding to unliganded $Sema1b_{1-2}$ and $PlexA_{1-4}$ and $Sema1b_{1-2}$ in complex with $PlexA_{1-4}$ with experimental mass of 131 kDa corresponding to 1:1 stoichiometry.

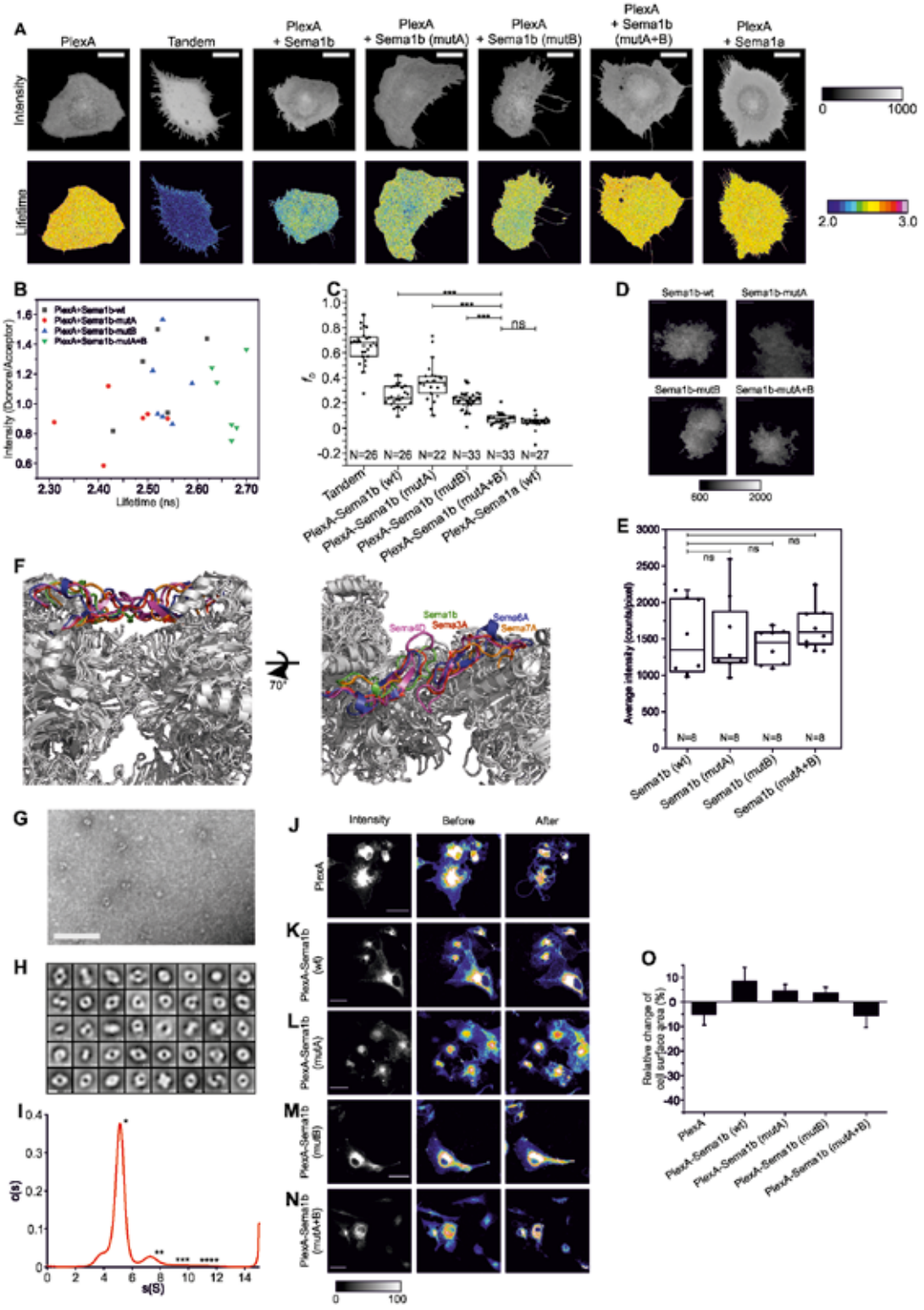
A
PlexA
Tandem
PlexA + Sema1b
PlexA + Sema1b (mutA)
PlexA + Sema1b (mutB)
PlexA + Sema1b (mutA+B)
PlexA + Sema1a
Intensity
Lifetime
0
1000
2.0
3.0
B
PlexA+Sema1b-wt
PlexA+Sema1b-mutA
PlexA+Sema1b-mutB
PlexA+Sema1b-mutA+B
Intensity (Donore/Acceptor)
Lifetime (ns)
C
fb
N=26 N=26 N=22 N=33 N=33 N=27
ns
Tandem
PlexA-Sema1b (wt)
PlexA-Sema1b (mutA)
PlexA-Sema1b (mutB)
PlexA-Sema1b (mutA+B)
PlexA-Sema1a (wt)
D
Sema1b-wt
Sema1b-mutA
Sema1b-mutB
Sema1b-mutA+B
600
2000
E
Average intensity (counts/pixel)
ns
N=8 N=8 N=8 N=8
Sema1b (wt)
Sema1b (mutA)
Sema1b (mutB)
Sema1b (mutA+B)
F
70°
Sema1b
Sema3A
Sema6A
Sema7A
Sema3F
G
H
I
c(s)
s(S)
J
Intensity
Before
After
PlexA
K
PlexA-Sema1b (wt)
L
PlexA-Sema1b (mutA)
M
PlexA-Sema1b (mutB)
N
PlexA-Sema1b (mutA+B)
0
100
O
Relative change of cell surface area (%)
PlexA
PlexA-Sema1b (wt)
PlexA-Sema1b (mutA)
PlexA-Sema1b (mutB)
PlexA-Sema1b (mutA+B)

< Figure EV3. Binding of Sema1b and PlexA in *cis* leads to opening of the PlexA ring-like conformation

A. Representative intensity and FLIM images of COS-7 cells transiently expressing FRET donor (PlexA-mClover), FRET acceptor (Sema1b-mRuby2 or Sema1a-mRuby2) or tandem mClover-mRuby2 .The FLIM images are pseudocolored. Scale bar, 20 μm. B. Calculated lifetimes are independent of donor/acceptor fluorescence intensity ratio as shown by the random distribution of the PlexA-mClover/Sema1b-mRuby2 intensity ratio against the average lifetime. The scatter chart was made from 23 randomly sampled cells. C. Distribution of the average fraction of the interacting donor (f_D) in the FRET-FLIM experiment. The boxcharts represent the average lifetime. Box limits indicate the 25th and 75th percentiles, centred lines show the median, squares represent sample means, whiskers extend 1.5-fold the interquartile range from the 25th and 75th percentiles, p-value calculated by one-way analysis of variance (ANOVA). ***P<0.001. D. Representative average fluorescence intensity images showing expression of Sema1b-wild-type-mClover, Sema1b-mutA-mClover, Sema1b-mutB-mClover or Sema1b-mutA+B-mClover on the cell surface of live COS7 cells. Scale bar, 10 μm. E. Distribution of the average fluorescence intensity of Sema1b and all three mutants on the cell surface of live COS-7 cells. The images were collected from two independent experiments. The box limits indicate the 25th and 75th percentiles, centred lines show the median, squares represent sample means, whiskers extend 1.5-fold the interquartile range from the 25th and 75th percentiles, p-value was calculated by t-test, ns: P>0.05. F. Structural superposition of Sema1b, Sema3A (4gz8), Sema6A (3okw), Sema4D (1olz) and Sema7A (3nvq) indicating the αEx1-αEx2 loop in Sema1b or corresponding loop in the other semaphorins. The loop is involved in the semaphorin homodimerization in Sema3A, Sema4D and Sema6A but not in Sema7A and A39R (not shown). However, in monomeric Sema1b, the loop is accessible for engagement with PlexA through the interaction site B. G. Representative negative stain electron micrograph of $PlexA_{ecto}$ particles. Scale bar, 100 nm. H. Negative stain 2D class averages of $PlexA_{ecto}$ obtained by classifying 12164 particles into 50 classes. The number of particles within each class is listed in the bottom right corner. Scale bar, 10 nm. I. Sedimentation coefficient distribution of $PlexA_{ecto}$ determined by sedimentation velocity analytical ultracentrifugation at a concentration of 2.2 μM. The predicted sedimentation coefficients of different oligomeric states that best correspond to the peak values are indicated by asterisk. J-N. COS-7 cells collapse assay showing representative images of collapsed and non-collapsed cells (second and third column from the left, pseudocolor) and average intensity images of non-collapsed cells (first column from the left, grey color). COS-7 cells transiently expressing $PlexA_{FL}$-mClover (J) or co-expressing $PlexA_{FL}$-mClover with Sema1b wild type (K) or Sema1b mutants (L,M,N) were treated with purified Sema1a-Fc at a final concetration of 5.8 μM. Images were acquired every minute for 30 minutes. Cell surface area was calculated using ImageJ before and after stimulation. Scale bar, 30 μm. O. Relative change of COS-7 cells surface area upon treatment with vehicle only. Cells expressing $PlexA_{FL}$-mClover or $PlexA_{FL}$-mCover and Sema1b-mRuby2 wild-type or mutants were treated with vehicle only (medium without semaphorin). Images were acquired every minute for 30 minutes. Cell surface area was calculated using ImageJ before and after stimulation. Data are presented as means ± sem. The images were collected from two independent experiments.

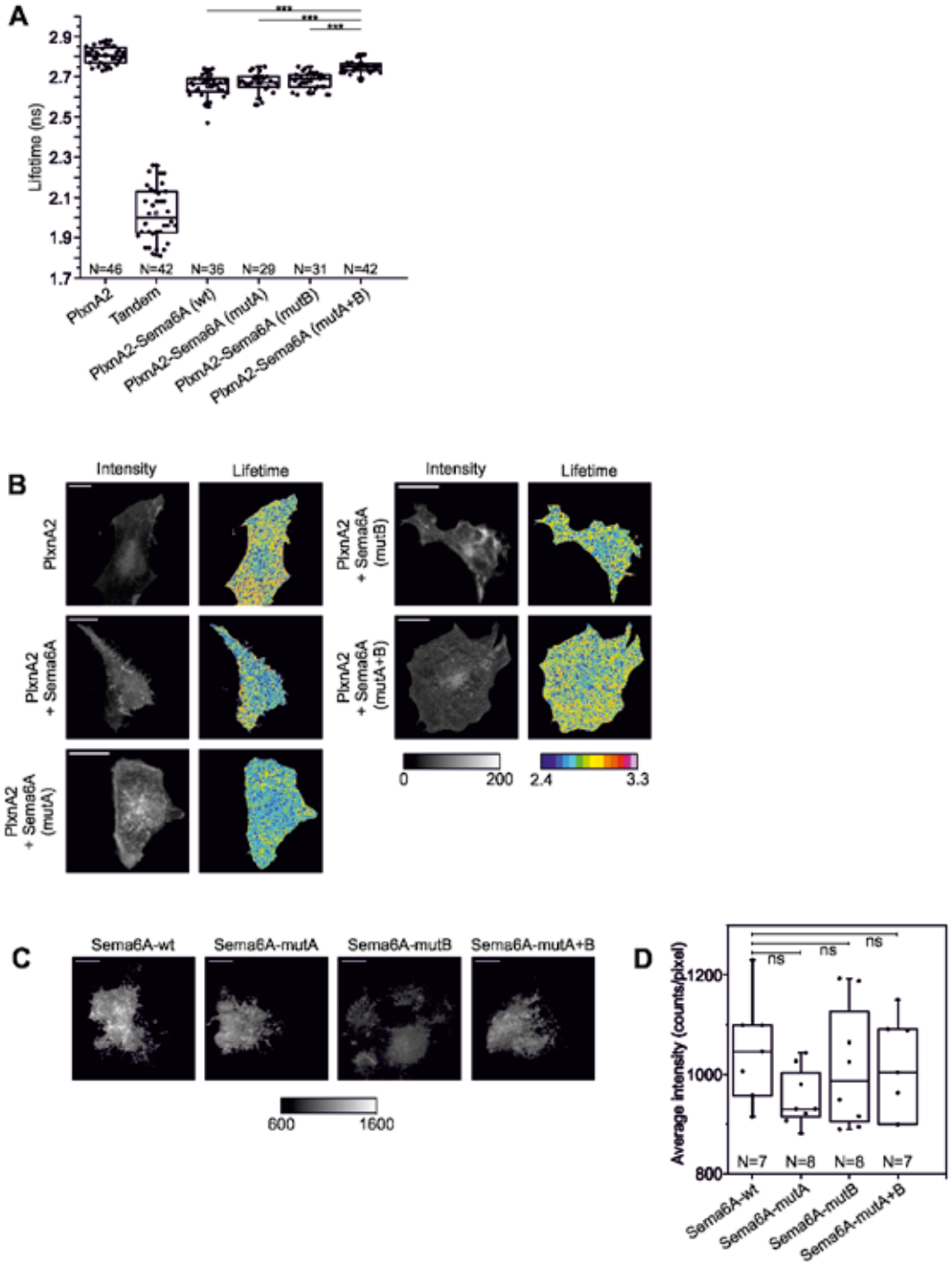
A
Lifetime (ns)
2.9
2.7
2.5
2.3
2.1
1.9
1.7
***
***
***
N=46
N=42
N=36
N=29
N=31
N=42
PlxnA2
Tandem
PlxnA2-Sema6A (wt)
PlxnA2-Sema6A (mutA)
PlxnA2-Sema6A (mutB)
PlxnA2-Sema6A (mutA+B)
B
Intensity
Lifetime
PlxnA2
PlxnA2 + Sema6A
PlxnA2 + Sema6A (mutA)
PlxnA2 + Sema6A (mutB)
PlxnA2 + Sema6A (mutA+B)
0
200
2.4
3.3
C
Sema6A-wt
Sema6A-mutA
Sema6A-mutB
Sema6A-mutA+B
600
1600
D
Average intensity (counts/pixel)
1200
1000
800
ns
ns
ns
N=7
N=8
N=8
N=7
Sema6A-wt
Sema6A-mutA
Sema6A-mutB
Sema6A-mutA+B

< Figure EV4. Mouse Sema6A utilises the same head-to-head and side-on binding modes to interact with PlxnA2 in *cis* as that observed for *Drosophila* Sema1b.

A. FRET-FLIM in live COS-7 cells shows cell surface Sema6A-PlxnA2 *cis* interaction. Sema6A mutants reveal that both head-to-head and side-on orientations are involved in the *cis* interaction. The boxcharts represent the average lifetime. Box limits indicate the 25th and 75th percentiles, centred lines show the median, squares represent sample means, whiskers extend 1.5-fold the interquartile range from the 25th and 75th percentiles. ***P<0.001, p-value calculated by one-way analysis of variance (ANOVA). B. Representative time correlated single photon counting intensity (first column from the left) and FLIM images (second column from the left) of COS-7 cells transiently expressing FRET donor (PlxnA2-mClover), FRET acceptor (Sema1b-mRuby2 or Sema1a-mRuby2) or tandem mClover-mRuby2. The FLIM images are pseudocolored. Scale bar, 20 μm. C. Representative average fluorescence intensity images showing co-expression of PlxnA2 with Sema6A-wild-type-mClover, Sema6A-mutA-mClover, Sema6A-mutB-mClover or Sema6A-mutA+B-mClover on the cell surface of live COS7 cells. Scale bar, 10 μm. D. Distribution of the average fluorescence intensity of Sema6A and all three mutants on the cell surface of live COS-7 cells. The images were collected from two independent experiments. The box limits indicate the 25th and 75th percentiles, centered lines show the median, squares represent sample means, whiskers extend 1.5-fold the interquartile range from the 25th and 75th percentiles, p-value was calculated by t-test, ns: P>0.05.

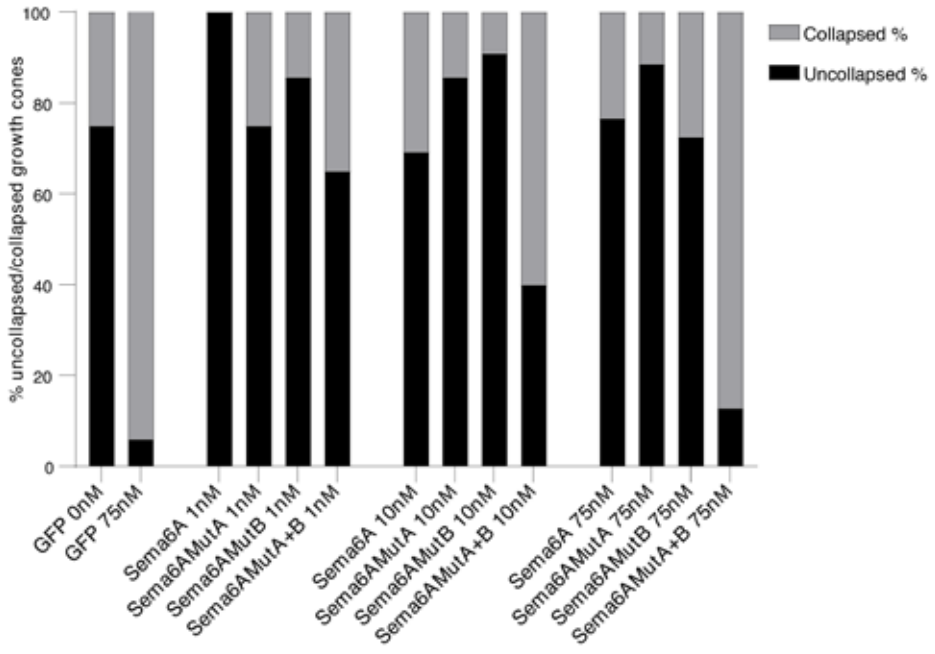

Figure EV5. DRG neurons transfected with Sema6A-mutA+B show growth cone collapse with increasing Sema6A-Fc concentrations.

Growth cone collapse responses for DRG neurons from E12.5 *Sema6A* KO embryos transfected with EGFP-pCAG (GFP), Sema6A-WT-EGFP-pCAG (Sema6A), Sema6A-mutA-EGFP-pCAG Sema6AMutA), Sema6A-mutB-EGFP-pCAG (Sema6AMutB) or Sema6A-mutA+B-EGFP-pCAG (Sema6AMutA+B) constructs after stimulation with different Sema6A-Fc protein concentrations (1, 10 or 75 nM) (see also Figure 3 for a more extensive analysis at 75 nM). DRG neurons transfected with EGFP-pCAG displayed robust collapse following treatment with 75 nM Sema6A-Fc, as compared to control (0 nM). Transfection of Sema6A-WT-EGFP-pCAG, Sema6A-mutA-EGFP-pCAG, or Sema6A-mutB-EGFP-pCAG inhibited Sema6A-Fc-induced growth cone collapse. In contrast, DRG neurons transfected with Sema6A-mutA+B-EGFP-pCAG acquired collapse sensitivity with increasing ligand concentrations. Growth cone collapse was assessed using the growth cone matrix shown in Figure 3 (category 1-4; uncollapsed, category 5-8; collapsed). 4-10 growth cones were analysed per condition per experiment in 2-3 independent experiments.

REFERENCES

1. Kolodkin, A. L. *et al.* Fasciclin IV: Sequence, expression, and function during growth cone guidance in the grasshopper embryo. *Neuron* (1992). doi:10.1016/0896-6273(92)90237-8
2. Kolodkin, A. L., Matthes, D. J. & Goodman, C. S. The semaphorin genes encode a family of transmembrane and secreted growth cone guidance molecules. *Cell* (1993). doi:10.1016/0092-8674(93)90625-Z
3. Luo, Y., Raible, D. & Raper, J. A. Collapsin: A protein in brain that induces the collapse and paralysis of neuronal growth cones. *Cell* 75, 217–227 (1993).
4. Tamagnone, L. *et al.* Plexins Are a Large Family of Receptors for Transmembrane, Secreted, and GPI-Anchored Semaphorins in Vertebrates. *Cell* 99, 71–80 (1999).
5. Pasterkamp, R. J. Getting neural circuits into shape with semaphorins. 13, 605–618 (2012).
6. Tran, T. S., Kolodkin, A. L. & Bharadwaj, R. Semaphorin Regulation of Cellular Morphology. *Annu. Dev.Biol.* (2007).
7. Takamatsu, H. & Kumanogoh, A. Diverse roles for semaphorin-plexin signaling in the immune system. *Trends in Immunology* (2012). doi:10.1016/j.it.2012.01.008
8. Tamagnone, L. Emerging Role of Semaphorins as Major Regulatory Signals and Potential Therapeutic Targets in Cancer. *Cancer Cell* (2012). doi:10.1016/j.ccr.2012.06.031
9. Seiradake, E., Jones, E. Y. & Klein, R. Structural Perspectives on Axon Guidance. *Annu. Rev. Cell Dev. Biol.* 32, 577–608 (2016).
10. Renaud, J. *et al.* Plexin-A2 and its ligand, Sema6A, control nucleus-centrosome coupling in migrating granule cells. *Nat. Neurosci.* 11, 440–449 (2008).
11. Suto, F. *et al.* Interactions between Plexin-A2, Plexin-A4, and Semaphorin 6A Control Lamina-Restricted Projection of Hippocampal Mossy Fibers. *Neuron* (2007). doi:10.1016/j.neuron.2007.01.028
12. Tawarayama, H., Yoshida, Y., Suto, F., Mitchell, K. J. & Fujisawa, H. Roles of Semaphorin-6B and Plexin-A2 in Lamina-Restricted Projection of Hippocampal Mossy Fibers. *J. Neurosci.* 30, 7049–7060 (2010).
13. Haklai-topper, L., Mlechkovich, G., Savariego, D., Gokhman, I. & Yaron, A. Cis interaction between Semaphorin6A and Plexin-A4 modulates the repulsive response to Sema6A. *EMBO J.* 29, 2635–2645 (2010).
14. Andermatt, I. *et al.* Semaphorin 6B acts as a receptor in post-crossing commissural axon guidance. *Development* 141, 3709–3720 (2014).
15. Mizumoto, K. & Shen, K. Interaxonal Interaction Defines Tiled Presynaptic Innervation in C. elegans. *Neuron* (2013). doi:10.1016/j.neuron.2012.12.031

16. Duan, Y. *et al.* Semaphorin 5A inhibits synaptogenesis in early postnatal- and adult-born hippocampal dentate granule cells. *Elife* (2014). doi:10.7554/eLife.04390
17. Perez-Branguli, F. *et al.* Reverse Signaling by Semaphorin-6A Regulates Cellular Aggregation and Neuronal Morphology. *PLoS One* 11, e0158686 (2016).
18. Antipenko, A. et al. Structure of the Semaphorin-3A Receptor Binding Module. Neuron 39, 589–598 (2003).
19. Love, C. A. et al. The ligand-binding face of the semaphorins revealed by the high-resolution crystal structure of SEMA4D. Nat. Struct. Mol. Biol. 10, 843–848 (2003).
20. Klostermann, A., Lohrum, M., Adams, R. H. & Püschel, A. W. The chemorepulsive activity of the axonal guidance signal semaphorin D requires dimerization. *J. Biol. Chem.* (1998). doi:10.1074/jbc.273.13.7326
21. Koppel, A. M. & Raper, J. A. Collapsin-1 covalently dimerizes, and dimerization is necessary for collapsing activity. *J. Biol. Chem.* (1998). doi:10.1074/jbc.273.25.15708
22. Rozbesky, D. et al. Diversity of oligomerization in Drosophila semaphorins suggests a mechanism of functional fine-tuning. Nat. Commun. 10, 3691 (2019).
23. Bork, P., Doerks, T., Springer, T. A. & Snel, B. Domains in plexins: Links to integrins and transcription factors. *Trends Biochem. Sci.* (1999). doi:10.1016/S0968-0004(99)01416-4
24. Bamberg, J. A. *et al.* Unified nomenclature for the semaphorins/collapsins [1]. *Cell* (1999). doi:10.1016/S0092-8674(00)80766-7
25. Bell, C. H., Aricescu, A. R., Jones, E. Y. & Siebold, C. A Dual Binding Mode for RhoGTPases in Plexin Signalling. PLoS Biol. 9, e1001134 (2011).
26. He, H., Yang, T., Terman, J. R. & Zhang, X. Crystal structure of the plexin A3 intracellular region reveals an autoinhibited conformation through active site sequestration. Proc. Natl. Acad. Sci. 106, 15610–15615 (2009).
27. Wang, Y., Pascoe, H. G., Brautigam, C. A., He, H. & Zhang, X. Structural basis for activation and non-canonical catalysis of the Rap GTPase activating protein domain of plexin. *Elife* (2013). doi:10.7554/eLife.01279.001
28. Tong, Y. et al. Structure and Function of the Intracellular Region of the Plexin-B1 Transmembrane Receptor. J. Biol. Chem. 284, 35962–35972 (2009).
29. Wang, Y. *et al.* Plexins are GTPase-activating proteins for Rap and are activated by induced dimerization. *Sci. Signal.* (2012). doi:10.1126/scisignal.2002636
30. Kong, Y. et al. Structural Basis for Plexin Activation and Regulation. Neuron 91, 548–60 (2016).
31. Marita, M. *et al.* Class A Plexins Are Organized as Preformed Inactive Dimers on the Cell Surface. *Biophys. J.* (2015). doi:10.1016/j.bpj.2015.04.043

32. Janssen, B. J. C. et al. Structural basis of semaphorin–plexin signalling. Nature 467, 1118–1122 (2010).
33. Liu, H. et al. Structural Basis of Semaphorin-Plexin Recognition and Viral Mimicry from Sema7A and A39R Complexes with PlexinC1. Cell 142, 749–761 (2010).
34. Nogi, T. et al. Structural basis for semaphorin signalling through the plexin receptor. Nature 467, 1123–1127 (2010).
35. Lam, A. J. *et al.* Improving FRET dynamic range with bright green and red fluorescent proteins. *Nat. Methods* (2012). doi:10.1038/nmeth.2171
36. Digman, M. A., Dalal, R., Horwitz, A. F. & Gratton, E. Mapping the number of molecules and brightness in the laser scanning microscope. *Biophys. J.* (2008). doi:10.1529/biophysj.107.114645
37. Iliopoulou, M. *et al.* A dynamic three-step mechanism drives the HIV-1 pre-fusion reaction. *Nat. Struct. Mol. Biol.* (2018). doi:10.1038/s41594-018-0113-x
38. Nolan, R., Alvarez, L. & Padilla-Parra, S. Detrending: How to Correct Images for Bleaching. Biophys. J. 114, 345a (2018).
39. Nolan, R. *et al.* nandb-number and brightness in R with a novel automatic detrending algorithm. *Bioinformatics* (2017). doi:10.1093/bioinformatics/btx434
40. Nolan, R. *et al.* Calibration-free In Vitro Quantification of Protein Homo-oligomerization Using Commercial Instrumentation and Free, Open Source Brightness Analysis Software. *J. Vis. Exp.* (2018). doi:10.3791/58157
41. Janssen, B. J. C. et al. Neuropilins lock secreted semaphorins onto plexins in a ternary signaling complex. Nat. Struct. Mol. Biol. 19, 1293–1299 (2012).
42. Siebold, C. & Jones, E. Y. Structural insights into semaphorins and their receptors. *Seminars in Cell and Developmental Biology* (2013). doi:10.1016/j.semcdb.2012.11.003
43. Padilla-Parra, S., Audugé, N., Coppey-Moisan, M. & Tramier, M. Quantitative FRET analysis by fast acquisition time domain FLIM at high spatial resolution in living cells. *Biophys. J.* (2008). doi:10.1529/biophysj.108.131276
44. Padilla-Parra, S. & Tramier, M. FRET microscopy in the living cell: Different approaches, strengths and weaknesses. *BioEssays* (2012). doi:10.1002/bies.201100086
45. Winberg, M. L. *et al.* Plexin A is a neuronal semaphorin receptor that controls axon guidance. *Cell* (1998). doi:10.1016/S0092-8674(00)81715-8
46. Suzuki, K. *et al.* Structure of the plexin ectodomain bound by semaphorin-mimicking antibodies. *PLoS One* (2016). doi:10.1371/journal.pone.0156719
47. Turner, L. J. & Hall, A. Plexin-induced collapse assay in COS cells. *Methods in Enzymology* (2006). doi:10.1016/S0076-6879(06)06052-6
48. Suto, F. *et al.* Plexin-A4 mediates axon-repulsive activities of both secreted and transmembrane semaphorins and plays roles in nerve fiber guidance. *J. Neurosci.* (2005). doi:10.1523/JNEUROSCI.4480-04.2005

49. Van Erp, S. *et al.* Lrig2 Negatively Regulates Ectodomain Shedding of Axon Guidance Receptors by ADAM Proteases. *Dev. Cell* (2015). doi:10.1016/j.devcel.2015.11.008
50. Held, W. & Mariuzza, R. A. Cis interactions of immunoreceptors with MHC and non-MHC ligands. *Nature Reviews Immunology* (2008). doi:10.1038/nri2278
51. Yaron, A. & Sprinzak, D. The cis side of juxtacrine signaling: a new role in the development of the nervous system. Trends Neurosci. 35, 230–239 (2012).
52. Sun, L. O. et al. On and Off Retinal Circuit Assembly by Divergent Molecular Mechanisms. Science (80-.). 342, 1241974–1241974 (2013).
53. Jones, E. Y. Understanding cell signalling systems: paving the way for new therapies. Philos. Trans. A. Math. Phys. Eng. Sci. 373, (2015).
54. Aricescu, A. R., Lu, W. & Jones, E. Y. A time- and cost-efficient system for high-level protein production in mammalian cells. *Acta Crystallogr. Sect. D Biol. Crystallogr.* (2006). doi:10.1107/S0907444906029799
55. Chang, V. T. *et al.* Glycoprotein Structural Genomics: Solving the Glycosylation Problem. *Structure* (2007). doi:10.1016/j.str.2007.01.011
56. Walter, T. S. *et al.* A procedure for setting up high-throughput nanolitre crystallization experiments. Crystallization workflow for initial screening, automated storage, imaging and optimization. in *Acta Crystallographica Section D: Biological Crystallography* (2005). doi:10.1107/S0907444905007808
57. Winter, G. Xia2: An expert system for macromolecular crystallography data reduction. *J. Appl. Crystallogr.* (2010). doi:10.1107/S0021889809045701
58. Dimaio, F. *et al.* Improved low-resolution crystallographic refinement with Phenix and Rosetta. *Nat. Methods* (2013). doi:10.1038/nmeth.2648
59. Davis, I. W. *et al.* MolProbity: All-atom contacts and structure validation for proteins and nucleic acids. *Nucleic Acids Res.* (2007). doi:10.1093/nar/gkm216
60. Krissinel, E. & Henrick, K. Inference of Macromolecular Assemblies from Crystalline State. *J. Mol. Biol.* (2007). doi:10.1016/j.jmb.2007.05.022
61. Sievers, F. *et al.* Fast, scalable generation of high-quality protein multiple sequence alignments using Clustal Omega. *Mol. Syst. Biol.* (2011). doi:10.1038/msb.2011.75
62. Baker, N. A., Sept, D., Joseph, S., Holst, M. J. & McCammon, J. A. Electrostatics of nanosystems: Application to microtubules and the ribosome. *Proc. Natl. Acad. Sci. U. S. A.* (2001). doi:10.1073/pnas.181342398
63. Gouet, P., Courcelle, E., Stuart, D. I. & Métoz, F. ESPript: Analysis of multiple sequence alignments in PostScript. *Bioinformatics* (1999). doi:10.1093/bioinformatics/15.4.305
64. Schuck, P. Size-distribution analysis of macromolecules by sedimentation velocity ultracentrifugation and Lamm equation modeling. *Biophys. J.* (2000). doi:10.1016/S0006-3495(00)76713-0

65. Ortega, A., Amorós, D. & García De La Torre, J. Prediction of hydrodynamic and other solution properties of rigid proteins from atomic- and residue-level models. *Biophys. J.* (2011). doi:10.1016/j.bpj.2011.06.046
66. Booth, D. S., Avila-Sakar, A. & Cheng, Y. Visualizing proteins and macromolecular complexes by negative stain EM: from grid preparation to image acquisition. *J. Vis. Exp.* (2011). doi:10.3791/3227
67. Tang, G. *et al.* EMAN2: An extensible image processing suite for electron microscopy. *J. Struct. Biol.* (2007). doi:10.1016/j.jsb.2006.05.009
68. van Heel, M. & Keegstra, W. IMAGIC: A fast, flexible and friendly image analysis software system. *Ultramicroscopy* (1981). doi:10.1016/0304-3991(81)90001-2
69. Elegheert, J. *et al.* Lentiviral transduction of mammalian cells for fast, scalable and high-level production of soluble and membrane proteins. *Nat. Protoc.* (2018). doi:10.1038/s41596-018-0075-9
70. Padilla-Parra, S. *et al.* Quantitative comparison of different fluorescent protein couples for fast FRET-FLIM acquisition. *Biophys. J.* (2009). doi:10.1016/j.bpj.2009.07.044
71. Lam, A. J. *et al.* Improving FRET Dynamic Range with Bright Green and Red Fluorescent Proteins. *Biophys. J.* (2013). doi:10.1016/j.bpj.2012.11.3773
72. Schindelin, J. *et al.* Fiji: An open-source platform for biological-image analysis. *Nature Methods* (2012). doi:10.1038/nmeth.2019
73. Van Battum, E. Y. *et al.* The intracellular redox protein MICAL-1 regulates the development of hippocampal mossy fibre connections. *Nat. Commun.* (2014). doi:10.1038/ncomms5317
74. Lilley, B. N. *et al.* Genetic access to neurons in the accessory optic system reveals a role for Sema6A in midbrain circuitry mediating motion perception. *J. Comp. Neurol.* (2019). doi:10.1002/cne.24507

CHAPTER 6

The role of *SEMA6A* in the GnRH neuronal system controlling puberty onset as revealed by *in vivo, in silico* and *in vitro* studies

Lettieri A.[1,*], Verhagen M.G.[2,*], Oleari R.[1,*], Tacconi C.[2], Paganoni A.[1], Azzarelli R.[3], Andre' V.[1], Demartini L.[1], Parravicini C.[1], Eberini I.[1], Dunkel L.[4], Fantin. A.[5], Howard S.[4], Pasterkamp R. J.[2,§] and Cariboni A.[1,§]

[1] University of Milan, Department of Pharmacological and Biomolecular Sciences, Via Balzaretti 9, 20133 Milan, Italy

[2] Department of Translational Neuroscience, UMC Utrecht Brain Center, University Medical Center Utrecht, Utrecht University, 3584 CG Utrecht, The Netherlands

*equal contribution

§ Correspondence: anna.cariboni@unimi.it / r.j.pasterkamp@umcutrecht.nl

R.J.P. and A.C. are co-last authors

ABSTRACT

Puberty is the maturational process of the reproductive endocrine system that results in the achievement of adult height and body proportion, in addition to development of the genital organs and the capacity to reproduce. Puberty onset is driven by the pulsatile release of GnRH by the hypothalamic GnRH-secreting neurons, that project to the median eminence where they secrete the decapeptide GnRH into the pituitary portal vessels. Defects in GnRH secretion result in low levels of gonadotropins, and consequently in transient delayed puberty or permanent hypothalamic-pituitary-gonadal axis failure. In this study, we investigated with next generation sequencing a large cohort of patients with extreme pubertal delay for pathogenic variants in genes of the semaphorin family. A mutation in the *Sema6A* gene was found that substitutes a hydrophobic residue (Isoleucine) with a charged threonine residue. This mutation is predicted to be damaging and disease causing *in silico*. *In vitro* experiments demonstrated a loss of function effect of the mutation on the production and localization of the protein; the mutated form is unable to reach the cell membrane and remains in the cytoplasm with a perinuclear position. Expression analysis in mice confirms the involvement of *Sema6A* in the GnRH system. In conclusion, we study the impact of the novel identified mutation of *SEMA6A* on protein structure, stability and function, by applying *in silico*, *in vitro* and *in vivo* models, and found a physiological role for SEMA6A in GnRH neuron development and puberty onset.

INTRODUCTION

Mammalian fertility is completely dependent upon a small number of scattered hypothalamic neurons that secrete gonadotropin-releasing hormone (GnRH), which directs the synthesis and secretion of gonadotropins (LH and FSH) in the pituitary. In turn, gonadotropins stimulate the gonads to produce and release sex steroids, which control gametogenesis and therefore reproduction in both sexes [1]. GnRH neuron development has been extensively studied in mouse where GnRH neurons are first detected in the nasal placode at embryonic day (E) 10.5 and then migrate in association with peripherin (PRPH)-positive axons of the terminal nerve (TN) and surrounded by olfactory ensheathing cells (OECs) to reach the forebrain (FB) [2–4]. Several molecules have been found to play crucial roles in the development of GnRH neurons, acting to control directly GnRH neuron migration or survival, or indirectly to control nasal axon patterning [5]. Around birth (E18.5-P0), GnRH neurons have reached their final position in the medial preoptic area (MPOA) in the hypothalamus, where in adulthood most of their cell bodies are found. At this stage, their projections towards the median eminence (ME) and the pituitary portal system of blood vessels, where GnRH is secreted, are also already established [6]. GnRH secretion is finely controlled by the action of several factors produced either centrally by other hypothalamic and extrahypothalamic neurons (e.g. Kiss1, Npy, Crh) [7] or deriving from peripheral tissues (e.g. leptin, Igf1, Ffgf21) [8–10]. Further, GnRH secretion can be modulated indirectly by molecules that act on ME plasticity, by remodelling the permeability of hypophyseal portal system through tanycytes (SEMA3A) or by controlling GnRH terminal extension (SEMA7A) [11,12]. Mutations in genes that control GnRH neuron development and/or function are thought to be the causes of a wide range of genetic disorders such as Delayed Puberty (DP), Hypogonadotropic Hypogonadism (HH) and Kallmann Syndrome (KS), characterized by reduced or absent levels of GnRH with consequent delayed or absent puberty [13–16].

Recent studies have highlighted the importance of semaphorins and their receptors/co-receptors in the GnRH neuronal system, where they control nasal axon patterning, GnRH neuron migration or survival, during development, as well as GnRH neuron plasticity, in adulthood [17,18]. SEMA6A is a transmembrane semaphorin which acts by binding to its canonical receptors PLXNA2 and PLXNA4 [19–22]. Interestingly, SEMA6A expression is reported in the olfactory system and hypothalamic regions of mouse embryo [23–25], but its function in the GnRH neuronal system that controls

fertility is not known. SEMA6A can act as ligand and as a receptor through a reverse signaling, to control several biological processes including cytoskeleton remodelling [26], cell survival [27], cell proliferation [28] and migration [25,29,30]. During development, SEMA6A is known mainly for its roles in axonal patterning [21,31] and neuronal positioning in the brain [19,32] but also in angiogenesis, by modulating VEGF signaling [33]. We aimed to investigate the role of SEMA6A in the GnRH neuroendocrine network and human pubertal development, by characterization through *in silico*, *in vivo*, and *in vitro* analysis and identification of deleterious genetic semaphorin variants in patients with delayed pubertal onset.

RESULTS

SEMA6A is expressed during GnRH neuron development

To study the physiological role of SEMA6A in the GnRH neuron system, we used mouse tissue to analyse SEMA6A expression in tissues and stages relevant to the GnRH neuron development, by *in situ* hybridization (ISH) and immunohistochemistry (IHC). First, we looked at the expression of *Sema6a* by ISH using a previously validated probe [21] on coronal sections of mouse heads at E12.5 and E14.5 which represent time-points for the start and peak of GnRH neuron migration (Suppl. Fig. 1). We found that *Sema6a* is expressed in the olfactory epithelium (OE), where olfactory neurons reside, in the vomeronasal organ (VNO), where GnRH neurons and the terminal nerve (TN) originate from, as well as in the nasal mesenchyme and in the external layer of the olfactory bulbs (OBs), at E12.5 (Suppl. Fig. 1A) and at E14.5 (Suppl. Fig. 1B). We also detected *Sema6a* expression in the forebrain (FB) at both E12.5 and E14.5, consistent with previous reports [21,34]. These results suggest a possible role of SEMA6A in the development of the GnRH system. To characterize the cell types expressing SEMA6A, we performed double immunofluorescent staining using antibodies against SEMA6A (AF1615, [33]) and specific markers for GnRH neurons, olfactory/terminal nerves and OECs on coronal sections from mouse heads at E12.5 and E14.5. As shown in Figure 1 and consistent with the ISH pattern, we detected SEMA6A expression at E12.5 in the OE, VNO and nasal mesenchyme (Fig. 1A-A', solid arrowheads in A'). Specifically, we found that SEMA6A is expressed by neurons in the VNO and axons emerging from the VNO (Fig. 1B-B', solid arrowheads in B') as well as by nasal axons targeting the OB (solid arrowhead in Fig. 1B), stained for the immature neuronal marker beta-3 tubulin (nTUBB3), at E12.5. Double labeling for SEMA6A

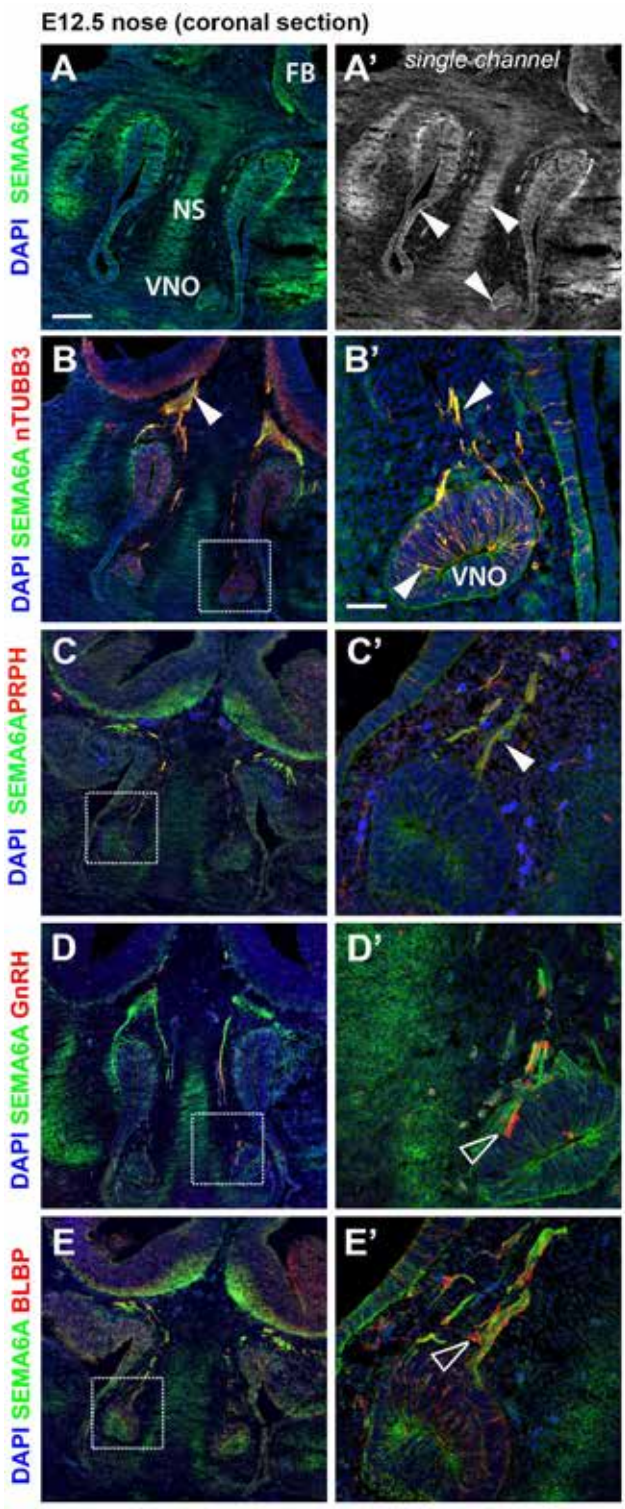

Figure 1. SEMA6A is expressed in the developing nose by neuronal cell bodies and nasal axons

(A-E) Coronal sections of E12.5 mouse heads were immunolabelled for SEMA6A (A) together with nTUBB3 (B), PRPH (C), GnRH (D) or BLBP (E). Sections are shown at the level of the developing nose and white boxes indicate VNO areas shown at higher magnification on the right of the corresponding panel (B'-E'); SEMA6A single channel is shown in panel A'. Solid arrowheads in A' indicate SEMA6A-expressing cells. Solid arrowheads in B'-C' indicate examples of nTUBB3- and PRPH-positive axons with SEMA6A, respectively. Empty arrowheads in D'-E' indicate examples of GnRH neurons and OECs that lack SEMA6A expression. All sections were counterstained with DAPI. VNO, vomeronasal organ; NS, nasal septum; FB, forebrain. Scale bars: 250 or 50 µm for lower and higher magnifications, respectively.

and peripherin (PRPH), a specific marker of the TN nerve, confirmed co-localisation of these proteins (Fig. 1C-C', solid arrowhead in panel C'). Instead, GnRH neurons and OECs cells, stained with anti-GnRH and anti-BLBP antibodies respectively, did not express SEMA6A (Fig. 1D-E', empty arrowheads in D' and E'). In the nasal compartment at E14.5, we found that SEMA6A is expressed by nTUBB3^{+} nasal axons along the septum (Fig. 2A, solid arrowheads) and specifically by PRPH-expressing fibers (Fig. 2B, solid arrowheads). Similar to E12.5, no co-localisation was found between SEMA6A and GnRH in migrating GnRH neurons within the nose (Fig. 2C, empty arrowhead). Further, as already observed at E12.5, SEMA6A was not expressed by BLBP^{+} OECs in the nasal compartment at E14.5 (Fig. 2D, empty arrowhead). Because at E14.5 GnRH neurons are scattered in the MPOA following TN fibers [2,17,35], we also studied SEMA6A expression in this compartment and found that SEMA6A is not expressed by GnRH neurons or PRPH^{+} TN fibers (Fig. 2E, F, empty arrowheads). Further, we localised expression of SEMA6A at E18.5 in the median eminence, next to GnRH neuron fibers (data not shown). Interestingly, we had access to a human embryo at CS19 and found expression of SEMA6A in the nasal region similar to what observed in mouse embryos at corresponding stage (Fig. 6D-E).

SEMA6A loss does not affect GnRH neuron development but reduces GnRH innervation of the ME at E18.5

Based on the expression pattern observed and the known role of SEMA6A in axon elongation [21,31], we first analysed the nasal axon patterning and GnRH neuron migration in wild-type (WT) and *Sema6a*$^{-/-}$ embryos at E14.5, by immunohistochemistry, as previously described [17,36]. Although SEMA6A was highly expressed by nasal axons in the nasal compartment, no obvious defects in the patterning of PRPH^{+} axons were observed in the *Sema6a*$^{-/-}$ embryos compared to WT littermates (Fig. 3A, white arrowheads). Accordingly, no differences were found in the number and positioning of GnRH neurons at E14.5 (Fig. 3B-C, black arrows and Supplemental table 1). We then analysed *Sema6a*$^{-/-}$ and WT embryos at E18.5, to assess whether the loss of SEMA6A may affect the final positioning of GnRH neurons in the MPOA and/or the innervation of ME, as at this stage GnRH terminals already innervate the ME [6] and we detected high expression of SEMA6A in this region (data not shown). The overall distribution of GnRH neurons between the OB and MPOA was similar between *Sema6a*$^{+/+}$ and *Sema6a*$^{-/-}$ mice (Fig. 3D and Supplemental table 1). However, despite all analysed *Sema6a*$^{-/-}$ mice (n=5) displayed a similar number of GnRH neurons in the MPOA similar to WT littermates, a significantly reduced GnRH neuron innervation (Fig. 3E,

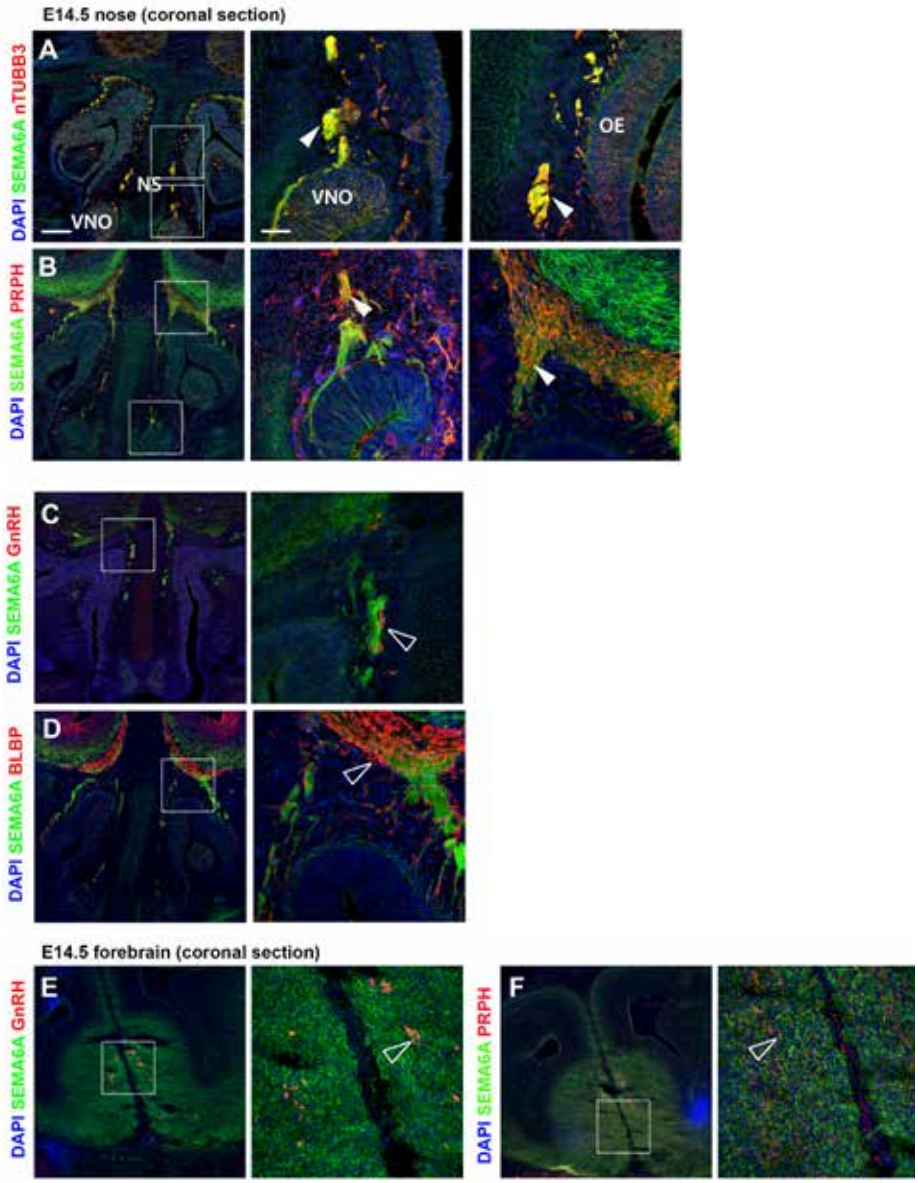

Figure 2. SEMA6A is expressed by PRPH⁺ axons in the nose but not in MPOA at E14.5

(A-F) Coronal sections of E14.5 mouse heads were immunolabelled for SEMA6A together with nTUBB3 (A), PRPH (B-F), GnRH (C-E) or BLBP (D). Sections are shown at the level of the nose (A-D) or forebrain (E-F). White boxes indicate areas shown at higher magnification on the right of the corresponding panel. Solid arrowheads in A-B indicate examples of nTUBB3- and specifically PRPH-positive axons with SEMA6A, respectively. Empty arrowheads in C-D indicate examples of GnRH neurons and OECs that lack SEMA6A expression. Empty arrowheads in E-F indicate the lack of expression of SEMA6A by TN fibers and GnRH neurons in the forebrain. All sections were counterstained with DAPI. OE, olfactory epithelium; VNO, vomeronasal organ; NS, nasal septum. Scale bars: 250 or 50 µm for lower and higher magnifications, respectively.

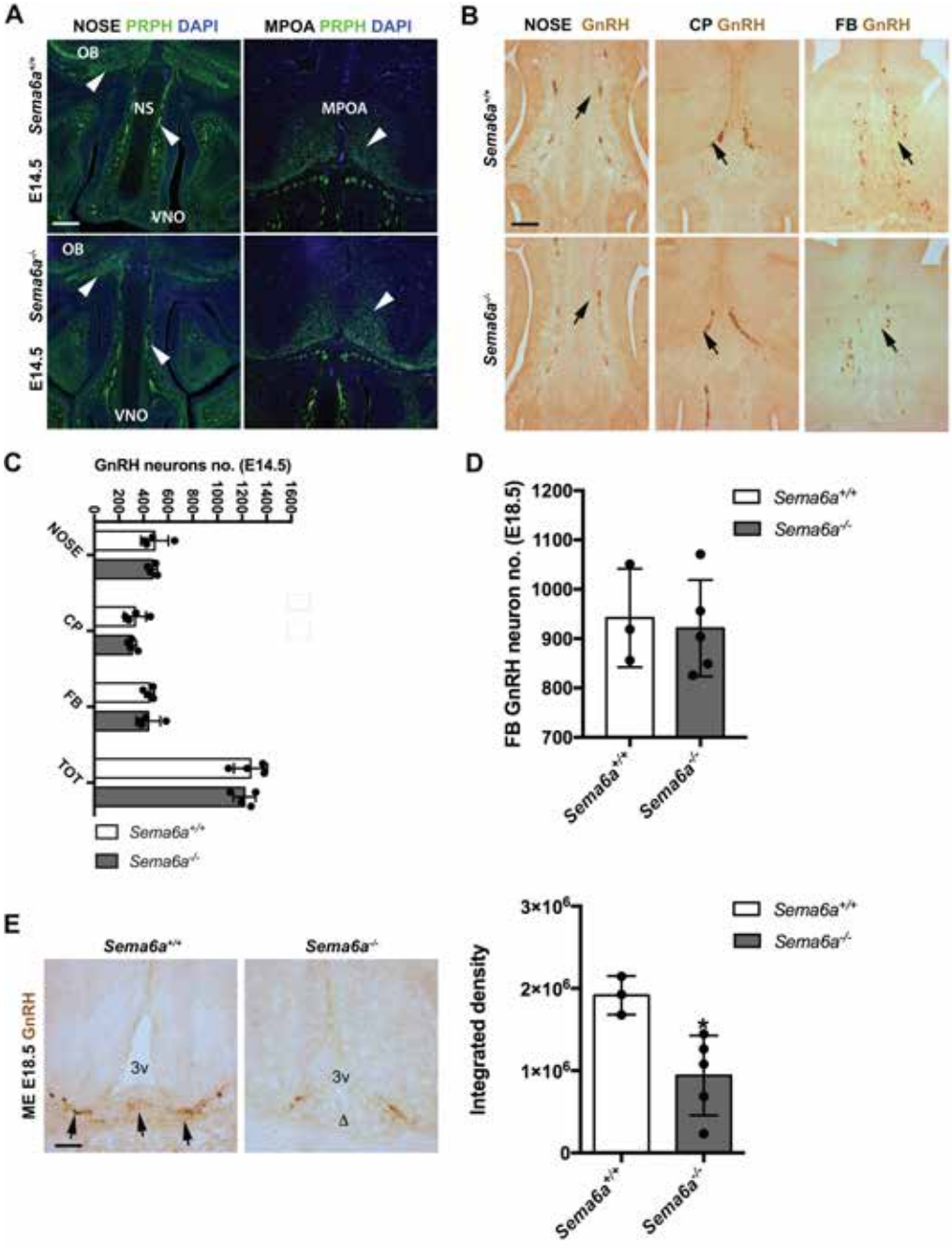
A
NOSE PRPH DAPI
MPOA PRPH DAPI
Sema6a+/+
E14.5
OB
NS
VNO
MPOA
Sema6a-/-
E14.5
OB
VNO
B
NOSE GnRH
CP GnRH
FB GnRH
Sema6a+/+
Sema6a-/-
C
GnRH neurons no. (E14.5)
0
200
400
600
800
1000
1200
1400
1600
NOSE
CP
FB
TOT
Sema6a+/+
Sema6a-/-
D
FB GnRH neuron no. (E18.5)
1200
1100
1000
900
800
700
Sema6a+/+
Sema6a-/-
Sema6a+/+
Sema6a-/-
E
Sema6a+/+
Sema6a-/-
ME E18.5 GnRH
3v
3v
Δ
Integrated density
3×10^6
2×10^6
1×10^6
0
*
Sema6a+/+
Sema6a-/-
Sema6a+/+
Sema6a-/-

< Figure 3. SEMA6A loss does not impair nasal axon and GnRH neuron development at E14.5, but reduces GnRH innervation of the ME at E18.5

(A) Coronal sections of E14.5 mouse heads of the indicated genotypes at the level of the nose (left panels) and MPOA (right panels) were immunolabeled for PRPH to reveal nasal axons. Solid arrowheads indicate normal nasal axon development in the nose and normal TN fibers in the MPOA. (B-C) E14.5 GnRH neuron analysis. (B) Coronal sections of E14.5 mouse heads with the indicated genotypes were immunolabelled for GnRH. Arrows indicate examples of normal GnRH neuron distribution in the nasal parenchyma (left panels) at the CP (middle panels) and in the FB (right panels). (C) Quantification of GnRH neuron number in the E14.5 head reveals no differences between the two groups (n = 3 for each group; n.s., Student's *t* test). (D-E) E18.5 GnRH neuron analysis. (D) Total GnRH neuron number in the FB (including OB and MPOA) is unaffected in *Sema6a*$^{-/-}$ (n=5) compared to *Sema6a*$^{+/+}$ (n=3) littermates (n.s., Student's *t* test). (E) Coronal sections of E18.5 brains with the indicated genotypes at the level of the ME were immunolabelled for GnRH. Arrows in the left panel indicate normal presence of GnRH neuron axon terminals in *Sema6a*$^{+/+}$ embryos; Δ in the right panel indicate decreased presence of GnRH neuron axon terminals. Quantification of ME innervation reveal a decreased GnRH staining in *Sema6a*$^{-/-}$ (n=5) compared to *Sema6a*$^{+/+}$ (n=3) littermates (* $p<0.05$, Student's *t* test). Data presented as mean ± sd. VNO, vomeronasal organ; NS, nasal septum; CP, cribriform plate; FB, forebrain; MPOA, medial preoptic area; OB, olfactory bulb; 3v, third ventricle. Scale bars: 250 µm (A-B), 125 µm (E).

indicated with Δ) of the ME was observed in *Sema6a*$^{-/-}$ mice compared to *Sema6a*$^{+/+}$ littermates (Fig. 3E; integrated density ± s.d.: *Sema6a*$^{+/+}$ $1.9 \times 10^6 \pm 2.3 \times 10^5$ (n=3) vs. *Sema6a*$^{-/-}$ $9.4 \times 10^5 \pm 4.9 \times 10^5$ (n=5), * $p<0.05$; Student's *t* test). Altogether these data suggest that SEMA6A is not essential for the migration of GnRH neurons, directly or indirectly, but rather imply a possible role for SEMA6A in GnRH neuron innervation/secretion.

SEMA6A is expressed in the ME in close contact with GnRH neuron terminals and blood vessels

Thus, to analyse whether SEMA6A has a role in the control of GnRH secretion postnatally, similarly to other semaphorins [11,12], we first examined its expression in the postnatal ME, where GnRH neurons secrete the decapeptide to stimulate gonadotropin release from the pituitary. To this purpose, we performed double immunofluorescence staining to localize SEMA6A expression in relation to GnRH neuron terminals, stained for GnRH, and blood vessels, stained for Ib4. We choose time-points P0, P24 and P60 for these analyses, corresponding to peri-pubertal (P0, P24) and post-pubertal stages (P60). Interestingly, we found high expression of SEMA6A in the ME also postnatally, at P0, P24 and P60, with a punctate pattern similar to neuroendocrine projections (Fig. 4). However, double immunofluorescence staining for SEMA6A and GnRH excluded the co-localisation between SEMA6A and GnRH neuron terminals, although the

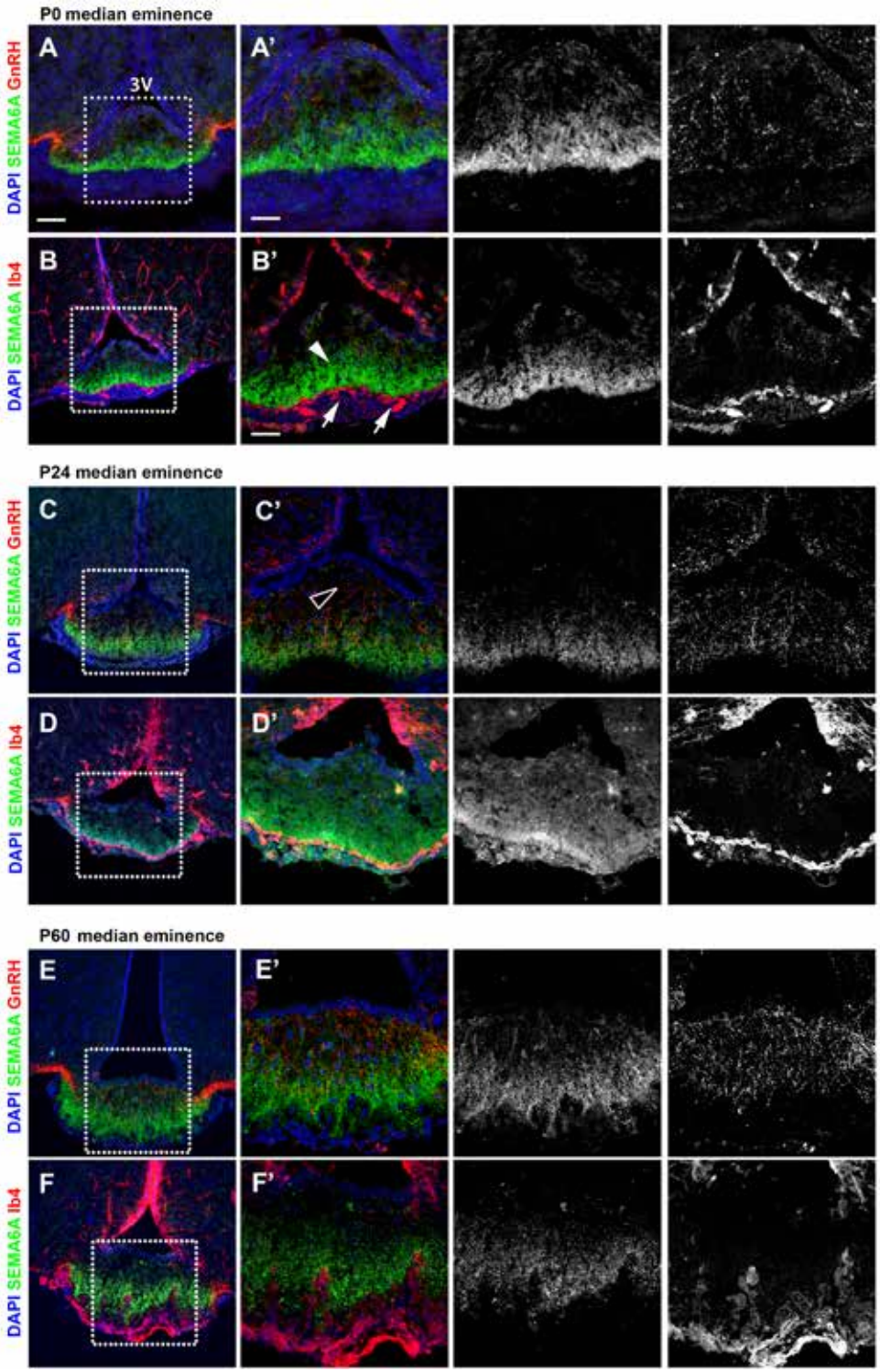
P0 median eminence
A
A'
3V
DAPI SEMA6A GnRH
B
B'
DAPI SEMA6A Ib4
P24 median eminence
C
C'
DAPI SEMA6A GnRH
D
D'
DAPI SEMA6A Ib4
P60 median eminence
E
E'
DAPI SEMA6A GnRH
F
F'
DAPI SEMA6A Ib4

< Figure 4. SEMA6A is expressed in the postnatal ME in close contact to GnRH neuron terminalis and blood vessels

(A-F) Coronal sections of P0 (A-B), P24 (C-D) and P60 (E-F) ME were immunolabelled for SEMA6A together with GnRH (A-C-E) or IB4 (B-D-F) to reveal GnRH axon terminals and blood vessels, respectively. White boxes indicate areas shown at higher magnification on the right of the corresponding panel (A'-F'). Single channels for SEMA6A, GnRH and IB4 of high magnification images are shown on the right of each image. Empty arrowhead indicates GnRH axon terminals. Arrows indicate Ib4^{+} blood vessels in D'-F'. All sections were counterstained with DAPI. 3V, third ventricle. Scale bars: 125 µm for lower magnifications and 50 µm higher magnifications.

two proteins were found in close proximity (Fig. 4A-A', C-C', E-E'). Because SEMA6A staining is prominent on the basal part of the ME where neurohormones including GnRH should be released into the blood vessels to reach the pituitary, we performed double immunofluorescence staining for SEMA6A and Ib4, to localize SEMA6A expression in relation to blood vessels. Interestingly, at all stages analysed, we found that SEMA6A expression lines up to the blood vessels (Fig. 4B-B', D-D', F-F'). Altogether, these results are consistent with a possible role of SEMA6A in the control of GnRH secretion in the portal blood vessels that contact the pituitary.

Sema6a$^{-/-}$ mice showed significant delayed puberty onset

Because we found high expression of SEMA6A in the ME, the region where GnRH is secreted, at stages relevant to puberty onset, we compared the timing of puberty in *Sema6a*$^{-/-}$, *Sema6a*$^{+/-}$ and WT female mice by identifying the day of vagina opening (VO), a proxy measurement for pubertal activation of the HPG axis in mice [15,37]. A slight but not significant VO delay was observed in *Sema6a*$^{+/-}$ females compared to WT; instead 6/9 *Sema6a*$^{-/-}$ females displayed statistically significant delayed VO and 3/9 *Sema6A*$^{-/-}$ females displayed a closed vagina phenotype compared to WT female mice. Specifically, VO of 9/9 mutant mice analysed was delayed by on average 12.1 ± 2.9 days in *Sema6A*$^{-/-}$ compared with WT females and of 5.9 ± 0.7 days, when the 3 females who displayed a closed vagina were not considered (Fig. 5A; postnatal day (P) of VO ± s.d.: WT 27.6 ± 1.4 (n=15); *Sema6a*$^{+/-}$ 28.1 ± 2.0 (n=17), n.s. vs WT; *Sema6a*$^{-/-}$ 39.7 ± 10.0 (n=9), **** p<0.0001 vs WT; delayed *Sema6a*$^{-/-}$ only 33.50 ± 2.6, n = 6, **** p<0.0001; mice were pooled from 8 different litters for *Sema6a*$^{-/-}$ and *Sema6a*$^{+/-}$ mice and from 3 different litters for wild types; One-way ANOVA, Dunnett's post-hoc test). Consistent with their delayed puberty (DP) and thus older age at VO in the *Sema6a*$^{-/-}$ females, there was a significant trend towards greater weight at the time of VO in *Sema6a*$^{-/-}$ compared with WT females within the cohort examined (Fig.

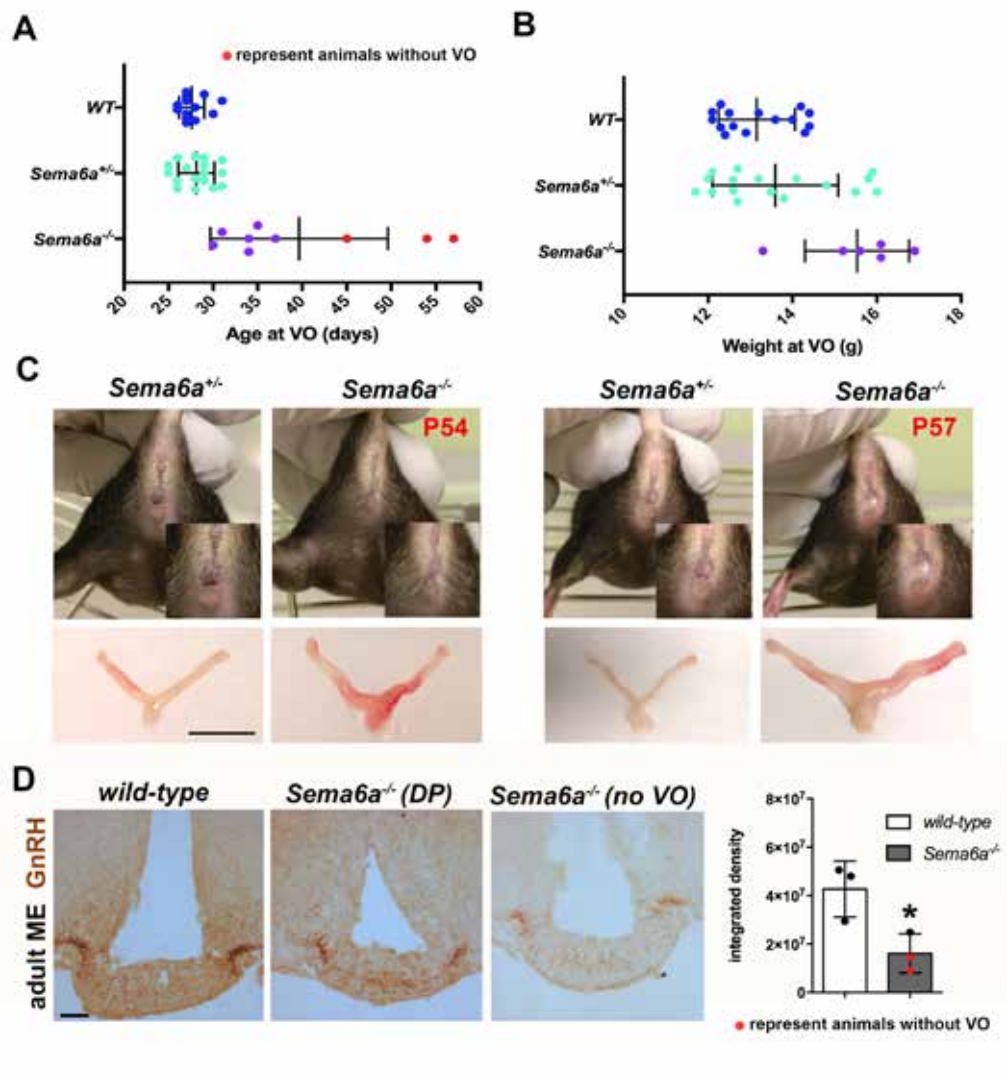

Figure 5. SEMA6A loss delays VO and decreases ME innervation in adult female mice

(A-B) Age (A) and weight (B) at the time of the VO in female WT (n=15), *Sema6a*$^{+/-}$ (n=17) and *Sema6a*$^{-/-}$ (n=9) mice. Red dots indicate *Sema6a*$^{-/-}$ females that displayed no VO (**** p<0.0001 and *** p<0.001, One-way ANOVA, Dunnett's post-hoc test). (C) External genitalia and uteri morphology of *Sema6a*$^{+/-}$ and *Sema6a*$^{-/-}$ adult females. *Sema6a*$^{-/-}$ females are examples of females which did not exhibit VO and displayed swelling uteri compared to *Sema6a*$^{+/-}$ littermates. (D) Coronal sections of adult brains with the indicated genotypes at the level of the ME were immunolabelled for GnRH. Quantification of ME innervation reveal a decreased GnRH staining in *Sema6a*$^{-/-}$ (n=3) compared to WT females (n=3); red dots indicate *Sema6a*$^{-/-}$ females that displayed no VO (* p<0.05, Student's *t* test). Data are mean ± sd. Scale bars: 2 cm (C), 125 µm (D).

5B; body weight on the day of VO ± s.d.: WT 13.2 ± 0.9 g (n=15); *Sema6a*$^{+/-}$ 13.6 ± 1.5 g (n=17), n.s. vs WT; *Sema6a*$^{-/-}$ 15.5 ± 1.2 g (n=6), *** p<0.001 vs WT, One-way ANOVA, Dunnett's post-hoc test). We also observed a distended uteri phenotype and swelling around the genital region in 2/9 *Sema6a*$^{-/-}$ females that did not display VO compared to *Sema6a*$^{+/-}$ mice (Fig. 5C). Consistent with a possible defect in GnRH secretion and with what observed at E18.5, we found that the ME of adult brains from 3/3 *Sema6a*$^{-/-}$ females were less innervated compared to stage-matched WT females (Fig. 5D, integrated density ± s.d.: WT 4.3 x 10^7 ± 6.7 x 10^6 vs *Sema6a*$^{-/-}$ 1.6 x 10^6 ± 4.7 x 10^6, * p<0.05; Student's *t* test; n=3 for each group). Notably, 2/2 *Sema6a*$^{-/-}$ females that did not reach VO (red dots in Fig. 5D) displayed a more pronounced reduction in ME innervation compared to the 1/1 female which exhibited a delayed VO. In agreement with E18.5 phenotype, the number of GnRH neurons in the MPOA of adult *Sema6a*$^{-/-}$ and WT females remained unaffected (Suppl. Table 1). Taken together, these findings show that *Sema6a* deficiency delays or impairs puberty in female mice through reduced GnRH neuron ME innervation.

Exome sequencing of patients with DP identifies a novel heterozygous variant in Semaphorin 6A in one family

We enquired exome sequencing data from our large cohort of patients with self-limited DP and identified a novel potentially pathogenic variant in the gene *SEMA6A* (ENSG00000092421, gene identification number 57556). This novel variant was carried by four affected members of one family from our cohort, and all individuals were heterozygous for this variant (Fig. 6A). The affected individuals from these pedigrees did not carry any other predicted pathogenic variants in known GnRH deficiency or gonadotropin deficiency causing genes. The affected individuals (both males and females) from this family have classical clinical and biochemical features of self-limited DP, with delayed onset of Tanner stage 2 and delayed peak height velocity. The male proband presented at 15.7 yrs with testes volume of 3.7 mL, bone age delayed by 3.6 yrs and short stature (height SDS – 2.75). He had normal olfaction and no evidence of chronic illness. His short stature was related to his pubertal delay, as height SDS at both 7 yrs and at adult height was -1.3, in keeping with his mid-parental target height. His delayed puberty was inherited from his mother, who had menarche aged 15 yrs, and his brother and maternal uncle also had delayed onset of puberty and growth spurt. Both the proband and his brother on follow up had spontaneous pubertal development without testosterone therapy, thus excluding idiopathic hypogonadotropic hypogonadism. The variant (NM_020796; c.1268T>C;

p.I432T) was not found in the gnomAD browser (accessed 28.10.2019) and affects an isoleucine residue at amino acid 423 within the SEMA domain of the protein that is highly conserved among species (Fig. 6B-C). The substitution of a threonine, a neutral polar amino acid, for an isoleucine, a neutral non-polar amino acid, at this position is predicted to be damaging or disease-causing to protein function by 3/3 (pMUT, SIFT and REVEL) bioinformatic tools, and has a CADD score of 31. To further predict the possible damaging impact of the I423T mutation, we performed *in silico* studies on protein stability using the CryoEM structure of the SEMA6A homodimer in complex with *C. sordellii* lethal toxin TcsL (PDB ID: 6WTS) [38]. The I423 residue lies in the SEMA domain, next to the central cavity of the beta-sheet structure of the 6th beta-propeller blade (Fig. 6B). It neither has direct contact to the SEMA6A dimerization surface nor to the SEMA6A-PLXNA2 interaction surface [38]. I423 residue forms hydrophobic contacts with surrounding residues (e.g. A298 T300 L312 A313 T314), thus an Ile to Thr substitution would reduce the size of the residue which would decrease its Van der Waals contact with some of the residues above. Additionally, it would make this local niche more accessible to the large solvent cavity of the SEMA domain hole. Accordingly, the stability of mutated SEMA6A homodimer is significantly decreased compared to wild-type SEMA6A homodimer (ΔStability: 16.22 ± 0.14 kcal/mol for each single SEMA6A protomer).

The SEMA6A^{I423T} mutation affects protein levels and localization *in vitro*

To functionally validate the *in silico* modelling predictions, we generated two vectors for the wild-type and the mutated form of human SEMA6A (SEMA6A^{WT} and SEMA6A^{I423T} respectively) that we transfected in COS-7 cells. Protein production and localization were then analysed, as previously described for other semaphorins [39] Western blotting analysis on lysates from cells expressing SEMA6A^{WT} or SEMA6A^{I423T} protein revealed that both proteins were normally synthetized, both at 24 and 48 hours after transfection. However, the mutated form was less abundant than SEMA6A^{WT} at both time-points analysed (Fig. 7A). To understand whether the mutation could have an effect also on protein localisation, we performed immunocytochemistry experiments using an anti-myc antibody to visualize SEMA6A^{WT} or SEMA6A^{I423T} in COS-7 cells, 24 and 48 hours post transfection (Fig. 7B-G). As expected, the SEMA6A^{WT} protein (green), both at 24 (B) and 48 (C) hours post transfection localised to the cellular membrane (Fig.7B-C, white arrowheads) [29]. Instead and interestingly, the

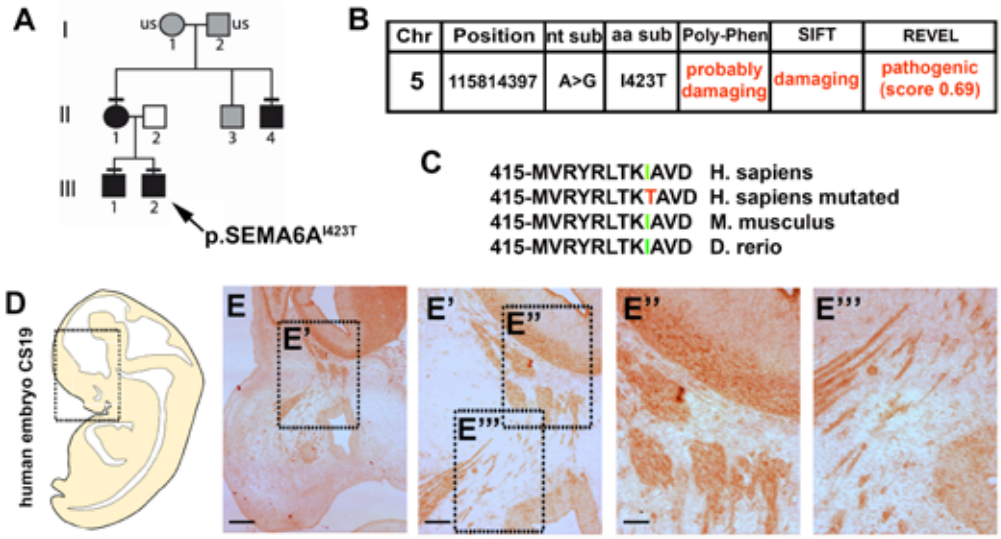

Figure 6. SEMA6A is mutated in patients with DP and is expressed in CS19 human embryo

(A) Pedigree of the proband with the p.I423T mutation. Squares indicate male family members; circles indicate female family members. Black symbols represent clinically affected family members, grey symbols represent family members with unknown phenotype and clear symbols represent unaffected individuals. The arrow labels the proband in the family. A horizontal black line above or adjacent to an individual's symbol indicates that they are heterozygous for the p.I423T mutation as identified by WES and verified by Sanger sequencing. (B) Chromosome position, nucleotide substitution, amino acid substitution, and bioinformatic predictions of the identified SEMA6A mutation. The p.I423T mutation is damaging and pathogenic according Poly-Phen, SIFT and REVEL software. (C) Alignment of partial protein sequences of vertebrate SEMA6A orthologs shows that the I423 residue is evolutionarily conserved in mouse and zebrafish. (D-E) Sagittal view of a CS19 human embryo in a schematic drawing (D) and sagittal sections of squared area of D immunolabeled for SEMA6A (E). Black boxes indicate areas shown at higher magnification on the right of the corresponding panel. Scale bars: 500 µm (E), 250 µm (E'), 125 µm (E''-E''').

overexpression of SEMA6A^{I423T} protein (green), both at 24 and 48 hours post transfection induced an abnormal localisation of the protein, which remains perinuclear and does not localise in the membrane (Fig. 7D-E, empty arrowheads). To confirm that the mutant form of SEMA6A is retained in the endoplasmic reticulum (ER), because of altered stability of the protein, as predicted by *in silico* analyses, we co-transfected COS-7 cells with SEMA6A ^{I423T} and a fluorescent ER-localisation vector (mEmerald-ER-3). As shown in figure 7 (F-G), SEMA6A ^{I423T} is retained in the ER, both at 24h and 48h post-transfection, as confirmed by the co-localisation of both signals (Fig. 7F-

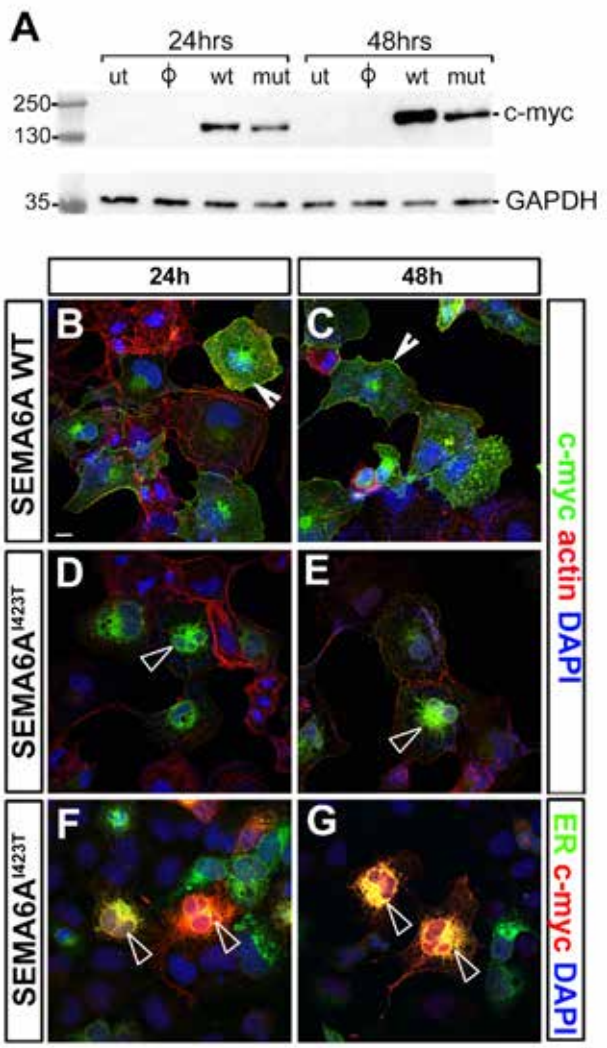

Figure 7. The SEMA6A^{I423T} mutation impairs protein synthesis due to ER retention

(A) Generation of wild-type and mutant human SEMA6A proteins. COS-7 cells were transfected with a control expression vector (Ø) or vectors encoding c-myc tagged human SEMA6A (wt) or mutant SEMA6A^{I423T} (mut). Cells were immunoblotted with an antibody against c-myc. Cells lysates contained a band of approximately 130 kDa. GAPDH (37 kDa) was used as a loading control. (B-E) COS-7 cells were transfected with vector encoding for SEMA6A WT (B-C) or SEMA6A^{I423T} (D-E). Cells were immunolabeled at 24 h (B-D) or 48 h (C-E) post transfection for c-myc (green) and actin (red). Solid arrowheads in B-C indicate examples of expression of SEMA6A WT in the membrane. Empty arrowheads in D-E indicate the lack of SEMA6A^{I423T} on the membrane and point at its intracellular and perinuclear expression. Nuclei were counterstained with DAPI. (F-G) COS-7 cells were co-transfected with vector encoding for SEMA6A^{I423T} and ER-emerald plasmid to visualizes ER (green). Cells were immunolabeled at 24 h (F) or 48 h (G) post transfection for c-myc (red). Solid arrowheads indicate examples of ER retention of SEMA6A^{I423T}. Nuclei were counterstained with DAPI. Scale bars: 50 µm (B-G).

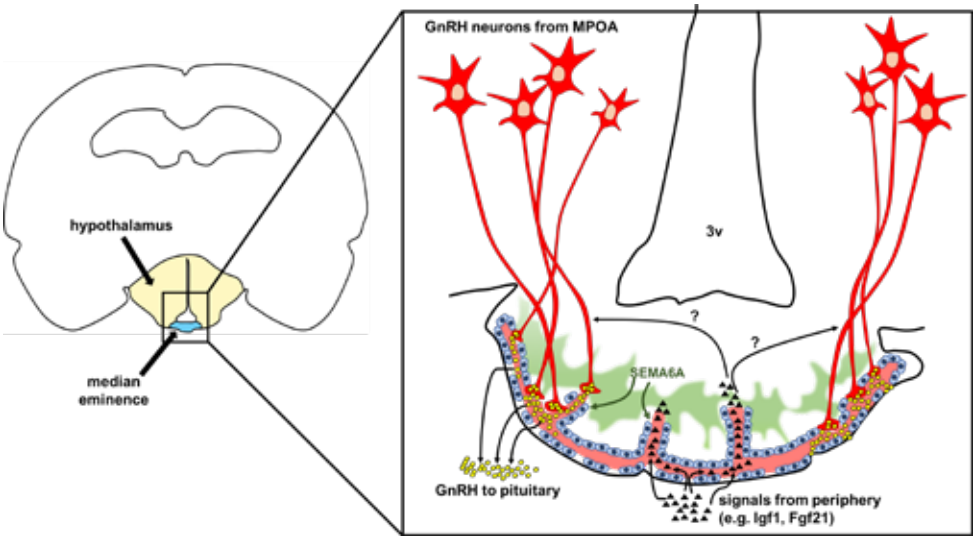

Figure 8. SEMA6A modulate blood vessel permeability and molecules exchange in the ME

Schematic drawing representing the proposed molecular mechanism through which SEMA6A modulate GnRH secretion. Coronal section of an adult brain at the level of the caudal hypothalamus (light yellow) is shown on the left. The region around the ME (light blue) is shown in detail on the right. GnRH neuron terminals (in red) reach the hypophyseal portal system to release GnRH peptide (yellow granule), which stimulate the pituitary. As the endothelium (blue cells) is fenestrated, the molecules can pass from the brain to periphery (e.g. GnRH peptide) and vice versa. Thus, several molecules synthetized by peripheral tissues (e.g. Igf1, Fgf21; black triangles) can modulate the release of GnRH. In this context, SEMA6A (in green) acts on fenestrated endothelium by modulating the permeability of blood vessels to regulate flux of molecules from the SNC and the periphery.

G, empty arrowheads). Together, the *in vitro* results strongly validate our *in silico* results, supporting the hypothesis that the mutation affects SEMA6A stability and impairs membrane localisation, thus suggesting a loss of function effect of the mutated SEMA6A in our patients.

DISCUSSION

The proper development and functionality of hypothalamic GnRH-secreting neurons strictly depends by the concerted action of several factors, whose lack may ultimately lead to a defective GnRH release/action with a consequent delayed or absent puberty. Among these molecules, different members of the semaphorin family were shown to play key roles during GnRH neuron development and GnRH peptide release by controlling their migration or ME plasticity, respectively [17,18]. For example, SEMA3A

via Neuropilin (NRP) 1 and 2 and members of the Plexin (PLXN) A family controls indirectly the FB entry of GnRH neurons by patterning nasal axons, whereas in adulthood SEMA3A via NRP1 controls the plasticity of the median eminence and indirectly the secretion of GnRH [11,17,36,40]. Similarly, while SEMA7A directly promotes GnRH neuron migration in the nasal compartment during development, it is also expressed by tanycytes in the ME, where it induces retraction of GnRH neuron terminals to control its secretion [12,41]. Here, we showed that SEMA6A is highly and exclusively expressed by nasal axons during embryonic development at both E12.5 and E14.5. These data were suggestive of a role of SEMA6A in nasal axon patterning in agreement with previous reports showing the involvement of SEMA6A in the guidance of several brain axons [42]. Altogether, these data prompted us to investigate a possible action of SEMA6A in GnRH secretion and to exclude a pivotal role in GnRH neuron migration.

Interestingly and in agreement with a previous report [25], we found robust expression of SEMA6A in the adult ME, both at pre-pubertal (P24) and post-pubertal stages (P60). In this area, SEMA6A does not colocalise with GnRH neuron terminals or Ib4+ blood vessels, but it is expressed in close contact to both. Our results refer to a role of SEMA6A in the GnRH neuron innervation of the ME or most likely in the release of GnRH. In agreement with our hypothesis and the observation of SEMA6A expression in the ME with a decreased ME innervation at E18.5, we found that adult females lacking SEMA6A displayed impaired puberty onset with delayed VO and reduced ME innervation by GnRH terminals. From E18.5 GnRH neuroendocrine terminals already reach the ME and the vasculature of the ME displays the essential characteristics of primary portal capillaries, including a fenestrated endothelium, designed to facilitate the free exchange of molecules between the portal circulation and the brain by passing the blood–brain barrier (BBB) [6]. The ME is a unique region where the blood brain barrier (BBB) is absent and the presence of fenestrated vessels allows both the release of neurohormones and the uptake of peripherally-derived factors that may control hormones secretion [43]. It's known that vascular endothelial growth factor (VEGF) and its receptor VEGF receptor 2 (VEGFR2) are key regulators of angiogenesis and may also control permeability [44,45]. At the level of the ME, VEGF is highly expressed in somatodendrites, astrocytes, tanycytes and neuronal terminals, while VEGFR2 is expressed in the endothelial cells of the portal circulation [43,45,46] supporting a role of VEGF/VEGFR2 in the regulation of permeability. Segarra et al. demonstrated a relationship between *Sema6A* deficiency and VEGFR2 expression [33]. In particular, *in vitro*,

the silencing of Sema6A in endothelial cells impaired VEGFR2 signaling; *in vivo*, *Sema6a*$^{-/-}$ mice showed vascular development defects [33]. Based on this knowledge, we hypothesised that the lack of SEMA6A could affect VEGFR2 functionality in the endothelial cells of the ME causing a consequent reduced permeability of fenestrated capillaries (Fig.8). This condition could result in a limited access of soluble factors coming from periphery and acting on GnRH neurons elongation or secretion.

Accordingly, previous studies displayed the importance of soluble factors coming from peripheral sources and acting within the hypothalamus/ ME [43,47]. Among them, IGF1 is known to be a trophic factor that exerts its function by its receptor IGF1-R, and is required *for the oestradiol-induced release of gonadotrophins* [47]. Interestingly, a high amount of IGF1 mRNA was found in the ME both at P0 and just before puberty [48]. At this time point, tanycytes capture Ifg1 entering from fenestrated blood vessels and deliver it inside the hypothalamus [48]. Moreover, an *in vivo* study demonstrated the presence of a high concentration of Ifg1-r at the level of the ME (and also its presence on GnRH neurons, supposing that Igf1 can act on GnRH neurons to stimulate GnRH release [49,50]. Accordingly, conditional knockout mice with Ifg1-r deleted from GnRH neurons exhibited delayed puberty phenotype [51]. In addition, Xu et al. recently showed, by using diffusion assays, that peripheral Fgf21 is able to extravasate from the fenestrated capillaries in the ME and the OVLT and act on GnRH neuronal dendrites and terminals suggesting a novel role for Fgf21 in controlling fertility by modulating GnRH neuron structural plasticity [9].

Mice lacking SEMA6A did not display defects in the development of PRPH^{+} nasal axons. Accordingly, the GnRH neuron migration from the nose to the brain, that occurs during development, was normal in these mice. This may be due to compensatory mechanisms of other semaphorins, which are known to be expressed in the nasal compartment to control nasal axon patterning such as SEMA3A and 3F, or by redundant roles of other members of the class 6 semaphorins such as SEMA6B or SEMA6D, which share the same PlexinA receptors. Similarly, at E18.5, when GnRH neurons are finally set in the MPOA, there were no significant differences in the positioning of GnRH neurons between *Sema6a*$^{-/-}$ and WT mice. Yet, mice lacking SEMA6A displayed a significant decrease in the GnRH neuron innervation of the ME, where normally SEMA6A is highly expressed.

In conclusion, we dissected the role of SEMA6A in the GnRH neuronal system in mice by showing that it is highly expressed in regions relevant to the GnRH neuron system both embryonically and postnatally. Our findings (summarized in figure 8) demonstrate that SEMA6A is not required for the patterning of nasal axons or for the migration of GnRH neurons, but is required for GnRH neuron innervation in the ME and consequently for puberty onset, possibly by modulating vascular permeability.

METHODS

Animals and tissue preparation

HASema6A^{fl} mice were crossed with *EIIa-Cre* mice (JAX stock #003724, Lakso et al., 1996) to create a germline deletion, *EIIa-Cre;HASema6A*$^{\Delta/\Delta}$ (referred to as *Sema6a*$^{-/-}$) maintained on a C57BL/6 background. The genotype of the mice was determined by PCR using DNA from mouse tail or ear tissue as a template and primers flanking the HA tag sequence using forward primer '5-CCTTGTCACACATGCAGTTG-3' and reverse primer '5-TGAAGTAGAGAAGCA-3'. For all experiments, we used mice that were housed socially and kept under a normal 12:12 h light-dark cycle with chow diet and water ad libitum. All experiments were conducted in compliance with the Animal Ethics Committee of Utrecht University (Dierexperimenten Ethische Commissie) (CCD licence: AVD115002016532) and in agreement with Dutch laws (Wet op de Dierproeven, 1996; revised 2014) and European regulations (Guideline 86/609/EEC; Directive 2010/63/EU). *HASema6A*^{fl} mice (conditional exon 3 deletion) were generated in the lab of Alex Kolodkin. The morning of vaginal plug observation was defined as embryonic day 0 (E0). The day of birth was defined as postnatal day 0 (P0). Timed pregnant females were sacrificed by cervical dislocation to collect embryos at E12.5, E14.5 and E18.5. Embryo heads were fixed for 3-6 hours in 4% formaldehyde at 4°C. Adult female mice were transcardially perfused with ice-cold PBS. Subsequently, brains and vaginal tissue were isolated and fixed in 4% PFA overnight at 4°C. Pituitaries, ovaries and uterus were collected for RNA extraction and analysis. All samples for cryosectioning were cryoprotected overnight in 30% sucrose prior to OCT-embedding.

In situ hybridization

Formaldehyde-fixed 20 µm cryosections of E12.5 and E14.5 embryos were incubated with digoxigenin (DIG)-labelled an anti-sense riboprobe for mouse Sema6a [21]. For labeling, we used the DIG RNA labeling kit (Roche).

Hybridisation was performed in 50% formamide, 0.3 M sodium chloride, 20 mM Tris pH 7.5, 5 mM EDTA, 10% dextran sulphate and 1x Denhardt's solution overnight at 65°C. Sections were washed in a saline sodium citrate buffer (50% formamide, 1x saline sodium citrate buffer, 0.1% Tween20), incubated overnight with alkaline phosphatase (AP)-conjugated anti-DIG IgG (1:1500; Roche) and developed overnight at 37°C with 4-nitro blue tetrazolium chloride and 5-bromo-4-chloro-3-indolyl phosphate disodium salt (Roche) dissolved in a buffer comprised of 100 mM Tris pH 9.5, 50 mM MgCl2, 100 mM NaCl and 1% Tween 20.

Immunofluorescence labeling

20 µm cryostat sections of formaldehyde-fixed embryos were incubated with serum-free protein block (DAKO) after permeabilization of sections with 0.1% TritonX-100. We used as primary antibodies rabbit anti-peripherin (1:100; Merck Millipore, cat. no. AB1530), rabbit anti-GnRH, (1:400; Immunostar, cat. no. 20075), anti-blbp (1:200, Sigma-Aldrich), mouse anti-nTUBB3 (1:500, clone Tuj1, Covance, cat. no. MMS- 435P), goat anti-SEMA6A (1:200; R&D Systems, cat. no. AF1615). Secondary antibodies used were Cy3-conjugated donkey anti-goat and 488-conjugated donkey anti-rabbit Fab fragments (1:200; Jackson Immunoresearch). Blood vessels were labelled using isolectin B4 (IB4; 1:100, Vector laboratories) followed by 488- or Cy3-conjugated streptavidin. Nuclei were counterstained with DAPI (1:10000; Sigma).

Immunoperoxidase labeling

20 µm cryostat sections of formaldehyde-fixed samples were incubated with hydrogen peroxide to quench endogenous peroxidase activity, and sequentially incubated with 10% heat-inactivated normal goat serum in PBS or serum-free blocking solution (DAKO) and then immunostained with rabbit anti-GnRH (1:1000; Immunostar), previously validated to recognize both the pre-hormone and the processed hormone [52] and anti-rabbit biotinylated antibody (1:400; Vector Laboratories). Sections were developed with the ABC kit (Vector Laboratories) and 3,3-diaminobenzidine (DAB; Sigma). To determine the total number of GnRH neurons at E14.5 and E18.5, 20 µm coronal sections through each entire head (E14.5) or FB (E18.5) were immunolabelled for GnRH and all GnRH-positive cells in the nose, CP area and FB were counted, as previously reported [17,36,39]. To help distinguish individual GnRH neurons found in cell clumps at the CP of double mutants, high magnification images were analysed.

Vagina opening

Sema6a$^{-/-}$, *Sema6a*$^{+/-}$ and WT females were checked for VO [15,53] and weighted daily at a fixed timepoint, starting from P25 onwards.

Human genetic analysis

Patients from two cohorts were analysed for this study. The first, a large Finnish cohort with self-limited DP, has been described in previous reports from our group (Mancini JCI Insight 2020). The second is a UK cohort referred for genetic evaluation for self-limited DP from Paediatric Endocrinology and Paediatric services around the UK. Inclusion criteria for both cohorts was the onset of Tanner genital stage II (testicular volume > 3 ml) >13.5 years in boys or Tanner breast stage II > 13.0 years in girls (i.e., two SD later than average pubertal development) and their unaffected relatives [54]. Chronic illness as a cause for functional hypogonadotropic hypogonadism was excluded by medical history, clinical examination, and biochemical investigations. Congenital or acquired hypogonadotropic hypogonadism, if suspected, was excluded by spontaneous pubertal development by 18 years of age at follow-up. Ethical approval was granted by the UK London-Chelsea NRES committee (13/LO/0257). All participants provided written informed consent prior to study participation. The study was conducted in accordance with the guidelines of The Declaration of Helsinki.

Bioinformatics

Whole exome sequencing (WES) was performed on DNA extracted from peripheral blood leukocytes of 157 probands (100 Finnish and 57 UK), using an Agilent V5 platform and Illumina HiSeq 2000 sequencing. The exome sequences were aligned to the UCSC hg19 reference genome using the Burrows-Wheeler Aligner software (BWA-MEM [bwa-0.7.12]. Picard tools [picard-tools-1.119] was used to sort alignments and mark PCR duplicates. The genome analysis toolkit (GATK-3.4-46) was used to realign around indels and recalibrate quality scores using dbSNP, Mills and 1000 genomes as reference resources. Variant calling and joint genotyping using pedigree information was performed using HaplotypeCaller in GVCF mode from the genome analysis toolkit. The resulting variants were filtered using the variant quality score recalibration (VQSR) function from GATK. An analysis of the called variants was performed using Ingenuity Variant Analysis (QIAGEN Redwood City, www.qiagen.com/ingenuity). Filtering for potential causal variants was carried out using filters for quality control (read depth and Phred strand bias), minor allele frequency (MAF <0.5% in the ExAC and

Genome Aggregation Database (gnomAD) databases), predicted functional annotation (pMUT, SIFT, REVEL, CADD score) and conservation score (phyloP and GERP).

In silico mutagenesis

The CryoEM structure of the SEMA6A homodimer in complex with *C. sordellii* lethal toxin TcsL (PDB ID: 6WTS) [38] was retrieved from the RCSB Protein Data Bank. After a structure preparation procedure *via* Schrödinger BioLuminate Protein Preparation Tool, including an energy minimization using the OPLS3e [55] force field, the TcsL toxin was removed. The evaluation of the impact of I423T mutation on the protein stability has been carried out with the Schrödinger BioLuminate Residue Scanning Tool. Stability is computed from a thermodynamic cycle which considers the relative stability of each entity: unfolded SEMA6A, folded SEMA6A, unfolded mutated SEMA6A and folded mutated SEMA6A [56].

Cloning

The pAPtag-5 vector (6,6 kb) has been chosen; it contains the replication origin of Simian Virus (SV) 40, the strong promoter of Citomegalovirus (PCMV), the gene for ampicillin resistance, the gene cassette in frame with alkaline phosphatase (AP) gene, the c-Myc and six histidine tags that allow easy purification, detection and interaction assay of the cloned proteins. Two different vectors have been prepared with *hSEMA6A*-wt and *hSEMA6A*-I423T genes inserted between the NheI and the XhoI restriction enzyme sites, in frame with c-Myc, cutting off the AP protein. The empty vector has been used as a control vector. The shorter isoform of *SEMA6A* gene (1030 amino acids, 114 kDa) is the one used for the cloning. For the staining of the Endoplasmic Reticulum (ER), the mEmerald-ER-3 vector (gift from Michael Davidson - Addgene plasmid # 54082) was co-transfected with the *hSEMA6A*-I423T vector (ratio 1:4).

Cell culture experiments

COS-7 cells (American Type Culture Collection, Manassas, VA) were grown as a monolayer at 37°C in a humidified CO_2 incubator in complete DMEM (Euroclone) and supplemented with 10% fetal bovine serum (FBS; Gibco). Subconfluent cells were harvested by trypsinization and cultured in 57 cm^2 dishes. For transfection, COS-7 cells (at 80% confluence) were grown in culture plates in complete culture medium for 24 h and incubated for 24h or 48h with the selected expression vector (1 µg/ml) in the presence of Lipofectamine 3000 (Invitrogen) according to the manufacturer's

instructions. To visualize the endoplasmic reticulum (ER), the mEmerald-ER-3 vector (gift from Michael Davidson, Addgene plasmid #54082) was co-transfected with hSEMA6A-I423T vector (ratio 1:4).

Immunoblotting

Transfected COS7 cells were lysed in 150 mM NaCl, 50 mM Tris-HCl (pH 7.4), and 1% Triton X-100, supplemented with protease and phosphatase inhibitors (Roche) Lysates were centrifuged at 10,000 g for 10 minutes at 4°C and protein concentration determined with the Bradford assay (Bio-Rad). Protein lysate (20 µg) were used for SDS-PAGE. Proteins were transferred to nitrocellulose membranes (Bio-Rad) and immunoblotted with mouse anti–MYC followed by anti-mouse antibodies.

Acknowledgements

We would like to thank Chiara Parravicini, Silvia Manfro and Marta Frisa for technical help; we also would like to thank Diego De Stefani for sharing the ER-vector; part of this work was carried out at NOLIMITS, an advanced imaging facility established by the Università degli Studi di Milano. A.C. was funded by the Italian Ministry of Health (GR-2016-02362389). R.J.P. was funded by the Netherlands Organization for Scientific Research (ALW-NWO VICI).

REFERENCES

1. Herbison, A. E. Control of puberty onset and fertility by gonadotropin-releasing hormone neurons. *Nature Reviews Endocrinology* (2016). doi:10.1038/nrendo.2016.70
2. Taroc, E. Z. M., Prasad, A., Lin, J. M. & Forni, P. E. The terminal nerve plays a prominent role in GnRH-1 neuronal migration independent from proper olfactory and vomeronasal connections to the olfactory bulbs. *Biol. Open* (2017). doi:10.1242/bio.029074
3. Barraud, P. *et al.* Neural crest origin of olfactory ensheathing glia. *Proc. Natl. Acad. Sci. U. S. A.* (2010). doi:10.1073/pnas.1012248107
4. Forni, P. E. & Wray, S. GnRH, anosmia and hypogonadotropic hypogonadism - Where are we? *Frontiers in Neuroendocrinology* (2015). doi:10.1016/j.yfrne.2014.09.004
5. Wierman, M. E., Kiseljak-Vassiliades, K. & Tobet, S. Gonadotropin-releasing hormone (GnRH) neuron migration: Initiation, maintenance and cessation as critical steps to ensure normal reproductive function. *Frontiers in Neuroendocrinology* (2011). doi:10.1016/j.yfrne.2010.07.005
6. Prevot, V. Puberty in Mice and Rats. in *Knobil and Neill's Physiology of Reproduction: Two-Volume Set* (2015). doi:10.1016/B978-0-12-397175-3.00030-2
7. Spergel, D. J. Neuropeptidergic modulation of GnRH neuronal activity and GnRH secretion controlling reproduction: insights from recent mouse studies. *Cell and Tissue Research* (2019). doi:10.1007/s00441-018-2893-z
8. Quennell, J. H. *et al.* Leptin indirectly regulates gonadotropin-releasing hormone neuronal function. *Endocrinology* (2009). doi:10.1210/en.2008-1693
9. Xu, C. *et al.* KLB , encoding αKlotho, is mutated in patients with congenital hypogonadotropic hypogonadism . *EMBO Mol. Med.* (2017). doi:10.15252/emmm.201607376
10. Daftary, S. S. & Gore, A. C. IGF-1 in the brain as a regulator of reproductive neuroendocrine function. *Experimental Biology and Medicine* (2005). doi:10.1177/153537020523000503
11. Giacobini, P. *et al.* Brain Endothelial Cells Control Fertility through Ovarian-Steroid-Dependent Release of Semaphorin 3A. *PLoS Biol.* (2014). doi:10.1371/journal.pbio.1001808
12. Parkash, J. *et al.* Semaphorin7A regulates neuroglial plasticity in the adult hypothalamic median eminence. *Nat. Commun.* (2015). doi:10.1038/ncomms7385
13. Boehm, U. *et al.* Expert consensus document: European Consensus Statement on congenital hypogonadotropic hypogonadism-pathogenesis, diagnosis and treatment. *Nature Reviews Endocrinology* (2015). doi:10.1038/nrendo.2015.112

14. Stamou, M. I. & Georgopoulos, N. A. Kallmann syndrome: phenotype and genotype of hypogonadotropic hypogonadism. *Metabolism* 86, 124–134 (2018).
15. Howard, S. R. *et al.* HS6ST1 Insufficiency Causes Self-Limited Delayed Puberty in Contrast with Other GnRH Deficiency Genes. *J. Clin. Endocrinol. Metab.* (2018). doi:10.1210/jc.2018-00646
16. Kim, S. H. Congenital hypogonadotropic hypogonadism and Kallmann syndrome: Past, present, and future. *Endocrinology and Metabolism* (2015). doi:10.3803/EnM.2015.30.4.456
17. Oleari, R., Lettieri, A., Paganoni, A., Zanieri, L. & Cariboni, A. Semaphorin Signaling in GnRH Neurons: From Development to Disease. *Neuroendocrinology* (2019). doi:10.1159/000495916
18. Messina, A. & Giacobini, P. Semaphorin signaling in the development and function of the gonadotropin hormone-releasing hormone system. *Frontiers in Endocrinology* (2013). doi:10.3389/fendo.2013.00133
19. Hatanaka, Y. *et al.* Semaphorin 6A–Plexin A2/A4 Interactions with Radial Glia Regulate Migration Termination of Superficial Layer Cortical Neurons. *iScience* (2019). doi:10.1016/j.isci.2019.10.034
20. Suto, F. *et al.* Interactions between Plexin-A2, Plexin-A4, and Semaphorin 6A Control Lamina-Restricted Projection of Hippocampal Mossy Fibers. *Neuron* (2007). doi:10.1016/j.neuron.2007.01.028
21. Mitsogiannis, M. D., Little, G. E. & Mitchell, K. J. Semaphorin-Plexin signaling influences early ventral telencephalic development and thalamocortical axon guidance. *Neural Dev.* 12, 6 (2017).
22. Janssen, B. J. C. *et al.* Structural basis of semaphorin–plexin signalling. *Nature* 467, 1118–1122 (2010).
23. Zhou, L. *et al.* Cloning and expression of a novel murine semaphorin with structural similarity to insect semaphorin I. *Mol. Cell. Neurosci.* (1997). doi:10.1006/mcne.1997.0607
24. Xu, X. *et al.* The Transmembrane Protein Semaphorin 6A Repels Embryonic Sympathetic Axons. 20, 2638–2648 (2000).
25. Klostermann, A., Lutz, B., Gertler, F. & Behl, C. The Orthologous Human and Murine Semaphorin 6A-1 Proteins (SEMA6A-1 / Sema6A-1) Bind to the Enabled / Vasodilator-stimulated Phosphoprotein-like Protein (EVL) via a Novel Carboxyl-terminal Zyxin-like Domain *. 275, 39647–39653 (2000).
26. Prislei, S. *et al.* From plasma membrane to cytoskeleton: A novel function for semaphorin 6A. *Mol. Cancer Ther.* (2008). doi:10.1158/1535-7163.MCT-07-0390
27. Loria, R. *et al.* Sema6A and Mical1 control cell growth and survival of BRAFV600E human melanoma cells. *Oncotarget* (2015). doi:10.18632/oncotarget.2995

28. Shen, C. Y. *et al.* The extracellular SEMA domain attenuates intracellular apoptotic signaling of semaphorin 6A in lung cancer cells. *Oncogenesis* (2018). doi:10.1038/s41389-018-0105-z
29. Perez-Branguli, F. *et al.* Reverse Signaling by Semaphorin-6A Regulates Cellular Aggregation and Neuronal Morphology. *PLoS One* 11, e0158686 (2016).
30. Belle, M., Parray, A., Belle, M., Chédotal, A. & Nguyen-Ba-Charvet, K. T. PlexinA2 and Sema6A are required for retinal progenitor cell migration. *Dev. Growth Differ.* (2016). doi:10.1111/dgd.12298
31. Okada, T., Keino-Masu, K., Suto, F., Mitchell, K. J. & Masu, M. Remarkable complexity and variability of corticospinal tract defects in adult Semaphorin 6A knockout mice. *Brain Res.* (2019). doi:10.1016/j.brainres.2018.12.041
32. Renaud, J. & Chédotal, A. Time-lapse analysis of tangential migration in Sema6A and PlexinA2 knockouts. *Mol. Cell. Neurosci.* 63, 49–59 (2014).
33. Segarra, M. *et al.* Semaphorin 6A regulates angiogenesis by modulating VEGF signaling. *Blood* (2012). doi:10.1182/blood-2012-02-410076
34. Little, G. E. *et al.* Specificity and plasticity of thalamocortical connections in Sema6A mutant mice. *PLoS Biol.* (2009). doi:10.1371/journal.pbio.1000098
35. Casoni, F. *et al.* Development of the neurons controlling fertility in humans: New insights from 3D imaging and transparent fetal brains. *Dev.* (2016). doi:10.1242/dev.139444
36. Cariboni, A. *et al.* Defective gonadotropin-releasing hormone neuron migration in mice lacking SEMA3A signalling through NRP1 and NRP2: Implications for the aetiology of hypogonadotropic hypogonadism. *Hum. Mol. Genet.* (2011). doi:10.1093/hmg/ddq468
37. Messina, A. *et al.* A microRNA switch regulates the rise in hypothalamic GnRH production before puberty. *Nat. Neurosci.* (2016). doi:10.1038/nn.4298
38. Lee, H. *et al.* Recognition of Semaphorin Proteins by P. sordellii Lethal Toxin Reveals Principles of Receptor Specificity in Clostridial Toxins. *Cell* (2020). doi:10.1016/j.cell.2020.06.005
39. Cariboni, A. *et al.* Dysfunctional SEMA3E signaling underlies gonadotropin-releasing hormone neuron deficiency in Kallmann syndrome. *J. Clin. Invest.* (2015). doi:10.1172/JCI78448
40. Cariboni, A., Maggi, R. & Parnavelas, J. G. From nose to fertility: the long migratory journey of gonadotropin-releasing hormone neurons. *Trends in Neurosciences* (2007). doi:10.1016/j.tins.2007.09.002
41. Messina, A. *et al.* Dysregulation of semaphorin7A/α1-integrin signaling leads to defective GnRH-1 cell migration, abnormal gonadal development and altered fertility. *Hum. Mol. Genet.* (2011). doi:10.1093/hmg/ddr403
42. Leighton, P. A. *et al.* Defining brain wiring patterns and mechanisms through gene trapping in mice. 410, (2001).

43. Morita-Takemura, S. & Wanaka, A. Blood-to-brain communication in the hypothalamus for energy intake regulation. *Neurochemistry International* (2019). doi:10.1016/j.neuint.2019.04.007
44. Greenberg, D. A. & Jin, K. From angiogenesis to neuropathology. *Nature* (2005). doi:10.1038/nature04481
45. Langlet, F. *et al.* Tanycytic VEGF-A boosts blood-hypothalamus barrier plasticity and access of metabolic signals to the arcuate nucleus in response to fasting. *Cell Metab.* (2013). doi:10.1016/j.cmet.2013.03.004
46. Morita, S., Ukai, S. & Miyata, S. VEGF-dependent continuous angiogenesis in the median eminence of adult mice. *Eur. J. Neurosci.* (2013). doi:10.1111/ejn.12047
47. Ojeda, S. R., Lomniczi, A. & Sandau, U. S. Glial-gonadotrophin hormone (GnRH) neurone interactions in the median eminence and the control of gnrh secretion. *Journal of Neuroendocrinology* (2008). doi:10.1111/j.1365-2826.2008.01712.x
48. Daftary, S. S. & Gore, A. C. Developmental changes in hypothalamic insulin-like growth factor-1: Relationship to gonadotropin-releasing hormone neurons. *Endocrinology* (2003). doi:10.1210/en.2002-221025
49. Daftary, S. S. & Gore, A. C. The hypothalamic insulin-like growth factor-1 receptor and its relationship to gonadotropin-releasing hormones neurones during postnatal development. *J. Neuroendocrinol.* (2004). doi:10.1111/j.0953-8194.2004.01149.x
50. Hiney, J. K., Srivastava, V. K., Pine, M. D. & Dees, W. Les. Insulin-like growth factor-I activates KiSS-1 gene expression in the brain of the prepubertal female rat. *Endocrinology* (2009). doi:10.1210/en.2008-0954
51. DiVall, S. A. *et al.* Divergent roles of growth factors in the GnRH regulation of puberty in mice. *J. Clin. Invest.* 120, 2900–2909 (2010).
52. Taroc, E. Z. M., Lin, J. M., Tulloch, A. J., Jaworski, A. & Forni, P. E. GnRH-1 neural migration from the nose to the brain is independent from slit2, robo3 and NELL2 signaling. *Front. Cell. Neurosci.* (2019). doi:10.3389/fncel.2019.00070
53. Caligioni, C. S. Assessing reproductive status/stages in mice. *Curr. Protoc. Neurosci.* (2009). doi:10.1002/0471142301.nsa04is48
54. Mancini, A. *et al.* LGR4 deficiency results in delayed puberty through impaired Wnt/αcatenin signaling. *JCI Insight* 5, (2020).
55. Harder, E. *et al.* OPLS3: A Force Field Providing Broad Coverage of Drug-like Small Molecules and Proteins. *J. Chem. Theory Comput.* (2016). doi:10.1021/acs.jctc.5b00864
56. Beard, H., Cholleti, A., Pearlman, D., Sherman, W. & Loving, K. A. Applying physics-based scoring to calculate free energies of binding for single amino acid mutations in protein-protein complexes. *PLoS One* (2013). doi:10.1371/journal.pone.0082849

CHAPTER 7

General Discussion

DISCUSSION

The brain is a highly complex structure that is organized in a specific manner to execute many different functions. In order to establish this structural organization, axon guidance cues such as semaphorins provide direction and context-specific signals to cells. This is essential in order to establish distinct functional regions and complex neural circuitry needed for proper brain function. The work described in this thesis focuses on the diverse roles of transmembrane Semaphorin6A (Sema6A) during the crucial stages of the development of the nervous system when directive cues and proper signals are imperative (Fig. 1). The findings provide evidence that Sema6A utilizes a wide range of signaling routes to control a large number of different cellular processes during brain development. Here, the three main findings and implications for future research of the three main topics of this thesis are discussed: Sema6A reverse signaling *in vivo* (**Chapters 3 and 4**), Sema6A *cis* interaction structural domains (**Chapter 5**), and a novel function of Sema6A in the gonadotropin-releasing hormone (GnRH) neuronal system and genetic mutation of Sema6A is causing disease. (**Chapter 6**).

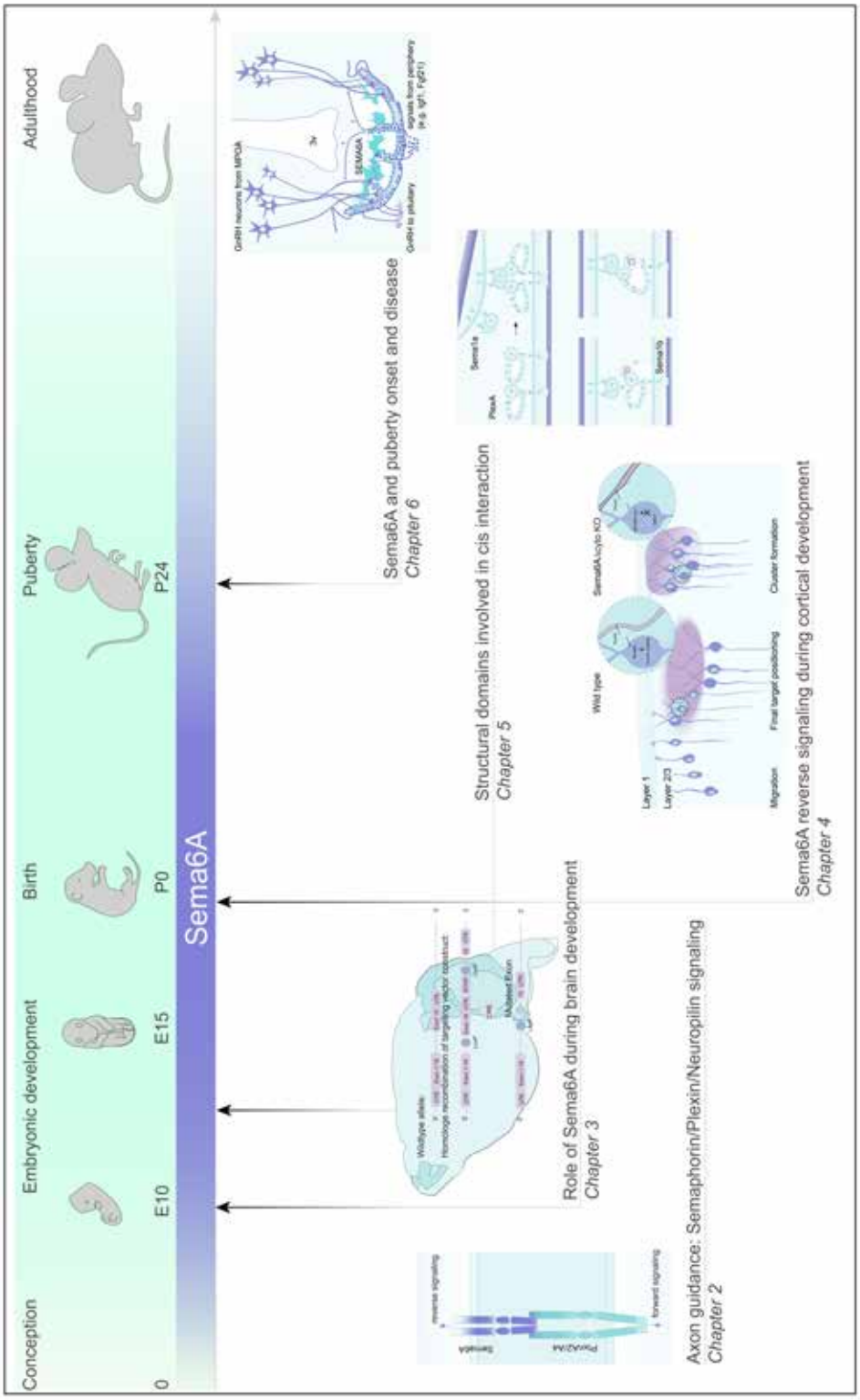
Conception
Embryonic development
Birth
Puberty
Adulthood
0
E10
E15
P0
P24
Sema6A
Axon guidance: Semaphorin/Plexin/Neuropilin signaling
Chapter 2
Role of Sema6A during brain development
Chapter 3
Structural domains involved in cis interaction
Chapter 5
Sema6A and puberty onset and disease
Chapter 6
Sema6A reverse signaling during cortical development
Chapter 4

Figure 1. 'The multifunctional role of Semaphorin6A during brain development and disease'. Schematic overview of diverse roles of transmembrane Sema6A at crucial stages of brain development. The black arrows indicate an approximation of the developmental timepoint studied in **Chapter 2** provides an introduction and description of general features of semaphorin, plexin and neuropilin signaling. In the consecutive chapters of the thesis, the focus is on Sema6A during brain development and to identify the specific role of the intracellular domain of Sema6A (**Chapter 3**). The intracellular domain of Sema6A was found to be important for proper brain development. In addition, the Sema6A reverse signaling pathway was found to be essential for the laminar formation of layer 2/3 of the cerebral cortex (**Chapter 4**). **In Chapter 5**, the interaction of Sema6A *in cis* was found to play a role during growth cone collapse in dorsal root ganglion neurons (DRGs). Future studies are needed to determine the *in vivo* role of the identified *cis* interaction domains. In **Chapter 6**, Sema6A was found to play an important role in the gonadotropin-releasing hormone neuronal system (GnRH). Genetic mutation of Sema6A results in altered brain development and delayed puberty onset. Together, these findings help to understand the complexity of semaphorin signaling pathways, specifically Sema6A, during brain development and disease.

Sema6A reverse signaling

Semaphorins are well known to play important roles during the development of the nervous system (**Chapter 2**). Sema6A is a transmembrane semaphorin and its activation can trigger different effects, and forward and reverse signaling. Therefore, it is imperative to design experimental assays that enable the study of these different functions and to distinguish between them. The multifunctional character of Sema6A is studied in this thesis using novel mouse genetics tools and experimental assays. Results show that in the absence of only the intracellular domain of Sema6A multiple neurodevelopmental defects occur (**Chapter 3**). Following up on these findings, a novel role for Sema6A reverse signaling upon PlexinA2/A4 interaction was found during layer 2/3 neuron positioning and laminar organization in the cerebral cortex (**Chapter 4**). In the following sections the implications of these findings are discussed concerning main themes and open questions in the field of axon guidance proteins. Potential downstream interactors that were identified in **Chapter 4** and possible regulatory mechanisms of Sema6A signaling pathways are discussed. Furthermore, the findings presented in **Chapter 4** suggest compartmentalization of Sema6A and PlxnA2/A4, on the cell soma and dendrites of layer 2/3 neurons respectively. Three modes of interaction and possible mechanisms for local functions of Sema6A and PlxnA2/A4 in specific compartments of the cell are presented in the context of Sema6A reverse signaling during layer 2/3 neuron positioning and laminar organization. Lastly, the potential consequences of layer 2/3 neuron mispositioning and cluster formation on developing neural circuitry and, eventually, brain function are discussed.

Downstream interactors of Sema6A

Sema6A forward and reverse signaling pathways are highly context- and region-specific. In the cerebral cortex, Sema6A reverse signaling was found essential for the proper positioning of layer 2/3 neurons (**Chapter 4**). This is the first record of Sema6A reverse signaling *in vivo*. Previously, *in vitro* assays showed that Sema6A reverse signaling depends on the downstream interaction with Abl to alter the interaction between cells of cerebellar explants triggered by external PlxnA2 [1]. The interaction between cerebellar cells is changed suggesting reverse signaling affects levels of cell adhesion *in vitro* [1]. Together, these findings suggest that Sema6A triggers different signaling pathways depending on specific location and context. It is therefore important to study potential interactors and proteins involved that together are responsible to trigger a context-specific response (**Chapter 4**). In **Chapter 4**, following rescue experiments using a Sema6AΔAbl

construct lacking intracellular binding to Abl, layer 2/3 neuron still display mispositioning and layer malformation phenotypes in Sema6A knockout mice (**Chapter 4**). On the contrary, overexpression of Sema6A with an intact Abl binding domain partially rescues layer 2/3 neuron mispositioning in Sema6A knockout mice. This provides, for the first time, *in vivo* evidence for Sema6A reverse signaling involving the downstream interaction with Abl. Other known downstream interactors of semaphorins and plexins, for example small GTPases, play an important role in intracellular signaling pathway transduction (**Chapter 2**). In the global and phospho-proteome of upper cortical layers, multiple members of a family of Rho GTPases were identified that might be involved in the Sema6A reverse signaling pathway in the cerebral cortex (**Chapter 4**). These include Rho1, Rho12, Srgap1, Cdc42, RhoA, RhoB, RhoF and Rac1. In *Drosophila*, Rho1 mediates Sema1a reverse signaling pathway to regulate the actin cytoskeleton [2,3]. It was suggested that PlexA, or another as of yet unidentified ligand, activates the Sema1a receptor and triggers the reverse signaling pathway [2-10]. Pebble (Rho guanine nucleotide exchange factor GEF) and RhoGAPp190 (GTPase activating protein GAP) also mediate Sema1a reverse signaling through Rho1 regulation [3]. More recently, two Sema1a interacting proteins, varicose (Vari) and cheerio (Cher), were identified and specifically linked to the Sema1a reverse signaling pathway in motor axon pathfinding [2]. There might be a similar modulatory role for of Rho GTPases and associated proteins involved in vertebrate Sema6A reverse signaling. Interestingly, Rho GTPases were recently found to be involved in the regulation of responses to irrelevant guidance signals. Signaling following binding of P190RhoGAP was found to bind the receptor Deleted in Colorectal Cancer (DCC) to suppress guidance molecule Netrin-1. This allows motor axons to exit the embryonic spinal cord [11]. Similar suppressive mechanisms might be involved to regulate the bidirectional properties of Sema6A, possibly enabling forward versus reverse signaling pathway activation in a non-simultaneous manner. For example, a specific role for the extracellular domain of Sema6A was found during the development of the dentate gyrus in the hippocampus independent of the intracellular domain (**Chapter 3**). Granule cells of the infrapyramidal blade are mispositioned in Sema6A knockout mice (*Sema6A*$^{-/-}$), while Sema6AΔcyto mice that lack the intracellular domain of Sema6A (*Ella-Cre;Sema6AΔcyto*$^{\Delta/\Delta}$), display a normal organization suggesting the Sema6A ligand is of importance here possibly activating the forward signaling pathway (**Chapter 3**). The receptor and downstream proteins involved remain to be determined. Proper development of this region of the hippocampus is independent of

the intracellular domain of Sema6A and in wild-type situation the receptor functions of Sema6A might be blocked by suppressive mechanisms involving Rho GTPases. In other systems, forward and reverse signaling pathways might be triggered simultaneously, as described for the ligand and receptor functions of Sema6D during heart development [12]. The question remains if Sema6A exerts a dual, simultaneous role during cortical development (**Chapter 4**). Although we found a clear role for Sema6A reverse signaling, forward signaling might be involved as well. Interestingly, a significant increase in the phosphorylation of the FERM Rho-GEF protein (Farp1) was identified in the phospho-proteome of the defective upper cortical layers of Sema6AΔcyto mice. Farp1 was previously found to promote dendritic growth in spinal motor neurons through the Sema6A/PlexinA4 forward signaling [13]. In motor neurons, Farp1 binds PlexinA4 to promote dendrite extension. The Rho-GEF domain of Farp1 is essential in this process suggesting modulation of small GTPase protein activity. How this modulatory function might affect dendritic morphology in other systems such as the cerebral cortex studied in **Chapter 4,** remains unknown. Future experiments are needed to study the function of Farp1 during cortical development. In summary, Sema6A triggers different signaling pathways depending on specific location and context. *In vivo* evidence shows that in the cortex, Sema6A reverse signaling involves downstream interaction with Abl. Future experiments are needed to study potential other interactors and proteins that together might be responsible for mediating a context-specific response and forward or reverse signaling events.

Transcriptional regulation

Axon guidance protein expression is suggested to be under tight control of transcription factors and regulatory factors, such as miRNAs, to regulate appropriate responses [14,15]. A recent example is transcriptional regulation of PlxnC1 by two LIM-homeodomain transcription factors Lmx1a, Lmx1b and orthodenticle homeobox 2 (Otx2). This mechanism is essential for regulating proper midbrain dopaminergic neuron (mDA) innervation in the striatum [16]. Multiple transcription factors were identified in the phospho-proteome of upper cortical layers (**Chapter 4**). Specifically, phosphorylated Satb2 was upregulated in *Emx1-Cre;Sema6AΔcyto*$^{fl/fl}$ mice, while phosphorylated Ctip2 was downregulated. Interestingly, Satb2 is associated with layer 2/3 neuron positioning and laminar organization [17] which suggests a role in the Sema6A reverse signaling pathway. Possibly, Satb2 is involved in the regulation of downstream interactors of Sema6A reverse signaling (extensively discussed in **Chapter 4**). Alternatively, it was previously suggested that axon guidance

molecules themselves might regulate gene expression by controlling local translation and transcription in specific areas of the cell [18]. Sema6A reverse signaling perhaps influences Satb2 activity and its role in transcription. An example of axon guidance molecules regulating gene expression is for example the regulating of transcription during neurogenesis by Eph-ephrin signaling [19]. In short, transmembrane ephrinBs are cleaved to act as a transcription factor themselves or interact with transcription factors to regulate transcription indirectly. Future studies are needed to determine the mechanisms involved in the regulation of gene expression by axon guidance molecules, and if such mechanisms apply for Sema6A.

Sema6A-dependent laminar organization

In the nervous system, there are several anatomical structures containing neuronal cell subtypes and projections that are organized in particular regions or laminae in order to establish specific connectivity patterns [20–25]. One well-known example is the laminar organization of the cerebral cortex studied in **Chapter 4**. A novel role for the Sema6A receptor and reverse signaling involved in the positioning of layer 2/3 neurons and laminar organization is described here. The proposed model suggests that the presence of PlxnA2/A4 on layer 2/3 neuronal dendrites extending into layer 1 creates a 'non-permissive zone'. At the cell soma membrane Sema6A expression prevents layer 2/3 neurons from entering layer 1. This results in a strict border between the cell sparse layer 1 and the densely populated layer 2/3 of the cerebral cortex. Previously, border organization regulated by axon guidance molecules was found to be important to prevent intermingling of cells during growth and development [26,27]. For example, the border between epithelium and hindbrain segments is restricted by Eph-ephrin signaling to prevent mixing of cells subtypes [28–31]. Eph and ephrin forward and reverse signaling is involved in cell segregation *in vitro* and possibly important to form and maintain sharp borders in epithelial tissues *in vivo* [32]. A similar bidirectional role for Sema6A might be important for border formation between layer 1 and layer 2/3 during cortical development. Other systems where semaphorins are known to contribute to the organization of specific laminae are the retina and hippocampus (**Chapter 2**). In the hippocampus, PlxnA4-positive mossy fibers are prevented from entering Sema6A-expressing regions but are permitted to grow into proximal parts of the CA3 neurons were the repulsive activity of Sema6A is suppressed by PlxnA2 interaction *in cis* [22]. In addition, a recent study shows that forward signaling through PlxinA2 GAP domain activation is dispensable for mossy fiber innervation suggesting alternative signaling routes might be involved [33].

Interestingly, *Emx1-Cre;Sema6AΔcyto*$^{fl/fl}$ mice show mossy fiber derailment suggesting role for the intracellular domain (**Chapter 3**). Hypothetically, the presence of Sema6A in the CA3 region suggests it could act as a receptor in reverse signaling for proper cell organization avoiding local PlxnA2-positive areas. In other words, perhaps Sema6A reverse signaling is important for the initial organization of the stratum pyramidale. Similar to the permissive zone for innervating mossy fibers in the hippocampus, the PlxnA2-positive zone in the cerebral cortex (**Chapter 4**) might be permissive for innervating fibers in layer 1 establishing cortical circuitry.

Compartmentalization

The model presented in **Chapter 4** suggests compartmentalization of axon guidance molecules. The question remains how Sema6A and PlxnA2/A4 expressed in different compartments of the cell might affect each other? In the present study (**Chapter 4**), PlxnA2 is expressed on dendrites and Sema6A is expressed at the cell soma membrane. In this model, PlxnA2 interacts *in trans* with Sema6A in close proximity (Fig. 2A and **Chapter 4**, Figure 18). Next to this potential mode of interaction, two alternatives are discussed here. First, Sema6A and PlxnnA2 might interact *in cis* at the same cell surface, similar as was suggested for the laminar organization in the hippocampus [22]. In the hippocampus, PlxnA2 may create a permissive zone for mossy fibers to innervate specifically at the proximal part of the CA3 neurons. The interaction *in cis* suppresses Sema6A repulsion *in trans* (Fig. 2B). However, in the cerebral cortex this would mean both molecules are expressed in the same cellular compartments (Fig. 2B). Based on our insights (**Chapter 4**) this is an unlikely scenario. In addition, it is known that upon *cis* interaction, the Plexin receptor can be activated in *C. elegans* (Mizomuto & Shen, 2013). However, the question remains if the interaction *in cis* could trigger Sema6A reverse signaling and future experiments are needed to study this. A second alternative mode of interaction, is through posttranslational regulatory processes such as proteolytic cleavage [34–38]. Hypothetically, PlxnA2 is cleaved from the cell surface into the local environment where it interacts only as a ligand with Sema6A expressed on layer 2/3 neurons triggering reverse signaling (Fig. 2C). An overview of the potential modes of interaction discussed are presented in Figure 2.

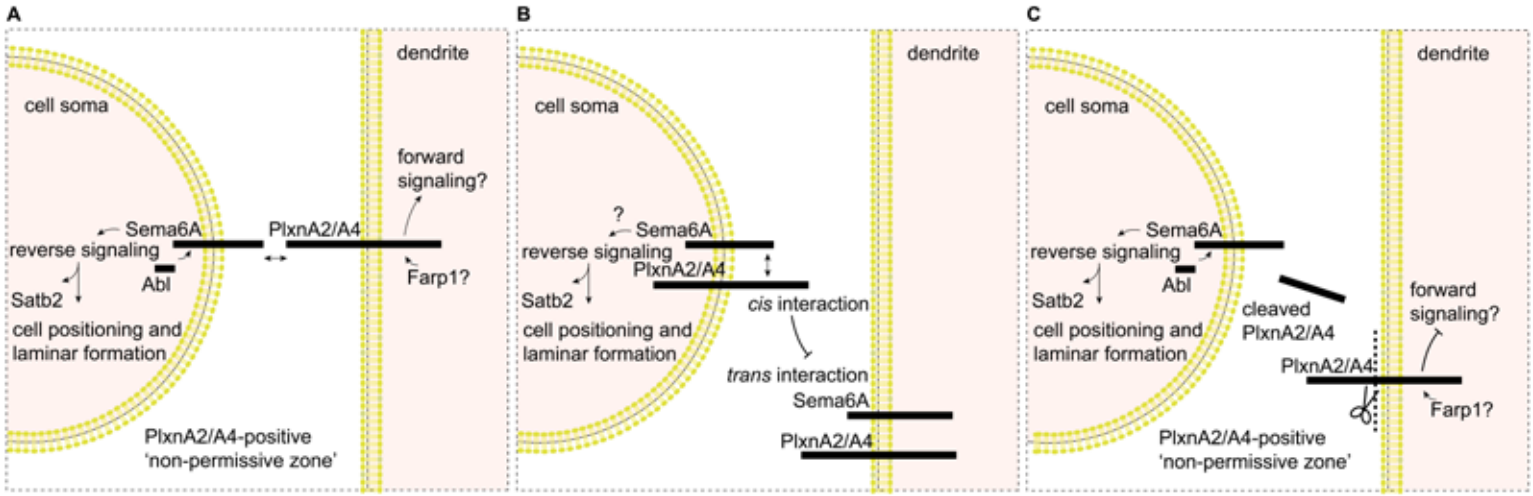

Figure 2. Schematic representation of interaction modes and compartmentalization of Sema6A and PlxnA2/A4 on layer 2/3 neurons in the cerebral cortex. A) Proposed model (**Chapter 4**) where Sema6A-PlexinA2/A4 reverse signaling through the intracellular interaction with Abl triggers cell positioning and laminar organization of layer 2/3 involving Satb2. Note that forward signaling could be activated, possibly regulated by Farp1, through the PlxnA2/A4 receptor. B) Alternative interaction mode *in cis* blocking interaction *in trans* thereby inhibiting forward signaling pathway activation. In this scenario it is unclear if reverse signaling is potentially triggered through intracellular interactions or currently unknown regulatory mechanisms. C) Third interaction mode involving proteolytic cleavage of PlxnA2/A4 from the cellular membrane into the local environment, where layer 2/3 neuron apical dendrites extend, and consequently blocking forward signaling. Reverse signaling through the intracellular domain of Sema6A involving Abl and Satb2 affects neuron positioning and laminar organization of layer 2/3 in the cerebral cortex.

Future directions

In **Chapter 4**, the final experimental directions taken were based on recent findings by Hatanaka et al. (Hatanaka et al., 2019). The proposed model by Hatanaka and authors suggests a role for Sema6A in radial glia cells where it interacts with PlxnA2/A4 expressed on layer 2/3 neurons during radial migration [39]. We set out to test this hypothesis, and to study how these molecules together are responsible for the organization of upper cortical laminae. Considering the suggested role for radial glia, we demonstrate that upon conditional deletion of Sema6A from radial glia cells at E17.5, the moment when layer 2/3 neurons are about to start their radial migration pattern out of the intermediate [40]. At P10 no neuronal mispositioning or laminar disturbance is detected (**Chapter 4**). Interestingly, mispositioning and cluster formation is observed in the medial cortical regions, however this only occurs when layer 2/3 neurons are targeted at E17.5. Since radial glia diminished during the first postnatal weeks [41–43]. To control for this, we analyzed not only at P10 but also at P3, when radial glia fibers are still abundant (**Chapter 4**). The absence of Sema6A in layer 2/3 neurons affects their positioning with non-cell autonomous consequences for neighboring cells. The non-cell autonomous effect can be explained due to the mispositioned neurons in layer 1 that express PlxnA2 on their apical dendrites. This signal enhances the mispositioning for neighboring neurons that still express Sema6A and interact with the mispositioned PlxnA2-positive apical dendrites.

Hatanaka et al. propose in their model that the process of radial migration of layer 2/3 neurons is involved. It is thought that Sema6A gradually increases towards the pial surface, suggesting high expression in radial glia endfeet [39]. The question remains what is the mechanism involved here to enable layer 2/3 neurons to detach from the radial glia, at the appropriate height in the cortex, before reaching the end feet at the pial surface. In other words, how do the layer 2/3 neurons end up in layer 2/3 and not in layer 1 or at the pial surface? Possibly, Sema6A is expressed in a gradient along the radial glial fibers, however future experiments are needed to determine this. According to the model by Hatanaka et al., in the absence of Sema6A, layer 2/3 neurons no longer detach from the radial glia and display an overmigration phenotype at the pial surface [39]. Our insights contrast this hypothesis by finding that layer 2/3 neurons display a branched phenotype with dendrites innervating layer 1 suggesting a post-radial migration effect since dendrites in cortical neurons form after migration ends [44]. Also, early arrived layer 2/3 neurons settle around E18.5-P0 before the defect onset at

P2 (**Chapter 4**, Fig. 9) [45,46] and do not display a 'build-up' of over-migrating cells towards the pial surface as hypothesized by Hatanaka et al. [39]. We did not detect such a phenotype in the absence of the intracellular domain or in the complete absence of Sema6A. Instead, spatiotemporal analysis showed that when most layer 2/3 neurons have settled the initial neuron mispositioning is characterized by an overall shift of layer 2/3 invading the cell sparse layer 1 at P2. At this time, the brain is expanding rapidly and our findings suggest that the normally sharp border between layer 2/3 and layer 1 is no longer controlled in the absence of Sema6A intracellular domain. The increased innervation and growth of layer 1 during at stages seem to coincide with PlxnA2 expression on apical dendrites that creates a non-permissive zone for neurons in layer 2/3 that change their position accordingly. Interestingly, a change in position of layer 2/3 neurons that shift to a slightly deeper position was observed previously [40]. This was found in the lateral cortex specifically while it was not observed in the medial cortex [40]. Since the shift is normally more dramatic in the lateral region of the cortex it could explain why the mispositioning and the largest clusters are found in the lateral cortical regions in the absence of Sema6A. Also, rescue experiments by Hanataka et al., figure 5C', showed that overexpression of PlxnA2 in neurons located in the middle and lower compartment of layer 2/3 creates a cell sparse zone right above [39]. However, authors did not observe this or comment on this finding. Our close observation contributes to the idea that the high expression of PlxnA2, irrespective of its location, acts as a non-permissive zone for neurons. In addition, our findings show a strong and specific expression pattern for PlxnA2 in the apical dendrites of layer 2/3 neurons not previously identified. It would be interesting to continue to study the role of PlxnA2 overexpression in lower cortical regions that cause an alternatively placed non-permissive zone for cortical neurons. To contribute to previous observations, it would important to study the consequences for the local neural circuitry by using for example fiber-specific antibodies in the cerebral cortex. Possibly, fiber innervation increases in the cells sparse zones that are PlxnA2-dependent. Together with studying the compartmentalization of PlxnA2 specifically in the apical dendrites of the neurons in these experiments will provide more information on spatial and temporal dynamics of Sema6A-PlxnA2/A4 signaling in the cerebral cortex.

Considering the multifunctional character of Sema6A and the increasing examples of the diverse signaling pathways involved during development of the cerebral cortex, there may be two temporally distinct sequential

processes at play, combining the publication by Hatanaka et al. [39] together with our findings presented in **Chapter 4** (Fig. 3). When assuming that there are two possibly independent processes at play, the first involves Sema6A expression on radial glia cells triggering forward signaling in layer 2/3 neurons during radial migration, as proposed by Hatanaka et al. [39], which we refer to as the process of **radial glia detachment** (Fig. 3). After detachment from radial glia, we show that Sema6A reverse signaling in layer 2/3 neurons is involved in laminar boundary formation between layer 1 and layer 2/3 during postnatal stages (**Chapter 4**), which we refer to as the process of **laminar organization** (Fig. 3). According to Hatanaka and authors [39], Sema6A-PlxnA2/A4 forward signaling is important for the first process of **radial glia detachment**. Therefore, for future experiments, it would be interesting to study potential differences between Sema6AΔcyto mice, that have an intact Sema6A ligand capable of forward signaling, and Sema6A full knockout mice. Possibly, Sema6A full knockout mice show overmigration and neuronal clusters at the far edge of the pial surface, where layer 2/3 are unable to detach and no longer respond to the repulsive effects of Sema6A in forward signaling. Whereas in Sema6AΔcyto mice, forward signaling is intact and the process of radial glia detachment through the interaction between Sema6AΔcyto and PlxnA2/A4 is possible suggesting the mispositioning of layer 2/3 neurons in Sema6AΔcyto mice involves a different mechanism. Sema6AΔcyto mice show neuronal clusters that are located around the border between layer 1 and layer 2/3 and the affected border organization depends on Sema6A-PlxnA2/A4 reverse signaling during the process of **laminar organization** (**Chapter 4**). Theoretically, defects in either of these processes may result in mispositioning and eventually neuronal clusters. The clustering might be a consequence due to increased layer 1 innervation from postnatal stages onward, affecting connectivity patterns and neural circuitry (**Chapter 4**). Future studies are needed to study potential differences in cluster location between the two mouse lines. In addition, to study the process of **radial glia detachment**, the exact role for PlxnA2 should be determined in more detail. Hatanaka and authors suggest that Sema6A might be specifically expressed in the end feet of radial gia cells [39]. It would be interesting to study the effects of overexpression of PlxnA2 in lower cortical layers that might result in early detachment from radial glia. If Sema6A is indeed highly expressed at the end feet, no early detachment can be observed. To study the process of **laminar organization**, the expected non-permissive zone around PlxnA2 transfected cells in lower cortical regions (based on previously explained close observation of microscopy images Hatanaka et

al.) would argue for the role of PlxnA2 in **laminar organization**. Sema6A-positive neurons are expected to be unable to migrate in this local PlxnA2-positive region. It is possible to test this effect in the cortical layers below layer 2/3 since IHC experiments using antibodies against Sema6A showed expression throughout the different cortical layers (**Chapter 4**). In addition, primary cortical neurons showed Sema6A expression throughout the cell *in vitro* (data not shown). To further confirm the presence of Sema6A, RNAseq data showed that upper cortical layer neurons express *Sema6A* (**Chapter 4**). Considering these findings, it would be interesting to analyze the subcellular distribution of Sema6A and PlxnnA2/A4 in primary cortical neurons in culture. The exposure to high protein expression levels of PlxnA2, for example, using stripe assays, might trigger a repulsive response in cortical neurons expressing Sema6A **Chapter 4**. Lastly, considering the proposed model by Hatanaka and authors, the question remains how reverse signaling in radial glia might be involved. Preliminary IHC data using antibodies against vimentin and nestin, which are markers for radial glial fibers, shows no change in radial glia organization. However, this could be studied in more detail in future experiments. We found clear evidence for the role of Sema6A reverse signaling in our study (**Chapter 4**). Note that the conditional deletion of Sema6A from radial glia did not result in layer 2/3 defects. In contrast, neuronal clusters where only detected in the regions where layer 2/3 neurons conditionally lack Sema6A (**Chapter 4**).

The border between cortical layer 1 and layer 2/3 studied in **Chapter 4** is unique due to the high contrast between cell density of the layers. Therefore, it is not surprising that complex mechanisms are involved to establish the strict border and specific laminar organization. We found a role for Sema6A-PlxnA2/A4 reverse signaling in layer 2/3 neurons for proper laminar organization. This process enables exclusive dendritic growth in layer 1 which is important to maintain this unique and cell sparse cortical layer. A recent study found that PlxnA4 is expressed on interneurons that migrate through the marginal zone (future layer 1) during development [47]. This specific expression pattern might enhance the non-permissive area, together with PlxnA2 on layer 2/3 apical dendrites (**Chapter 4**). In addition to this recent finding, Prox1-positieve neurons and GFAP-positive astrocytes were found in the neural clusters (**Chapter 4**). Similar signaling mechanisms might be involved to establish proper laminar organization. Differences in expression patterns should be compared between different mouse lines. For example, Prox1-positive might be affected in Sema6A full knockout mice. Although Prox1-positive cells are not targeted in Emx1-Cre

crosses, clustering might occur as a consequence of the location of these cells in the upper cortical layers. Therefore, future experiments are needed to identify Sema6A and PlxnA2/A4 expression patterns of these and other cell types that are located in layer 1. The presence of Sema6A might indicate a similar mechanism as compared to layer 2/3 neurons (**Chapter 4**).

The establishment of complex neural circuitry might be affected due to mispositioning of layer 2/3 neurons and laminar disruption (**Chapter 4**). Proper axonal development is essential to establish neural connectivity and brain function. The correct cellular organization in cortical layer 1 and layer 2/3 dependent on Sema6A-PlxnA2/A4 signaling might be essential for the formation of specific neuronal circuitry. Emerging evidence suggests an important role for altered or uncontrolled semaphorin expression and function in neural disease for example in the prefrontal cortex of schizophrenia patients [48]. Specifically, axon guidance defects in Sema6A knockout mice (**Chapter 3**) and the consequences of these developmental changes on neuronal circuitry are associated with altered behavioral phenotypes related to neuropsychiatric disorders [49,50]. In short, Sema6A knockout mice display altered exploratory and habituation behavior, motor learning deficits and an overall hyperactive phenotype that reflects psychotic symptoms in comparison with animal models of schizophrenia disorder [50]. Furthermore, a risk gene associated with neuropsychiatric illness, C11orf46/ADP ribosylation factor like GTPase 14 effector protein (Arl14ep), was identified as a chromatin regulator of Sema6A [51]. C11orf46 haploinsuffiency in patients is associated with transcallosal dysconnectivity and hypoplasia of the corpus callosum. Electroporation of dCas9-SunTag-mediated recruitment of C11orf46, to initialize RNA-guided epigenetic editing of the Sema6A promotor in layer 2/3 transcallosal projection neurons *in utero*, showed 'reversed hyperexpression' of Sema6A at an early stage of development and rescue of transcallosal dysconnectivity [51]. This finding on the epigenetic regulation of Sema6A together with the previously mentioned behavioral studies provide insight into signaling pathways important for proper brain function with a direct link to a during neuropsychiatric disease.

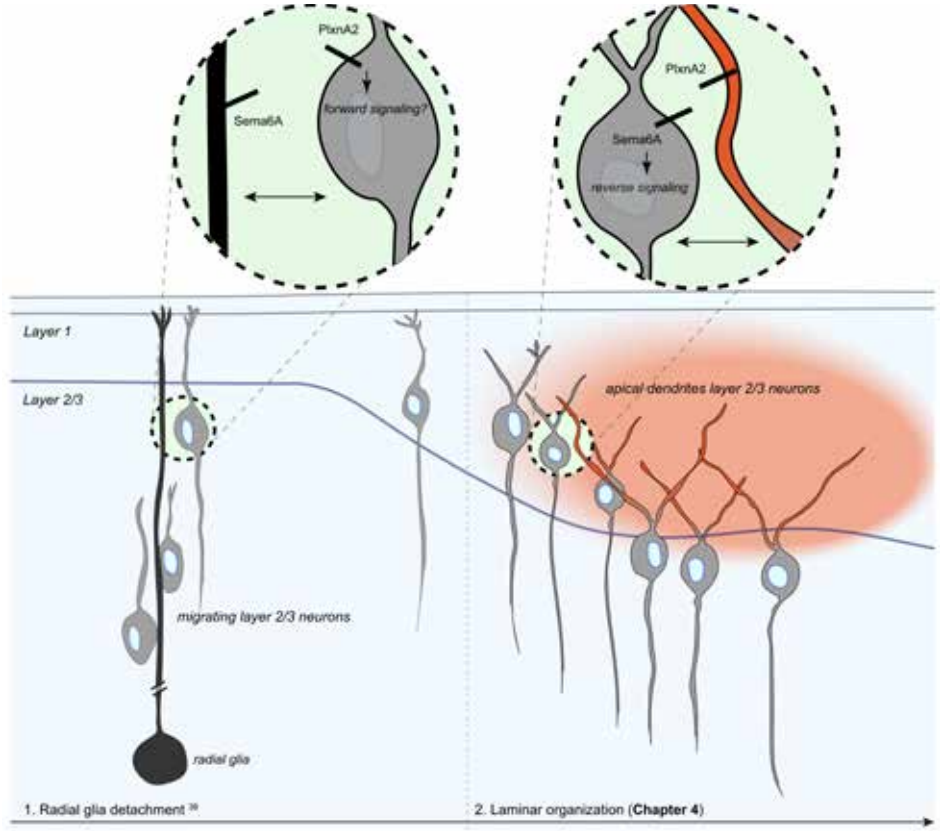

Figure 3. Radial glia detachment [39] and laminar organization (Chapter 4), two temporally distinct processes involved during cortical development. Analyzing novel insights presented in this thesis (**Chapter 4**) in the context of published literature [39], two distinct processes of **radial glia detachment**, as proposed by Hatanaka and authors, and **laminar organization** (**Chapter 4**) are suggested. During **radial glia detachment**, Sema6A expressed on radial glia cells triggers a repulsive, forward signaling response in migrating cortical neurons expressing PlxnA2/A4. Sema6A was suggested to be specifically expressed towards radial glia end feet triggering forward signaling in layer 2/3 of the cortex. After the completion of radial migration and detachment, a strict and precise border is established between layer 1 and layer 2/3 during the process of **laminar organization**. This process is dependent on Sema6A-PlxnA2/A4 reverse signaling in layer 2/3 neurons. PlxnA2/A4 expressed on the apical dendrites triggers reverse signaling through Sema6A expressed on neighboring layer 2/3 neurons resulting in the organization of the border between layer 1 and layer 2/3. This process is important during postnatal growth and expansion of layer 1 that is highly innervated by deeper cortical layers during postnatal stages.

Sema6A *cis* interaction

Over the past decades, crystal structures of distinct semaphorins and plexins, individually and in signaling complexes, have been reported and highlight key residues and structural features required for protein-protein interactions and signaling (**Chapter 2, Box I**). Apart from the bidirectional properties of forward and reverse signaling, Sema6A is known to interact *in cis* thereby inhibiting the interaction *in trans* [52,53]. In **Chapter 5**, two structural domains were found to be specifically involved in *cis* inhibitory functions of invertebrate Sema1a and its vertebrate orthologue Sema6A (**Chapter 5**). These findings, together with previous structural work, greatly contribute to the understanding of how semaphorins interact and may signal, and provide information on the multifunctional character of Sema6A (**Chapter 2 and 5**).

Cis interaction domain identification

In *Drosophila*, transmembrane Sema1b can interact *in cis* with the PlexA receptor thereby regulating signaling outputs (**Chapter 5**). In this study, two independent binding sides were identified for monomeric Sema1b to bind PlexA in a 'side-on' interaction mode. This mode of interaction *in cis* inhibits plexin dimeric engagement and activation *in trans*. Interestingly, invertebrate Sema1b highly resembles vertebrate Sema6A that can interact with PlxnAs *in cis* through the two identified binding domains. Sema1b uniquely shows predominantly monomeric states [54]. It is known that both monomeric and dimeric states of Sema6A are found in solution [55,56]. Sema1a and Sema6A potentially share biological properties and common general functions. Binding of Sema6A to PlxnA4 *in cis*, through the two identified domains that are essential for this interaction, prevents growth cone collapse in dorsal root ganglion (DRG) neurons by Sema6A *in trans* (**Chapter 5**).

To follow up on these findings, a big challenge is to identify the biological role and function of the *cis* interaction in a physiological context. Semaphorin-plexin *cis* interaction has been proposed to act as a threshold-generating mechanism to modulate the signaling response in different cell types during the development of the nervous system [57]. In short, when the cell expresses more receptor than ligand, *cis* interactions block most receptors but not all, the cell can receive signals through the free receptors. The other way around, if there is more ligand than receptor expressed, the cell can send out signals but not receive due to *cis* inhibition. This would mean signaling responses only occur above a certain threshold and enabling

a strong and clear response in an all-or-nothing fashion, exclusively sending or receiving. The interactions *in cis* enable fast responses and signaling dynamics [57]. The Semaphorin-Plexin *cis* interaction inhibits receptor binding *in trans* [52,53]. Interestingly, Semaphorin-Plexin activation *in cis* can lead to Plexin receptor activation in *C. elegans* [58]. Transmembrane semaphorins are known to also function as receptors themselves in reverse signaling (**Chapter 3 and 4**) [59]. How the interaction *in cis* can influence downstream Sema6A reverse signaling remains unclear. It is difficult to disentangle *cis* and *trans* interactions in tissue when both are possibly simultaneously present. There might be a balance between *cis* inhibition and activation events that perhaps rely on distinct types of complexes.

Biological relevance cis interaction

Inhibitory *cis* interactions between Sema6s and PlxnAs have been previously reported to modulate repulsive cell guidance signaling in dorsal root ganglion neurons and other systems such as spinal cord, star burst amacrine cells in the retina and the previously mentioned mossy fiber axons of granule cells in the hippocampus [22,33,52,60–63]. Recent data show that the interaction between PlxnA2 and Sema6A during mossy fiber innervation in the hippocampus is reliant on the *cis* inhibitory effect of Sema6A on the PlxnA2 receptor. In the absence of the PlxnA2 GAP binding domain, which is essential for forward signaling, most mossy fibers innervate normally. This contributes to the idea that Sema6A and PlxnA2 interact *in cis* and thereby create a permissive zone for mossy fibers to innervate [33]. Together with previous work, these data show distinct functional outcomes for *cis* and *trans* binding between semaphorins and plexins. Inhibitory *cis* interactions between semaphorins and plexins contribute to the complexity and multifunctionality of semaphorin ligand-receptor interactions and signaling. **Chapter 5** provides a first insight into the *cis* binding modes of monomeric semaphorins. The characterization of the *cis* interaction in this study provides novel information about this modulatory role contributing to the multifunctional character of semaphorin-plexin signaling pathways.

Cis inhibition in other signaling pathways

Besides semaphorin-plexin signaling, c*is* inhibition is observed in other major signaling systems such as Notch-Delta and ephrin-Eph during neurogenesis and axonal guidance [57,64–67]. Notch signaling is an essential cell communication pathway affecting gene expression and differentiation during development [67]. A well-studied example of *cis* inhibition of Notch signaling is the organization of the dorsal-ventral boundary in the

Drosophila wing [68–70]. The interaction between Notch and Delta proteins *in cis* acts as a regulatory mechanism resulting in the mutual inactivation for Notch and Delta interactions *in trans*. *Cis* inhibition is important for generating a sensitive switch between sending and receiving signaling states involved in cell specification events [71–73]. The Notch signaling pathway consist of multiple receptors and ligands that control the specificity and directionality in different contexts. The combinatorial action of the different molecules adds another level of complexity and diversity of interactions *in cis* and *trans*. Additional modulatory proteins such as Fringe enzymes control and specifiy the Notch signaling pathway further by blocking or promoting the formation of specific ligand-receptor pairs [74]. Eph and ephrin signaling molecules are bidirectional cues interacting *in trans* that can trigger forward and reverse signaling simultaneously [75,76]. The interaction by ephrin *in cis* has a attenuating role on the Eph receptor and inhibits the interaction *in trans* and tyrosine kinase activation [77]. Eph-eprhin signaling also involves alternative mechanisms for pathway attenuation through local expression of Ephs or ephins in specific compartments of the growth cone thereby influencing trajectory choices. This means the Eph receptors are expressed in separate microdomains from ephrin ligands or they can be both expressed in the same domain enabling bidirectional signaling or inhibition *in cis* [78]. How these microdomains are regulated remains unknown. Although *cis* inhibition is observed in multiple signaling systems such as Notch-Delta and Eph-ephrin, *cis* activation is not so well studied. Cis activation potentially expands the signaling capabilities even further. Interestingly, a recent study shows that the *cis* interaction can activate Notch signaling *in vitro* [79]. Different ligands might affect *cis* activation differently, for example, Notch2 shows a strong *cis* activation response compared to Notch1 that triggers *cis* inhibition. RNA sequencing data shows that high Notch1 levels can be found in neuronal stem cells, suggesting *cis* activation might be important in these cells [79]. *Cis* activation adds an additional mode of signaling in the Notch pathway. Other examples of *cis* activation are described for cell adhesion molecules (CAMs) that can be activated *in cis* to induce neurite outgrowth during neuronal development [80,81]. These signaling pathways potentially share common mechanisms for the interaction *in cis* and similar functional consequences.

Future directions

The neuronal system used in this study (**Chapter 5**), is a clear example of the interaction between semaphorin and plexin *in cis*. In the nervous system, dorsal root and sympathetic ganglions express PlxnA4 and only axons of the

sympathetic ganglions are sensitive to Sema6A repulsion. The dorsal root ganglions co-express Sema6A *in cis* to inhibit interaction *in trans* [52,53]. The interaction in *cis* by Sema6A is also found in the hippocampus, retina and oligodendrocytes [22,62,82]. In **Chapter 5**, we find that two identified binding domains are essential for the interaction between Sema6A to PlxnA4 in *cis* to prevent growth cone collapse in dorsal root ganglion neurons by Sema6A in *trans.* The question remains if the interaction *in cis* might trigger downstream signaling events in this system. PlxnA2 binds Sema6A *in trans* when co-expressed *in cis* with PlxnA2 (Perez-Branguli et al., 2016). For future experiments, CRISPR/Cas9 genome editing techniques (Jinek et al., 2012), could be used to study Sema6A and the specific *cis* interaction domains identified in this study *in vivo* (**Chapter 5**). It would be interesting to study the *cis* interaction in the context of the Sema6A reverse signaling pathway. For example, oligodendrocyte precursor cells (OPCs) cultured from Sema6A knockout mice show a maturation delay while PlxnA2 or PlxnA4 knockout mice do not [83]. It was suggested, PlxnA2 and PlxnA4 might both drive the same process and compensate for each other or alternatively, another currently unknown molecule might interact with Sema6A here. In addition, it was found that Sema6A affects the migration pattern of OPCs upon the interaction with PlxnA4 expressed in surrounding cells [82]. The role of interactions *in cis* and reverse signaling could be explored in this system. For example, Sema6A reverse signaling in OPC might affect the cells morphologically during the process of maturation. It would be interesting study the *cis* interaction domains identified here and also to activate the reverse signaling pathway in cultured OPCs to study if the maturation process is restored. To trigger the reverse signaling pathway, intracellular domain of Sema6A can be activated using a tool for chemical induction of multimerization [1]. Further read-outs from these cultured cells could include protein identification using mass spectrometry and proteomics analysis, and single cell RNA sequencing (scRNA-Seq) to profile the transcriptome of dissociated neurons. For future approaches, novel techniques such as spatial transcriptomics are interesting tools to determine the spatial orientation of these molecules during development [84–86].

Novel function of Sema6A in the GnRH system

In addition to studying the bidirectional and regulatory functions of Sema6A, a novel role for this cue was found in the Gonadotropin-releasing hormone (GnRH) system. The GnRH system comprises GnRH neurons that originate in the nasal placode and migrate to the hypothalamus during embryonic development, guided by various axon guidance cues. In the hypothalamus,

GnRH is released at the level of the median eminence (ME) into the blood vessels. GnRH reaches the pituitary and stimulates luteinizing hormone (LH) and follicle-stimulating hormone (FSH) release that reach the gonads and directly stimulate the synthesis of sex steroids, androgens and estrogens to control puberty onset, gametogenesis and estrous cycling [87]. Deficiencies in GnRH neuron function can lead to multiple syndromes that are characterized by low LH and FSH, low concentrations of sex steroids and consequently delayed or absence of puberty onset and reproductive failure [88]. Identifying the underlying genetic defect helps to understand the associated nonreproductive phenotypes seen in patients. Exome sequencing in patients with self-limited delayed puberty (i.e. puberty is delayed for a certain time and will eventually commence) identified a novel pathogenic mutation in the SEMA6A gene. In female mice, the absence of Sema6A affects the GnRH system resulting in delayed puberty onset and disease (**Chapter 6**).

Sema6A is required for GnRH neuron innervation in the ME

Semaphorins are expressed during GnRH neuron migration and their loss results in abnormal migratory paths and reproductive defects (**Chapter 2**). Female Sema6A knockout mice display decreased GnRH axon innervation in the ME during embryonic development and delayed puberty onset. Since Sema6A knockout mice show less innervation by GnRH neurons in the ME, Sema6A might be involved in controlling ME permeability to regulate GnRH secretion into the blood system. Sema6A was found to be highly expressed in regions of the GnRH neuronal system, both embryonically and postnatally. Preliminary data show that in the presence of Sema6A ectodomain permeability of HUVECs cells is increased *in vitro*. Interestingly, recently published work shows that melatonin-concentrating hormone (MCH) neurons can modulate the permeability of the ME barrier. In addition, *Sema6A* was identified in scRNAseq experiments suggesting expression in MCH neurons [89]. Possibly, MCH neurons provide the source of Sema6A affecting permeability of the ME barrier.

Future directions

To further confirm the role of Sema6A in the development of the GnRH system it would be interesting to study Sema6A expression in neurons in the hypothalamus *in vivo*. In addition, antibodies against MECA32 can be used to visualize the vasculature of the ME in Sema6A knockout brain tissue. Alterations in the vasculature of the ME would further suggest a dual role for Sema6A in regulating GnRH neuronal and vascular patterning. Defective

vascularization in Sema6A knockout mice is described for the retina [90]. In this paper, Sema6A downregulation using shRNA constructs in HUVECs cells were found to affect vascular endothelial growth factor receptor 2 (VEGFR2) expression *in vitro*. Sema6A was found to play a critical role in blood vessel development, modulating VEFGR2 which, together with vascular endothelial growth factor (VEGF), is a key regulator of angiogenesis [90–92]. PlxnA2/A4 were found to not be involved in mediating Sema6A-VEGFR2 signaling and other potential interactors for Sema6A remain to be determined. Recombinant Sema6A-Fc rescued the expression of VEGF2 *in vitro*. These data suggest that, Sema6A may possibly affect VEGF and VEGF2 functionality in endothelial cells of the ME thereby reducing permeability. As a consequence, other factors from the periphery might be affected as well for example, Fgf21 that is known act on the vasculature thereby affecting the GnRH neuronal function and secretion [93]. As a final remark, both male and female patients with SEMA6A mutations studied display features of self-limited delayed puberty onset (**Chapter 6**). Therefore, sex specific effects should be studied further in Sema6A mutants, for example, by studying gonadal development in male mice. Delayed puberty phenotypes for male Sema6A knockout mice remain to be determined.

Conclusions

The work described in this thesis outlines three main findings regarding the diverse roles of semaphorins and specifically the multifunctional character of Sema6A (Fig. 1). First, using a novel mouse model to study the multifunctional character of Sema6A, the intracellular domain of Sema6A was found essential for proper development of the brain (**Chapter 3**). The Sema6A reverse signaling pathway was found to play an important role in layer 2/3 neuron positioning and laminar organization during cortical development (**Chapter 4**). Second, in-depth study of the *cis* regulatory function of Sema1a and Sema6A identified two structural domains involved in this form of signaling (**Chapter 5**). Lastly, novel roles for Sema6A were found in the GnRH neuronal system and surrounding vasculature. Altered expression of Sema6A during development caused delayed puberty onset (**Chapter 6**). Taken together, this thesis provides novel insights into signaling pathways of Sema6A and its ability to exert diverse and highly complex functions that are tightly regulated and context-dependent. The knowledge on these signaling pathways, that play a critical role in the nervous system, progress our understanding of the principles of brain development and disease.

REFERENCES

1. Perez-Branguli, F. et al. Reverse Signaling by Semaphorin-6A Regulates Cellular Aggregation and Neuronal Morphology. PLoS One 11, e0158686 (2016).
2. Jeong, S. *et al.* Varicose and cheerio collaborate with pebble to mediate semaphorin-1a reverse signaling in Drosophila. *Proc. Natl. Acad. Sci. U. S. A.* (2017). doi:10.1073/pnas.1713010114
3. Jeong, S., Juhaszova, K. & Kolodkin, A. L. The Control of Semaphorin-1a-Mediated Reverse Signaling by Opposing Pebble and RhoGAPp190 Functions in Drosophila. *Neuron* (2012). doi:10.1016/j.neuron.2012.09.018
4. Pecot, M. Y. *et al.* Multiple Interactions Control Synaptic Layer Specificity in the Drosophila Visual System. *Neuron* (2013). doi:10.1016/j.neuron.2012.11.007
5. Sweeney, L. B. *et al.* Secreted semaphorins from degenerating larval ORN axons direct adult projection neuron dendrite targeting. *Neuron* (2011). doi:10.1016/j.neuron.2011.09.026
6. Cafferty, P., Yu, L., Long, H. & Rao, Y. Semaphorin-1a functions as a guidance receptor in the Drosophila visual system. *J. Neurosci.* (2006). doi:10.1523/JNEUROSCI.3845-05.2006
7. Godenschwege, T. A., Hu, H., Shan-Crofts, X., Goodman, C. S. & Murphey, R. K. Bi-directional signaling by semaphorin 1a during central synapse formation in Drosophila. *Nat. Neurosci.* (2002). doi:10.1038/nn976
8. Komiyama, T., Sweeney, L. B., Schuldiner, O., Garcia, K. C. & Luo, L. Graded Expression of Semaphorin-1a Cell-Autonomously Directs Dendritic Targeting of Olfactory Projection Neurons. *Cell* (2007). doi:10.1016/j.cell.2006.12.028
9. Yu, L., Zhou, Y., Cheng, S. & Rao, Y. Plexin A-Semaphorin-1a Reverse Signaling Regulates Photoreceptor Axon Guidance in Drosophila. *J. Neurosci.* (2010). doi:10.1523/JNEUROSCI.1494-10.2010
10. Hernandez-Fleming, M., Rohrbach, E. W. & Bashaw, G. J. Sema-1a Reverse Signaling Promotes Midline Crossing in Response to Secreted Semaphorins. *Cell Rep.* (2017). doi:10.1016/j.celrep.2016.12.027
11. Bonanomi, D. *et al.* p190RhoGAP Filters Competing Signals to Resolve Axon Guidance Conflicts. *Neuron* (2019). doi:10.1016/j.neuron.2019.02.034
12. Toyofuku, T. *et al.* Guidance of myocardial patterning in cardiac development by Sema6D reverse signalling. *Nat. Cell Biol.* (2004). doi:10.1038/ncb1193
13. Zhuang, B., Su, Y. S. & Sockanathan, S. FARP1 Promotes the Dendritic Growth of Spinal Motor Neuron Subtypes through Transmembrane Semaphorin6A and PlexinA4 Signaling. *Neuron* (2009). doi:10.1016/j.neuron.2008.12.022
14. Jongbloets, B. C. & Pasterkamp, R. J. Semaphorin signalling during development. Development 141, 3292–3297 (2014).

15. Polleux, F., Ince-Dunn, G. & Ghosh, A. Transcriptional regulation of vertebrate axon guidance and synapse formation. *Nature Reviews Neuroscience* (2007). doi:10.1038/nrn2118
16. Chabrat, A. *et al.* Transcriptional repression of Plxnc1 by Lmx1a and Lmx1b directs topographic dopaminergic circuit formation. *Nat. Commun.* (2017). doi:10.1038/s41467-017-01042-0
17. Zhang, L. et al. Satb2 Is Required for Dendritic Arborization and Soma Spacing in Mouse Cerebral Cortex. Cereb. Cortex 22, 1510–1519 (2012).
18. Russell, S. A. & Bashaw, G. J. Axon guidance pathways and the control of gene expression. *Developmental Dynamics* (2018). doi:10.1002/dvdy.24609
19. Laussu, J., Khuong, A., Gautrais, J. & Davy, A. Beyond boundaries - Eph: Ephrin signaling in neurogenesis. *Cell Adhesion and Migration* (2014). doi:10.4161/19336918.2014.969990
20. Sanes, J. R. & Yamagata, M. Formation of lamina-specific synaptic connections. *Curr. Opin. Neurobiol.* (1999). doi:10.1016/S0959-4388(99)80010-5
21. Yamagata, M., Weiner, J. A. & Sanes, J. R. Sidekicks: Synaptic adhesion molecules that promote lamina-specific connectivity in the retina. *Cell* (2002). doi:10.1016/S0092-8674(02)00910-8
22. Suto, F. *et al.* Interactions between Plexin-A2, Plexin-A4, and Semaphorin 6A Control Lamina-Restricted Projection of Hippocampal Mossy Fibers. *Neuron* (2007). doi:10.1016/j.neuron.2007.01.028
23. Poskanzer, K., Needleman, L. A., Bozdagi, O. & Huntley, G. W. N-cadherin regulates ingrowth and laminar targeting of thalamocortical axons. *J. Neurosci.* (2003). doi:10.1523/jneurosci.23-06-02294.2003
24. Inoue, A. & Sanes, J. R. Lamina-specific connectivity in the brain: Regulation by N-cadherin, neurotrophins, and glycoconjugates. *Science (80-.).* (1997). doi:10.1126/science.276.5317.1428
25. Mumm, J. S. *et al.* Laminar circuit formation in the vertebrate retina. *Progress in Brain Research* (2005). doi:10.1016/S0079-6123(04)47012-5
26. Mellitzer, G., Xu, Q. & Wilkinson, D. G. Eph receptors and ephrins restrict cell intermingling and communication. *Nature* (1999). doi:10.1038/21907
27. Xu, Q., Mellitzer, G., Robinson, V. & Wilkinson, D. G. In vivo cell sorting in complementary segmental domains mediated by Eph receptors and ephrins. *Nature* (1999). doi:10.1038/20452
28. Kemp, H. A., Cooke, J. E. & Moens, C. B. EphA4 and EfnB2a maintain rhombomere coherence by independently regulating intercalation of progenitor cells in the zebrafish neural keel. *Dev. Biol.* (2009). doi:10.1016/j.ydbio.2008.12.010
29. Cooke, J. E., Kemp, H. A. & Moens, C. B. EphA4 is required for cell adhesion and rhombomere-boundary formation in the zebrafish. *Curr. Biol.* (2005). doi:10.1016/j.cub.2005.02.019

30. Terriente, J., Gerety, S. S., Watanabe-Asaka, T., Gonzalez-Quevedo, R. & Wilkinson, D. G. Signalling from hindbrain boundaries regulates neuronal clustering that patterns neurogenesis. *Dev.* (2012). doi:10.1242/dev.080135
31. Cayuso, J., Xu, Q., Addison, M. & Wilkinson, D. G. Actomyosin regulation by eph receptor signaling couples boundary cell formation to border sharpness. *Elife* (2019). doi:10.7554/eLife.49696
32. Wu, Z., Ashlin, T. G., Xu, Q. & Wilkinson, D. G. Role of forward and reverse signaling in Eph receptor and ephrin mediated cell segregation. *Exp. Cell Res.* (2019). doi:10.1016/j.yexcr.2019.04.040
33. Zhao, X.-F. et al. PlexinA2 Forward Signaling through Rap1 GTPases Regulates Dentate Gyrus Development and Schizophrenia-like Behaviors. Cell Rep. 22, 456–470 (2018).
34. O'Donnell, M., Chance, R. K. & Bashaw, G. J. Axon growth and guidance: Receptor regulation and signal transduction. *Annual Review of Neuroscience* (2009). doi:10.1146/annurev.neuro.051508.135614
35. Ch'ng, E. S. & Kumanogoh, A. Roles of Sema4D and Plexin-B1 in tumor progression. Mol. Cancer 9, 251 (2010).
36. Ito, T. et al. Estrogen-Dependent Proteolytic Cleavage of Semaphorin 4D and Plexin-B1 Enhances Semaphorin 4D-Induced Apoptosis during Postnatal Vaginal Remodeling in Pubescent Mice. PLoS One 9, e97909 (2014).
37. St. Clair, R. M. et al. Fyn-dependent phosphorylation of PlexinA1 and PlexinA2 at conserved tyrosines is essential for zebrafish eye development. FEBS J. 285, 72–86 (2018).
38. Kellermeyer, R. *et al.* Proteolytic cleavage of Slit by the Tolkin protease converts an axon repulsion cue to an axon growth cue in vivo. *Development* (2020). doi:10.1242/dev.196055
39. Hatanaka, Y. *et al.* Semaphorin 6A–Plexin A2/A4 Interactions with Radial Glia Regulate Migration Termination of Superficial Layer Cortical Neurons. *iScience* (2019). doi:10.1016/j.isci.2019.10.034
40. Yoshinaga, S. *et al.* Comprehensive Characterization of Migration Profiles of Murine Cerebral Cortical Neurons During Development Using FlashTag Labeling. *SSRN Electron. J.* (2020). doi:10.2139/ssrn.3696753
41. Schmechel, D. E. & Rakic, P. A golgi study of radial glial cells in developing monkey telencephalon: Morphogenesis and transformation into astrocytes. *Anat. Embryol. (Berl).* (1979). doi:10.1007/BF00300010
42. Tramontin, A. D., García-Verdugo, J. M., Lim, D. A. & Alvarez-Buylla, A. Postnatal development of radial glia and the ventricular zone (VZ): A continuum of the neural stem cell compartment. *Cerebral Cortex* (2003). doi:10.1093/cercor/13.6.580

43. Voigt, T. Development of glial cells in the cerebral wall of ferrets: Direct tracing of their transformation from radial glia into astrocytes. *J. Comp. Neurol.* (1989). doi:10.1002/cne.902890106
44. Whitford, K. L., Dijkhuizen, P., Polleux, F. & Ghosh, A. Molecular control of cortical dendrite development. *Annual Review of Neuroscience* (2002). doi:10.1146/annurev.neuro.25.112701.142932
45. Chai, X. *et al.* Reelin induces branching of neurons and radial glial cells during corticogenesis. *Cereb. Cortex* (2015). doi:10.1093/cercor/bhu216
46. Ignacio, M. P. D., Kimm, E. J., Kageyama, G. H., Yu, J. & Robertson, R. T. Postnatal migration of neurons and formation of laminae in rat cerebral cortex. *Anat. Embryol. (Berl).* (1995). doi:10.1007/BF00186782
47. Limoni, G., Murthy, S., Jabaudon, D., Dayer, A. & Niquille, M. PlexinA4-Semaphorin3A-mediated crosstalk between main cortical interneuron classes is required for superficial interneuron lamination. Cell Rep. 34, 108644 (2021).
48. Gilabert-Juan, J. *et al.* Semaphorin and plexin gene expression is altered in the prefrontal cortex of schizophrenia patients with and without auditory hallucinations. *Psychiatry Res.* (2015). doi:10.1016/j.psychres.2015.07.074
49. Rünker, A. E. et al. Mutation of Semaphorin-6A Disrupts Limbic and Cortical Connectivity and Models Neurodevelopmental Psychopathology. PLoS One 6, e26488 (2011).
50. Håkansson, K. et al. Semaphorin 6A knockout mice display abnormalities across ethologically-based topographies of exploration and in motor learning. Neurosci. Lett. 641, 70–76 (2017).
51. Peter, C. J. et al. In vivo epigenetic editing of Sema6a promoter reverses transcallosal dysconnectivity caused by C11orf46/Arl14ep risk gene. Nat. Commun. 10, 4112 (2019).
52. Haklai-topper, L., Mlechkovich, G., Savariego, D., Gokhman, I. & Yaron, A. Cis interaction between Semaphorin6A and Plexin-A4 modulates the repulsive response to Sema6A. EMBO J. 29, 2635–2645 (2010).
53. Suto, F. *et al.* Plexin-A4 mediates axon-repulsive activities of both secreted and transmembrane semaphorins and plays roles in nerve fiber guidance. *J. Neurosci.* (2005). doi:10.1523/JNEUROSCI.4480-04.2005
54. Rozbesky, D. et al. Diversity of oligomerization in Drosophila semaphorins suggests a mechanism of functional fine-tuning. Nat. Commun. 10, 3691 (2019).
55. Janssen, B. J. C. et al. Structural basis of semaphorin–plexin signalling. Nature 467, 1118–1122 (2010).
56. Nogi, T. Structural basis for semaphorin signalling through the plexin receptor. 3–9 (2010). doi:10.1038/nature09473
57. Yaron, A. & Sprinzak, D. The cis side of juxtacrine signaling: a new role in the development of the nervous system. Trends Neurosci. 35, 230–239 (2012).

58. Mizumoto, K. & Shen, K. Interaxonal Interaction Defines Tiled Presynaptic Innervation in C. elegans. *Neuron* (2013). doi:10.1016/j.neuron.2012.12.031
59. Yu, L., Zhou, Y., Cheng, S. & Rao, Y. Plexin A-Semaphorin-1a reverse signaling regulates photoreceptor axon guidance in Drosophila. *J. Neurosci.* (2010). doi:10.1523/JNEUROSCI.1494-10.2010
60. Andermatt, I. et al. Semaphorin 6B acts as a receptor in post-crossing commissural axon guidance. Development 141, 3709–3720 (2014).
61. Renaud, J. et al. Plexin-A2 and its ligand, Sema6A, control nucleus-centrosome coupling in migrating granule cells. Nat. Neurosci. 11, 440–449 (2008).
62. Sun, L. O. et al. On and Off Retinal Circuit Assembly by Divergent Molecular Mechanisms. Science (80-.). 342, 1241974–1241974 (2013).
63. Tawarayama, H., Yoshida, Y., Suto, F., Mitchell, K. J. & Fujisawa, H. Roles of Semaphorin-6B and Plexin-A2 in Lamina-Restricted Projection of Hippocampal Mossy Fibers. J. Neurosci. 30, 7049–7060 (2010).
64. Stahl, B., Müller, B., von Boxberg, Y., Cox, E. C. & Bonhoeffer, F. Biochemical characterization of a putative axonal guidance molecule of the chick visual system. *Neuron* (1990). doi:10.1016/0896-6273(90)90227-7
65. Dudanova, I. & Klein, R. The Axon's Balancing Act: Cis- and trans-Interactions between Ephs and Ephrins. *Neuron* (2011). doi:10.1016/j.neuron.2011.06.030
66. Del Álamo, D., Rouault, H. & Schweisguth, F. Mechanism and significance of cis-inhibition in notch signalling. *Current Biology* (2011). doi:10.1016/j.cub.2010.10.034
67. Artavanis-Tsakonas, S., Rand, M. D. & Lake, R. J. Notch signaling: Cell fate control and signal integration in development. *Science* (1999). doi:10.1126/science.284.5415.770
68. De Celis, J. F. & Bray, S. Feed-back mechanisms affecting Notch activation at the dorsoventral boundary in the Drosophila wing. *Development* (1997).
69. Brückner, K., Pasquale, E. B. & Klein, R. Tyrosine phosphorylation of transmembrane ligands for Eph receptors. *Science (80-.).* (1997). doi:10.1126/science.275.5306.1640
70. Glittenberg, M., Pitsouli, C., Garvey, C., Delidakis, C. & Bray, S. Role of conserved intracellular motifs in Serrate signalling, cis-inhibition and endocytosis. *EMBO J.* (2006). doi:10.1038/sj.emboj.7601337
71. Jacobsen, T. L., Brennan, K., Arias, A. M. & Muskavitch, M. A. T. Cis-interactions between Delta and Notch modulate neurogenic signalling in Drosophila. *Development* (1998).
72. Sprinzak, D. *et al.* Cis-interactions between Notch and Delta generate mutually exclusive signalling states. *Nature* (2010). doi:10.1038/nature08959
73. Jolly, M. K. *et al.* Operating principles of Notch-Delta-Jagged module of cell-cell communication. *New J. Phys.* (2015). doi:10.1088/1367-2630/17/5/055021

74. Panin, V. M., Papayannopoulos, V., Wilson, R. & Irvine, K. D. Fringe modulates Notch-ligand interactions. *Nature* (1997). doi:10.1038/43191
75. Holland, S. J. *et al.* Bidirectional signalling through the EPH-family receptor Nuk and its transmembrane ligands. *Nature* (1996). doi:10.1038/383722a0
76. Murai, K. K. & Pasquale, E. B. 'Eph'ective signaling: Forward, reverse and crosstalk. *Journal of Cell Science* (2003). doi:10.1242/jcs.00625
77. Carvalho, R. F. *et al.* Silencing of EphA3 through a cis interaction with ephrinA5. *Nat. Neurosci.* (2006). doi:10.1038/nn1655
78. Kao, T. J. & Kania, A. Ephrin-Mediated cis-Attenuation of Eph Receptor Signaling Is Essential for Spinal Motor Axon Guidance. *Neuron* (2011). doi:10.1016/j.neuron.2011.05.031
79. Nandagopal, N., Santat, L. A. & Elowitz, M. B. Cis-activation in the Notch signaling pathway. Elife 8, (2019).
80. Bechara, A. *et al.* FAK-MAPK-dependent adhesion disassembly downstream of L1 contributes to semaphorin3A-induced collapse. *EMBO J.* (2008). doi:10.1038/emboj.2008.86
81. Sonderegger, P. & Rathjen, F. G. Regulation of axonal growth in the vertebrate nervous system by interactions between glycoproteins belonging to two subgroups of the immunoglobulin superfamily. *Journal of Cell Biology* (1992). doi:10.1083/jcb.119.6.1387
82. Okada, A. & Tomooka, Y. A role of Sema6A expressed in oligodendrocyte precursor cells. *Neurosci. Lett.* (2013). doi:10.1016/j.neulet.2013.01.026
83. Bernard, F. et al. Role of transmembrane semaphorin Sema6A in oligodendrocyte differentiation and myelination. Glia 60, 1590–1604 (2012).
84. Crosetto, N., Bienko, M. & Van Oudenaarden, A. Spatially resolved transcriptomics and beyond. *Nature Reviews Genetics* (2015). doi:10.1038/nrg3832
85. Lein, E., Borm, L. E. & Linnarsson, S. The promise of spatial transcriptomics for neuroscience in the era of molecular cell typing. *Science* (2017). doi:10.1126/science.aan6827
86. Asp, M., Bergenstråhle, J. & Lundeberg, J. Spatially Resolved Transcriptomes–Next Generation Tools for Tissue Exploration. *BioEssays* (2020). doi:10.1002/bies.201900221
87. Ojeda, S. R. *et al.* Minireview: The neuroendocrine regulation of puberty: Is the time ripe for a systems biology approach? *Endocrinology* (2006). doi:10.1210/en.2005-1136
88. Cariboni, A., Oleari, R., Lettieri, A., Paganoni, A. & Zanieri, L. Semaphorin signalling in GnRH neurons: from development to disease. *Neuroendocrinology* (2018). doi:10.1159/000495916
89. Jiang, H. *et al.* MCH Neurons Regulate Permeability of the Median Eminence Barrier. *Neuron* (2020). doi:10.1016/j.neuron.2020.04.020

90. Segarra, M. *et al.* Semaphorin 6A regulates angiogenesis by modulating VEGF signaling. *Blood* (2012). doi:10.1182/blood-2012-02-410076
91. Greenberg, D. A. & Jin, K. From angiogenesis to neuropathology. *Nature* (2005). doi:10.1038/nature04481
92. Langlet, F. *et al.* Tanycytic VEGF-A boosts blood-hypothalamus barrier plasticity and access of metabolic signals to the arcuate nucleus in response to fasting. *Cell Metab.* (2013). doi:10.1016/j.cmet.2013.03.004
93. Xu, C. *et al.* KLB , encoding αKlotho, is mutated in patients with congenital hypogonadotropic hypogonadism . *EMBO Mol. Med.* (2017). doi:10.15252/emmm.201607376

Addendum

Samenvatting in het Nederlands

De multifunctionele rol van Semaforine6A tijdens de ontwikkeling van de hersenen en hersenziekten

Voorwaarts met tegengestelde signalering

De hersenen zijn het meest complexe en veelzijdige orgaan van het menselijk lichaam. Denk aan dagelijkse dingen zoals bewegen, horen en zien, maar ook hogere cognitieve functies zoals taal, geheugen en intelligentie, de hersenen sturen dit allemaal aan. De hersenen zijn opgebouwd uit verschillende gebieden en bevatten miljarden hersencellen. Tijdens de ontwikkeling van de hersenen moeten de hersencellen allemaal op de juiste plek komen en verbindingen met elkaar maken. Via lange en korte routes verbinden de hersencellen zich met elkaar om netwerken te vormen, zodat belangrijke informatie naar de juiste plek gestuurd kan worden. Dit proces wordt nauwkeurig gereguleerd om ervoor te zorgen dat alle hersencellen en verbindingen goed aangelegd en georganiseerd worden. De hersencellen hebben een vertakkende structuur die vergeleken kan worden met de groeiende takken van een boom, deze takken worden axonen en dendrieten genoemd. Verschillende stoffen geven signalen aan de vertakkingen en zorgen dat ze de juiste kant op groeien, zodat alles op de juiste plek komt. Alle verbindingen samen vormen complexe circuits die nodig zijn voor een goede hersenfunctie. Dit principe wordt in het Engels 'axon guidance' genoemd, in het Nederlands 'axon begeleiding' of 'sturing'. Door middel van wetenschappelijk onderzoek wordt stukje bij beetje meer informatie verzameld over de vorming en organisatie van de hersenen. Deze kennis draagt bij aan het begrijpen van het functioneren van de hersenen en de problemen die kunnen leiden tot hersenziekten en ontwikkelingsstoornissen zoals schizofrenie en autisme.

Semaforines zijn eiwitten die een belangrijke rol hebben in het hierboven genoemde proces van axon guidance. Deze eiwitten functioneren als begeleidende stoffen die sturende en richtinggevende signalen geven waarmee de hersencellen op de juiste plek terecht komen, en zich aan elkaar kunnen verbinden.

Het werk dat in dit proefschrift wordt beschreven richt zich op het semaforine eiwit genaamd semaforine6A (Sema6A). Dit eiwit speelt een onmisbare rol tijdens de ontwikkeling van de hersenen. Sema6A is een

bijzonder eiwit, omdat het veel verschillende functies kan uitvoeren. Zo kan het signalen doorgeven aan andere cellen in zogenaamde 'voorwaartse signalering' ('forward signaling'), maar ook signalen ontvangen op de cel waar Sema6A zich bevindt en dit direct verwerken in 'tegengestelde signalering' ('reverse signaling'). Het onderzoek in dit proefschrift richt zich op de cruciale momenten van de ontwikkeling van de hersenen wanneer sturende signalen en aanwijzingen noodzakelijk zijn. De bevindingen leveren bewijs dat Sema6A een multifunctioneel eiwit is dat tijdens de ontwikkeling van de hersenen verschillende signaleringsfuncties uitvoert en laten zien in welke delen van de hersenen dit gebeurd. De functies van Sema6A zijn essentieel om ervoor te zorgen dat aanleg van de hersenen op een juiste manier verloopt.

Er zijn in dit proefschrift een aantal belangrijke bevindingen beschreven met betrekking tot de diverse rollen van semaforines met als hoofddoel het in kaart brengen van het multifunctionele karakter van Sema6A tijdens de ontwikkeling van de hersenen. De belangrijkste bevindingen zijn in drie hoofdonderwerpen in te delen: 1) de rol van tegengestelde signalering, 2) de identificatie van nieuwe domeinen betrokken bij Sema6A signalering, 3) de consequenties van een genetische mutatie van Sema6A.

Ten eerste, wetenschappelijk onderzoek laat zien dat Sema6A een duidelijke functie heeft in axon guidance via andere eiwitten PlexineA2 (PlxnA2) en PlexineA4 (PlxnA4) in 'voorwaartse signalering'. In dit proefschrift ligt de nadruk juist op een minder bekende functie van signalering door Sema6A zelf, de 'tegengestelde signalering' (Hoofdstukken 2 en 3). Met behulp van een nieuw muismodel is vastgesteld dat een specifieke component van het Sema6A eiwit, dat onder andere nodig is voor tegengestelde signalering, essentieel is voor een goede ontwikkeling van een aantal hersenengebieden (Hoofdstuk 2). We leren hieruit op welke locatie in de hersenen de tegengestelde signalering van het eiwit van belang is, en waar niet. De hersenschors is een locatie waar een nieuwe rol voor Sema6A tegengestelde signalering werd gevonden. Dit gebied omvat de buitenkant van de hersenen en bestaat uit 6 lagen waar zich in elke laag een ander soort hersencellen met bijbehorende functies bevinden (zie ook de grafische weergave op de cover van dit proefschrift). Voor een juiste organisatie blijven de hersencellen normaal gesproken binnen de grenzen van elke laag. Wanneer door een defect de tegengestelde signalering niet langer mogelijk is, komen de hersencellen niet op de goede plek in de twee bovenste lagen van de hersenschors. De grens tussen laag 1 en laag 2

blijkt bepaald te worden door PlxnA2 en PlxnA4 die Sema6A tegengestelde signalering activeren. Dit proces is van essentieel belang voor een juiste organisatie van de hersencellen in de hersenschors tijdens de ontwikkeling (Hoofdstuk 3).

Ten tweede, het Sema6A eiwit is opgebouwd uit verschillende domeinen die verschillende functies hebben en bijdragen aan het multifunctionele karakter van het eiwit. In hoofdstuk 4, zijn twee, tot nu toe onbekende, domeinen van Sema1a en Sema6A geïdentificeerd. We hebben vastgesteld dat deze domeinen van belang zijn bij het uitvoeren van nóg een vorm van signalering, namelijk '*in cis*'. *Cis* is latijn voor 'aan deze kant' en betekent dat het Sema6A en PlxnA2 of PlxnA4 eiwit zich naast elkaar op dezelfde hersencel bevinden. Deze vorm van signalering kan ervoor zorgen dat plexine eiwitten geblokkeerd worden en de voorwaartse signalering op andere hersencellen *in trans (*Latijn voor 'aan de andere kant') in de omgeving niet mogelijk is. Dit is een vorm van regulatie van de signaleringprocessen die ervoor zorgt dat de signalering alleen plaatsvindt op het juiste moment (Hoofdstuk 4).

Ten derde, wanneer Sema6A afwezig is in de hersenen blijkt dit gevolgen te hebben voor de ontwikkeling van de hersenen en te leiden tot een hersenziekte. Bij patiënten blijkt een nog niet eerder beschreven genetische mutatie (een afwijking in het erfelijk materiaal) van het Sema6A gen in het hersengebied van het hormoon genaamd gonadotropine-releasing hormone (GnRH) problemen te geven. Bij patiënten leidt deze mutatie tot een vertraagde ontwikkeling van de puberteit of zelfs tot volledige afwezigheid hiervan en dit heeft gevolgen voor het functioneren van het voortplantingssysteem (Hoofdstuk 5). In dit hoofdstuk wordt de rol van Sema6A onderzocht in patiënten en met behulp van diermodellen in kaart gebracht wat er precies mis gaat in de hersenen. Dit onderzoek geeft nieuwe inzichten in hersenaandoeningen die gevolgen hebben voor ontwikkeling van puberteit en kan bijdragen aan het ontwikkelen van behandelingen voor patiënten.

Samengevat levert dit proefschrift een belangrijke bijdrage aan ons begrip van het vermogen van Sema6A, als multifunctioneel eiwit, om diverse en zeer complexe functies uit te oefenen die strak gereguleerd en per hersengebied verschillend zijn. Sema6A speelt een belangrijke rol tijdens de ontwikkeling van de hersenen en het in kaart brengen van deze functies is van cruciaal belang om te kunnen begrijpen hoe de hersenen werken en hoe hersenziektes zich kunnen ontwikkelen.

Dankwoord

Iedereen die betrokken is geweest bij mijn onderzoek wil ik bedanken. Ik noem een aantal mensen in het bijzonder.

Professor Pasterkamp, Jeroen, bedankt voor alle mogelijkheden, kansen, samenwerkingen en gesprekken. Het bezoek aan een groot aantal congressen, met de presentaties op AXON2019 en CSHL2020 als absolute hoogtepunten, blijven me voor altijd bij. Mijn ervaringen als PhD student in het Pasterkamplab hebben me ontzettend veel gebracht en ze hebben me gevormd als wetenschapper. Ik ben trots dat het onderzoek naar Sema6A blijft doorgaan.

Dr. Ramakers, Geert, na mijn bachelor Biologie wilde ik meer weten van de neurowetenschappen en nam ik contact met je op. Dankzij jou was in 2012 mijn introductie op de afdeling Translationele Neurowetenschappen een feit. Ik mocht binnen het PhD project van Bart Jongbloets kijken naar de morfologie van Sema7A knockout neuronen en dat was een geweldig leuke ervaring. Dankzij deze stage, en jouw colleges bij BMW en die van Prof. Albert Postma bij Psychologie, was de keuze voor de master opleiding Neuroscience and Cognition snel gemaakt. Daarom vind ik het ontzettend leuk dat je nu mijn copromotor bent geworden. Veel dank voor je input op het manuscript van mijn proefschrift.

Leden van de beoordelingscommissie, Prof. dr. J. Verhaagen, Prof. dr. F.E. Hoebeek, Prof. dr. M.J.N. Benders, Prof. dr. E.J.M. Storkebaum en Prof. dr. J.P.H. Burbach, hartelijk dank voor het plaats nemen in de leescommissie en het beoordelen van dit proefschrift.

Beste paranimfen, Suzanne en Anna,
Suzanne, ik had me geen betere collega kunnen wensen. Je bent altijd kritisch, oprecht en een voorbeeld voor elke onderzoeker. Daarnaast hebben we werkelijk waar van alles met elkaar kunnen delen en ik waardeer onze vriendschap enorm. Dank voor de steun, de prachtige Sema6A experimenten, en alle discussies over experimenten en gesprekken over wetenschap door de jaren heen. We ontmoetten elkaar voor het eerst op de hogeschool Utrecht, jaren later weer bij het RMI, en werden collega's in het Pasterkamplab; wij zullen elkaar ongetwijfeld steeds weer blijven tegenkomen. Samenwerken met jou was echt een hoogtepunt en ik hoop dat we dat in de toekomst weer zullen doen.

Anna, you are a scientist in heart and soul. I greatly admire your knowledge and broad interests. Thank you for your messages and support. You immediately drop everything when somebody needs help in the lab. The sometimes long days or weekend visits at the lab were so much better with your piano concerts and coffee moments together with Suzanne and Divya. Now that you are busy writing your thesis yourself I wish you all the strength and inspiration to decide your direction for the future. The truffle festival in Italy is still on my bucket list and of course I hope to see you in Leuven!

Divya, colleague and dear friend, I miss you very much but I am happy that we manage to stay in touch and I am sure we will continue to do so. I admire your honesty, perseverance, passion for science and your love and care for your dear Anuj, sweet Advik and family. I hope we will visit each other in the future, in India and beautiful Kerala, or Chicago and Belgium.

Kristel, Emma, Danielle en Tamar, met jullie was het een hele gezellig tijd op ons mooie kantoor. Kantoor 4.133 stond niet alleen bekend om het koffiezetapparaat en de snoeppot, maar ook om de Halloween kantoorborrel (toen er nog zo'n 25 man op 10 m^2 mochten staan). Het decoratieve spinrag kan waarschijnlijk de komende jaren nog uit het plafond geplukt worden. Danielle, samen posters voor de PR maken hoorde daar zeker bij en dat niet alleen met Halloween, maar ook het filmen en editen van de Pasterkamplab thesis movies was bloedserieus. Niet te vergeten, de befaamde ugly Christmas sweater day was een dag met de nodige creatieve voorbereidingen en dat was altijd super gezellig. Ik hoop dat we nog veel creatieve acties met elkaar zullen ondernemen.

Youri, 7 maanden lang hebben we gewacht op een antilichaam dat steeds maar niet kwam. Na de tientallen emails (elke maand gestuurd naar een andere werknemer van Abcam: Christel, Leslie, Coby, Tanja, Jessica en anderen) kwam het dan toch eindelijk binnen! Tussendoor was er gelukkig thee (of toch maar koffie). En even zonder gekheid, de lightsheet experimenten voor mijn onderzoek waren dankzij jouw hulp een hoogtepunt, plus ik citeer: 'Als er licht is, is er licht', was voor al het microscopie gerelateerde werk een onmisbare leus. Verder hielden we ons ook bezig met reorganisatie en dataopslag samen met het Databaseteam met Anna, Pavol, Melissa, Renata en later ook Özge en Astrid. Het uitruimen van een -80 vriezer of een lang vergeten bewaardoos was verschrikkelijk, maar met jouw humor en oog voor organisatie een feest tegelijk.

Christiaan, wat was ik blij toen ik hoorde dat je nog tot juni 2020 zou blijven werken in het Pasterkamplab. Dankzij jouw ondersteuning konden we de ene na de andere IUE uitvoeren met prachtige resultaten. Ik vond het onwijs gezellig en heerlijk efficiënt om met jou naar de planning en organisatie van de 5e te kijken, jij hield de boel scherp. Ook schreven we het ene na het andere werkprotocol en hadden we nuttige gesprekken met de IVD. In de laatste maanden lieten we de strak georganiseerde experimentele set-ups zien aan de NVWA met het zweet op ons voorhoofd. Veel dank voor alles en ik hoop je eens te zien in Litouwen of in Leuven, want ze hebben hier namelijk Chinchilla's.

Nicky, met jouw aanwezigheid kwam er op de 5e nog eens een berg gezelligheid bovenop. De laatste experimenten waren twee keer zo leuk met jou erbij. Jij weet van aanpakken en ik weet zeker dat jij alles op de 5e verdieping goed laat lopen. Enne, die Brabanste worstenbroodjes, das goei voeier!

Dr. Jongbloets, Bart, ik zei het net al, mijn tijd bij het BCRM begon met Sema7A. Dank voor de inspanningen met twee studenten tegelijk (is die ene blonde nou Tamar of was dat nou Marieke?) en voor de kans aan mij als onervaren bachelor student. Tijdens het analyseren van data kon ik je keuze voor muziek ook wel waarderen (het nummer 'Shuffle' van Bombay Bicycle Club luisterde jij bijna dagelijks waardoor het er zo ingeramd is dat ik daar tot op de dag van vandaag nog regelmatig naar luister). Wie weet kunnen we in de toekomst nog eens samenwerken.

Leo en Henk, dat gaat even terug in de tijd natuurlijk, maar jullie waren essentieel in de beginjaren van mijn PhD dus ik wil jullie hier ook bedanken. Naast de gezelligheid aan de lunchtafel waren jullie altijd beschikbaar voor een vraag en boden een helpende hand. Leo, jij in het bijzonder veel dank voor je hulp. Je kon je af en toe verbazen over mijn schoonmaakaanvallen op het lab, maar hielp dan gewoon gezellig een handje mee.

Ketharini, besides the fact that we were part of the same masters program and that we worked in the same research group, you are a very dear friend, living in one of the most beautiful little streets in the city center of Utrecht. Now you will start a new adventure and move to Nijmegen which is not so far from Leuven! We always have so much to share and talk about and I am looking forward to meeting you in your new city.

Vamshi, I always enjoyed our conversations and coffee moments very much. I hope to see you soon in Zeist or welcome you and your family in Leuven. Although our bbq plan was not possible because of corona, I am sure we will plan one some day and celebrate good times.

Emma, the Spanish dinner under the Dutch sun in Lombok I will never forget. Thank you for your relaxtheid. 100 montaditos is waiting for us.

Kati, although we did not work together for a very long time, you were there to kick start the very first steps of my PhD project. Back then, it started with genotyping a single mouseline and this now resulted in a enormous increase in setups and possibilities to study Sema6A. We had regular brainstorm sessions with a cup of coffee which were very useful and I want to thank you for your efforts and help in the first phase of the Sema6A research.

Studenten Klara, Melissa en Josien. Zonder jullie was ik nu nog bezig met heel wat experimenten. Dank voor jullie inzet en tijd in het Pasterkamplab! Melissa, ik hoop je snel eens te zien in Putten!

Eljo, tijdens mijn stage maakte ik dankzij jou voor het eerst kennis met de IUE techniek. Nadat je naar Parijs vertrok had ik niet gedacht ooit als collega's te werken op dezelfde afdeling, maar jij kwam terug bij het Pasterkamplab en werkt nu samen met Marleen aan allerlei projecten en aan Sema6A.

De Pasterkamplab Thursday Meetings waren voor mij goud. Niet alleen hadden we hierdoor een extra centraal moment om elkaar gewoon even te ontmoeten en te lunchen, maar ook konden we praktische problemen delen en experimenten bespreken. In coronatijd is zo'n extra online meeting erbij niet ideaal, maar ik hoop dat het toch zal doorzetten.

To all the other (former) colleagues that were part of the Pasterkamplab during my PhD: Dianne, Sara, Renata, Mark, Lill Eva, Sandra, Lieke, Mateja, Andreia, Marloes, Tijana, Astrid, Noora, Pavol, Xandor, Svetlana, Özge, Danielle V, Rianne, Laurens, Marta: many thanks for sharing your research and for all the good chats and coffee moments, keep up the good work! Mark B, the klimbos in the Ardennen I will never forget! Marina, thank you for your help with all kinds of things in the lab!

Department of TN, Vicki, Sandra, Ria, Krista, Joke en Rianne. Allen bedankt voor jullie beschikbaarheid en de ruimte om vragen te stellen of hulp om administratieve zaken te regelen.

All people and research groups of the TN department: thank you for sharing your research during seminars or symposia and for all the nice lunch or coffee breaks, fun borrels and yearly labdays.

Dorinde, Vera en Nadieh, dank voor jullie gezelligheid de afgelopen jaren met etentjes en koffie/thee momenten. Al wonen we door het hele land ik hoop dat we elkaar snel weer eens zien. Dorinde, dank voor jouw lieve kaarten en interesse in mijn onderzoek door de jaren heen.

Trineke en Dianne, dank voor alle geweldige muzieksessies in de kerk, in huis of buiten in het park. Ik hoop dat we nog zeer regelmatig zullen spelen samen, dank voor jullie vriendschap, steun en interesse in mijn onderzoek. Daarbij betrek ik ook de muziekgroep van de Jacobikerk in Utrecht in zijn huidige vorm, en alle muzikanten die de afgelopen jaren mee hebben gedaan, de muziek die we samen maken brengt heel veel goeds!

Magda en Diane, dank voor jullie vriendschap die altijd blijft. Met daarbij jullie mannen Matthijs en Laurens-Jan en lieve kids. Ik hoop dat we nog veel film-marathons, spelletjesavonden en etentjes mogen beleven samen met drapjes en hankjes zoals biertjes en wijntjes en kaasjes en witte bakstenen. En daarbij natuurlijk weer eens muziek maken als Tak3 band met Tsjaikovski, Michael Jackson, Eric Clapton of Billy Joel covers.

Edward, dank voor de interesse in mijn onderzoek, in mij als wetenschapper en als mens. Jij hielp me te zien wat echt belangrijk is. Dat wist ik diep van binnen misschien ook wel zou je zeggen, maar dankzij jou kwam alles in een stroomversnelling en had ik daar tijdens mijn PhD en voor altijd heel veel aan. Ik hoop van harte dat we nog veel goede gesprekken zullen voeren.

Reinalda, met jou is het altijd goed. Ik heb geweldige herinneringen aan als kind rondcrossen op een skelter door wijk Frankrijk, kamperen in de achtertuin, overleden goudvissen ceremonieel begraven, rotjes afsteken, de kermis in Harderwijk, de krommekamp, de vlierburgweg, de basisschool en nog heel veel meer. Dat we op een andere middelbare school kwamen te zitten maakte niet uit, elke vakantie zagen we elkaar elke dag. Jouw vriendschap is onmisbaar. Dank voor je onvoorwaardelijke steun en interesse in mijn werk. Alhoewel ik

heel graag met je meegegaan was op wereldreis kon dat niet, omdat die laatste fase PhD toch wel een dingetje was. Ik hoop ooit nog eens met je op reis te gaan en ik heb heel veel zin in de roadtrips met de camper a.k.a de bezemwagen.

Lieve ouders, Piet en Ineke, jullie waren er altijd en nog steeds. Dank voor de interesse in mijn onderzoek en alle aanmoedigingen. Toen het hoofdstuk in het studieboek uitkwam bestelde Piet het gelijk en nog voor ik het zelf in huis had keken jullie er al vol bewondering naar. Lieve Ineke, dankzij jou bleef er ook ruimte voor tekenen en schilderen. Ook al was het soms onmogelijk om een workshop te plannen ik weet zeker dat we er samen nog veel zullen volgen. Lieve Piet, ik zie uit naar de komende jaren in Leuven en vind het geweldig leuk dat jullie regelmatig in de buurt zullen zijn.

Elise, Pieterjan, Peter, Floor en Mark, dank voor jullie interesse in mijn onderzoek. Elise, de eerste promotieceremonie die ik bijwoonde was die van jou. In jouw werk als kinderarts bent je ook altijd met onderzoek bezig. Wie weet kunnen we in de toekomst nog eens samen aan een onderzoek werken. Pieterjan, ik weet nog goed dat jij er, in India, 2018, achter kwam waar dat onderzoek van mij nou eigenlijk over ging toen we op een prachtig eiland in gesprek waren met een alleraardigst, hoog bejaard stel uit Engeland. Ik denk nog vaak aan dat gesprek en de aanmoedigende woorden van die Britten: 'Good luck with the research!'. Peter, ook al ging het gespreksonderwerp al snel richting 'z'n vriendje dommel' zodra het woord semaforine viel, jij was altijd benieuwd naar de status en voortgang van mijn onderzoek. Ik hoop dat je samen met Floor en Lizzie nog lang om de hoek blijft wonen. Mark, jij weet ook hoe het is om grote projecten te moeten uitvoeren en zo konden we met elkaar praten over de leuke en moeilijke kanten. Ik vind het echt geweldig leuk dat je in Utrecht woont en dat we onze liefde voor de Aziatische keuken kunnen delen en insta-waardige maaltijden op tafel zetten.

Lieve Viktor en Lizzie, jullie zijn de jongste familieleden en ik denk de belangrijkste. Als tante wil ik er altijd voor jullie zijn.

Oma Bep, wat vind ik het mooi dat ik dit boek aan u kan geven. Dank voor alle aandacht en belangstelling voor mijn proefschrift. Ontzettend jammer dat Opa Gerard, Opa Piet en Oma Rijkje er niet meer zijn. Oma Rijkje heeft me nog laten zien dat er ruimte was voor een foto van mijn promotiedag aan de 'wall of fame'. Ze ging er helemaal vanuit dat het goed zou komen en ik daardoor ook. Tante Cora, waar ik toch wel erg op zou lijken, had het vast ook mooi gevonden. Ik stel me voor dat we als onderzoekers een goede discussie hadden kunnen voeren.

Lieve schoonfamilie, in het bijzonder opa Biesbroek, dank voor alle hartelijke woorden en interesse in Matthijs en mij. Ans, Chris, Jolien, Timon, Esmee, Giske, Sven, Jesse, Sofie, Stefan en Lotte, het familieweekend in het mooie Bundenbach in 2019 vond ik geweldig en ik hoop dat we dat nog eens kunnen doen!

Allerliefste Matthijs, jij weet als geen ander hoe het is om een PhD project te runnen. Naast dat we tijdens het avondeten helemaal kunnen opgaan in gesprekken over onderzoek en wetenschap hebben we zoveel te delen en te beleven samen! Dank voor alle rust die je gaf wanneer ik niet kon slapen, omdat er te lang was doorgewerkt of als er de volgende dag een belangrijke afspraak op de agenda stond. Met jou aan het Oppenheimplein in Utrecht en op de Sint-Quintensberg in Leuven wonen is het mooiste wat er is en ik wil er altijd voor je zijn.

About the author

Marieke Geerte Verhagen was born on the 10th of July 1989 in Gouda, the Netherlands. She grew up in Breda and Harderwijk. After completing high school at the Christelijk College Nassau Veluwe, she started her studies at the Hogeschool Utrecht studying Life Sciences. After obtaining the first degree (*propedeuse*) she applied at Utrecht University and started the Biology bachelor program. During the third year she followed courses in Neuropsychology and Biomedical Sciences focusing on neuroscience and extra-curricular courses in Music Theory. After the bachelor program, she contributed to a research project at the Brain Center Rudolf Magnus under the supervision of Dr. G.M.J. Ramakers and Dr. B.C. Jongbloets. This project, focusing on axon guidance and neuronal morphology sparked her interest in neuroscience further. In 2013, she started the master program Neuroscience and Cognition following the Experimental and Clinical Neuroscience track and worked on miRNA135ab involved in neurite outgrowth and targets Krüppel-like Factor 4 and Adenomatous Polyposis Coli during a 9-month internship under supervision of Prof. dr. R.J. Pasterkamp and Dr. E.Y. van Battum. This project resulted in a scientific publication. She moved to the United Kingdom, London, King's college for a 6-month internship to train in microsurgery techniques and cortical development at the MRC Centre for Neurodevelopmental Disorders under supervision of Prof. dr. O. Marín and Dr. L. Lim. In 2016, she started her PhD project studying the role of Sema6A during nervous system development and specifically the reverse signaling pathway under supervision of Prof. dr. R.J. Pasterkamp. The results of her research are found in this thesis and she presented her research at several international conferences, including oral presentations at the Circuits Development and Axon Regeneration meeting (AXON2019) and at the Molecular Mechanisms of Neuronal Connectivity meeting (CSHL2020). Music has been a weekly activity since she was 9 years old and Marieke will continue to study the piano and flute. In July 2021, Marieke started her new job as a postdoctoral fellow in Belgium at KU Leuven and VIB in the group of Dr. L. Lim, studying the development and function of long-range GABAergic neurons in the cerebral cortex.

List of publications

MG Verhagen and RJ Pasterkamp. Axon guidance: semaphorin/neuropilin/plexin signaling. Cellular Migration and Formation of Axons and Dendrites, 109-122, 2020, doi.org/10.1016/B978-0-12-814407-7.00005-5

D Rozbesky, MG Verhagen, D Karia, GN Nagy, L Alvarez, RA Robinson, K Harlos, S Padilla-Parra, RJ Pasterkamp, EY Jones. Structural basis of semaphorin-plexin cis interaction. The EMBO Journal 2020, 39:e102926, doi.org/10.15252/embj.2019102926

EY Van Battum, MG Verhagen, VR Vangoor, Y Fujita, AAHA Derijck, E O'Duibhir, G Giuliani, T de Gunst, Y Adolfs, D Lelieveld, D Egan, RQJ Schaapveld, T Yamashita, RJ Pasterkamp. An Image-Based miRNA screen identifies miRNA-135s as regulators of CNS axon growth and regeneration by targeting Krüppel-like factor. Journal of Neuroscience 2018, 38(3):613-630, doi.org/10.1523/JNEUROSCI.0662-17.2017

S Brignani, DDA Raj, ERE Schmidt, Ö Düdükcü, Y Adolfs, AA De Ruiter, M Rybiczka-Tesulov, MG Verhagen, C van der Meer, MH Broekhoven, JA Moreno-Bravo, LM Grossouw, E Dumontier, JF Cloutier, A Chédotal, RJ Pasterkamp. Remotely Produced and Axon-Derived Netrin-1 Instructs GABAergic Neuron Migration and Dopaminergic Substantia Nigra Development. Neuron 2020, 107(4):684-702.e9, doi.org/10.1016/j.neuron.2020.05.037